

# The mechanisms of microtubule associated proteins in chromosome segregation

---

Vukušić, Kruno

Doctoral thesis / Disertacija

2020

Degree Grantor / Ustanova koja je dodijelila akademski / stručni stupanj: **University of Zagreb, Faculty of Science / Sveučilište u Zagrebu, Prirodoslovno-matematički fakultet**

Permanent link / Trajna poveznica: <https://um.nsk.hr/um:nbn:hr:217:732521>

Rights / Prava: [In copyright](#) / [Zaštićeno autorskim pravom.](#)

Download date / Datum preuzimanja: **2024-07-20**



Repository / Repozitorij:

[Repository of the Faculty of Science - University of Zagreb](#)





University of Zagreb

FACULTY OF SCIENCE  
DEPARTMENT OF BIOLOGY

Kruno Vukušić

**THE MECHANISMS OF MICROTUBULE  
ASSOCIATED PROTEINS IN  
CHROMOSOME SEGREGATION**

DOCTORAL THESIS

Zagreb, 2020





University of Zagreb

FACULTY OF SCIENCE  
DEPARTMENT OF BIOLOGY

Kruno Vukušić

**THE MECHANISMS OF MICROTUBULE  
ASSOCIATED PROTEINS IN  
CHROMOSOME SEGREGATION**

DOCTORAL THESIS

Iva Tolić, PhD, Senior Research Group Leader

Zagreb, 2020



Sveučilište u Zagrebu

PRIRODOSLOVNO-MATEMATIČKI FAKULTET  
BIOLOŠKI ODSJEK

Kruno Vukušić

**MEHANIZMI DJELOVANJA PROTEINA  
POVEZANIH S MIKROTUBULIMA U  
SEGREGACIJI KROMOSOMA**

DOKTORSKI RAD

dr. sc. Iva Tolić, znanstvena savjetnica u trajnom zvanju

Zagreb, 2020.

This work was done in laboratory of Iva M. Tolić, PhD, Senior Research Group Leader at Ruđer Bošković Institute, Zagreb, under supervision of Iva M. Tolić, PhD, Senior Research Group Leader. As a part of Postgraduate doctoral programme of Biology, this thesis is submitted for review to Department of Biology at Faculty of Science, University of Zagreb in order to achieve the academic degree Doctor of Biology.

## **Supervisor biography**

Professor Iva M. Tolić was born in Zagreb, Croatia. She graduated Molecular biology at Faculty of Science, University of Zagreb, Croatia in 1996. During graduate studies, she worked as Research assistant in the group of Prof. Nenad Trinajstić, Ruđer Bošković Institute. Her PhD work was done with Prof. Ning Wang, Harvard School of Public Health, Boston, USA. She achieved the academic degree Doctor of biology at University of Zagreb in 2002. After this, she worked as a postdoctoral fellow with Prof. Kirstine Berg-Sørensen, Niels Bohr Institute, Copenhagen, Denmark and later with Prof. Francesco Pavone, LENS - European Laboratory for Non-Linear Spectroscopy, Florence, Italy. From 2005 until 2014 she worked as a Research Group Leader at Max Planck Institute of Molecular Cell Biology and Genetics in Dresden, Germany. Her research areas are mitosis, mitotic spindle mechanics, microtubules, motor proteins and other processes in the cell that rely on cytoskeletal components and motor proteins. Professor Tolić has received 14 research grants including the prestigious projects funded by the European Research Council (ERC), *Consolidator* and *Synergy*. She has published more than 80 papers in peer-reviewed journals including *Science*, *Cell*, and *Nature Cell Biology*, cited more than 3500 times, and served as reviewer for these and various other journals. She has been elected to EMBO membership and received numerous awards such as the Ignaz Lieben Award of the Austrian Academy of Sciences and European Biophysical Societies Association (EBSA) Young Investigators' Medal and Prize. To this date she has mentored 8 PhD and 4 Master theses. As an invited speaker, she has participated in more than 100 conferences and research seminars worldwide. She organized several scientific meetings including the EMBO Conference on Meiosis in Hvar. Currently, professor Tolić is a Senior Research Group Leader with tenure at Ruđer Bošković Institute in Zagreb.

## Acknowledgements

First and foremost, I would like to thank my mentor and advisor Iva Tolić, for the opportunity to work on fundamental and exiting scientific problems using state of the art approaches. Thank you for your guidance through all those years of working together, for my scientific development, for freedom in organising experiments and for all the knowledge you passed on to me. Your scientific enthusiasm is encouraging for young scientist entering the field.

Special thanks to my amazing lab partner and friend Renata Buđa, for wonderful scientific cooperation, for all years we spent together trying to find our place in science and in the world. You always looked on the bright side of life opposing my pessimism. Thank you for all the laughs, all the bears and for being yourself, you are the greatest pal the bloke could ever have. Huge thanks also to Ivana Ponjavić, for being amazing lab partner, for work you did with me and Renata in times when we needed help the most. Huge thanks also to my lab partners Bruno Polak, Barbara Kuzmić and Ana Milas, for great atmosphere we made together in our office at Institute, you made hard days pass easily with laughter.

Many thanks to Patrik Risteski, for following anaphase project and for all the talks, Ivana Šarić for all advices, her general understanding and a help in Illustrator. Thanks to all other lab members from whom I learned a lot: Juraj Simunić, Sonja Lesjak, Jelena Martinčić and Mihaela Jagrić. Big thanks also to Nenad Pavin group, for all the knowledge I learned from you and new perspectives you gave me, special thanks to Agneza for her participation in anaphase project and Marcel for being so wonderfully different. Thanks to Marko Marjanović, Marieta Kralj group and Igor Weber group, for their help with a start of the project. Also, special thanks to all other colleagues at Ruđer Bošković Institute, MPI-CBG Dresden and all others who helped by providing us with consumables and equipment.

I would like to thank all professors from my elementary and high schools in Split and from Faculty of Science in Zagreb who all took part in my education as a scientist. Special thanks to professor Dalibor Vladović who saw in me a good scientist when I didn't see anything.

Thanks to all my beautiful friends, especially my two Ivans, for amazing time, memories and for enduring me all those years. I don't even know where to start to thank my family, my mother Silvana for all the support and patience she gave me, my father Miro for supporting and encouraging my personal and professional development, my sisters for their love, my grandparents for their sacrifice and all my other relatives who supported me no matter what.

Finally, biggest thank to by wonderful wife and a little girl for all the beautiful moments you gave me in life.

University of Zagreb  
Faculty of Science  
Department of Biology

Doctoral thesis

## **The mechanisms of microtubule associated proteins in chromosome segregation**

Kruno Vukušić  
Ruđer Bošković Institute

Successful cell division requires chromosomes to be separated on opposite sides of the cell. This is achieved by depolymerisation of kinetochore fibers and spindle elongation. Forces required for spindle elongation in human cells are linked to sliding of antiparallel microtubules and sliding capacity has been demonstrated *in vitro* for multiple motor proteins, but the molecular mechanism of sliding during anaphase in the spindles of human cells remains unknown. Here I show, by using combined depletion and inactivation assays to explore redundancy between multiple targets together with CRISPR technology, that PRC1-dependent motor KIF4A/kinesin-4, together with EG5/kinesin-5 motor is essential for spindle elongation in human cells. Depletion of KIF4A, or its partner PRC1, together with EG5 inhibition, completely arrests cell division in early anaphase while depletion of other PRC1-interacting partners had minor effect on anaphase progression. On the other hand, decreased stability of midzone microtubules measured by photoactivation assay or their structural changes studied by expansion microscopy cannot explain the observed anaphase arrest. Conclusively, my work demonstrates that two independent sliding modules power sliding mechanism that drives anaphase spindle elongation in human cells thus resolving longstanding question in the field and bridging the gap between extensive *in vitro* work on sliding motors and their concrete actions within the cell.

(192 pages, 67 figures, 367 references, original in English)

Key words: mitosis, anaphase, motor proteins, spindle elongation, bridging fibers

Supervisor: Iva M. Tolić, PhD, Senior Research Group Leader

Reviewers: Juraj Simunić, PhD, Research Associate

Helder Maiato, PhD, Principal Investigator

Maja Matulić, PhD, Associate Professor

## **Mehanizmi djelovanja proteina povezanih s mikrotubulima u segregaciji kromosoma**

Kruno Vukušić  
Institut Ruđer Bošković

Uspješna stanična dioba rezultat je točnog razdvajanja genetičkog materijala tijekom anafaze u dvije stanice kćeri. Iako su sile koje su potrebne kako bi se kromosomi razdvojili u ljudskim stanicama povezane s klizanjem premošćujućih antiparalelnih mikrotubula i poznati su mnogi motorni proteini koji mogu klizati antiparalelne mikrotubule u sustavima *in vitro*, molekularni mehanizam klizanja mikrotubula u živim stanicama tijekom anafaze još je uvijek nepoznat. Koristeći se kombiniranim utišavanjem i inhibicijom mnogih proteina zajedno s CRISPR tehnologijom u svrhu otkrivanja mogućega nadomjesnog mehanizma u anafazi ljudskih stanica, u ovom radu pokazao sam kako PRC1-ovisni motor KIF4A/kinezin-4 djeluje zajedno s motornim proteinom EG5/kinezin-5 te kako su oba ključna za produljivanje diobenog vretena u ljudskim stanicama. Eksperimenti fotoaktivacije tubulina kombinirani s ekspanzijskom mikroskopijom pokazuju kako perturbacija oba proteina značajno utječe na klizanje mikrotubula, dok njihova smanjena stabilnost ne može objasniti opisano zaustavljanje anafaze. Zaključno, elongacija diobenog vretena u anafazi ljudskih stanica rezultat je klizanja premošćujućih mikrotubula koje pokreću dva motorna proteina.

(192 stranice, 67 slika, 367 literaturnih navoda, jezik izvornika engleski)

Ključne riječi: mitoz, anafaza, motorni proteini, premošćujući mikrotubuli, diobeno vreteno

Mentor: dr. sc. Iva M. Tolić, znanstvena savjetnica u trajnom zvanju

Ocjenjivači: dr. sc. Juraj Simunić, znanstveni suradnik

dr. sc. Helder Maiato, principal investigator

izv. prof. dr. sc. Maja Matulić

# CONTENTS

<b>1</b>	<b>INTRODUCTION</b> .....	<b>1</b>
<b>2</b>	<b>OVERVIEWS OF RESEARCH</b> .....	<b>8</b>
2.1	HISTORICAL PERSPECTIVE OF CELL DIVISION .....	8
2.2	CELL CYCLE .....	10
2.3	MITOSIS IN GENERAL.....	12
2.4	MICROTUBULE STRUCTURE, ORGANISATION AND DYNAMICS .....	15
2.5	CURRENT MODELS OF MICROTUBULE POPULATIONS WITHIN THE SPINDLE .....	18
2.6	EMERGING CONCEPT OF BRIDGING MTs.....	22
2.7	MOLECULAR MOTORS AS FORCE-GENERATORS IN MITOSIS .....	24
2.8	REGULATION OF MOLECULAR MOTORS .....	30
2.9	ANAPHASE IN GENERAL.....	32
2.10	QUANTITATIVE DESCRIPTION OF ANAPHASE.....	36
2.11	SPINDLE MECHANICS DURING ANAPHASE A .....	37
2.12	ROLE OF MOLECULAR MOTORS DURING ANAPHASE A.....	42
2.13	ROLE OF NON-MOTOR PROTEINS DURING ANAPHASE A .....	43
2.14	FORCE-GENERATING MECHANISMS DURING ANAPHASE B.....	44
2.15	ASTRAL MICROTUBULES DURING ANAPHASE SPINDLE ELONGATION IN HUMAN CELLS.....	45
2.16	ANTIPARALLEL MICROTUBULES DURING ANAPHASE SPINDLE ELONGATION IN HUMAN CELLS .....	48
2.17	STRUCTURE OF BRIDGING MICROTUBULE DURING ANAPHASE.....	50
2.18	SLIDING OF BRIDGING MICROTUBULES CONTRIBUTES TO CHROMOSOME SEGREGATION IN HUMAN CELLS..	51
2.19	MECHANISMS THAT CONTROL MICROTUBULE OVERLAPS.....	53
2.20	REGULATION OF SPINDLE ELONGATION AND AURORA KINASES .....	56
2.21	PRC1 AS A MAIN SCAFFOLD FOR RECRUITMENT OF MULTIPLE MOTORS .....	60
2.22	PRC1-INTERACTING PROTEINS.....	62
2.22.1	<i>Kinesins-6 (MKLP1, MKLP2 and MPP1)</i> .....	62
2.22.2	<i>Kinesin-4 (KIF4A)</i> .....	64
2.22.3	<i>Other motor proteins</i> .....	65
2.23	KINESIN-5 AS A MAJOR PROTEIN INVOLVED IN SLIDING OF ANTIPARALLEL MICROTUBULES .....	65
2.24	SPINDLE ELONGATION BY MOTOR-DRIVEN SLIDING IN HUMAN CELLS .....	69
<b>3</b>	<b>MATERIALS AND METHODS</b> .....	<b>71</b>
3.1	CELL LINES .....	71
3.2	CONSTRUCTS, TRANSFECTIONS AND RNAI .....	72
3.3	DRUGS .....	73
3.4	SAMPLE PREPARATION.....	74
3.5	LIVE CELL IMAGING .....	75
3.6	PHOTOACTIVATION (PA) STABILITY AND SLIDING ASSAYS .....	76
3.7	IMMUNOFLUORESCENCE.....	76
3.8	EXPANSION MICROSCOPY.....	77
3.9	IMAGING OF FIXED CELLS.....	78
3.10	PARAMETERS USED TO DEFINE METAPHASE-TO-ANAPHASE TRANSITION .....	79
3.11	TRACKING OF KINETOCHORE, CENTROSOME AND CHROMOSOME MOTIONS.....	79
3.12	QUANTIFICATION OF MICROTUBULE STABILITY .....	80
3.13	QUANTIFICATION OF SLIDING VELOCITY .....	81
3.14	QUANTIFICATION OF PRC1 OVEREXPRESSION.....	81
3.15	CRISPR KO CELL SCORING .....	81
3.16	IMAGE PROCESSING AND STATISTICAL ANALYSIS .....	82
<b>4</b>	<b>RESULTS AND DISCUSSION</b> .....	<b>83</b>
4.1	MOTORS THAT GENERATE SLIDING FORCES DURING ANAPHASE .....	83



4.1.1	<i>Expansion microscopy of mitotic spindles</i>	83
4.1.2	<i>Role of EG5 and KIF15 redundancy during anaphase</i>	85
4.1.3	<i>Depletion of PRC1 does not affect velocity of spindle elongation</i>	96
4.1.4	<i>Depletion of PRC1 does not influence spindle elongation velocities</i>	100
4.1.5	<i>PRC1 depletion and EG5 inhibition induce a complete block in spindle elongation</i>	103
4.1.6	<i>EG5 motor protein and PRC1-interacting motor protein KIF4A are crucial for spindle elongation in human cells</i>	111
4.1.7	<i>Depletion of both kinesins-6, when combined with EG5 inhibition, can mimic the effect of KIF4A and EG5 perturbations</i>	112
4.1.8	<i>CENP-E and KIF14 cannot mimic the observed block in spindle elongation</i>	116
4.1.9	<i>Both Auroras are regulating spindle elongation</i>	120
4.1.10	<i>All tested perturbations have a little effect on structure of midzone microtubules</i>	124
4.1.11	<i>Decrease in protein stability cannot explain the block in spindle elongation</i>	129
4.1.12	<i>Sliding is greatly perturbed in conditions that block spindle elongation</i>	133
4.2	ADDITIONAL EXPERIMENTS ON U2OS CELLS	140
<b>5</b>	<b>CONCLUDING DISCUSSION</b>	<b>148</b>
5.1	REGULATION OF SPINDLE LENGTH AND MAIN MOTORS INVOLVED	148
5.2	KINESINS KIF4A AND EG5 DRIVE ELONGATION OF THE ANAPHASE SPINDLE	152
5.3	REGULATION OF KIF4A AND EG5 SLIDING MODULES	154
5.4	ROLE OF MICROTUBULE STABILITY DURING EARLY AND LATE ANAPHASE	158
5.5	REGULATION OF ANTIPARALLEL OVERLAP LENGTH	161
5.6	TRANSMISSION OF SLIDING FORCE TO CHROMOSOMES AND POLES	162
5.7	RETHINKING THE ANAPHASE MOVEMENTS	164
<b>6</b>	<b>CONCLUSIONS</b>	<b>168</b>
<b>7</b>	<b>REFERENCES</b>	<b>173</b>
<b>8</b>	<b>AUTHOR BIOGRAPHY</b>	<b>191</b>

# 1 INTRODUCTION

The cell cycle in eukaryotic organisms can be divided into four phases. The main fluctuations during cell cycle are happening in the S phase (S for synthesis) when DNA is duplicated and in the M phase (M for mitosis) when duplicated chromosomes are distributed into two daughter cells. In most human cells, we can observe two G (G for gap) phases which separate the events in S and M phase. G1, S and G2 phases together are called interphase. In a typical human cell proliferating in culture, interphase might occupy 23 hours of a 24-hour cycle, with 1 hour reserved for the M-phase. The typical M phase, on the other hand, can be separated into mitosis, the division of nucleus, and cytokinesis, the division of cytoplasm (Lodish, 2014). Mitosis itself can be subdivided into few stages in which the mitotic spindle is self-assembled, the chromosomes are incorporated into the spindle and are separated into two daughter cells. The beginning of mitosis in most eukaryotic cells is marked by nuclear envelope breakdown (NEBD) marking end of the prophase. In prometaphase, microtubules are nucleated, the mitotic spindle gradually forms and chromosomes are congressing to the future metaphase plate (Maiato et al., 2017). In metaphase, all chromosomes are arranged in tight metaphase plate at the cell equator and the cell checkpoint system is testing if all sister chromatids are correctly attached to microtubules from opposite spindle poles. If all the chromosomes are correctly positioned and attached to spindle poles, the securin is abruptly ubiquitinated which enables a separation of sister chromatids in anaphase. In telophase, the chromosomes are decondensed, the nuclear envelope is reformed around new daughter nuclei and microtubules are restructured into interphase arrays (McIntosh et al., 2012).

Almost all mitotic processes are orchestrated by the mitotic spindle, structure composed of microtubules and associated proteins whose role is to accurately separate chromosomes between two daughter cells (Pavin and Tolić, 2016). Microtubules are protein hollow cylindrical structures made by polymerization of tubulin subunits. The tubulin subunit is itself a heterodimer formed from two closely related globular proteins called  $\alpha$ -tubulin and  $\beta$ -tubulin, tightly bound together by noncovalent bonds. One microtubule is made of 13 parallel arranged protofilaments which finally make a hollow cylindrical structure of microtubule (Akhmanova and Steinmetz, 2008). Protofilaments, and consequently microtubules, are polar structures with  $\alpha$ -tubulins exposed at one end (called the minus – end) and  $\beta$ -tubulins exposed at the other end (called the plus + end) (Lodish, 2014). Microtubules in the mitotic spindle are organized into fibers made up of different number of microtubules.

Depending on microtubule orientation within the fiber we can distinguish parallel (all microtubules pointing in the same direction) and antiparallel (microtubules pointing in opposite directions) fibers. Kinetochore fibers (k-fibers) are connected with (+) ends of their microtubules to the kinetochores, protein complexes on the chromosomes. In this way, chromosomes are connected to the mitotic spindle, and can be separated to opposite spindle poles during anaphase (Tolić, 2018). These fibers are the most important and the most stable fibers within the mitotic spindle (Musacchio and Desai, 2017). Electron microscopy studies in the human tumour cell lines determined that k-fibers contain roughly 12-22 parallel interconnected microtubules (Wendell et al., 1993). Except k-fibers, in human cell lines we can distinguish two more subpopulations – interporal and astral microtubules. Interporal microtubules are organized into antiparallel bundles of microtubules nucleating from opposite sides of the spindle and they are overlapping in the central part of the mitotic spindle. Astral microtubules are nucleated from the spindle poles into the cytoplasm on the cortical side and are participating in spindle positioning by interactions with the cell cortex machinery (Dumont and Mitchison, 2009).

Process of chromosome segregation in mitosis is known as anaphase which relies on multiple mechanisms, even within an individual cell (Asbury, 2017; Maiato and Lince-Faria, 2010). In most model systems studied to date, segregation includes chromosome-to-pole motility (anaphase A) and spindle elongation (anaphase B) (Asbury, 2017; Pavin and Tolić, 2016; Scholey et al., 2016), and in unperturbed human cells both are equal contributors to chromosome segregation (Vukusic et al., 2017). One of the mechanisms that can contribute to anaphase A is the Pac-Man activity in which kinetochores stimulate the depolymerization of k-fibers at their plus ends and move towards the spindle poles by „chewing them up“ (Gorbsky et al., 1987; Mitchison et al., 1986). Supplementary mechanism involved is poleward flux of k-fibers, i.e., their translation toward the spindle pole accompanied by disassembly at the pole (Mitchison, 1989). Sliding of overlap microtubules (MTs) (Saxton and McIntosh, 1987) and pulling from the cortex on astral MTs (Aist et al., 1993; Grill et al., 2001) can drive spindle pole separation in anaphase B, and thus also contribute to kinetochore separation. To date, there is no comprehensive model combining all forces driving chromosome segregation in anaphase of human cells (Scholey et al., 2016).

Previous research on anaphase in human cells have marked the importance of dynamic ends of K-fibers in chromosome motion (Ganem et al., 2005; Sikirzhytski et al., 2014; Stumpff et al., 2008; Yang et al., 2007) while the contribution of forces that could arise from the central part of the spindle or the cell cortex was scarcely studied (Vukusic et al.,

2019). On the other hand, it was thought that interpolar MTs do not interact with kinetochores, while their interaction with k-fibers is weak and limited to the spindle pole region far from the kinetochores (Tolić, 2018). Interestingly, by using experimental approach involving laser ablation (Buda et al., 2017), we have recently shown that k-fibers are in strong interaction with interpolar MTs in metaphase spindles of human cells. These MTs are called bridging MTs, which assemble into bridging fibers, because they balance the forces between two sister kinetochores by bridging their k-fibers into single mechanical unit (Kajtez et al., 2016). Afterwards, it has been shown that most interpolar MTs in the metaphase spindle of human cells are connected with a pair of sister k-fibers and these can be considered as bridging fibers (Polak et al., 2017). Also, the existence of bridging MTs in vicinity of k-fibers in metaphase and anaphase spindles of human cells has recently been confirmed by electron microscopy studies (Nixon et al., 2017; Yu et al., 2019). Finally, by using laser ablation and photoactivation assays it has been shown recently by our group that sliding of MTs within the bridging fibers drives pole separation and pushes k-fibers poleward in anaphase by the friction of passive crosslinks between these fibers (Vukusic et al., 2017), establishing bridging MTs as important part of anaphase segregation machinery.

Aside from MTs, the crucial role in the organization and function of mitotic spindles have microtubule associated proteins (MAPs) that can be divided into four subgroups. The first group consists of motor proteins that have the ability to convert chemical energy into mechanical one that enables their directional movement along the MTs (Lodish, 2014). The main motor proteins in the mitotic spindle are dynein and members of the various kinesin families. Dynein is a motor protein that walks towards (-) ends of MTs, while kinesins differ in a direction of their movement depending on each subfamily and specific environmental conditions (Sharp et al., 2000). The second group of MAP proteins consists of proteins that specifically localise at the (+) end of MTs (+TIPs, plus end tracking proteins). The third group consists of proteins that regulate the extent of microtubule dynamic instability at both ends of MTs. The last group of MAP proteins consists of proteins that passively crosslink parallel or antiparallel MTs, which means that they do not have the ability to walk along the MTs (Lodish, 2014). All groups of MAP proteins are well studied in all phases of mitosis (Wordeman, 2010), while their studies in anaphase have been limited. Specifically, by using available experimental techniques it is challenging to test to role of specific proteins in anaphase if these proteins are essential in previous phases of mitosis. Moreover, modification of proteins or their concentrations in the cell can disable the entry into anaphase by inhibiting the spindle assembly checkpoint. Furthermore, interpreting the data in anaphase, even if

protein is not essential in previous phases, is complicated because the observed effects can be consequence of defects caused in phases preceding anaphase onset (Maiato and Lince-Faria, 2010). In that regard, development of small molecule inhibitors for multiple mitotic kinesins that are fast acting and easily penetrating molecules, has proved to be very useful in study of protein function during later stages of mitosis (Lampson and Kapoor, 2006).

The anaphase protein machinery studied in human cells has been linked primarily with depolymerisation of MTs at both ends, regarding mostly anaphase A mechanisms (Maiato and Lince-Faria, 2010). In that regard, depolymerization of MTs at spindle poles in anaphase has been attributed to Kif2A protein from a kinesin-13 family of kinesins (Ganem et al., 2005). However, depolymerisation at (-) ends of MTs in anaphase of human cells is not contributing significantly to overall chromosome movement (Ganem et al., 2005; Vukusic et al., 2019). Furthermore, it has been proposed that Kif18A protein from kinesin-8 family limits the overall speed of chromosomes in anaphase through regulation of depolymerization at (+) ends of MTs (Stumpff et al., 2008). This result is unexpected because it has been shown that Kif18A depolymerizes MTs using *in vitro* assays (Mayr et al., 2007). Another protein that has been well studied in human anaphase is dynein, protein characterized by walking towards (-) ends of MTs (Maiato and Lince-Faria, 2010). It has been shown that depletion of kinetochore pool of dynein in human cells dramatically reduces the velocity of chromosomes moving towards their respective poles (Yang et al., 2007) but it remains to be clarified whether the observed reduction is a direct result of lack of dynein processive motion along k-fiber MTs, or whether it is due to unstable microtubule attachments at kinetochores, possibly associated with a defective SAC, which is a known effect of dynein perturbations (Varma et al., 2008). On the other hand, non-motor proteins that connect kinetochores with MTs, like Ncd80 complex, appear essential for depolymerisation driven movement of chromosomes (McIntosh et al., 2010).

Regarding anaphase B protein machinery experimental approaches in human cells thus far have been limited to study of proteins that influence either microtubule bundling and stability or those that regulate plus-ends of interpolar MTs (Vukusic et al., 2019). On the other hand, the proteins that could have effect on anaphase through direct sliding of bridging MTs, structures shown to contribute to chromosome segregation (Vukušić et al., 2017), have not been directly experimentally tested. Specifically, some of these proteins could directly slide antiparallel MTs apart within the bridging fiber in anaphase by walking toward plus-end of MTs and in that way, they can, by exerting pushing forces, contribute to movement of k-fibers and centrosomes (Vukušić et al., 2019). Similar mechanisms of pushing from the spindle

midzone by sliding action of antiparallel MTs were proposed years ago (McIntosh et al., 1969). In that category falls primarily Eg5 protein (KIF11), from a family of kinesins-5, who can slide antiparallel MTs *in vitro* (Kapitein et al., 2005) and whose orthologues drive spindle elongation by antiparallel sliding mechanism in the yeast spindle (Straight et al., 1998). On the other hand, some proteins could passively connect parallel or antiparallel MTs within the bridging fiber and thus regulate stability and number of bridging MTs or could act as a brake on sliding between the MTs (Collins et al., 2014). The most obvious candidates in this category are PRC1 (protein regulator of cytokinesis 1) protein that specifically binds only antiparallel overlapping regions in metaphase and anaphase (Polak et al., 2017; Vukusic et al., 2017) and KIF23/MKLP1 protein from family of kinesins-6 that binds antiparallel MTs in late anaphase (Glotzer, 2009), but also slides antiparallel MTs *in vitro* (Nislow et al., 1992) and is itself known interacting partner of PRC1 (Kurasawa et al., 2004). Alongside direct sliding of overlapping bridging MTs the dynamics of their ends could be also important because it can regulate the length of the overlap region. In that regard, previous experiments have shown that depletion of KIF4A, protein from a family of kinesins-4, causes overlap regions to lengthen during anaphase (Zhu and Jiang, 2005). On the other hand, there is possibility that growing (+) ends of bridging MTs can directly push sister k-fibers by polymerization pressure and in that way, they could move chromosomes (Vleugel et al., 2016). The similar mechanism has been recently proposed for chromosome segregation in the oocytes of *Caenorhabditis elegans* (Laband et al., 2017). Taken together, it is necessary to experimentally test the contribution of aforementioned proteins in anaphase in multiple combinations using various techniques of protein perturbation to test if some of them exert their function through sliding of bridging MTs.

Although forces required for spindle elongation can be generated at the cell cortex, this is unlikely scenario in human cells given that depletion of dynein adaptors on the cortex does not impact chromosome segregation during early anaphase (Kiyomitsu and Cheeseman, 2013). While the sliding mechanism has been proposed years ago (McIntosh et al., 1969), and *in vitro* experiments demonstrated antiparallel sliding capacity of multiple motors (Bieling et al., 2010; Kapitein et al., 2005; Nislow et al., 1992; Su et al., 2013) which proteins drive sliding of MTs in mitotic spindle and what is exact molecular mechanism of spindle elongation in human cells remains a longstanding open question. While spindle elongation can be specifically altered by changing temperature (Afonso et al., 2014), global MT dynamics (Hu et al., 2011) or interfering with top signalling effectors like Aurora kinases, PLK1, Cyclin B or CDK1 (Afonso et al., 2019; Afonso et al., 2014; Brennan et al., 2007;

Wolf et al., 2006), the aim of this thesis was to find the force-producing proteins whose depletion stops spindle elongation during anaphase and uncover the mechanisms that regulate them thereby unravelling one of the most perplexing problems in the field of mitosis. We can say we will use a bottom-to-top approach, when regarding signalling pathways, in which we will try to elucidate the bottom force-generating proteins, and after that, middle and top regulatory networks that control them.

The first step in this study will be imaging of control human non-transformed RPE-1 and tumour U2OS cells without modifications of protein function or concentration to determine the referent measurement of anaphase dynamics for all cell types and to exclude the negative nonspecific effects of used inhibitors. Next, the depletion or inhibition of all groups of proteins known from literature (candidate-based approach) will be performed by using techniques of RNA interference, available small molecule inhibitors of motor proteins and CRISPR knock-out (KO) technology. Main technique of protein perturbation will be RNA interference (RNAi) which depletes protein levels in a cell by using small interfering RNAs (siRNAs) who interferes with translation of protein by specifically binding to mRNA. Next, available small molecule inhibitors of mitotic kinesins will be used which specifically interfere with protein function mainly by binding to important protein domains responsible for normal function of mitotic protein within the spindle. Finally, CRISPR technology will be used for most-promising candidates which specifically induces breaks within DNA sequences of interest thereby generating stable knock-outs (KOs), if those candidates are available in published bases of RPE-1 cell line KOs. To determine the efficiency of protein depletion and inhibition we will use an immunostaining of cells to determine that protein is not localizing to the mitotic spindle as in control cells, where applicable. Furthermore, to precisely quantify the exact amount of protein that was depleted in cells the Western-blot analysis will be performed for every protein that was inhibited. To enrich cells in mitosis, the synchronization of cells will be performed using conventional inhibitors of S/G1 transition, G1/M transition and SAC. After establishing that level of protein depletion reached maximum levels by specific technique, the velocity of kinetochore separation, spindle pole separation and poleward movement of kinetochores to poles will be measured in all conditions. The obtained results will be compared with control cells to determine if any of the candidate proteins have a significant effect on parameters of anaphase dynamics. For proteins that are affecting anaphase velocities, the depletion will be performed again but this time combined with photoactivation of bridging MTs in anaphase to determine if these proteins affect the sliding velocities directly or if they affect microtubule stability through microtubule bundling. Also,

to check if candidates are affecting global structure of antiparallel bridging MTs fixation combined with expansion microscopy of mitotic spindle will be used enabling super-resolution imaging of mitotic spindle MTs. Furthermore, for proteins that are showing similar and significant effects on anaphase the combined inhibition will be performed to examine if these proteins work by the same or similar mechanism in the mitotic spindle thereby defining redundant pathways in spindle elongation. Finally, the goal is to determine which proteins are responsible for direct generation of forces in the bridging fibers and which proteins have an indirect effect on dynamic properties of those fibers. The main goal of study as a whole is to build a first comprehensive model of spindle elongation in human cells, incorporating all important mechanisms and protein players by checking redundant pathway of force-generation and deciphering regulatory mechanisms that control mitotic kinesins in antiparallel overlaps. The hypothesis of the study is that candidate motor proteins specifically localise to bridging MTs and actively push k-fibers by sliding antiparallel bridging MTs apart and, in that way, separate centrosomes and segregate chromosomes in anaphase of human cells.



## 2 OVERVIEWS OF RESEARCH

### 2.1 Historical perspective of cell division

Cell division is the process in which parent cell divides into two nascent daughter cells. This process forms the basis of existence and continuity of all life and it can be reasoned that the most critical part of this process is the ability of cells to accurately duplicate and then faithfully segregate their duplicated genetic material at each cell division (McIntosh et al., 2012). This ensures stability of genomic information that is fundamental to life. For that reason, this process has to be very precise because some loss or gain in DNA material can be either lethal to the cell, in which case it is not detected at the level of organism, or can cause severe complications for the cell (Lodish, 2014). For example, it is estimated that missegregation rate in human non-transformed cell lines is extremely low (Worrall et al., 2018). Thus, tightly controlled and timed cell divisions at level of organism are essential for normal differentiation and complex organ development because loss of these controls is common defect observed in various types of cancers, infertility disorders and multiple congenital abnormalities (Lodish, 2014). In that regard, aneuploidy - deviation from a multiple of the haploid chromosome number - is the leading cause of spontaneous miscarriages and birth defects in humans (Nagaoka et al., 2012) and it represents a key hallmark of cancer, in which recurrent patterns of aneuploidy are observed (Ben-David et al., 2016).

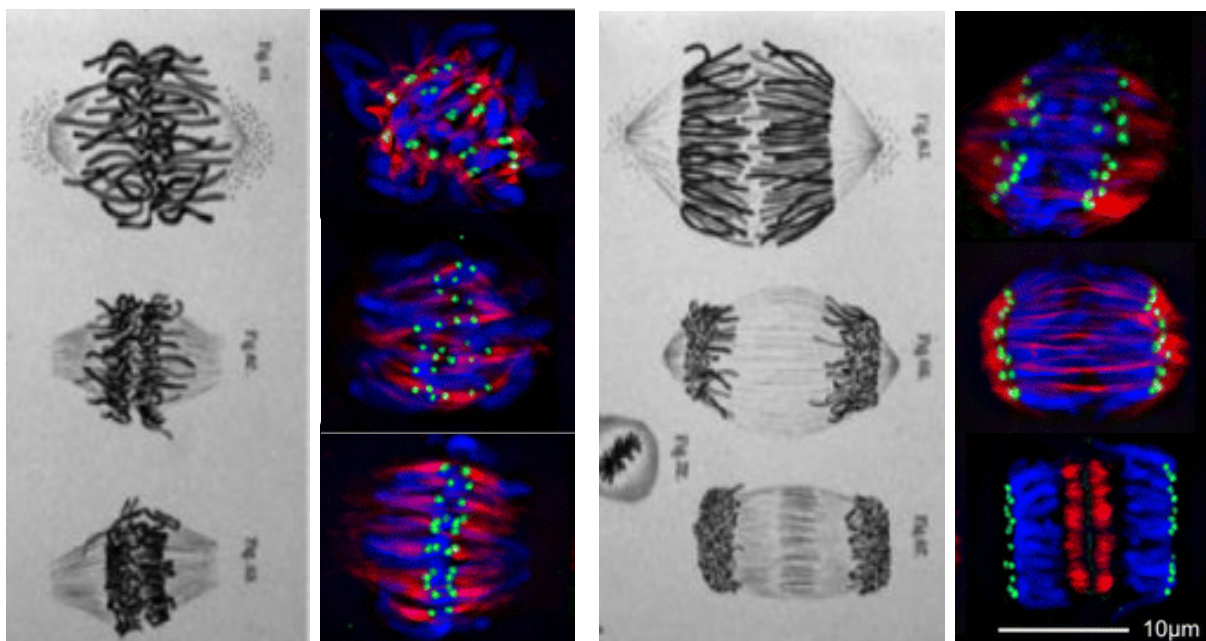


**Figure 1. Old and new representations of same stages of mitosis, depicting mitotic spindle in a plant cell.** Black and white images represent drawings done by Walther Flemming and coloured images represent modern fluorescent images depicting MTs in red, chromosomes in blue and kinetochores in green (Assembled from Figure parts from: <https://www.nature.com/scitable/content/drawing-of-mitosis-by-walther-flemming-43904/> and Zhang and Dawe, 2011).

Mitosis (Greek  $\mu\acute{\iota}\tau\omicron\varsigma$  mitos, meaning thread) is a term first used by Walther Flemming in 1880 which now describes a process by which the duplicated chromosomes are segregated to the nascent daughter cells. Even though he worked with cells subjected to rather crude fixation and staining methods, Flemming was able to describe bipolar shape of the spindle and its characteristic filamentous organisation, in principle not much different than modern spindle seen under fluorescence microscopy (Figure 1) (Paweletz, 2001). In 1950s, polarisation microscopy proved that spindles are built from filaments that run in parallel with chromosome motion and later it was proposed that polymerisation dynamics of these filaments produce mechanical forces needed for powering chromosome motion during anaphase (Inoue and Sato, 1967). Later, by combination of different techniques and rapid expansion in field of molecular biology these filaments were identified as MTs, non-covalent polymers of protein tubulin (Mohri, 1968). Due to its large size and major role in mitosis, many have studied molecular components of mitotic spindle in the last 40 years by various techniques and many proteins were identified that are essential for mitosis (Walczak and Heald, 2008). In addition, emergence of techniques such as phase contrast microscopy allowed the first live-cell imaging of a highly dynamic structures such is mitotic spindle. Further, discovery and development of green fluorescent protein (GFP) and its many sister forms allowed for fast visualisation, tracking and quantification of molecular structures within mitotic spindle (Rieder and Khodjakov, 2003). Further, micro-manipulation techniques and laser ablation of some components of spindle gave us insight into mechanical principles of the mitotic spindle, mainly force generation mechanisms involved (Recouvreur and Dogterom, 2012). Lastly, development of small molecule inhibitors for different spindle components enabled temporally precise and fast perturbations elucidating the previously unknown roles of some proteins (Lampson and Kapoor, 2006). However, our understanding of the basic mechanical principles and architecture of this essential cellular structure remains rudimentary, since we cannot explain how the spindle maintains its structural and functional stability in the face of different forces (Shimamoto et al., 2011). These complex questions regarding mitotic

spindle and its riddles still remain in scope of modern biophysical research (McIntosh and Hays, 2016).

## 2.2 Cell cycle

Cell cycle is an ordered series of events that lead to cell division and the production of two daughter cells, each containing chromosomes identical to those in the parental cells (Lodish, 2014). The cell cycle is divided into four main phases: G1 (gap one), S (synthesis), G2 (gap two) and M (mitosis) (Figure 2). To complete the whole cell cycle, human cell need ~24 hours. In G1 phase (~15 hours) cells grow in size and synthesize proteins and RNAs required for DNA replication. When cell has synthesized all required molecules and reached appropriate size, it enters next cell cycle phase by passing a point in G1 known as restriction point. When cells pass this point, they are irreversibly committed to cell division (Meraldi et al., 2004). Next, cells enter the S phase (~6 h), where genetic material of each chromosome is duplicated to form two identical sister chromatids duplicated in the process of semiconservative replication. In the next gap phase, G2 (~2 h), cells synthesize more proteins and grow to prepare for the last phase of cell cycle, M phase (~1 h). M phase consists of two major processes: division of the nucleus, or mitosis, and division of the cytoplasm, or cytokinesis, when the cell itself divides in two. Main function of mitosis is to successfully distribute sister chromatids to each daughter cell (Lodish, 2014). Despite conserved proteins and basic principles of cell cycle that are shared by many eukaryotic organisms, the process can differ significantly in some details, so many analogous principles exist that can exert the same function with different mechanisms (McIntosh et al., 2012). Therefore, as this project was done on multiple human cell lines, I will discuss mainly mitotic mechanisms in these model systems.

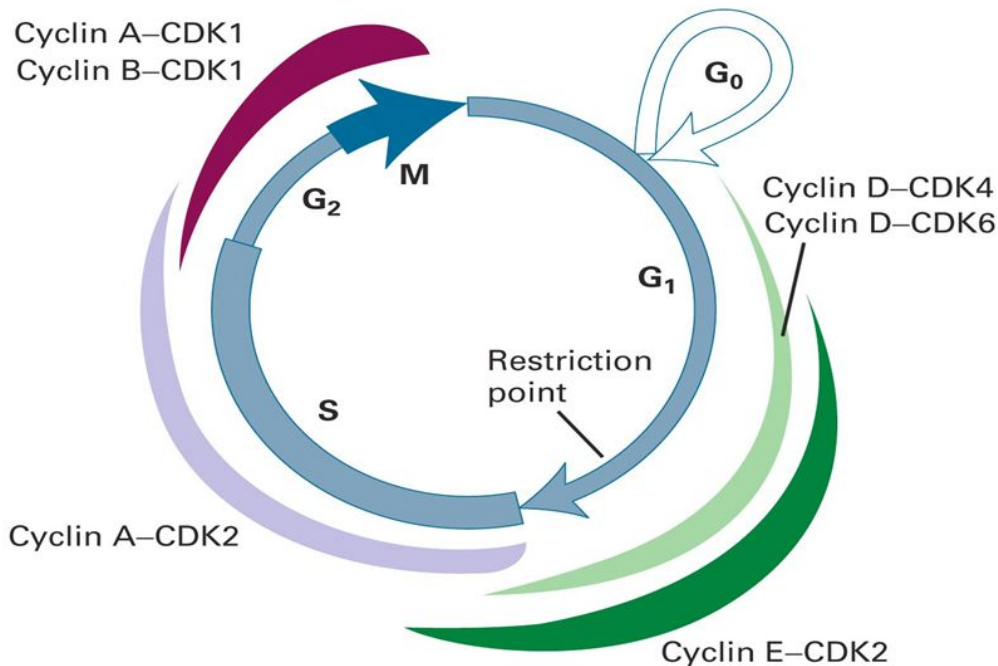


**Figure 2. Overview of main phases of the cell cycle in animal cells.** S phase of the cell cycle is period of DNA replication followed by gap two ( $G_2$ ) period of protein synthesis. Start of mitosis is marked with breakdown of nuclear envelope and chromosome condensation and at metaphase-anaphase transition of mitosis sister chromatids segregate. After mitosis, M phase of cell cycle finishes with cytokinesis followed by gap one ( $G_1$ ) phase of protein synthesis. In  $G_1$ , cell passes through Restriction point, after which cell is irreversibly committed to cell cycle. Interphase is defined as the time between two mitoses.  $G_0$  represents a quiescent state in which cell does not proliferate. Involvement of cyclin-CDK complexes that are specific for every transition event between phases is also represented. Taken from Lodish et al., 2014.

It is essential that cell can control each step in a cell cycle because it must ensure that DNA replication is carried out correctly and that each daughter cell inherits the correct number of each chromosome. Accuracy and fidelity are achieved because cell division is controlled by mechanisms known as checkpoint pathways that prevent initiation of next step in cell cycle until earlier steps have been completed and all discernible errors corrected (Meraldi et al., 2004). The main controllers of cell cycle progression are highly conserved heterodimeric protein serine-threonine kinases that contain a regulatory subunit (cyclin) and a catalytic subunit (cyclin-dependent kinase, CDK) (Figure 2) (Hochegger et al., 2008). While

CDK expression levels are rather constant during cell cycle, the cyclin expression varies from phase to phase thus controlling the kinase activity. These complexes regulate some key checkpoints, transition from G1 to S phase and from G2 to M phase. This regulative progression, involved in entry of different stages of cell cycle, is achieved by phosphorylation of various proteins at specific regulatory sites. In that way, phosphorylation can activate some proteins and inhibit others in complex regulatory networks. Interestingly, CDKs are also subjects of regulation by phosphorylation (Hochegger et al., 2008). In addition, regulated degradation in proteasomes of the same proteins plays an important role in cell cycle transitions and because it is irreversible, it ensures that the whole cycle moves in only one direction, from G1 phase to the M phase. Cells produce different type of CDKs that have a role in initiation of specific events in each cell phase (G1 CDKs, G1/S CDKs, S phase CDKs and mitotic CDKs) and CDKs that trigger one cell cycle phase are active only during that phase (Lodish, 2014) (Figure 2).

## 2.3 Mitosis in general

For mitosis to proceed correctly, cells must first duplicate their microtubule-organizing centres (MTOCs), in animal cells called centrosomes, in coordination with replication of chromosomes in the S phase. The duplicated centrosomes separate in prophase of mitosis and will become two spindle poles of mitotic spindle (Lodish, 2014) thus making a characteristic bipolar spindle form. It is important to note that this process has to be properly regulated because multipolar spindles that result from failure in this process contribute to mis-segregation of chromosomes leading to high genomic instability resulting in aneuploidy seen in many tumour cell lines (Godinho and Pellman, 2014).

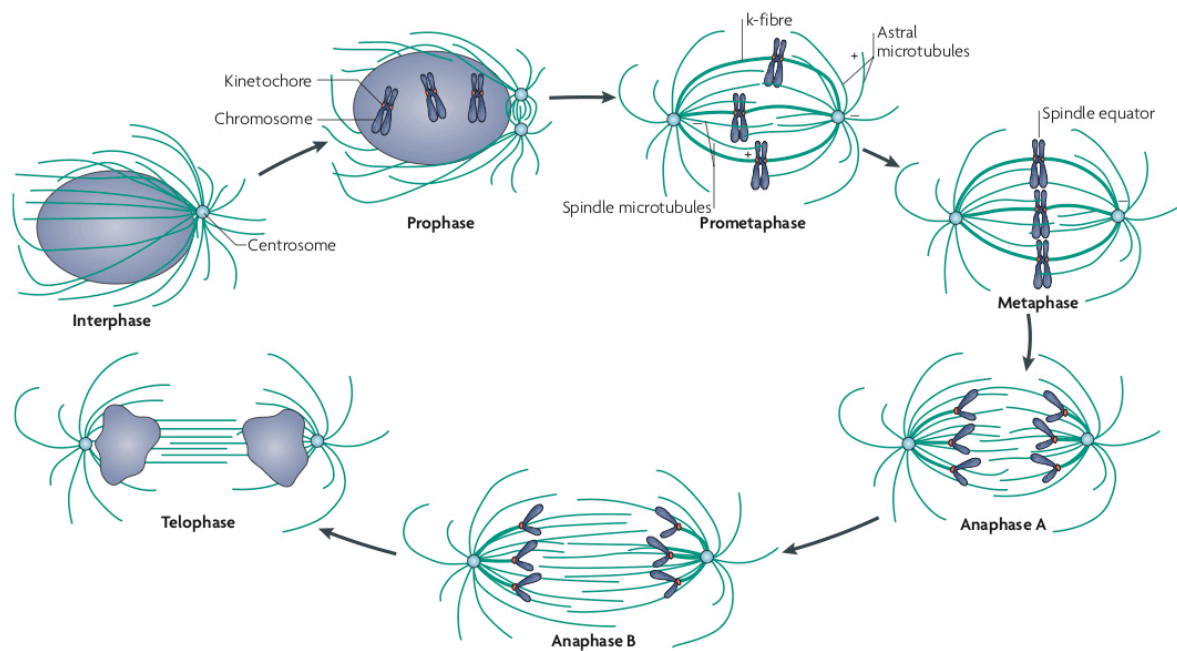


**Figure 3. The stages of mitosis with some key components of mitotic spindle noted.** Although mitosis is a continuous process it has been divided into stages for ease of description. During interphase, chromosomes are duplicated, bound by cohesin complexes and in the same time, centrosomes are duplicated. During prophase, chromatin condense into chromosomes concurrently with reorganisation of interphase microtubule array. During prometaphase, chromosomes attach to MTs and congress to establish a metaphase plate. In metaphase, chromosomes are aligned in metaphase plate at spindle equator, and in anaphase, they are segregated to two poles by depolymerisation of k-fibers, anaphase A, and spindle elongation, anaphase B. During telophase, nuclear envelope reforms around two daughter nuclei. More details in the text. Taken from Walczak et al., 2010.

Although mitosis is a continuous process, it has been commonly divided in five stages for ease of description (Lodish, 2014) (Figure 3). First phase of mitosis, prophase, is characterized by increased activity of centrosomes, as they begin to nucleate MTs which replaces interphase array of MTs with mitotic asters, structures consisting of centrosome and its radial arrays of MTs that converge at the centrosome (Mogilner and Craig, 2010) (Figure 3). Additionally, the dynamics of growing MTs increase at their plus-ends and two mitotic asters are moving to opposite sides of the nucleus by the action of bipolar kinesin-5 motor protein. Separated centrosomes will form two spindle poles of mitotic spindle (Figure 3). This pathway of centrosome separation in human cells is called the prophase pathway (Kaseda et

al., 2012), because centrosomes can be also separated in prometaphase. Furthermore, internal order of membrane system is disrupted; endocytosis and exocytosis stop and actin microfilaments are rearranged to give rise to rounded cell. In addition, chromosomes begin to condense extensively; each DNA duplex must be reduced in length by >1000-fold after which it forms tight structures called chromosomes (McIntosh et al., 2012) (Figure 3). Next, cohesin complexes at chromosome arms are degraded leaving only those in centromeric region and protein complexes that represent sites of microtubule attachment, called kinetochores, begin to assemble at the centromeric region of each sister chromatid (Musacchio and Desai, 2017). In prometaphase, nuclear envelope and nuclear pores breakdown and nuclear lamina disassemble. Nuclear envelope breakdown (NEBD) allows MTs to search and capture the chromosome pairs by associating with their kinetochores (model first proposed in (Kirschner and Mitchison, 1986) (Figure 3). This first interaction between chromosomes and growing MTs marks the beginning of assembly of mitotic spindle. When both sister chromatids become captured to opposite spindle poles they are said to be bi-oriented (also called amphitelic attachment) (Mogilner and Craig, 2010). Such pairs begin a process of chromosome congression, movement that finally results in aligned sister chromatids in equatorial plane and finalisation of that process defines beginning of metaphase (Maiato et al., 2017) (Figure 3). Some cells can separate their centrosomes extensively in this phase thereby taking the prometaphase pathway of centrosome separation (Kaseda et al., 2012).

Metaphase in human cells is defined as a stage when paired sister chromosomes oscillate at the center of the spindle (Figure 3). Metaphase is known as a biophysical steady state. That means that despite large fluctuations and directed fluxes in both physical and chemical processes during metaphase average amount and position of spindle components is constant over time (Dumont and Mitchison, 2009). The next stage, anaphase, is induced only when quality control is passed on. That quality control process is called spindle assembly checkpoint (SAC) and it controls segregation in a way that it prevents segregation until chromosomes are attached to poles and kinetochores are under sufficient tension (Cheeseman and Desai, 2008). If these conditions are fulfilled, anaphase-promoting complex/cyclosome (APC/C) is activated and cohesin complexes in centromeric part are broken, chromosomes are separated and pulled to different poles by the forces exerted by MTs depolymerization (anaphase A) (Figure 3). Separate movement also occurs, spindle poles move apart from each other, elongating the spindle extensively, mediated probably by sliding of antiparallel MTs (anaphase B) (Figure 3). In the next phase, telophase, after chromosomes have separated, nuclear envelope reforms and chromosomes decondense (Figure 3). Finally, last phase of the

cell cycle, cytokinesis, is characterized by division of the cell cytoplasm through formation of a contractile ring (Lodish, 2014) (Figure 3).

## 2.4 Microtubule structure, organisation and dynamics

MTs are ubiquitous cytoskeletal polymers essential for life of all eukaryotic cells. Although they are essential parts of many biological processes and structures, I will focus here on their role in mitotic spindle, as they are his fundamental components defining both its organisation and dynamics. Every microtubule is dynamic and polar polymer composed of 13 parallel, laterally associated protofilaments that form the hollow cylindrical structure with an outer diameter of 25 nm (Downing and Nogales, 1998) (Figure 4). Each protofilament is a string of  $\alpha\beta$ -tubulin heterodimers connected by non-covalent bonds and arranged in a head-to-tail configuration, with each subunit type repeating every 8 nm (Figure 4). As the subunits are oriented in a same way throughout whole protofilament, they have intrinsic polarity, and as all protofilaments within microtubule have the same polarity, whole microtubule has an overall polarity (Akhmanova and Steinmetz, 2008). By convention, the end with exposed  $\beta$ -subunit is called plus-end, while the end with exposed  $\alpha$ -subunit is the minus-end (Lodish et al., 2014) (Figure 4). Microtubule polarity is a crucial property important for spindle morphogenesis because, for example, microtubule-based motor proteins, including dynein and a large set of kinesin-like proteins, recognize the surface of MTs, read their polarity, and move their cargo accordingly (Wittmann et al., 2001). In addition, because of structural differences between subunits, that define two ends of MTs, growing and shrinking rates are much higher at the plus-end of microtubule (Akhmanova and Steinmetz, 2008). That follows to second important microtubule property important for spindle morphogenesis – dynamic instability. Dynamic instability is a process that describes microtubule fluctuation between slow growing and fast shrinking rates (Mitchison and Kirschner, 1984) (Figure 4).

To better understand dynamic instability, we must first understand the molecular characteristics of tubulin. Each tubulin subunit in a heterodimer can bind one molecule of nucleotide guanine triphosphate (GTP). While in the  $\alpha$ -subunit, GTP is never hydrolysed because it is trapped by the interface of the subunits, while the in  $\beta$ -subunit GTP can be hydrolysed and reversibly bind because GTP-binding site is at surface of the dimer (Figure 4) (Downing and Nogales, 1998). Transition from slow growing to fast shrinking is referred to as catastrophe, and transition from fast shrinking to slow growing as rescue (Figure 4). Moreover, MTs sometimes pause for a period of time, during which their length remains



constant. Soluble free tubulin subunits have a very slow rate of GTP hydrolysis but this rate increases after subunit becomes incorporated into protofilament (Desai and Mitchison, 1997). Moreover, nucleotide guanine diphosphate (GDP), which is a product of hydrolysis of GTP, does not exchange while  $\beta$ -tubulin remains in the polymer. So, each protofilament in a growing microtubule is composed mostly of GDP-bound  $\beta$ -tubulin subunits while only at the growing tip it is capped by one or two terminal heterodimers containing GTP-bound  $\beta$ -tubulin subunits. This part of growing end is called *GTP cap*. The whole model is after it called GTP-CAP model, developed by Mitchison and Kirschner in 1984 (Mitchison and Kirschner, 1984) (Figure 4). As GTP dissociates four times slower than GDP that causes GTP cap at plus-end to stabilize MTs (Howard and Hyman, 2009). The infrequent loss of such GTP cap would result in a microtubule catastrophe, whereas the reacquisition of such a cap by a polymerisation would result in a rescue. All these processes are carefully regulated by microtubule associated proteins (MAPs) of three classes: polymerases that promote growth, depolymerases that promote shrinking and microtubule plus-end tracking proteins that stabilize plus-ends (Howard and Hyman, 2009). The importance of the dynamic instability is realised from the fact that energy, released by GTP hydrolysis of the subunits behind the GTP cap, is stored as structural strain in microtubule lattice which can be released when the cap is lost. It is thought that this process is crucial for the movement of chromosomes during metaphase and anaphase (McIntosh et al., 2010).

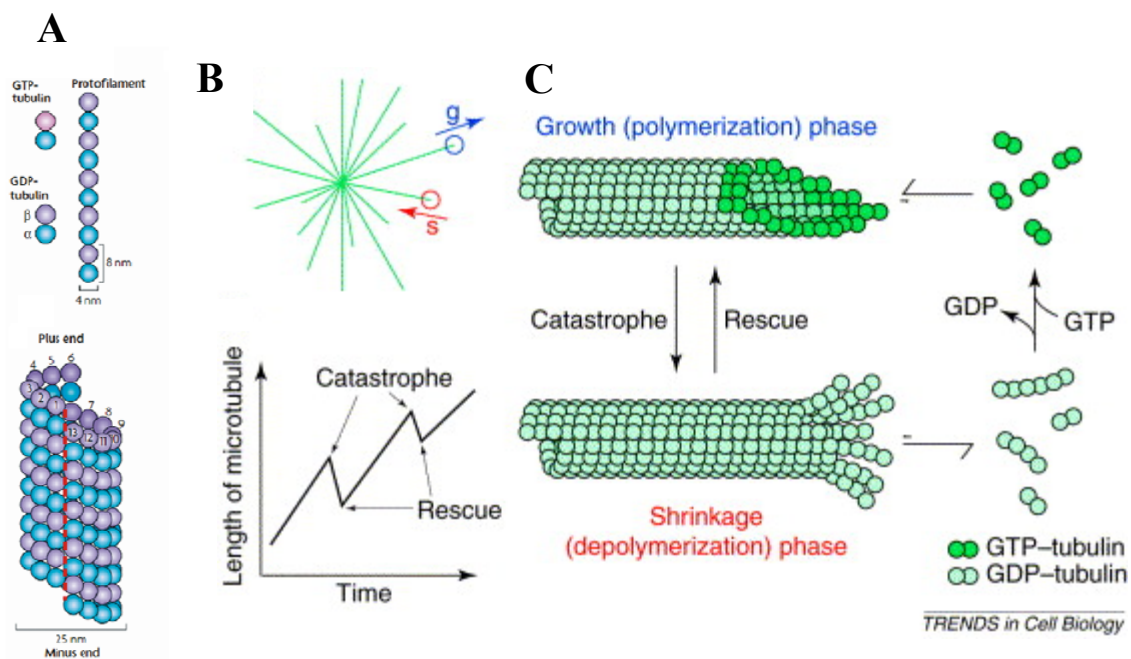


**Figure 4. Structure and dynamic instability of MTs.** (A) Structure of aligned polar microtubule protofilament with alpha and beta-tubulin heterodimer colour coded. The cylindrical and helical microtubule wall typically comprises 13 parallel protofilaments *in vivo*. (B) Dynamic instability of MTs within microtubule aster *in vitro* (top, s depicts shortening, and g growth). Microtubule length plotted as function of time (bottom). Assembly and disassembly each proceed at uniform rates but, as can be seen from different slopes of the lines, shortening of microtubule is much more rapid than growth. (C) Growing microtubule with blunter plus-end (top) had GTP- $\beta$ -tubulin cap whereas shrinking one with curved structure terminate in GDP- $\beta$ -tubulin (bottom). Microtubule dynamics, as can be seen, is higher at the plus-ends of MTs. Adapted Figure parts are from Kinoshita et al., 2002 and Akhmanova and Steinmetz, 2008.

All MTs are nucleated from structures known as microtubule-organizing centers (MTOCs) and spontaneous nucleation does not play a significant role in microtubule assembly *in vivo* (Wiese and Zheng, 2006). In animal cell, primary MTOC is called the centrosome and in most cases, minus-end of microtubule is located near the centrosome and plus-end radiates from it (McIntosh et al., 2012), although with possible exceptions. In interphase, centrosome is located near the nucleus producing interphase radial array of MTs (Lodish, 2014). Centrosomes are composed of a pair of orthogonally arranged cylindrical structures called centrioles, that are highly stable and surrounded by pericentriolar material (PCM) (Wiese and Zheng, 2006). Despite variations in morphology of centrosomes, all include in their PCM more than 50 copies of the  $\gamma$ -tubulin ring complex ( $\gamma$ TuRC), the conserved, essential core of the microtubule nucleating machinery. Every  $\gamma$ TuRC contains about 13 copies of the  $\gamma$ -isoform of tubulin and several associated proteins. This complex defines the position of MT nucleation, the polar orientation of the polymer, and the fiber into which tubulin assembles (McIntosh et al., 2012).

As I mentioned above, prerequisite for successful mitosis is the duplication of centrosomes, in coordination with replication of chromosomes in S phase (Figure 3). These duplicated centrosomes separate usually in prophase of mitosis and these will become two spindle poles of mitotic spindle (Godinho and Pellman, 2014). Interestingly, it has been noted that, at the beginning of mitosis, microtubule nucleation rate can increase about 5-fold compared with that of interphase cells. This can be explained by a process called centrosome maturation in which abrupt increase in centrosome-localized  $\gamma$ -tubulin at beginning of mitosis has been noticed (Piehl et al., 2004). In addition, dynamic behaviour of MTs increases

considerably in mitosis, mainly through increase in dynamic instability behaviour. This is accomplished by increased catastrophes (mainly through depolymerisation activity of kinesin-13 family of proteins) and fewer rescues (mainly through activity of stabilizing microtubule-associated proteins) (Lodish, 2014).

Recently, another pathway has been described for nucleation of MTs including the augmin complex, protein complex consisting of eight polypeptides that can bind to existing MTs, where it recruits  $\gamma$ TuRC that nucleate assembly of new MTs. It is one example of centrosome-independent microtubule formation in dividing cells (Hsia et al., 2014). It is believed that this complex is not essential for spindle formation, but in absence of this pathway, levels of spindle MTs are greatly reduced (Goshima et al., 2008).

## 2.5 Current models of microtubule populations within the spindle

Current models accompanying structure of animal spindle describe three distant populations of MTs within mitotic spindle: kinetochore, nonkinetochore and astral MTs (Figure 5) (Lodish, 2014). Although they all assemble from the same pool of tubulin subunits, they differ in their architecture, dynamics and role they play in mitotic spindle (Dumont and Mitchison, 2009).

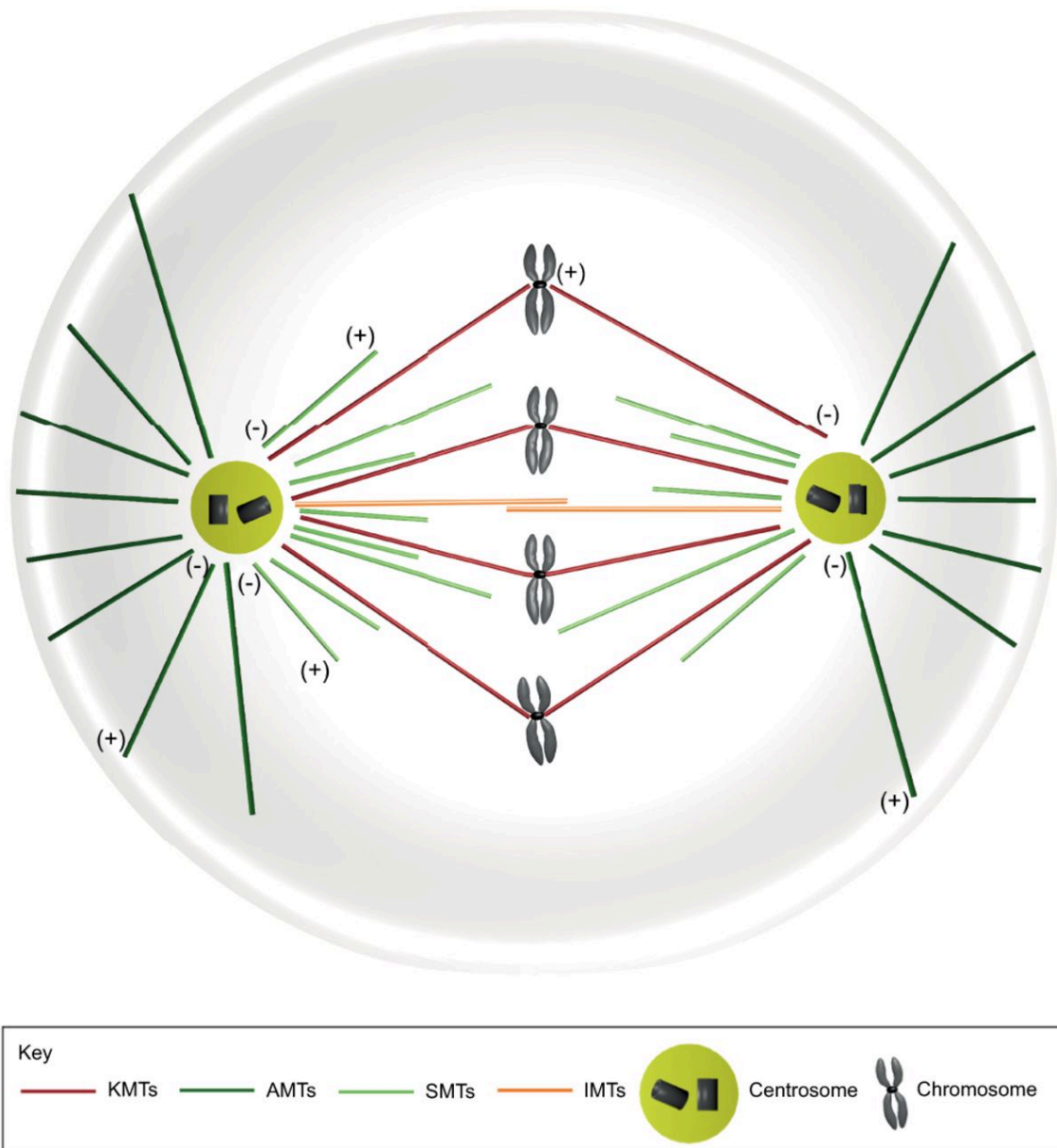


**Figure 5. Canonical view of mitotic spindle architecture in metaphase.** The bipolar metaphase spindle is nucleating MTs mainly from centrosomes (light green circles with two centrioles). MTs minus ends (-) are anchored at the centrosome while their plus-ends (+) are growing toward different sites within the dividing cell. Kinetochore MTs (KMT) are depicted in red, and are attached to chromosomes, via kinetochores (black), astral MTs are depicted in dark green and point towards the cell periphery. Interpolar MTs (SMTs) are depicted in light green when not in interaction with MTs from other pole and in orange when growing toward the spindle interior and interacting in the middle of the spindle with microtubule from other pole thus forming antiparallel overlaps. Taken from Muller-Reichert et al., 2018.

Kinetochore MTs (kMTs) have their plus-ends embedded in outer kinetochore layer and minus-ends at or near centrosomes (Figure 5). Main function of this population is to exert pulling forces on chromosomes at their kinetochores and they seem to be indispensable for proper spindle function, although some parts of mitosis to some degree, like congression of chromosomes to the equatorial plane of the spindle, can be accomplished without these MTs (Cai et al., 2009). As already described, they accomplish their tasks by exerting pulling forces on sister chromatids during metaphase and during anaphase they pull separated sister chromatids to different poles of the spindle when cohesin between chromatids is broken. They also silence the SAC, a special signalling system that is active on sister kinetochores when these are not attached to MTs and when kinetochores are not under sufficient tension (Dumont et al., 2012). Typical number of kMTs that bind to one kinetochore in mammalian cells is from 10-30, depending on cell type studied (McEwen et al., 1997, O'Toole et al., 2020). KMTs that are connected to the same kinetochore tend to assemble into a bundle called k-fiber, and most MTs within one fiber are continuous from kinetochore to the pole and run in parallel orientation. MTs within fiber are evenly spaced at 50-100 nm apart and interactions between them are weak along k-fiber, except near spindle poles where these interactions are strong (McDonald et al., 1992). Crosslinking proteins that have been shown to lock parallel microtubule together include kinesin-14 family members (Fink et al., 2009). Recently, using 3D electron microscopy, it was shown that k-fibers in human cells are connected by a complex network of MT connectors. This k-fiber mesh is made of linked multipolar connectors made primarily by TACC3 and associated proteins (Nixon et al., 2015). Thus, if k-fiber is perturbed using micromanipulation tools it behaves as single mechanical unit (Nicklas et al., 1982).

Origin of kMT has been described in previous section because origin of kMT reflects origin of spindle itself. These kMTs are not stationary tracks, as was once believed, yet they have a dynamical property named poleward flux. During poleward flux, polymerisation is occurring at plus-ends of MTs, where they are connected to kinetochore, and during steady-state such as metaphase, this is balanced by depolymerisation at minus-ends of MTs, located near spindle poles. Result of this process is the constant movement of kMT subunits to the pole (hence term poleward) at rate of  $0.5 \mu\text{m min}^{-1}$  (Rogers et al., 2005). It is perceived that flux can provide force that can perform work when steady state balancing at kMT polymerizing plus-end is suppressed (Waters et al., 1996).

Another population of MTs described in current models of mitotic spindle are astral MTs (aMTs). They are classically defined as MTs nucleated at centrosomes whose plus-ends

extend toward the cell cortex (Dumont and Mitchison, 2009) (Figure 5). Cell cortex is a network formed by actin filaments, organized into bundles especially abundant beneath the plasma membrane, that provides mechanical support, determines cell shape, and allows movement of the cell surface (Lodish et al., 2014). Astral MTs turnover by dynamic instability of their plus-ends, at growth and shrinkage rates that are very high when compared to other populations of MTs, about 10-15  $\mu\text{m min}^{-1}$ , but unlike other populations, they do not exhibit flux because their minus-ends do not depolymerize (Waterman-Storer et al., 1998). It is thought they perform the critical function of positioning the spindle with respect to the cell division plane by interacting with the cell cortex. There are many models that explain how this is achieved and one of them includes action of cytoplasmic dynein-dynactin complex associated with both cortex and astral microtubule and others include pulling action exerted by astral MTs tethered to spindle poles (Vukusic et al., 2019). In the dynein mechanism, this motor pulls astral MTs by walking to their minus-ends embedded in centrosome, thereby pulling the whole spindle with towards cortex (Lu and Johnston, 2013).

Last microtubule population within spindle are nonkinetochore or interpolar MTs (ipMTs or just polar MTs), which comprise a majority of MTs within large spindles such as vertebrate spindles (Lodish, 2014). They are defined as all MTs within the body of mitotic spindle that are not kMTs (Dumont and Mitchison, 2009) (Figure 5). Electron microscopy studies have revealed that ipMTs tend to bundle together in fibers just like k-fibers do, but each fiber typically contains 2-6 MTs, evenly spaced by 30-50 nm (Mastronarde et al., 1993) and anti-parallel bundling seems to be predominating, focusing primarily on region of spindle midzone (Figure 5). Their function in spindle is poorly understood and since they are numerous in spindle, it can be reasoned that our knowledge in this area is very limited. It is thought that their primary functions are to keep spindle pole apart through sliding between their antiparallel bundles by the action of molecular motors, to regulate spindle length and structure and to generate a force that moves poles apart during anaphase B (McIntosh et al., 2012). Their minus-ends are mostly located throughout whole spindle and seldom at spindle poles (O'Toole et al., 2020, Yu et al., 2019). Like kMTs, they also slide at an average rate of about 2  $\mu\text{m min}^{-1}$  (Vukusic et al., 2017), but it is unknown in human cells if this combination of sliding and fluxing is a synchronous process all the way to the poles (Yang et al., 2008). In PtK1 cells, the minus ends of interpolar MTs are found throughout the spindle (Mastronarde et al., 1993), while those of the kinetochore MTs are located mostly near the poles (McDonald et al., 1992). Interpolar MTs meet in the equatorial region of the spindle, where they form antiparallel overlaps (Brinkley and Cartwright, 1971). In addition, a substantial fraction of

non-kinetochore MTs end before they reach the spindle equator (McIntosh and Landis, 1971) and these have presumably free plus-ends and dynamic nature more similar to astral MTs. Furthermore, electron microscopy studies in multiple organisms (Brinkley and Cartwright, 1971; Jensen, 1982; Mastronarde et al., 1993; McDonald et al., 1992; McIntosh and Landis, 1971; Nixon et al., 2017; Ohi et al., 2003; Winey et al., 1995; Yu et al., 2019) have revealed that non-kinetochore MTs are often found in the vicinity of kinetochore MTs, which implies that MTs from these two groups may be physically linked (Tolić, 2017). It can be imagined that these connections may be very important for force transmission from force-generating sites, such as spindle midzone or kinetochores, to other sites within the spindle.

## 2.6 Emerging concept of bridging MTs

Our group have recently explored this exact relationship between interpolar and k-fibers during metaphase of human cells (Kajtez et al., 2016). By using fluorescence live-microscopy, we observed that a bundle of interpolar MTs follows a pair of k-fibers that are bound to sister kinetochores. This interpolar bundle looks like a bridge between sister k-fibers and we termed this structure a bridging fiber (Kajtez et al., 2016; Tolić and Pavin, 2016) (Figure 6). Moreover, we used laser ablation to sever a kinetochore fiber in HeLa, U2OS and PtK1 cells (Buda et al., 2017; Kajtez et al., 2016; Milas and Tolić, 2016), in approach similar to previous experiments (Elting et al., 2014; Sikirzhyski et al., 2014) and we reasoned that if strong connections exists between these two fibers, they will move together after the severing of one k-fiber. Indeed, we observed that the bridging fiber moved together with sister kinetochores, and their respective k-fibers, both perturbed and unperturbed (Kajtez et al., 2016). This outward movement, on the other hand, is a result of tension release which typifies k-fibers near kinetochores in metaphase spindles (Mcintosh and Dumont, 2009). All these structures moved as a single object away from the spindle (Kajtez et al., 2016), and later back towards the spindle, latter mechanism also described by others (Elting et al., 2014). Thus, the bridging fiber is strongly linked to its k-fibers, acting as a bridge between. Moreover, we proposed this microtubular combination is representing one functional module that is probably involved in chromosome segregation mechanisms (Tolić and Pavin, 2016). Severing of a kinetochore fiber at different locations revealed that the kinetochore fiber is laterally linked with the bridging fiber in a large region starting  $\sim 1 \mu\text{m}$  away from the kinetochore and extending towards the spindle pole (Kajtez et al., 2016; Milas and Tolić, 2016), although the end of this connections in term of location of bridging fiber minus ends is not known. In this

region, the kinetochore fiber and the bridging fiber separate (Figure 6), with a maximum distance between them of ~250 nm at the location of the kinetochore (Kajtez et al., 2016).

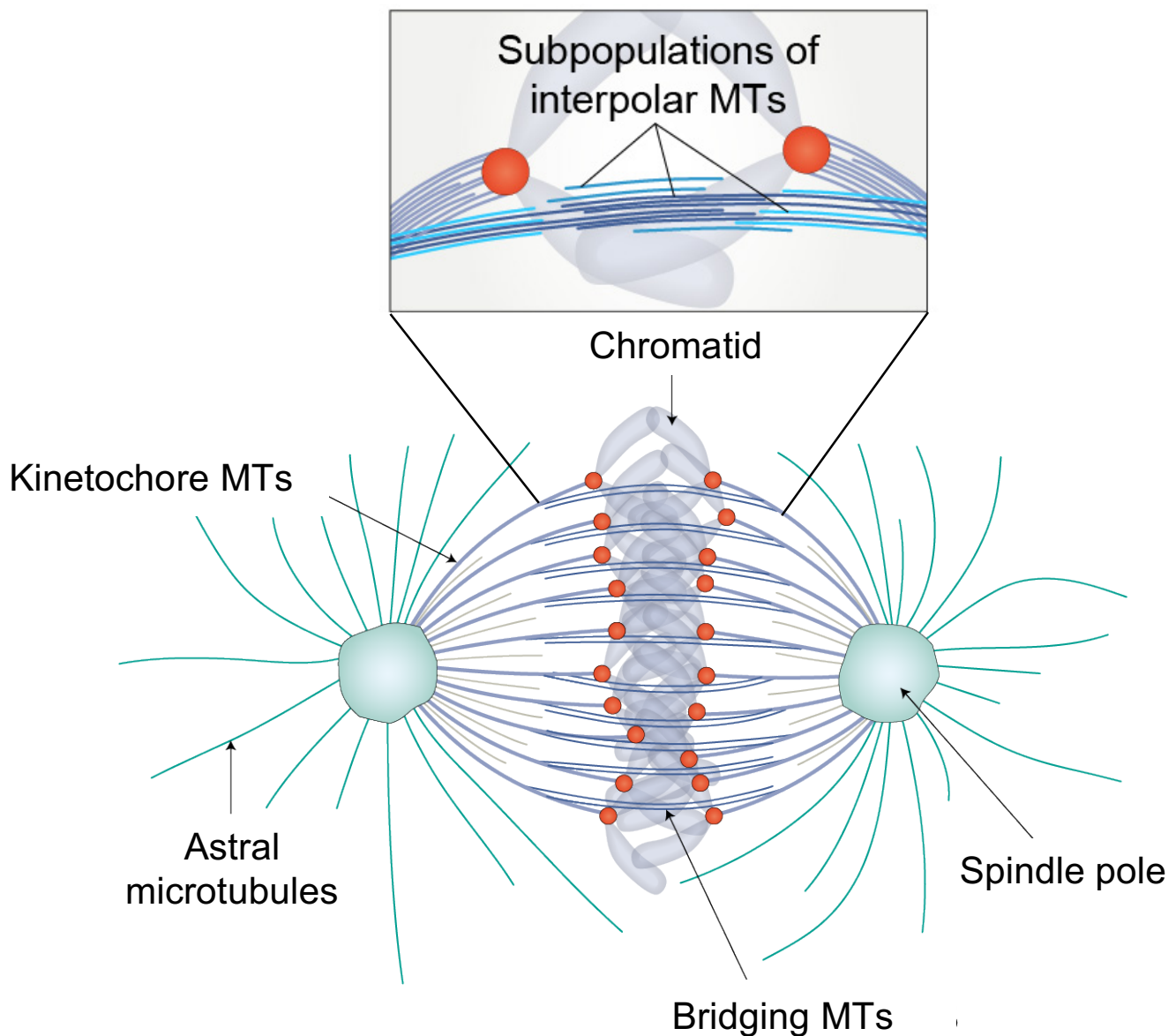


**Figure 6. Revised model of the mitotic spindle that includes bridging microtubules.** The spindle is composed of kinetochore microtubules (MTs) that are growing from the centrosome (here broadly defined as the region of spindle pole) to the kinetochores (red) connected with sister chromatids, astral MTs that are growing from the centrosome to the spindle periphery, and bridging MTs that are laterally linked with their respective kinetochore MTs into one mechanical unit and that make antiparallel overlap in the middle of the spindle. Free interpolar MTs are depicted in grey. Adapted from Vukušić et al., 2019.



Later, by comparing localization of the PRC1-labeled MT bundles in respect to kinetochores our group showed that more than 90% of PRC1 bundles are associated with a pair of sister kinetochores. Thus, almost all interpolar bundles in a metaphase spindle are bridging fibers (Polak et al., 2017). In other words, there are only few free overlap bundles in an unperturbed metaphase spindle that are not connected to k-fibers (Tolić, 2017). Interestingly, we also found that tension and compression coexist along the same kinetochore fiber (Kajtez et al., 2016). This mechanism resolved the old paradox of the simultaneous existence of tension and compression along a single kinetochore fiber (Dumont and Mitchison, 2009), showing that the compression in the bridging fiber balances the tension between sister kinetochores and the compression at the spindle poles. The kinetochore fiber is thus under tension in the region between the kinetochore and the junction points, and under compression along rest of its length, between the junction and the spindle pole, where lateral interaction between bridging fibers and k-fibers takes place (Tolić, 2018). However, it is not known if bridging MTs extend all the way to the poles, and recent EM studies do not support this notion (O'Toole et al., 2020), implying interconnections between bridging and f-fibers do not reach the poles. Also, one recent study reported that region where bridging MTs are located contains several MT sub-populations during early anaphase: dominant one includes MTs in close proximity to k-fibers that pass in between chromosomes and often bundle into antiparallel fibers, those that are located with both ends between chromosomes, and those that are contacting chromosomes with one end, while other end is located between chromosomes (Yu et al., 2019) (Figure 6).

## 2.7 Molecular motors as force-generators in mitosis

Highly purified tubulin heterodimers can assemble *in vitro* into MTs, but fast assembly and consequent formation of complex structures requires presence of microtubule-associated proteins (MAPs). Although, MAPs are very broad term that has recently been applied to any protein that can associate, directly or indirectly, to MTs *in vivo* or *in vitro* (Fisher et al., 2008) we can divide them into four groups. The first group consists of crosslinking side-binding proteins that stabilize and align MTs in specific structures. The second group of plus-end tracking proteins (+TIPs) either regulate MT growth at plus-end or link plus-ends to the other cellular structures. The third group consists of enzymes that regulate MT destabilisation and the fourth of motor proteins that move along MTs powered by chemical energy (Lodish, 2014). As can be seen from the previous sections where different

MAPs where mentioned, they are essential in control of MT dynamics and generation of forces that are needed for spindle assembly and proper function of the whole spindle.

Force production in mitotic spindle can be divided into active and passive force production. Active force production is defined by processes that convert chemical energy from ATP or GTP hydrolysis into mechanical work (Dumont and Mitchison, 2009). Two main active force production mechanisms are polymerisation dynamics of MTs and ATPase motor activity. Passive forces are defined by energy consumption that was put into system by one of the active processes. Two main passive spindle forces are elastic contraction and friction and they are often underappreciated in mitotic studies because they are poorly understood (Dumont and Mitchison, 2009).

Molecular motors are a group of proteins that can be broadly described as ATPase enzymes, which bind and catalyse the hydrolysis of ATP into ADP and a free phosphate ion (Barton and Goldstein, 1996). They couple chemical energy released during ATP hydrolysis to reversible conformational changes in their motor domain(s) to do mechanical work. It is this mechanochemically driven cycling between different conformational states that causes motor proteins to alternate between bound and unbound states allowing them to 'walk' along MTs (Lodish et al., 2014). Almost all of them have a motor domain conserved within one family or more motor domains at opposite sides that bind and hydrolyse ATP to walk along more than one track (Figure 7). Besides, they can also have some class-specific nonmotor domains, such as binding domain responsible for binding of their cargo molecules, some domains involved in dimerization and usually some domains involved in the propagation of the structural change (Gatlin and Bloom, 2010) (Figure 7). Their motion along MT in given circumstances is always unidirectional regarding mean direction of movement, and is connected to intrinsic polarity of MTs described above. So, some of these proteins are said to walk toward plus- and some toward a minus-end of MTs (Lodish et al., 2014). It is this direction of movement that determines the function of each motor protein in spindle assembly and maintenance. Every 'walking' motor has characteristic size of its step, characteristic rate of moving along MT and characteristic processivity which can be defined as a number of steps motor can do without dissociating from MT (Rath and Kozielski, 2012).

Family members (alias) [orthologues]	Directionality and properties	Structural organization		Length (nm)																	
		0	25		50	75	100	125	150	175	200										
<b>Kinesin-6</b> for example, KIF23 (MKLP1) and KIF20A (MKLP2) [ZEN-4 and Pavarotti]	<ul style="list-style-type: none"> <li>• Plus end</li> <li>• Non-processive</li> <li>• Oligomerizes</li> <li>• Crosslinks</li> </ul>	Motor domain	Predicted coiled-coil	Globular domain																	
<b>Kinesin-12</b> for example, KIF15 (hKLP2) [xklp2]	<ul style="list-style-type: none"> <li>• Plus end</li> <li>• Crosslinks with TPX2</li> </ul>																				
<b>Kinesin-7</b> for example, KIF10 (CENP-E) [CENP-meta and CENP-ana]	<ul style="list-style-type: none"> <li>• Plus end</li> <li>• Processive</li> <li>• <math>F_{stall} \approx -6</math> pN</li> </ul>																			Kinetochores-binding site Microtubule-binding site	
<b>Kinesin-5</b> KIF11 in humans (EG5) [Cin8, Klp61F and Cut7]	<ul style="list-style-type: none"> <li>• Plus and minus ends</li> <li>• Poor processivity</li> <li>• <math>F_{stall} \approx -4</math> pN</li> <li>• Tetrameric crosslinker</li> </ul>																				
<b>Kinesin-14</b> KIFC1 in mammals (HSET) [Ncd, Kar3, Klp2 and xctk2]	<ul style="list-style-type: none"> <li>• Minus end</li> <li>• Non-processive</li> <li>• Dimeric crosslinker</li> </ul>																				
<b>Kinesin-8</b> for example, KIF18A [Kip3, Klp5, Klp6 and Klp67a]	<ul style="list-style-type: none"> <li>• Plus end</li> <li>• Processive</li> <li>• <math>F_{stall} \approx -1</math> pN</li> <li>• Dampens microtubule dynamics</li> </ul>																				
<b>Kinesin-4</b> for example, KIF4 in mammals [xKlp1 and Klp3a]	<ul style="list-style-type: none"> <li>• Plus end</li> </ul>																				
<b>Kinesin-10</b> for example, KIF22 (KID) [Nod]	<ul style="list-style-type: none"> <li>• Plus end</li> <li>• Non-processive (some non-motile)</li> <li>• Dampens microtubule dynamics</li> </ul>																				
<b>Kinesin-13</b> for example, KIF2A, KIF2B and KIF2C in humans (MCAK) [xkcm1, Klp59C and Klp10A]	<ul style="list-style-type: none"> <li>• Non-motile</li> <li>• Microtubule depolymerase (minus and plus ends)</li> </ul>																				

**Figure 7. Mitotic kinesin motors.** Representation of mitotic kinesins in human cells with list of various nomenclatures used, alternative names and orthologues from other organisms together with directionality information, note about important properties and structural organization illustrations with the main domains depicted. See details through the text. Taken from Cross and McAinsh, 2014.

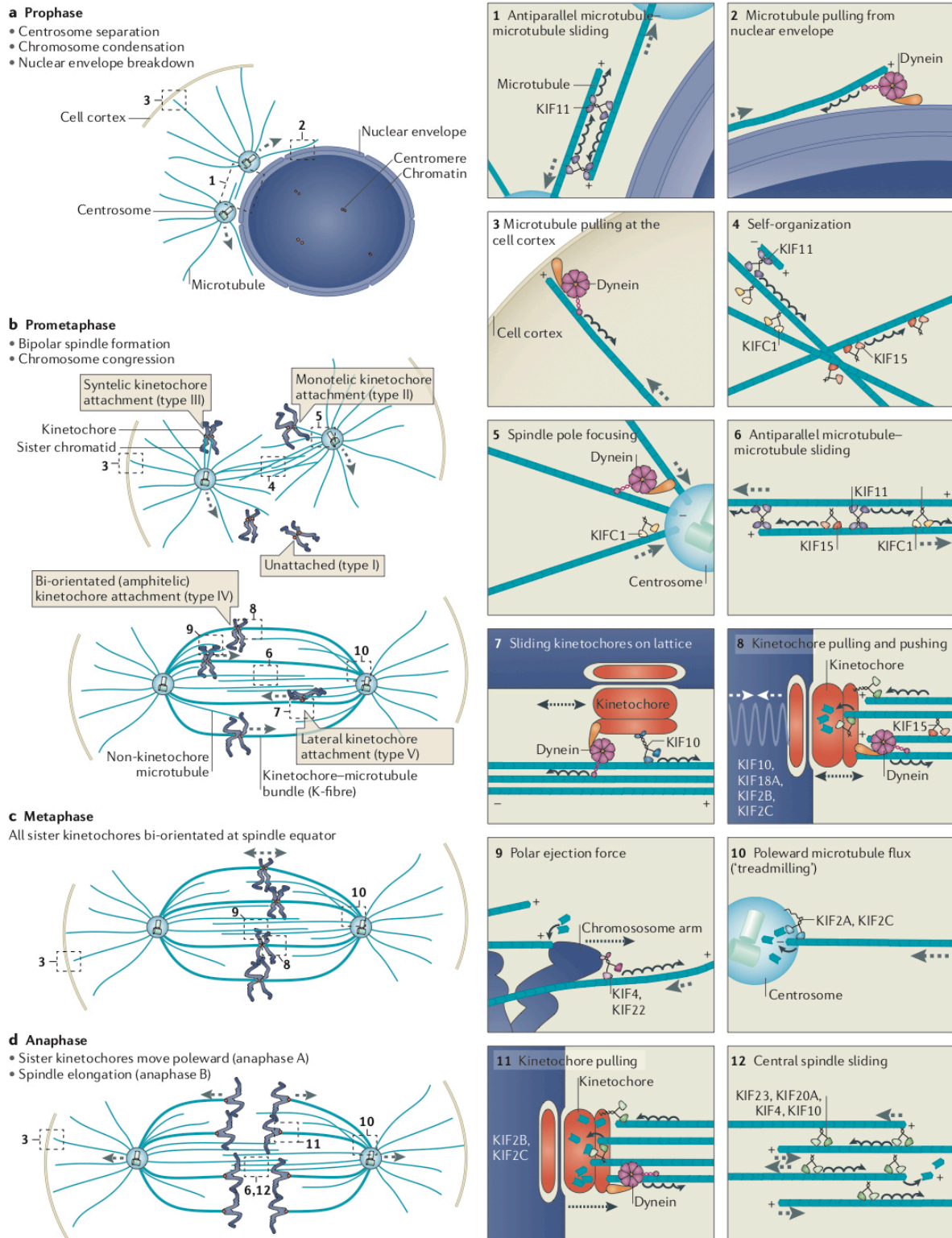


**Figure 8. Functional roles of motor proteins in mitosis of human cell.** Proposed involvement of multiple mitotic motors in the key mitotic processes noted on the left with some key mechanisms distinguished and numbered on the right incorporating all stages of mitosis. See details through the text. Taken from Cross and McAinsh, 2014.

The major plus-end directed motor in the mitotic spindle is the kinesin-5 member Kif11, a bipolar homotetramer complex with four heavy chains forming two motor domains that are capable of binding and cross-linking two MTs (Waitzman and Rice, 2014) (Figures 7 and 8). It moves along MTs at rates of  $0.1\text{-}0.01\text{ mm s}^{-1}$ , characteristic of mitotic motility in general, while these are almost 10-fold slower than those characterizing intracellular transport motors, such as kinesin-1 (Peterman and Scholey, 2009). Kif11, due to orientation of its motor domains, preferentially binds to antiparallel MTs and then slides them by walking to their plus-ends (Figures 7 and 8). Result of such motion is aligning of plus-ends of antiparallel MTs and pushing apart of their minus-ends (anti-parallel sliding filament mechanism) (McIntosh et al., 1969). Its main antagonist in sliding antiparallel MTs is a motor of opposite directionality such as minus-end directed motor protein kinesin-14 (for example KifC1 in humans) (Figure 8). This motor protein slides the minus-ends closer to each other while it pushes the plus-ends apart. This motor functional antagonism is an important mechanism of establishment of initial spindle bipolarity and possibly regulation of spindle length (Cross and McAinsh, 2014). In addition, it is important to note that activity of these antagonistic motors is changing as mitosis progresses. Following initial dominance of plus-end directed motors, at metaphase steady state is achieved where action of plus-end directed motor proteins is balanced by activity of minus-end directed proteins (van Heesbeen et al., 2014).

Although Kif11 is critical to establishment of mitotic spindle bipolarity by centrosome separation it is not required to maintain this bipolarity in all systems. It has been shown that kinesin-12 plus-end directed protein, Kif15 in humans, can have a redundant role with Eg5 in maintaining this bipolarity, probably by sliding parallel MTs apart (Drechsler et al., 2014) (Figures 7 and 8). Interestingly, one recent study reported that coordination between plus-end directed Eg5, Kif15, and minus-end directed dynein motor, controls proper spindle assembly, demonstrating the importance of a proper force balance in mitotic spindle. Hence, when excessive inward forces are present, monopolar spindles are formed; and when excessive outward forces are present, spindle poles splay (van Heesbeen et al., 2014). It would be interesting to explore how these mechanisms of spindle length maintenance during prometaphase and metaphase are connected with those in anaphase where spindle extensively elongates, since location and motor function of some candidates, mentioned as important in metaphase spindle length regulation, such as dynein, drastically change at transition from metaphase to anaphase in human cells (Goshima and Scholey, 2010).

Besides already mentioned kinesin-14, the dominant minus-end-directed motor in the mitotic spindle is the cytoplasmic dynein (Figure 8). These motors have the same overall organisation, they have two motor domains on one side and nucleotide-insensitive MT-binding tail domain on other. As we said before, by binding two antiparallel MTs, minus-end movements of these motors directly function to oppose the MT motion of kinesin-5s (She and Yang, 2017). These proteins have one interesting feature; they can bind one MT as a cargo and transport it toward the minus-end of another MT, thereby clustering the minus-ends of MTs together. This process constitutes the basis of slide-and-cluster mechanism of spindle length maintenance (Figure 8). These motors therefore have a main role in focusing MTs into a united pole, function obviously very important to maintain bipolar shape of the spindle (Civelekoglu-Scholey and Scholey, 2010). In addition to its role in organizing MTs in spindle, dynein can also bind different cargoes and transport them to minus-ends of MTs, located mainly at spindle poles. These cargoes can be special protein regulators of spindle assembly and maintenance; such is NuMa, which stabilizes the pole structure, or different motor proteins, mainly kinesins, who are transported from the plus-ends of MTs towards the minus-ends (Goshima and Scholey, 2010).

Lastly, a large number of motor proteins has been identified that bind not only to MTs but also to chromosome arms. Most important of them are called chromokinesins and these are involved in generation of so called polar ejection force (Rieder and Salmon, 1994), one of the mechanisms for force production on chromosomes (Figure 8). Chromokinesins are also involved to different degree in some other processes including chromosome segregation, spindle organisation and cytokinesis (Mazumdar and Misteli, 2005). Two members of these groups are plus-end directed Kid/kinesin-10 and kinesin-4 family members KIF4A and KIF4B, which have conserved motor domains but differ in organisation of other domains (Figure 7). Polar ejection force is one of the forces that acts on kinetochores during metaphase (others are poleward flux of k-fiber MTs and forces exerted through dynamic connections between kinetochores and MTs described above) presumably to prevent premature movement of chromosomes toward the poles (Figure 8) (Su et al., 2016). Kinesin-4 and kinesin-10 bind chromosome arms and interact with MTs emanating from centrosomes and in doing so they push chromosomes towards a MT plus-end and thus toward a metaphase plane (Mazumdar and Misteli, 2005) (Figure 8).

Besides motor proteins involved in transportation of MTs and other cargo in the spindle, there are many classes of MAPs involved in MT destabilisation, MT stabilisation or just binding of MTs.

Proteins involved in MT destabilisation are very important because they disassemble the interphase array of MTs in prophase and thus provide substrates for formation of all populations of spindle MTs. In addition, by affecting the lifetime of MTs they can influence the spindle size and organisation in processes such as chromosome attachment, MT flux or overall MT density and length (Helmke et al., 2013). To date, three major classes of this group of proteins have been described: destabilizing kinesin family members (kinesin-13 primarily but also kinesin-14 and kinesin-8 family members), MT-severing enzymes of the AAA ATPase family (like Katanin, Spastin, Fidgetin), and tubulin dimer-sequestering proteins (like OP18/Stathmin, RB3) (Helmke et al., 2013). Some of these proteins, like kinesins-13 are well known regulators of poleward MT flux, mechanism of force release important for chromosome positioning, in which they regulate depolymerisation at MT minus-ends (Figure 8).

In MT-stabilizing group, strictly speaking, we can include nucleation proteins, but these were analysed before, so I will not discuss them. Other MT stabilizing proteins include for example HURP, XMAP215/chTOG, Patronin, and MCRS proteins that are grouped by mechanism that they use to ensure stability of MTs. First group seems to form protofilament interactions that can stabilize tubulin heterodimers and protofilaments (HURP), second can increase growth rate of primarily ipMTs by interacting with plus-ends (XMAP215/chTOG) and third can reduce catastrophe frequency by interacting with plus- or minus-ends (Patronin, MCRS and EB proteins) (Lodish, 2014). The two latter groups, because they bind or 'track' plus-ends, are historically known as +TIPS (plus-end tracking proteins). All these stabilizing proteins are mediating establishment and maintenance of spindle architecture in general (Helmke et al., 2013).

## 2.8 Regulation of molecular motors

Many mitotic kinesins are regulated through temporal synthesis and degradation ensuring that protein is only present when needed during mitosis (Yount et al., 2015) (Figure 9). For example, binding of one or more mitosis-specific transcription factors, such as FOXM1, can promote expression of many cell cycle regulated genes at the G2/M transition (Alvarez-Fernandez and Medema, 2013). The levels of kinesin proteins are also controlled by their regulated destruction at the end of mitosis. Several kinesins contain destruction box (D-box) or KEN box sequences that are targeted by APCCdc20 and by APCCdh1, which are



ubiquitin ligases that tag proteins for destruction at the metaphase-to-anaphase transition and during early G1, respectively (Yount et al., 2015).

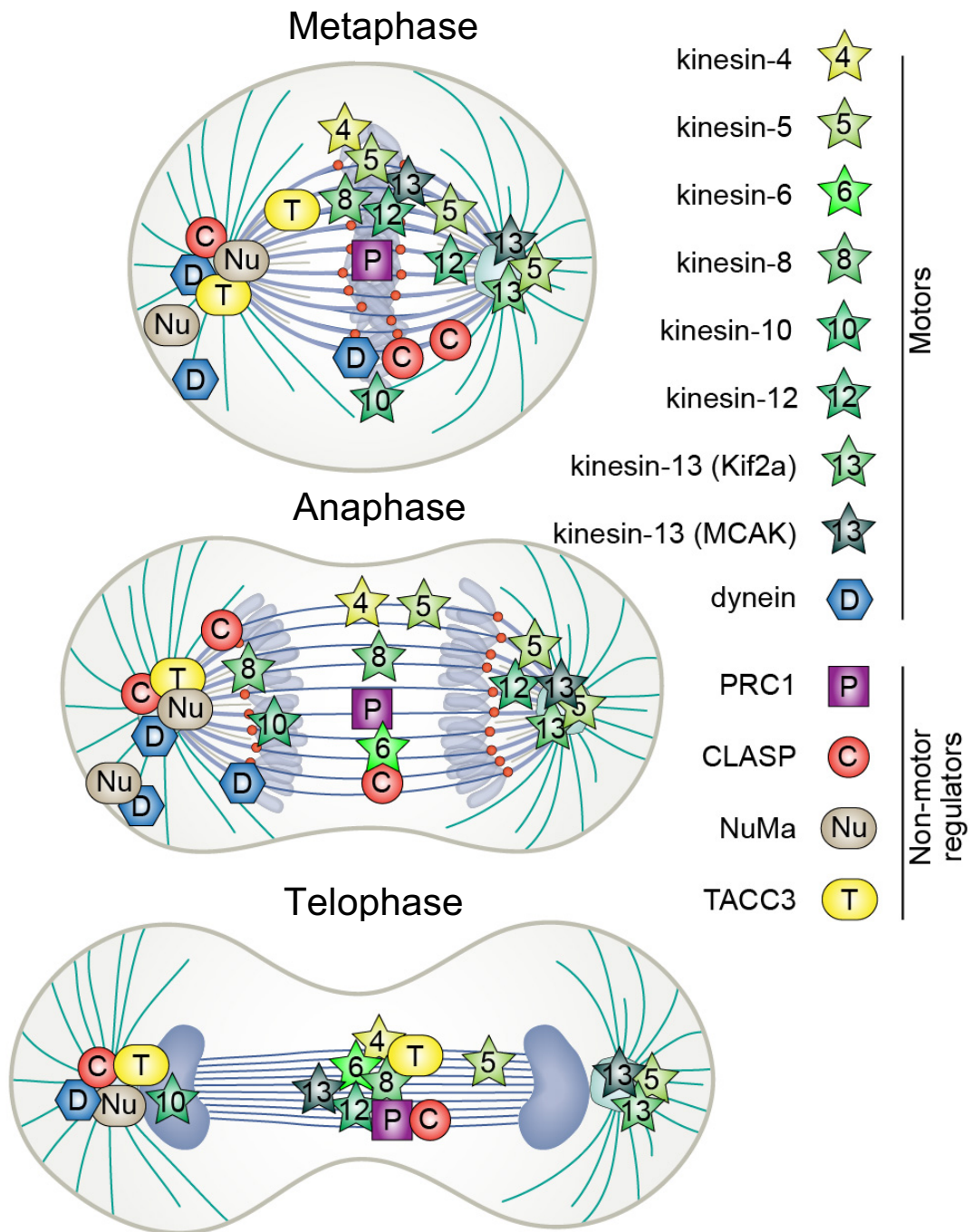


**Figure 9. Localization of molecular anaphase players during different stages of mitosis**  
Schemes of metaphase, anaphase and telophase cell showing the localization of motor and non-motor regulators of anaphase A and B mentioned throughout the thesis with legend on the right.



In addition to cell cycle temporal control, some motors act only at specific time during mitosis (Figure 9), and there are multiple cellular mechanisms that contribute to this type of motor regulation. The most notable examples are regulations of motor activity by modulating specific protein-protein interactions or control of the catalytic activity of the motor itself. These mechanisms often act through the action of mitotic kinases, such as Aurora A and B, Plk1, and Cdk1, which phosphorylate multiple kinesins to regulate their specific localizations and activities in the spindle (Yount et al., 2015). The localization of mitotic kinesins can be diverse as their functions, but the two are interconnected because kinesins must be localized properly to complete their proper functions. Kinesins accomplish this task by directly binding to subsets of MTs, to kinetochores, or to chromosomes (Figure 9). The affinities for specific localizations within the spindle are precisely controlled through gradients, intermolecular interactions with other proteins, and phosphorylation or other post-translational modifications (Yount et al., 2015).

On the other hand, post-translational modifications of tubulin itself could also impact localization and activity of mitotic proteins that are in direct contact with MTs on which they move. In that regard, a recent study showed that tyronisanated or detyronized states of tubulin, which are not evenly distributed on various populations of MTs within the spindle, can impact localization and activity of kinesin-7 CENP-E motor in human cells (Barisic et al., 2015). In that way, post-translational modifications of tubulin could serve as a navigational track system for movement of various molecular motors, defining exclusive zones for localisation or enhancing protein activity on particular locations within the spindle.

## 2.9 Anaphase in general

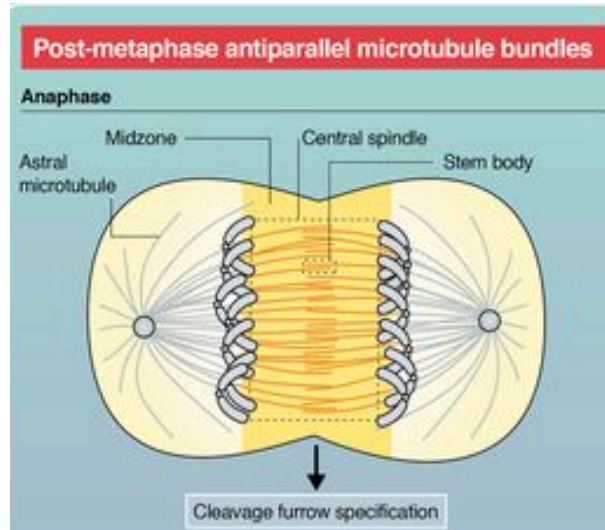
Anaphase, as part of the mitosis, is one of the most spectacular moments of the cell cycle, when coordinated splitting of replicated chromosomes and segregation of sister chromatids occurs. During anaphase, lagging chromosomes appear only rarely in human cells (Worrall et al., 2018), indicating the robustness of mechanisms acting during this phase.

Chromosome separation is accomplished, like all stages of mitosis before it, by the spindle, a structure composed of MTs and accompanying proteins, which self-assembles at the onset of mitosis (Pavin and Tolić, 2016), as described earlier. Anaphase starts when all chromosomes are bi-oriented, with sister kinetochores attached to MTs extending from opposite spindle poles and the spindle assembly checkpoint being satisfied (Joglekar, 2016).

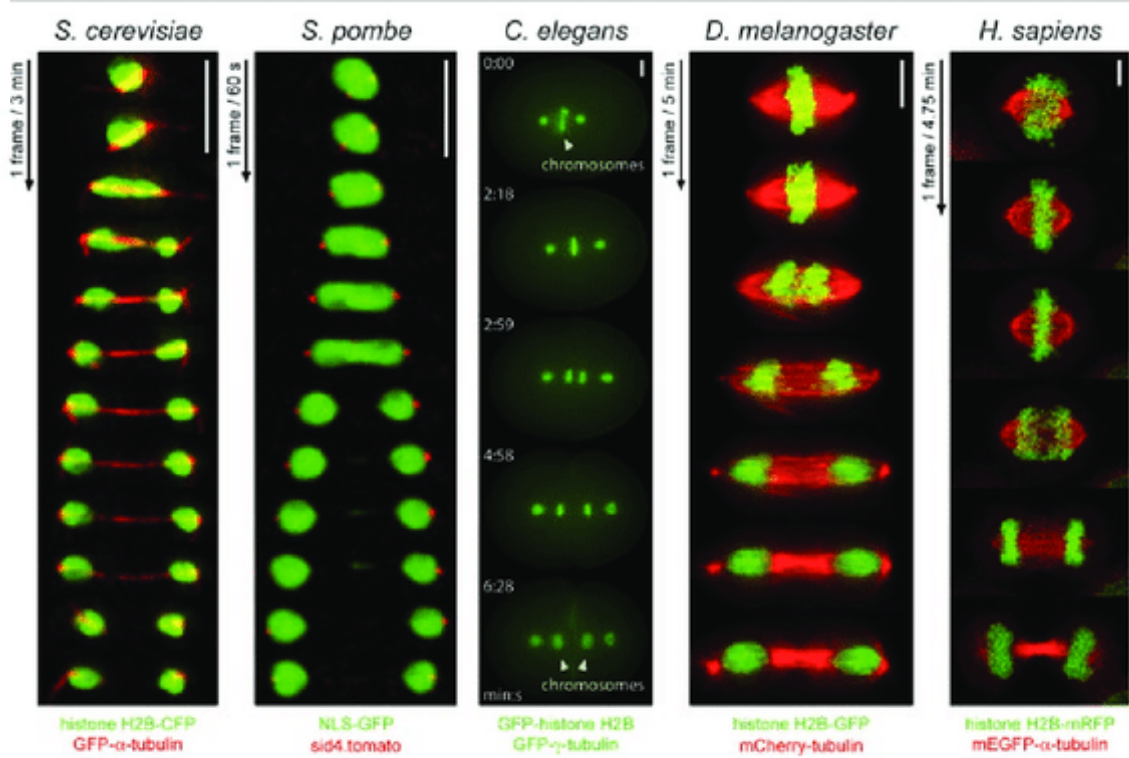
Subsequently, chromosome segregation initiates with proteolytic severing of cohesin links between sister chromatids (Hauf et al., 2001), accompanied by global protein dephosphorylation (Wurzenberger and Gerlich, 2011). This is accomplished by gradual inactivation of cyclin-dependent kinase 1 (CDK1) and increased activity of phosphatases reducing metaphase anti-poleward forces, which allows chromosomes to display net motion towards the spindle poles (Su et al., 2016).

The anaphase spindle is, similarly to metaphase spindle, composed of different populations of MTs, defined according to their structure, dynamics and function: kinetochore MTs, which connect kinetochores with the spindle poles, and non-kinetochore MTs (Vukusic et al., 2019). Kinetochore MTs form parallel bundles known as k-fibers. The main non-kinetochore MTs are interpolar MTs, which extend from the opposite sides to the center of the spindle forming an antiparallel bundle, and astral MTs, which grow from the spindle poles towards the cell cortex (Vukusic et al., 2019). In human cell lines, interpolar MT bundles interact laterally with sister k-fibers acting as a bridge between them and are thus termed bridging fibers (Kajtez et al., 2016, Polak et al., 2017). The accompanying anaphase proteins that are associated with spindle MTs or chromatin during anaphase can be divided into several classes – molecular motors from the kinesin and dynein families that convert chemical energy stored into ATP to do mechanical work, non-motor MT-associated proteins that crosslink, bundle or focus spindle MTs, various regulators of MT dynamics and global protein regulators, such as kinases (Civelekoglu-Scholey and Scholey, 2010; Cross and McAinsh, 2014; Raaijmakers and Medema, 2014; Verhey and Hammond, 2009).

A



B



C

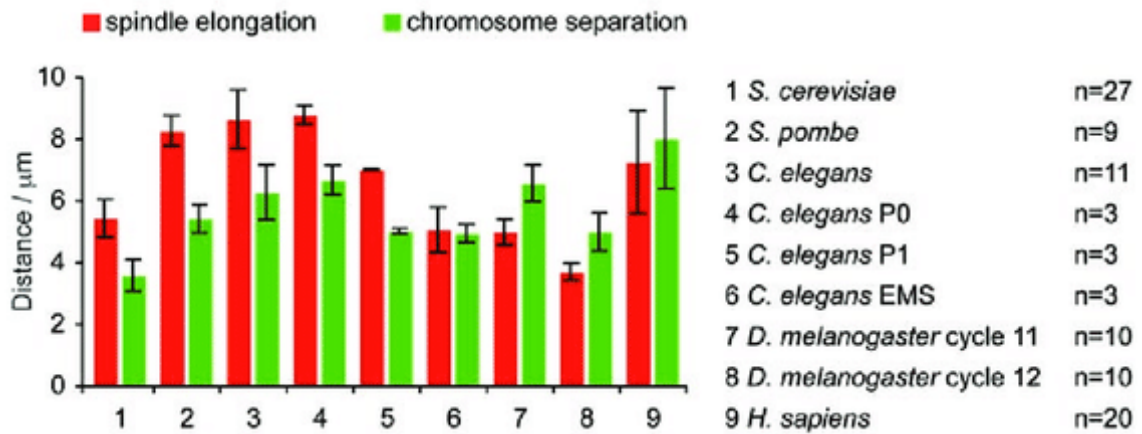


**Figure 10. Structure of the anaphase spindle and contribution of spindle elongation to chromosome segregation in various organisms.** (A) Structure of the anaphase spindle in human cells with main components noted. Taken from Lee et al., 2012. (B) Fluorescent live images of anaphase in different model systems. Representative time-lapse sequences are shown with MTs or spindle poles in red and chromosomes or nucleoplasm (*S. pombe*) in green. Scale bars are 5  $\mu\text{m}$ . (C) Contribution of anaphase A and B to chromosome segregation. Spindle elongation (measured as increase in spindle length by the end of anaphase, red bars) and chromosome separation (measured as increase in inner interchromosomal distance during anaphase, green bars) were measured in time-lapse sequences from A. Mean  $\pm$  SD values are shown. When spindle elongation is less than chromosome separation, anaphase A is the major contributor. If spindle elongation exceeds chromosome separation, anaphase B is more important. Taken from Roostalu et al., 2010.

Chromosome segregation is commonly described in two overlapping phases: anaphase A, where chromosomes move poleward, and anaphase B, where the spindle elongates (Asbury, 2017; Scholey et al., 2016) (Figures 10 and 11). Anaphase A and B were distinguished in pioneering experiments by Hans Ris on grasshopper spermatocytes where chloral hydrate stopped only anaphase B (Ris, 1949), and later on human somatic cells where inhibition of Polo-like kinase 1 (PLK1) also blocked only anaphase B (Brennan et al., 2007), suggesting distinct molecular mechanisms. Interestingly, the relative contribution of these two processes to chromosome segregation varies among organisms (Roostalu et al., 2010) (Figure 10). For example, one-cell stage *Caenorhabditis elegans* embryos display no anaphase A (Oegema et al., 2001) and in yeast spindles anaphase A does not significantly contribute to chromosome segregation (Mallavarapu et al., 1999; Straight et al., 1998), whereas *Xenopus* meiotic extract spindles rely entirely on anaphase A, lacking anaphase B (Desai et al., 1998). In human cells, both phases seem to be equally important contributors to chromosome segregation (Vukusic et al., 2017) (Figure 11). Although the process of anaphase has been well studied for decades, the mechanisms driving anaphase are still under debate, especially in human cells (Asbury, 2017; Maiato and Lince-Faria, 2010; McIntosh et al., 2012; Scholey et al., 2016).

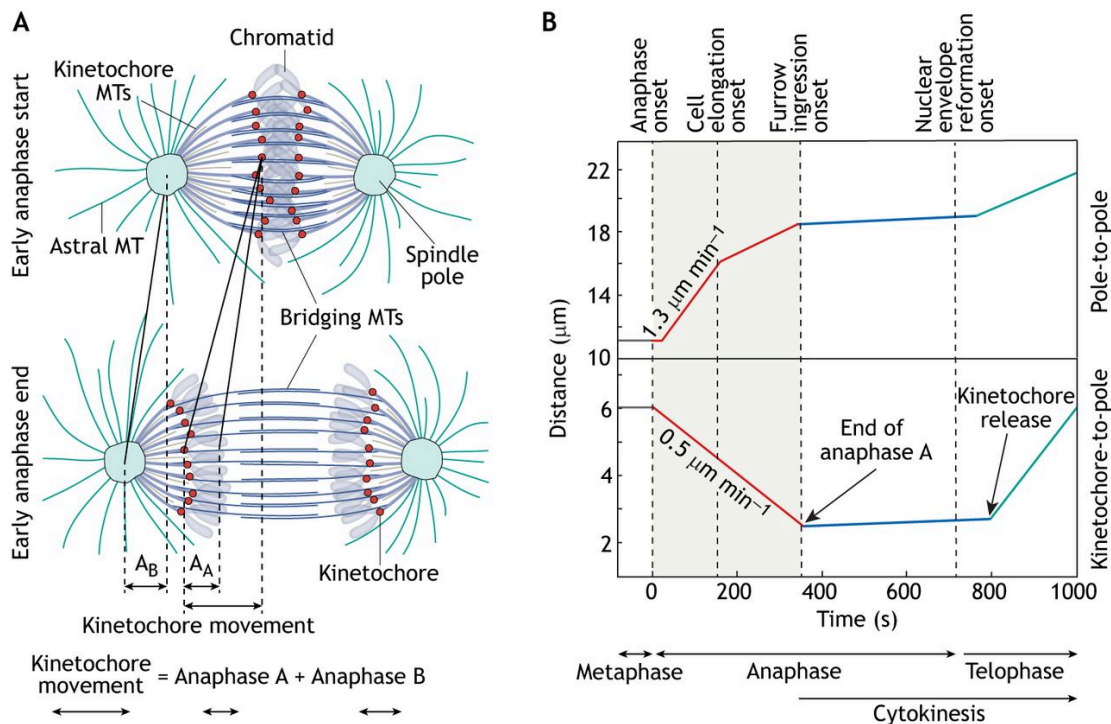


**Figure 11. An overview of anaphase spindle structures and dynamics.** (A) Anaphase A and B ( $A_A$  and  $A_B$ ) contribute roughly equally to kinetochore movement. Different spindle structures and microtubule (MT) populations are depicted. (B) Spindle elongation (top graph) and kinetochore poleward movement (bottom graph) are characterized by phases with different velocity regimes (color-coding). Chromosomes segregate mostly during early anaphase (0 to 360 s, shaded area). Onset of specific events that define the transition events between phases is noted. Taken from Vukusic et al., 2019.

## 2.10 Quantitative description of anaphase

Anaphase is marked by distinctive events regarding mainly poleward movement and spindle elongation (Figure 11). Poleward movement of kinetochores (anaphase A), in typical human cell, starts at an average kinetochore-to-pole distance of around  $6 \mu\text{m}$  (Su et al., 2016; Vukusic et al., 2017). The average poleward velocity is around  $0.5 \mu\text{m/min}$  during the first phase, which is almost linear and lasts for 6 minutes (Su et al., 2016; Vukusic et al., 2017) (Figure 11). Neighbouring chromosomes during this phase can move in different directions, both poleward and anti-poleward and these switches occur at different rates for individual chromosomes (Stumpff et al., 2008; Su et al., 2016), arguing that kinetochores in anaphase move individually, not as a group. Afterwards, anaphase A movement stops and the poleward

motion enters the stationary phase at a distance of around 3  $\mu\text{m}$  between kinetochores and spindle poles. At the transition from anaphase to telophase, around 13 min after anaphase onset, the distance between kinetochores and poles increases suddenly and synchronously, indicating kinetochore-MT detachment (Su et al., 2016) (Figure 11).

Spindle elongation (anaphase B) initiates shortly after anaphase onset (Su et al., 2016) and occurs in four distinct phases: an initial fast and linear spindle pole separation phase until 3 min after anaphase onset at a velocity of around 1.3  $\mu\text{m}/\text{min}$  (Vukusic et al., 2017); a second, somewhat slower phase that coincides with start of cell elongation; a third, almost stationary phase that lasts approximately 13 min from anaphase onset; and a fourth phase with an increase in velocity that coincides with kinetochore release from MTs (Afonso et al., 2014) (Figure 11). In parallel, the onset of cytokinesis in human cells is marked by the initiation of a furrow, which takes place around 6-8 minutes after anaphase onset (Janisch et al., 2018) (Figure 11). The first three phases of spindle elongation are commonly considered as anaphase B, whereas the fourth phase happens after nuclear reformation in telophase and is sometimes referred to as anaphase C (McIntosh, 1994). At the end of anaphase, tubulin is excluded from the new-born nuclei and Lamin B accumulates around the same structure, which marks nuclear envelope reformation and defines the onset of telophase (Afonso et al., 2014) (Figure 11). Since the chromosomes segregate the most during the first, almost linear phase of anaphase A that coincides with first two phases of anaphase B (Figure 11), this thesis will mainly focus on the events taking place during these time intervals and I will refer to them as early anaphase.

## 2.11 Spindle mechanics during anaphase A

The most important structures for anaphase A movement are k-fibers, whose kinetochore-attached MTs drive poleward movement of chromosomes (Maiato and Lince-Faria, 2010) (Figure 12). Early ground-breaking experiments in different organisms demonstrated that when the kinetochore of a single chromosome is damaged and its connection to k-fibers is severed, the movement of the rest of the chromosome stops; conversely, if chromosome arms are ablated, the movement is not affected (McNeill and Berns, 1981; Uretz et al., 1954). These experiments showed that chromosome connection to k-fiber is crucial for its poleward movement whereas chromosome arms are mainly passive players during this process. Movement of chromosomes is coupled to either growth or

shortening of the fibers to which they are attached (Cimini et al., 2004); the shortening of k-fibers seems to drag chromosomes poleward, one of the most conserved and fundamental features of mitosis (Asbury, 2017). In accordance, the induction of MT depolymerization by cold, colchicine or high pressure *in vivo* can generate the force able to induce or accelerate the rate of poleward movement of chromosomes (Inoue, 1952; Inoue and Ritter, 1975; Salmon et al., 1976). Furthermore, some studies reported that a rate of poleward movement was dependent on a rate of MTs depolymerisation itself, suggesting that depolymerization is a direct force producer or a main rate-limiting step in anaphase A.







particles close to the kinetochore and along the k-fiber in metaphase and their absence from the same places in anaphase. Reproduced and adapted from (Mitchison et al., 1986) **(B)** Schemes of early and late anaphase spindles (left). Magnified regions from left panel show contribution of Pac-man and poleward flux to anaphase A movement. Black arrow head indicates thicker k-fiber and faster poleward movement than the neighbour (middle). Time points of early and late anaphase from live U2OS cell with MTs in green labelled with tubulin-mCherry and kinetochores in magenta labelled with CENP-A-GFP and photoactivatable tubulin-GFP. Arrowheads indicate the photoactivated region (right). **(C)** Magnified regions from **(B)** depict k-fiber plus-end depolymerization. **(D)** Magnified regions from **(B)** depict k-fiber minus-end depolymerization.

Shortening of the k-fiber could occur through MT depolymerization at their plus- and minus-ends. Classic electron microscopy and photo-bleaching experiments in mammalian fibroblasts (BSC1 cells) showed that depolymerization occurs at the kinetochore - and thus MT plus-ends - concomitantly with chromosome poleward movement in anaphase (Mitchison et al., 1986) (Figure 12) and micromanipulation studies on grasshopper spindles demonstrated that chromosomes continue to move poleward in anaphase as long as the k-fiber stub is longer than 1  $\mu\text{m}$  (Nicklas, 1989). Therefore, the primary site of force generation in anaphase A is on or near kinetochores. In addition, the energy for poleward movement of isolated chromosomes and MTs *in vitro* is derived solely from MT depolymerization at kinetochores (Koshland et al., 1988). This coupling of chromosome movement to MT disassembly at kinetochores is referred as 'plus tip-coupling' (Asbury, 2017), while whole mechanism of kinetochore movement driven by coupled k-fiber depolymerisation, is known as the Pac-man model (Cassimeris et al., 1987) (Figure 12).

On the contrary, the contribution of depolymerization at the k-fiber minus-ends was revealed during metaphase of mammalian fibroblasts upon incorporation of labelled tubulin at k-fiber plus-ends and subsequent extension towards the pole (Mitchison et al., 1986), as well as poleward movement of k-fiber subunits in newt lung cells, which slowed down as anaphase progressed (Mitchison and Salmon, 1992). This data indicated a poleward flux of MT subunits coupled to depolymerization at the spindle pole (Figure 12). These observations define the modern version of classic traction fiber model (Inoue and Ritter, 1975; Maiato and Lince-Faria, 2010), in which, after the sudden increase in MT polymerization at kinetochore, the still active depolymerization at the pole pulls the k-fiber, along with the kinetochore, poleward.

The fraction of the observed k-fiber shortening at both MT ends varies greatly between different model organisms (Asbury, 2017). Poleward MT flux during anaphase in human cells accounts for about a 30-40% of anaphase A chromosome-to-pole movement when measured directly by photoactivation of tubulin (Vukusic et al., 2017), whereas the remaining 60-70% are due to plus-end disassembly (Figure 12). The molecular motor kinesin-13 (Kif2a) is required for flux of k-fibers during metaphase in human cells (Ganem et al., 2005) (Figure 12), similar to its fly homologue kinesin-like protein A (Klp10A) in flies (Rogers et al., 2004). However, the anaphase A chromosome movement rates in cells with inhibited flux during metaphase, following kinesin-13 depletion only decreased by 20% (Ganem et al., 2005), demonstrating that, in human cells, kinetochore-led depolymerization is sufficient and predominant in powering chromosome movements during anaphase. Similarly, in mammalian oocytes the disassembly of MTs at the plus-end makes a major contribution to anaphase A (FitzHarris, 2012).

Confirming the predominance of the plus-end force generation during anaphase A, it was recently shown that a reduction of number of MTs that are ending at kinetochores diminishes some of the forces acting on them and moreover these forces are important for anaphase A movement (Dudka et al., 2018). Hence, a reduction of MT occupancy at kinetochores by 30% led to a reduction of anaphase A movement by 40%, without disruption of spindle elongation rates (Dudka et al., 2018). Thus, in human cells, the ~17 MTs typically contacting a kinetochore per fibre (McEwen et al., 2001), are an important part of the anaphase A segregation machinery.

Furthermore, few recent studies pointed to additional anaphase mechanisms by observing fast poleward movement of short k-fibers generated by laser ablation during anaphase, and establishing this phenomenon was mediated by dynein-dynactin motor complexes interacting with NuMa crosslinker on MTs (Elting et al., 2014; Sikirzhytski et al., 2014). Also, authors reported existence of short k-fibers in metaphase spindles of human cells, whose minus ends presumably ended within another k-fiber. However, less than 10% of kinetochores exhibit frequent fast poleward motions mediated by dynein in unperturbed anaphase (Sikirzhytski et al., 2014), meaning this mechanism can be a surplus to normal anaphase segregation machinery.

In conclusion, chromosome-to-pole motion in human cells is a superposition of two mechanisms: the predominant MT plus-end disassembly at kinetochores and MT poleward flux that is linked with minus-end disassembly (Figure 12).

## 2.12 Role of molecular motors during anaphase A

Is chromosome poleward movement actively powered by molecular motors? Seminal works inhibiting ATP to test its requirement for anaphase A (Cande, 1982; Spurck et al., 1986) revealed that ATP is required for MT disassembly but not for a kinetochore motor actively pulling the kinetochore poleward (Spurck and Pickett-Heaps, 1987). Interestingly, a significant reduction of poleward velocity was seen upon minus-end-directed motor cytoplasmic dynein perturbations (Sikirzhytski et al., 2014; Yang et al., 2007). However, because dynein is barely detectable at kinetochores in anaphase (Pfarr et al., 1990), its effects are most likely indirect, either by regulating MT dynamics, stability of k-fibers or kinetochore orientation (Bader and Vaughan, 2010) (Figure 12). Further exciting candidates for powering poleward movement are CENP-F (Auckland and McAinsh, 2019), which is an efficient coupler to depolymerizing MTs (Volkov et al., 2015), and CENP-E, found to be required for depolymerization-dependent movement of chromosomes *in vitro* (Lombillo et al., 1995).

Interestingly, the kinesin-13 members KLP59C and KLP10A, can form rings around MTs (Tan et al., 2006) and contribute to anaphase A in *Drosophila* cells (Rogers et al., 2004), but the depletion of orthologues in human cells, known to localize to kinetochores or spindle poles (Howard and Hyman, 2007), did not affect anaphase A movement globally but on level of single kinetochores (Bakhoun et al., 2009; Ganem et al., 2005; Gupta et al., 2006), indicating that they are not crucial for chromosome segregation in anaphase. Another candidate, Kif18a (a kinesin-8 member) promotes MT disassembly at plus-ends and couples it to the movement of beads *in vitro* (Grissom et al., 2009). Interestingly, *in vivo*, depletion of Kif18a accelerates poleward velocity rates, whereas its overexpression lowers this rate (Stumpff et al., 2008), similar to what is seen in *Drosophila* somatic cells (Buster and Sharp, 2007), suggesting that Kif18a affects kinetochore velocity through reduction of kinetochore-MT plus-end dynamics. Regarding non-motor regulators, poleward velocity rates during anaphase are significantly lower in Clasp2-knockout mouse embryonic fibroblasts, implying that this protein has a role in the regulation of kinetochore MT depolymerization in anaphase (Pereira et al., 2006). Furthermore, depletion of the MT-severing protein fidgetin decreased metaphase poleward flux rates and anaphase poleward chromosome velocity, albeit to a minor extent (Mukherjee et al., 2012). An overall picture is that individual motors are dispensable for anaphase A movements and, together with non-motor proteins, have a regulatory role during depolymerization-driven poleward chromosome movement.

## 2.13 Role of non-motor proteins during anaphase A

Rather, non-motor proteins that bind to kinetochores seem to be central to plus tip-coupling and kinetochore movement (Figure 12). Primarily this involves the highly conserved Ndc80 complex (Powers et al., 2009; Volkov et al., 2018), a hetero-tetramer with a fibrillary structure with one end that binds MTs and the other end stably anchored into the constitutive centromere associated network (CCAN) of the inner kinetochore (Varma and Salmon, 2012) (Figure 12). Interestingly, inhibition of parts of this complex results in complete stop of poleward chromosome motion in *Xenopus* S3 cells (McClelland et al., 2003; Vorozhko et al., 2008) while in human cells, its depletion results in disrupted kinetochore-MT attachments, failure in chromosome alignment, abnormally long spindles and prometaphase block (DeLuca et al., 2003; DeLuca et al., 2002). Despite evidence that forcing the anaphase in the blocked cells results in anaphase completion with misaligned chromosomes (Meraldi et al., 2004) and fragmented nuclei (Martin-Lluesma et al., 2002), it is still not known if Ndc80 complex is indispensable for anaphase poleward movement as predicted by many authors (Kops et al., 2010). Additionally, the replacement of endogenous Ska (Schmidt et al., 2012; Welburn et al., 2009), that might bridge neighbouring Ndc80 complexes and serve as an attachment-stabilizer, with a mutant lacking the MT-binding domain does not induce a significant change in chromosome dynamics during anaphase A in human cells (Su et al., 2016).

A critical question in the mitotic field that is still under debate is how kinetochores or spindle poles can maintain a persistent connection with MT tips that are depolymerizing (Asbury, 2017). Evidence against simple models in which tip-coupling is based primarily on a single type of conventional molecular motor was gathered by depleting all kinetochore-localized proteins in fission yeast (Grishchuk and McIntosh, 2006) or all minus-end directed kinetochore motors in budding yeast (Tanaka et al., 2007) and poleward movement of chromosomes coupled with depolymerization still continued. In agreement with this, perturbation of various kinetochore or spindle pole motors and regulators in human cells (Auckland and McAinsh, 2019; Ganem et al., 2005; Maffini et al., 2009; Mukherjee et al., 2012; Stumpff et al., 2008; Su et al., 2016; Wandke et al., 2012; Zhu et al., 2005) did not completely abolish anaphase chromosome-to-pole movements. The current view is that motor proteins play a passive role in regulating tip-coupling in anaphase of human cells.

Conclusively, coupling is most probably mediated by fibrillary supra-complexes connecting the bending protofilaments of MTs to the outer kinetochore, visualized by electron microscopy (McIntosh et al., 2008), possibly including Ndc80 with contribution from long

kinetochore-associated motors like CENP-E and F (McIntosh et al., 2010). In brief, k-fiber depolymerization driving chromosome movement in human cells is largely independent of molecular motor and instead requires force exerted by depolymerizing MTs coupled to kinetochores (Figure 12). Lastly, the role of interpolar MTs during anaphase A movement has been theoretically predicted, but remained largely unexplored to date in human cells (Betterton and McIntosh, 2013).

## 2.14 Force-generating mechanisms during anaphase B

Origin of forces required for spindle elongation has been a matter of debate in the last 100 years since first experimental approaches were conducted in the field of anaphase, and the two dominant theories have emerged that tried to explain the movement of the spindle poles, and accompanying MTs with chromosomes, on opposite sides of the cell (Scholey et al., 2016). One theory relies on old ideas proposed first by Druner in 1894, who proposed that structures inside a spindle, later recognized as interpolar MTs, can generate force for elongation of the spindle by pushing two spindle halves apart, this idea was later termed as midzonal pushing mechanism (Maiato and Lince-Faria, 2010; McIntosh et al., 1969) (Figure 8). Subsequent light microscopy studies have documented the kinetics of anaphase B spindle elongation in a variety of eukaryotic cell types (Goshima and Scholey, 2010). An important advance was the proposal and subsequent testing of a ‘sliding filament hypothesis’ for mitosis (McIntosh et al., 1969), in which it was postulated that mitotic motors slide apart aligned antiparallel MTs to drive many of the movements of the mitotic spindle that contribute to overall chromosome movements, in a manner similar to class-II myosin filaments, which drive the sliding filament mechanism of muscle contraction (Scholey et al., 2016) (Figure 8). Testing the sliding filament model promoted detailed electron microscopy of the organization of mitotic spindle MTs and a biochemical search for the motors that mediate MT-MT sliding in multiple organisms (Scholey et al., 2016), but despite intense efforts only in yeasts nanoscale motors involved in spindle elongation have been characterized (Fu et al., 2009; Kruger et al., 2019; Straight et al., 1998).

While a significant body of evidence supports a midzone pushing model (Vukusic et al., 2019), other work has shown that the pulling apart of the spindle poles by motors located on the cell cortex can provide an alternative or complementary mechanism to accomplish midzonal MT-MT sliding and anaphase B spindle elongation in some organisms (Aist et al., 1991; Fink et al., 2006; Grill et al., 2001; Waters et al., 1993) (Figure 8). This theory in

general was proposed first by Boveri in 1888 and relies on an idea that spindle can elongate by pulling via structures, we now know as astral MTs, that connect spindle poles with cell membrane and cortex and this mechanism was later termed cortical pulling mechanism (Scholey et al., 2016).

## 2.15 Astral microtubules during anaphase spindle elongation in human cells

In most vertebrates, MTs emanate from spindle poles and grow towards the cell periphery (Figure 13). These astral MTs can be long enough to interact with proteins at the cell cortex, the actin layer beneath the inner surface of the plasma membrane (Kotak, 2019) (Figure 13). Not all cells have astral MTs (Bannigan et al., 2008; Dumont et al., 2010) and they seem to be non-essential for mitosis, but they contribute to spindle positioning in some systems, most notably the *C. elegans* embryo (Grill et al., 2003; Grill and Hyman, 2005). In human cells, at least in part, the position of the mitotic spindle is controlled by dynein-dependent cortical pulling forces exerted on astral MTs (Kiyomitsu and Cheeseman, 2012) (Figure 13). Specifically, the dynein-dynactin complex is recruited to the cell cortex in anaphase by parallel pathways including LGN and 4.1 family proteins, both interacting with nuclear mitotic apparatus protein (NuMA). Depletion of both pathways results in unequally-sized daughter cells after cell division and defects in spindle centering relative to cell boundaries (Kiyomitsu and Cheeseman, 2013) (Figure 13).

In some organisms, however, there is evidence for external pulling forces on the spindle poles in order to elongate the spindle (Aist et al., 1993; Grill et al., 2001). Potential mechanisms could involve depolymerization of the plus-ends of astral MTs (Grishchuk et al., 2005) or pulling by motors that walk towards the minus-end of astral MTs (Ananthanarayanan et al., 2013; Pavin and Tolić-Norrelykke, 2013) and it has been shown that dynein can participate in both mechanisms (Laan et al., 2012). This suggests a requirement for direct contact between astral MTs and the cell cortex (Kozlowski et al., 2007), although with possible exceptions including anchoring to cytoplasmic actin filament network as shown in cell-free *Drosophila* embryo extract (Telley et al., 2012).

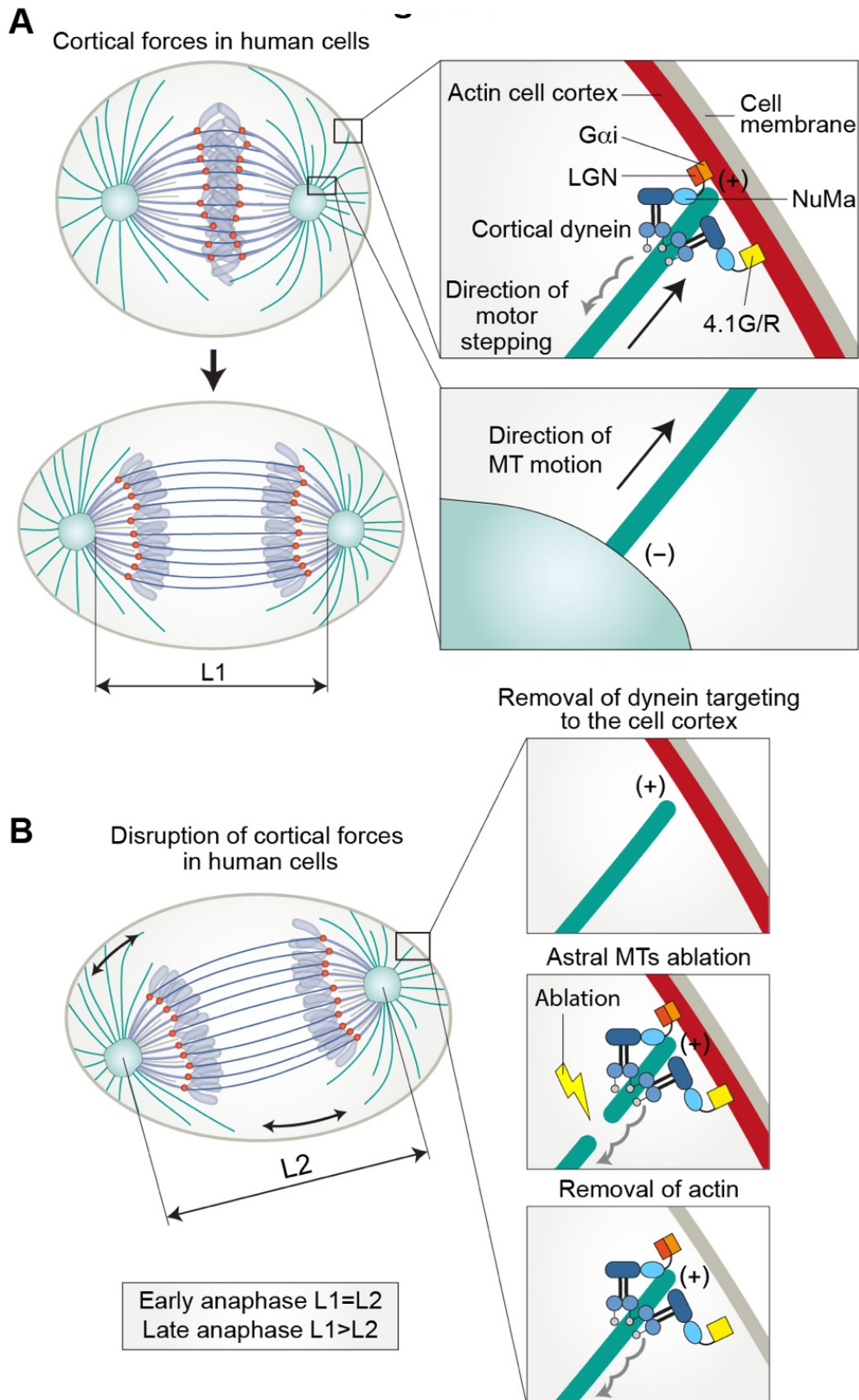


**Figure 13. Astral microtubules in force generation during anaphase.** (A) Schemes of early and late anaphase cell (left). L1 indicates spindle length at late anaphase in unperturbed

mitosis. Magnified regions from left show mechanism of cortical force generation and its impact on spindle pole (right). **(B)** Scheme of late anaphase cell after perturbation of cortical forces. L2 indicates spindle length in late anaphase in perturbed mitosis. Double headed arrows indicate increased oscillatory movement of perturbed spindle (left). Schemes depict the different perturbations of cortical force generation (right).

In human cells, the cortical NuMA and dynein distribution increases during transition from metaphase to anaphase and the final spindle length at the end of anaphase is reduced after NuMA depletion (Kotak et al., 2013). However, NuMA is during anaphase also located throughout mitotic spindle (Kotak et al., 2013), complicating conclusions based on its depletion. On the other hand, whereas it is important for spindle positioning during anaphase, removal of both LGN and a 4.1 family protein does not affect rates of sister chromatid segregation in HeLa cells during early anaphase, but only during later stages (Kiyomitsu and Cheeseman, 2013) (Figure 13). In this case, dynein, NuMA and the dynactin subunit p150 that regulates dynein motility are barely detectable at the cell cortex from the beginning of anaphase (Kiyomitsu and Cheeseman, 2013). In agreement, our laser ablation of astral MTs in U2OS cells did not slow down chromatid segregation and spindle elongation (Vukusic et al., 2017) (Figure 13) and there was no acceleration of spindle pole separation after cutting the spindle midzone region during early anaphase (Vukusic et al., 2017; Yu et al., 2019). Thus, contrary to *C. elegans* and PtK2 cells where astral MTs drive spindle elongation (Aist et al., 1993; Grill et al., 2001), cortical pulling forces seem dispensable for fast spindle elongation and chromosome segregation during early anaphase in human cells (Figure 13).

In line with this, disruption of the actin cytoskeleton by actin-antagonizing drugs, which abolishes astral MT connection to the cortex and thus forces they may impose on the spindle, does not affect spindle pole separation in human cells (Wheatley et al., 1997) (Figure 13). Yet, these treatments have an impact on spindle positioning, cytokinesis, and cell elongation (Charnley et al., 2013; Fernandez et al., 2011). These results support the role of astral MTs in spindle positioning and argue against a force-generating role during the phase of fast spindle elongation in early anaphase, leaving the role of astral MTs in late human anaphase and telophase movements to be investigated (Kotak and Gonczy, 2014) (Figure 13).



## 2.16 Antiparallel microtubules during anaphase spindle elongation in human cells

Interpolar MT bundles during anaphase in human cells are formed by two sets of MTs that emanate from opposite poles and form an antiparallel overlap region in the spindle midzone (McIntosh and Landis, 1971) (Figure 14). The arrangement of plus-ends of interpolar MTs changes slightly from metaphase to mid-anaphase, with a decrease in the overlap length at anaphase-to-telophase transition in long-nosed potoroos epithelial kidney cells (PtK1) (Mastronarde et al., 1993). Tubulin subunits are added to the plus-ends of these antiparallel MTs that slide apart, during late anaphase (Saxton and McIntosh, 1987) (Figure 14), while the overall dynamics of polymerization vary at different anaphase stages in PtK1 cells (Shelden and Wadsworth, 1990). Although k-fibers are the most stable MT subpopulation in metaphase, being more resistant to depolymerization-inducing cold treatment than interpolar or astral MTs in PtK1 cells (Brinkley and Cartwright, 1975), late anaphase central spindle MTs are also very stable and can resist high pressure forces in HeLa cells (Salmon et al., 1976). However, the details of interpolar MT dynamics, temporal regulation of the overlap length, stability and their impact on anaphase movements in human cells remain to be elucidated.

A similar structural organization of interpolar MTs has been found in most species studied (Ding et al., 1993; Mastronarde et al., 1993; McDonald et al., 1977; McIntosh and Landis, 1971; Winey et al., 1995), although MT numbers vary from less than ten in yeasts (Ding et al., 1993; Winey et al., 1995) to hundreds in cultured mammalian cells (McIntosh and Landis, 1971). In budding yeast (Winey et al., 1995), fission yeast (Ding et al., 1993) and diatom (McDonald et al., 1977) spindles, the minus-ends of interpolar MTs appear to interact with spindle poles; this could enable the outward pushing force of sliding interpolar MTs to be exerted on spindle poles in order to drive spindle elongation (McIntosh et al., 1969). On the other hand, the minus-ends of the most interpolar MTs in PtK1 spindles do not reach the poles (Mastronarde et al., 1993), suggesting that direct pushing of interpolar MTs on spindle poles is not likely to occur in all organisms.

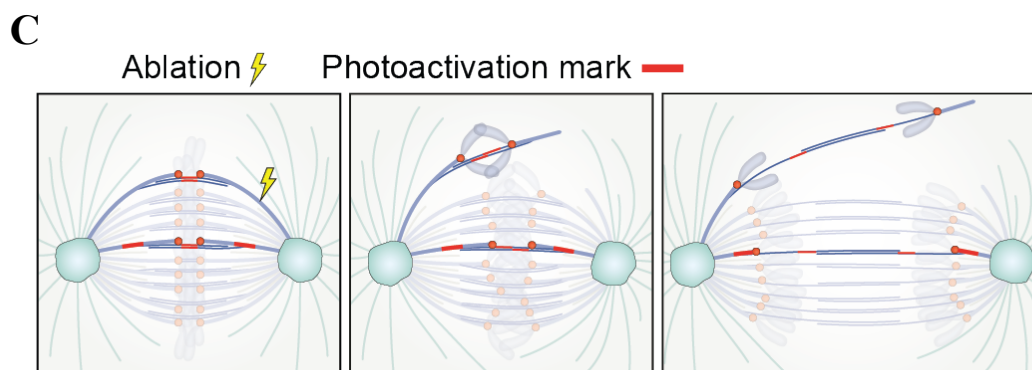
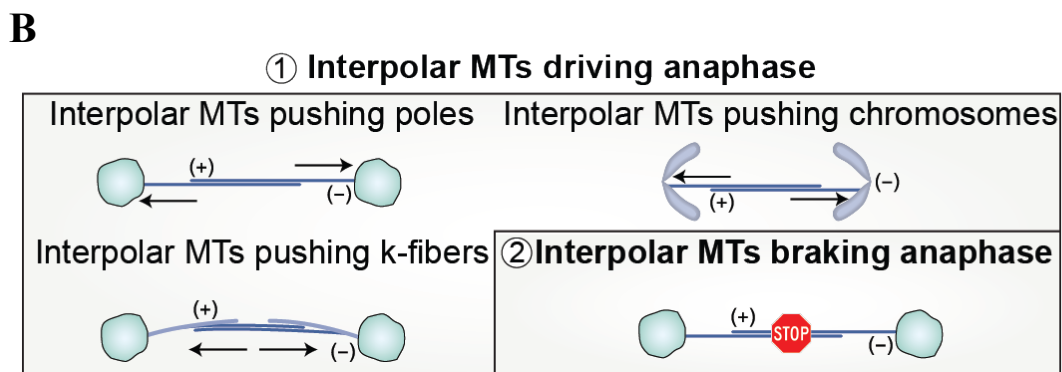
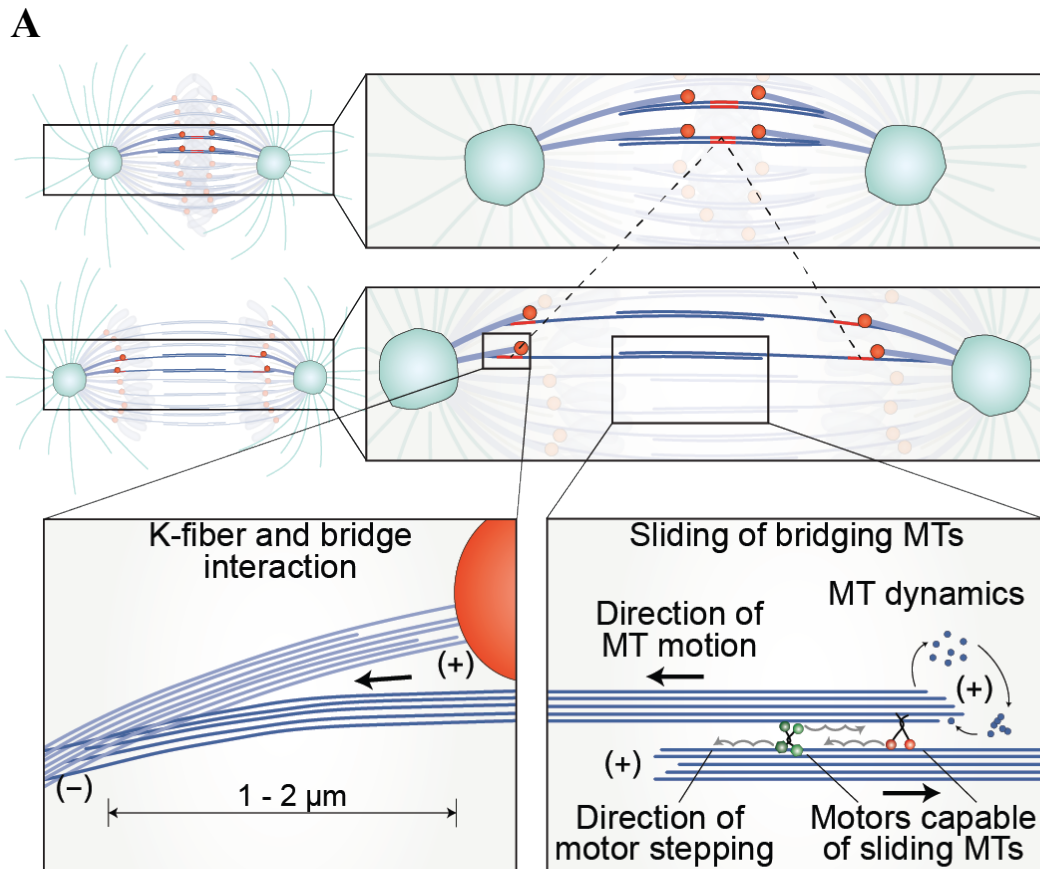


**Figure 14. Interpolar microtubules in force generation during anaphase.** (A) Bridging microtubules (MTs) slide apart (red lines, top). Bridging MTs interact with k-fibers (bottom left) and push them apart by sliding of plus-end directed motors, coupled with regulation of MT plus-end dynamics (bottom right). (B) Interpolar MTs can (1) drive anaphase by different means or (2) act as a brake (stop sign). Black arrows indicate where interpolar MTs exert pushing forces. (C) Schemes of experimental results on human cells showing that after laser ablation (yellow) of one k-fiber, kinetochores segregate independently of the spindle pole, driven by bridging MT sliding and k-fiber depolymerization. At the same time, intact k-fibers and their bridging MTs slide apart at a similar velocity. Adapted from Vukusic et al., 2019.

## 2.17 Structure of bridging microtubule during anaphase

It has been previously reported that non-kinetochore MTs could extend along the k-fiber to the region between sister kinetochores in the metaphase spindles of human cells (McIntosh and Landis, 1971; Nixon et al., 2017). Our group found that almost all of these nonkinetochore MT bundles act as a bridge between sister k-fibers in metaphase (Kajtez et al., 2016). By using a laser ablation assay (Buda et al., 2017), we observed that these bridging fibers moved together with sister kinetochores and their k-fibers, indicating strong crosslinking between these structures during metaphase (Kajtez et al., 2016) and anaphase (Vukusic et al., 2017) (Figure 14). Moreover, these isolated fibers contained PRC1 protein confirming their antiparallel nature (Kajtez et al., 2016; Vukusic et al., 2017). In agreement with the observation of bridging MTs in anaphase (Vukusic et al., 2017), recent large-scale electron tomography reconstructions of spindles in human cells reported different classes of interpolar MTs that were often tightly associated into bundles contacting k-fibers (Yu et al., 2019) (Figure 6). Interestingly, MTs that extend all the way from the pole to the region between chromosomes were not observed meaning that most interpolar MTs during anaphase do not reach poles in human cells, as suggested by previous electron tomography approaches (Kamasaki et al., 2013). This is important for force transmission because it implies that, in order to transmit force generated within the midzone, interpolar MTs must be strongly crosslinked with k-fibers, as shown by a series of recent papers from our group (Kajtez et al., 2016; Milas and Tolić, 2016; Vukusic et al., 2017). Moreover, all described classes of ipMTs were tightly associated into bundles contacting k-fibers, with the last class being the most abundant one in the spindle (Yu et al., 2019), which likely correspond to bridging MTs (Kajtez et al., 2016; Vukusic et al., 2017; Vukusic et al., 2019). Interestingly, it will be

important to identify the crosslinkers that keep k-fibers and bridging fibers laterally linked, with the kinesins Eg5 (also known as Kif11) and Kif15 being good candidates as they are involved in the regulation of neighbouring k-fiber coupling during metaphase (Vladimirou et al., 2013). Likewise, the mechanisms maintaining the connections between bridging and k-fiber as the k-fiber depolymerizes at both ends during anaphase also remain as an open question.

What about the origin of central spindle MTs? In addition to nucleation from centrosomes by MT nucleating  $\gamma$ -tubulin ring complex ( $\gamma$ TuRC), MTs can be also nucleated along pre-existing MTs (Petry and Vale, 2015) by action of the  $\gamma$ TuRC-recruiting human augmin complex (HAUS) (Lawo et al., 2009). In accordance, decreased density of MTs in the central spindle, observed in HAUS6-depleted cells during late anaphase (Uehara et al., 2009), indicated that HAUS complex participates in the generation of new interpolar MTs during anaphase B. However, depletion of this pathway only affects spindle elongation during late anaphase (Uehara et al., 2016), suggesting that most MTs in the antiparallel region during early anaphase are bridging MTs originating from the metaphase spindle, which can be also nucleated by augmin complex during prometaphase or metaphase (Kamasaki et al., 2013).

## 2.18 Sliding of bridging microtubules contributes to chromosome segregation in human cells

In principle, interpolar MTs can contribute to anaphase dynamics in different ways: in the first scenario, antiparallel MTs slide apart powered by motor proteins that walk towards their plus-end (Figure 14). As they slide, the interpolar MTs can push apart different parts of the spindle attached at or near their minus-ends, such as spindle poles (Brust-Mascher et al., 2004), neighbouring k-fibers (Vukusic et al., 2017), or the chromosomes (Dumont et al., 2010) (Figure 14). In the second scenario, antiparallel MTs are negative regulators of anaphase dynamics through a braking mechanism produced by molecular friction or crowding effects (Collins et al., 2014; Saunders et al., 2007) (Figure 14). In addition, the two mechanisms could work together with a temporally displaced activity where interpolar MTs may actively generate forces for chromosome movement in one phase while in the other they may act as a brake, possibly mediated by concentration of antiparallel crosslinkers in the midzone.

To distinguish between these scenarios, laser ablation of spindle MTs has proven to be a useful tool. The sufficiency and necessity of pushing from spindle midzone for spindle

elongation has been confirmed in diatom (Leslie and Pickett-Heaps, 1983) and fission yeast (Khodjakov et al., 2004; Tolić-Norrelykke et al., 2004) spindles. Interestingly, in other model organisms such as PtK2 (Aist et al., 1993), *Caenorhabditis elegans* (Grill et al., 2001) and *Nectria haematococca* (Aist et al., 1991), the same ablation experiments of interpolar MTs accelerated pole separation during anaphase B, revealing that midzone MTs are dispensable and instead act as a brake in spindle elongation.

In human cells, displacement of a pair of sister kinetochores from the rest of the spindle just before anaphase onset showed that kinetochores can segregate independently of attachment to one spindle pole, with antiparallel MTs sliding apart between them (Vukusic et al., 2017) (Figure 14). Moreover, our work revealed that the pushing forces exerted by the bridging fiber are able to segregate chromosomes independently of the spindle pole (Vukusic et al., 2017) (Figure 14). This result is unexpected because according to the current view, the processes that contribute to kinetochore separation require kinetochores to be linked, directly or indirectly, with the spindle pole (Vukusic et al., 2019). Pioneering micromanipulation experiments (Nicklas, 1989; Nicklas et al., 1982) in cricket and grasshopper spindles, where a centrosome was removed, have shown that chromosomes continue to move poleward in anaphase as long as the K-fiber stub is longer than 1  $\mu\text{m}$  (Nicklas, 1989). However, in these experiments K-fibers remained focused into a pole, and thus the role of kinetochore-pole connections remained unexplored. Moreover, recent studies have shown that direct kinetochore-pole connections are not required for chromosome segregation in mammalian cells, because short K-fibers can move chromosomes poleward through interactions with adjacent spindle MTs (Elting et al., 2014; Sikirzhytski et al., 2014). On the contrary, in our study the K-fiber stub was oriented away from the entire spindle and the kinetochore attached to the stub moved away from the pole to which it was originally connected. Thus, the kinetochores segregated without any connection, direct or indirect, to one spindle pole (Figure 14).

Also, we found bridging fibers to be essential for the separation of displaced kinetochores, and continuous cutting of most interpolar MTs in the central spindle decreased spindle elongation rates as well (Vukusic et al., 2017). In agreement with the latter result, short term laser ablation of all interpolar MTs in human cells immediately stopped anaphase chromosome motion for a short period of time (Yu et al., 2019). Additionally, we confirmed that ablation close to the kinetochore, less than a micrometer away, renders kinetochores incapable of separating (Vukusic et al., 2017), possibly due to disruption of the connection between the bridging and k-fiber given that they merge 1-2  $\mu\text{m}$  away from the kinetochores

(Kajtez et al., 2016), suggesting that bridging MTs are sites of active force generation essential for proper chromosome segregation (Figure 14).

How is this force transmitted to spindle poles? Together, data from human cells revoke old ideas that interpolar MTs can slide apart and generate forces that can be transmitted along the k-fibers (Belar, 1929; McIntosh et al., 1969; Ostergren, 1951) consequentially exerting forces on poles to push them apart and elongate the spindle. Accordingly, interpolar MTs originate mostly away from the pole in human cells (Yu et al., 2019), arguing for pushing via k-fibers (Figure 14). Consequentially, the velocity of interpolar MT sliding is greater than the velocity of spindle elongation (2.1  $\mu\text{m}/\text{min}$  and 1.3  $\mu\text{m}/\text{min}$ , respectively) (Vukusic et al., 2017). Such dynamics are expected in a system with MT depolymerization at the minus-end, dissipating some of the force of sliding. Interestingly, in *Drosophila*, reduction of interpolar MT minus-end dynamics at anaphase onset is sufficient to induce spindle elongation (Wang et al., 2013), but the existence of this mechanism in human cells remains to be explored.

## 2.19 Mechanisms that control microtubule overlaps

Regarding control of MT overlaps, several mechanisms have been proposed for stabilization and length control of antiparallel overlaps (Jongorius, 2017). One possible mechanism involves both plus and minus-end-directed motor proteins. These antagonistic motor proteins were thought to balance their forces in order to form a stable antiparallel overlap, at least in metaphase spindle (Gatlin and Bloom, 2010; Goshima and Scholey, 2010; Sharp et al., 2000) (Figure 15). This was supported by experiments *in vivo* that showed that the depletion of a minus end-directed motor could rescue the spindle collapse caused by the depletion of a plus end-directed motor (Saunders and Hoyt, 1992; Sharp et al., 1999a), but direct evidence that these motors are indeed acting through sliding of antiparallel MTs *in vivo* is still lacking. However, *in vitro* relative sliding assays with antagonistic motors do not lead to a stable overlaps and force-balanced steady state (Hentrich and Surrey, 2010). Instead, these experiments lead to bidirectional behaviour of the MT overlaps in which always some motor overrun his agonist in specific point in time. The stochastically changing amount of motors of both types in the overlap is thought to induce this frequent switches in directionality (Hentrich and Surrey, 2010).

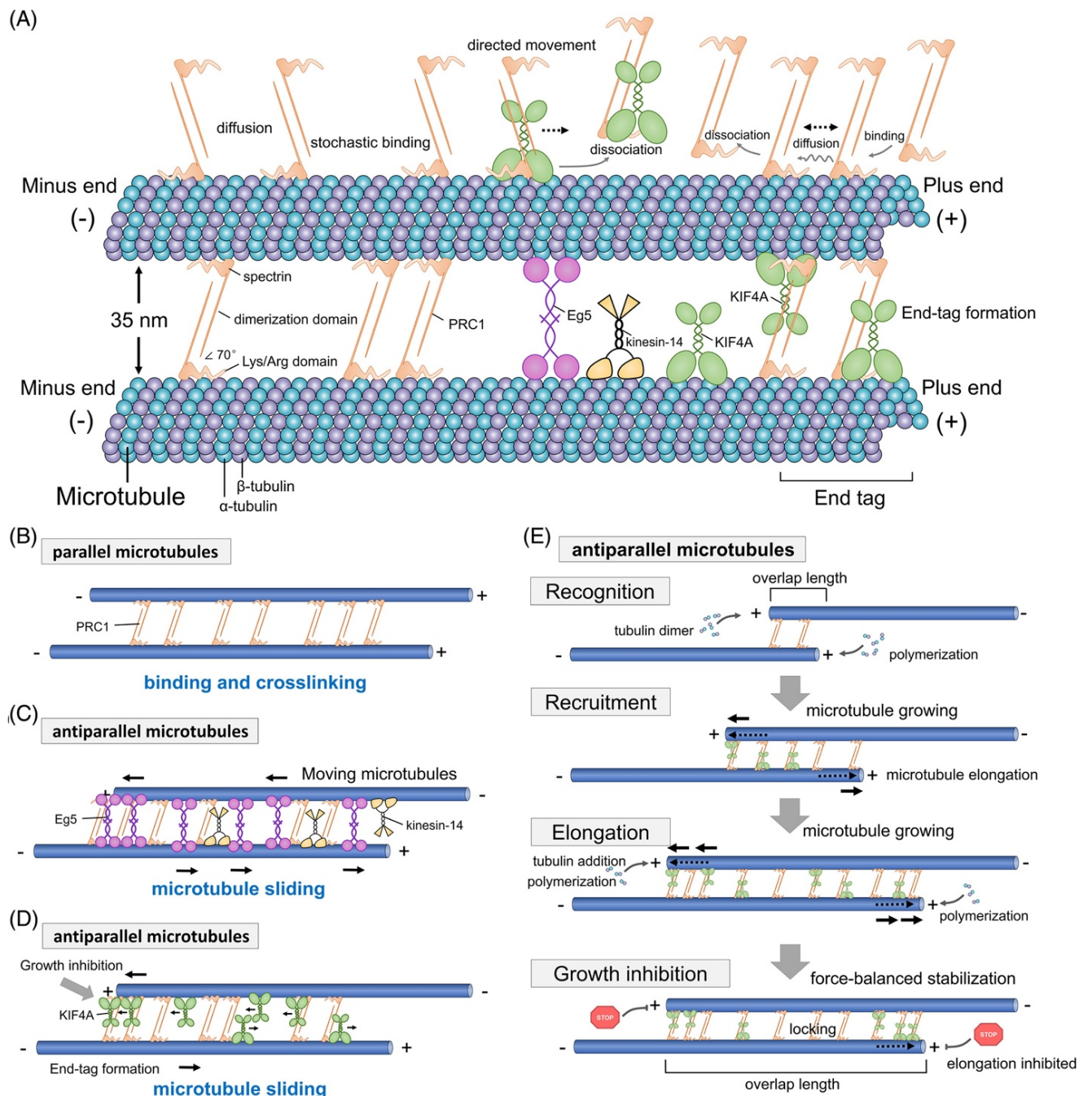


**Figure 15. Mechanisms involved in regulation of antiparallel overlap length. (A)** The mechanochemistry of PRC1 on MTs, including MT binding, diffusion, crosslinking, bundling, dissociation and length-dependent end-tag formation with kinesin-4 member KIF4A. Plus-end directed tetrameric motor EG5 and minus end dimeric kinesin-14 are also depicted. **(B)** PRC1 can weakly bundle parallel MTs. **(C)** PRC1-generated friction and entropic forces counterbalance forces from kinesin-14 and the kinesin-5 Eg5 and mediate MT bundling. **(D)** KIF4A has a weak MT-binding affinity and PRC1 recruits KIF4A to MT bundles. KIF4A–PRC1 interaction contributes to length-dependent end-tag formation in antiparallel MT overlaps and inhibition of MT growth at plus ends. **(E)** The mechanisms

behind PRC1-KIF4A complexes in binding, sliding and growth inhibition of antiparallel MTs in the spindle midzone. Taken from She et al., 2019.

Furthermore, constant length of the overlap is not the only concern since, at the same time, MTs have to slide apart for spindle elongation to happen as balance in forces will not generate constant sliding (Jongerijs, 2017). Moreover, the forces produced for spindle elongation could be regulated depending on the overlap length but how antagonistic motors in overlaps can permit constant sliding and on the other hand control overlap length was unclear. Hence, while antagonistic motor proteins are balanced *in vivo*, a mere combination of these motors alone does not seem to regulate overlap length *in vitro* (Jongerijs, 2017).

Other mechanisms that are proposed to regulate the overlap length involve not only motors but also MT cross linking proteins from a PRC1 family (Figure 15). A few *in vitro* studies that combine PRC1 or its orthologues with another MAP were done. In the first one, researchers combined ase1, an antiparallel bundling protein from *S. pombe*, with ncd, a minus end-directed motor from *Drosophila melanogaster* (Braun et al., 2011). Ncd is a dimeric motor with a second MT binding site at the tail that can slide two MTs apart (Fink et al., 2009). With only ncd present, MTs slide until they are completely separated. However, the presence of ase1 prevented MTs from sliding apart and retained the antiparallel overlap. Regarding this, authors noticed that, first, ncd sliding is slowed by ase1 in a dose-dependent manner and second, ase1 that is present in a bundle is confined to that bundle, while motors are lost in proportion with the decrease in overlap length. Thus, the MT ends form a diffusive barrier for ase1, retaining ase1 in shrinking overlaps. When MTs reach the end of the surface MT, the overlap length is reduced and this causes an increase of ase1 molecules per overlap length and a decrease in number of motor molecules. As a result, ase1 starts to reduce ncd velocity triggering a braking mechanism (Jongerijs, 2017). However, friction caused by high local densities of ase1 can slow sliding, but is not able to prevent MTs from sliding apart. Though, another mechanism that expands the overlaps is induced when MTs slide apart. The crowded environment with a high density of ase1 in the short overlap is unfavourable and the diffusing ase1 in the overlap creates an expanding force (Lansky et al., 2015). Presented mechanisms did not include MT dynamics and their relevance to human PRC1 are not known.

This is challenging because regulating growth of MT may also be a mechanism for length control since overlap is governed both by growth and sliding (Jongerijs, 2017). To investigate this, experiments were performed with assays using dynamic MTs (not stabilized with taxol) and some regulators of MT dynamic ends. In that regard, authors explored



antiparallel MT overlaps using PRC1 and kinesin-4 Xklp1, both from *Xenopus* (Bieling et al., 2010). They show that the two proteins have a direct interaction with each other and that PRC1 is needed to recruit kinesin-4 to antiparallel overlaps (Bieling et al., 2010). PRC1 then recruits kinesin-4 to the antiparallel overlaps where kinesin is supposed to move towards the MT plus ends. This leads to a kinesin-4 accumulation at the growing MT plus end, where it inhibits MT growth (Figure 15). In this mechanism, the length of the overlaps dictates the amount of kinesin-4 that binds there. This results in larger accumulations of kinesin-4 in longer overlaps, leading to more growth inhibition, and smaller accumulations in shorter overlaps, leading to less growth inhibition (Figure 15). Finally, this results in a stable steady state, in which the overlap length does not change (Bieling et al., 2010). This mechanism shows that the combination of a MT bundler and recruiter together with a processive motor or growth inhibitor can form a minimal system to obtain overlap length control (Jongerius, 2017).

Moreover, it is known that the collective activity of PRC1 and Kif4A results in their accumulation at MT plus-ends (termed ‘end-tag’) (Subramanian et al., 2013). More recently, one study reported that *in vitro* sliding system that include PRC1-KIF4A complex represents an alternative mechanism in which a motor and a non-motor proteins act synergistically on antiparallel MTs to first promote relative sliding and then stall MT movement by forming a molecular roadblock (Wijeratne and Subramanian, 2018) (Figure 15). To conclude, mechanisms of overlap length maintenance that are achieved through balance between MT bundling, sliding and growing/shrinking have been extensively explored *in vitro*, but translation of all these mechanisms to *in vivo* anaphase spindle of human cells is still lacking.

## 2.20 Regulation of spindle elongation and aurora kinases

In animal cells, the sequential ubiquitin-dependent proteolytic degradation of distinct mitotic cyclins is required for progression through mitosis, with cyclin A degradation allowing progression through metaphase and cyclin B degradation, which starts after the SAC is satisfied, being necessary for anaphase B (Sullivan and Morgan, 2007). During metaphase-to-anaphase transition, global protein phosphorylation state of the cell is reversed by the activation of E3 ubiquitin ligase APC/C which targets Cyclin B for degradation in proteasomes leading to downregulation of CDK1 activity and increase in PP1/PP2A phosphatase activity (Wurzenberger and Gerlich, 2011) (Figure 16). Importantly, the MT bundler protein from a PRC1/Ase1p family serves as a regulatory hub for control of anaphase

B in many model organisms (Roostalu et al., 2010). PRC1 accumulates at the anaphase spindle midzone in a phosphorylation- and motor-dependent manner, where it controls midzone structural organization via its crosslinking function, but also recruits many key anaphase B proteins (Roostalu et al., 2010) that can regulate PRC1 itself. Thus, the regulation of anaphase B spindle elongation is complex. It occurs at several levels and involves ubiquitin-dependent proteolytic degradation, CDK1 and phosphatase-dependent phosphorylation-dephosphorylation cycles, the key midzone regulatory MAP, PRC1/Ase1p, which is crucial for localization of key molecules to the midzone, and whose localization is on the other hand regulated by the same midzone molecules (Nasa and Kettenbach, 2018).

Moreover, exciting recent work indicates that the control of anaphase B involves the dynamic cooperation and antagonism between functionally interdependent kinases, phosphatases, MAPs and motors capable of producing spatially-controlled feedback loops that coordinate the dynamic turnover of phosphorylation sites to coordinate spindle midzone assembly and elongation (Afonso et al., 2014; Bastos et al., 2014; Su et al., 2016). However, although recent experiments unravelled a regulatory crosstalk behind mitotic exit (Afonso et al., 2019; Afonso et al., 2014; Potapova et al., 2006; Wolf et al., 2006), linkage between key modulating kinases and direct force producing proteins in human cells is still lacking, especially when compared to knowledge gathered in yeast spindles.

Main downstream protein regulators during anaphase are Aurora kinases (Afonso et al., 2017). Aurora A is localized mainly at centrosomes throughout mitosis where it plays a conserved role in centrosome maturation and separation, control of MT dynamics, and bipolar spindle assembly (Barr and Gergely, 2007). In contrast, Aurora B localizes at centromeres and chromosomes in early mitosis and re-localizes to the spindle midzone after anaphase onset and midbody during mitotic exit (Adams et al., 2000). Aurora B plays a role in the correction of incorrect kinetochore-MT attachments and SAC response, ensuring chromosome bi-orientation and faithful segregation during anaphase (Lampson and Cheeseman, 2011). Recently, two well-known Aurora A substrates from pre-anaphase cells, TACC3 and P150Glued, have also been implicated in spindle midzone stability and nucleation during anaphase, in a manner dependant on Aurora A (Lioutas and Vernos, 2013; Rebutier et al., 2013) (Figure 16). However, as Aurora A localizes mainly on centrosomes, accumulating at the midbody only in late anaphase and telophase it is unclear how it promotes spindle midzone stability (Rebutier et al., 2013).

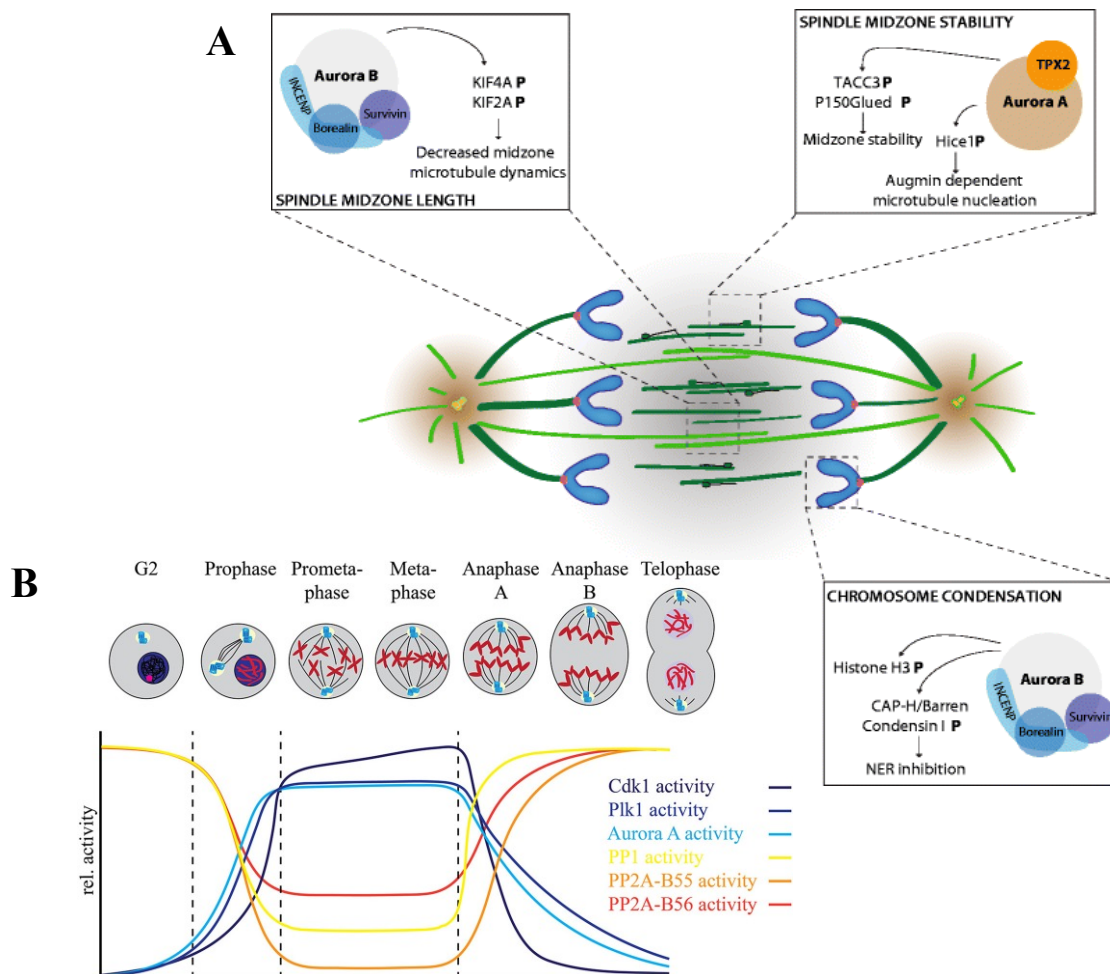


**Figure 16. Current models of regulation of spindle midzone length and stability that involves Aurora kinases. (A)** Aurora kinase B, in complex with INCEP, Borealin and Survivin, regulate spindle midzone length by phosphorylating KIF4A and KIF2A proteins thereby decreasing MT dynamics within the spindle midzone. Aurora A controls midzone stability by phosphorylating TACC3, p150Glued or Hice1 which leads to increased midzone MT stability and increased MT nucleation through action of augmin complex, respectively. Aurora B is also involved in chromosome condensation and inhibition of nuclear envelope reformation (NER) by phosphorylating CAP-H/Barren and Condensin I and Histone H3. **(B)** Mitotic progression is regulated by fine balance between the mitotic protein kinases and protein phosphatases. The relative activities of major mitotic protein kinases including Cdk1, AURKA, AURKB, and Plk1, indicated in blue spectrum, increase as the cells enter mitosis, and decrease as the cells enter anaphase. This trend is accompanied by opposite trend in the activities of major mitotic phosphatases including PP1, PP2A-B56 and PP2A-B55. Taken from Afonso et al., 2017 and Nasa and Kettenbach, 2018.

Aurora B kinase activity is dependent on its regulatory partner proteins INCENP, survivin, and borealin (Afonso et al., 2017). Together, these proteins constitute the chromosomal passenger complex (CPC) (Ruchaud et al., 2007). At the metaphase-anaphase transition, Aurora B is released from the centromeres, which is associated with a drop in Cyclin B1/Cdk1 activity (Hummer and Mayer, 2009). Cdk1 is a master kinase that negatively regulates several proteins required for spindle midzone formation such as PRC1 (Mollinari et al., 2002), INCENP (Hummer and Mayer, 2009), MKLP2 (Kitagawa et al., 2014), and MKLP1 (Mishima et al., 2004). INCEP interacts with MKLP2 only after inhibitory phosphorylation on this protein is removed (Hummer and Mayer, 2009) and this leads to relocalization of Aurora B from centromeres to the antiparallel MTs in the spindle midzone (Gruneberg et al., 2004). Here, Aurora B recruits and phosphorylates MKLP1 (Neef et al., 2006), which then recruits its partner CYK4 (Mishima et al., 2002), thereby initiating formation of the heterotetrameric centralspindlin complex between MKLP1 and CYK4, which has MT bundling properties and is essential for spindle midzone stabilization (Glotzer, 2009). Notably, the formation of the centralspindlin complex is negatively regulated by 14-3-3 binding to MKLP1 and this is counteracted by Aurora B-dependent phosphorylation of MKLP1 (Douglas et al., 2010), which consequentially induces clustering of centralspindlin complexes at the spindle midzone.

An Aurora B phosphorylation gradient also regulates spindle midzone length by two mechanisms that are opposed to each other (Figure 16). First includes an inhibitory phosphorylation of KIF2A, which blocks its depolymerizing activity at the spindle midzone, restricting KIF2A localization to the MT minus-ends (Uehara et al., 2013), and latter includes an activating phosphorylation of KIF4A that leads to stabilization of ipMTs plus-ends (Nunes Bastos et al., 2013) (Figure 16). An Aurora B activity gradient at the spindle midzone has also been shown to monitor chromosome position during anaphase, ensuring that completion of nuclear envelope reformation (NER) and chromosome decondensation occur only after sufficient sister chromatid separation (Afonso et al., 2014), defining chromosome segregation checkpoint in anaphase. Additional Aurora A and B substrates, with functions related to MT dynamics and direct force-production within spindle midzone, have been identified by large-scale phospho-proteomic studies, but their relevance for spindle midzone function remains to be elucidated (Afonso et al., 2017). Finally, one study reported that both Aurora kinases jointly coordinate chromosome segregation during anaphase by observing cells that exit mitosis without anaphase, forming polyploid daughter cells with a single nucleus, after

perturbation of both Aurora kinases (Hegarar et al., 2011), but detailed study of possible mechanisms behind this anaphase arrest is needed to further support this conclusion.

## 2.21 PRC1 as a main scaffold for recruitment of multiple motors

PRC1 (Jiang et al., 1998) is a MT bundling protein, which belongs to a highly conserved family of MAPs that includes plant MAP65 and yeast Ase1p (She et al., 2019). Crosslinks of ~35 nm in length are observed between anti-parallel MTs that are bundled by this protein (Subramanian et al., 2010) (Figure 15). Large part of the PRC1 molecule is predicted to form a rod-like homodimer consisting of repeated triple helix bundles similar to an actin bundling protein  $\alpha$ -actinin. The MT-binding region of PRC1 has been mapped to the C-terminal half of the molecule, termed spectrin domain, which covers the unfolded tail and the adjacent part of the  $\alpha$ -helical region (Subramanian et al., 2010). The N-terminal region of PRC1 is made up of  $\alpha$ -helices and is required for its midzone localization (She et al., 2019). The triple helix bundle structure in the MT-binding domain of human PRC1 has been confirmed by X-ray crystallography and cryo-EM helical reconstruction (Subramanian et al., 2010).

PRC1 is essential for the formation of the central spindle *in vivo* during late anaphase (Mollinari et al., 2002). Also, depletion of PRC1 causes accelerated spindle elongation (Pamula et al., 2019), in some cases only after cytokinesis furrowing, not effecting fast phase of spindle elongation, while the final spindle length after 16 minutes was unchanged when compared to controls (Uehara et al., 2016). Before the onset of anaphase, PRC1 is diffusely localised throughout the cytoplasm but a fraction of its population associates with the antiparallel MTs even in the metaphase spindle (Kajtez et al., 2016; Polak et al., 2017). At anaphase onset, PRC1 rapidly accumulates to the spindle midzone, forming the structure composed of multiple antiparallel MTs, termed central spindle (Lee et al., 2012) (Figure 17). Phosphorylation by cyclin-dependent kinase 1 (CDK1) has a crucial role in temporal regulation of PRC1 (Jiang et al., 1998; Mollinari et al., 2002; Zhu and Jiang, 2005), as described earlier. *In vitro* experiments at the single molecule level revealed that both PRC1 and Ase1p move diffusively along a single MT and have a higher preference for anti-parallel MTs when compared with parallel ones (Bieling et al., 2010; Subramanian et al., 2010). Moreover, PRC1 does not substantially resist the relative sliding of two MTs by kinesin-5 motors (Subramanian et al., 2010). PRC1 also interacts with various motors and MAPs

forming a main scaffold in antiparallel region of the spindle (Lee et al., 2012) (Figure 17), as discussed below.

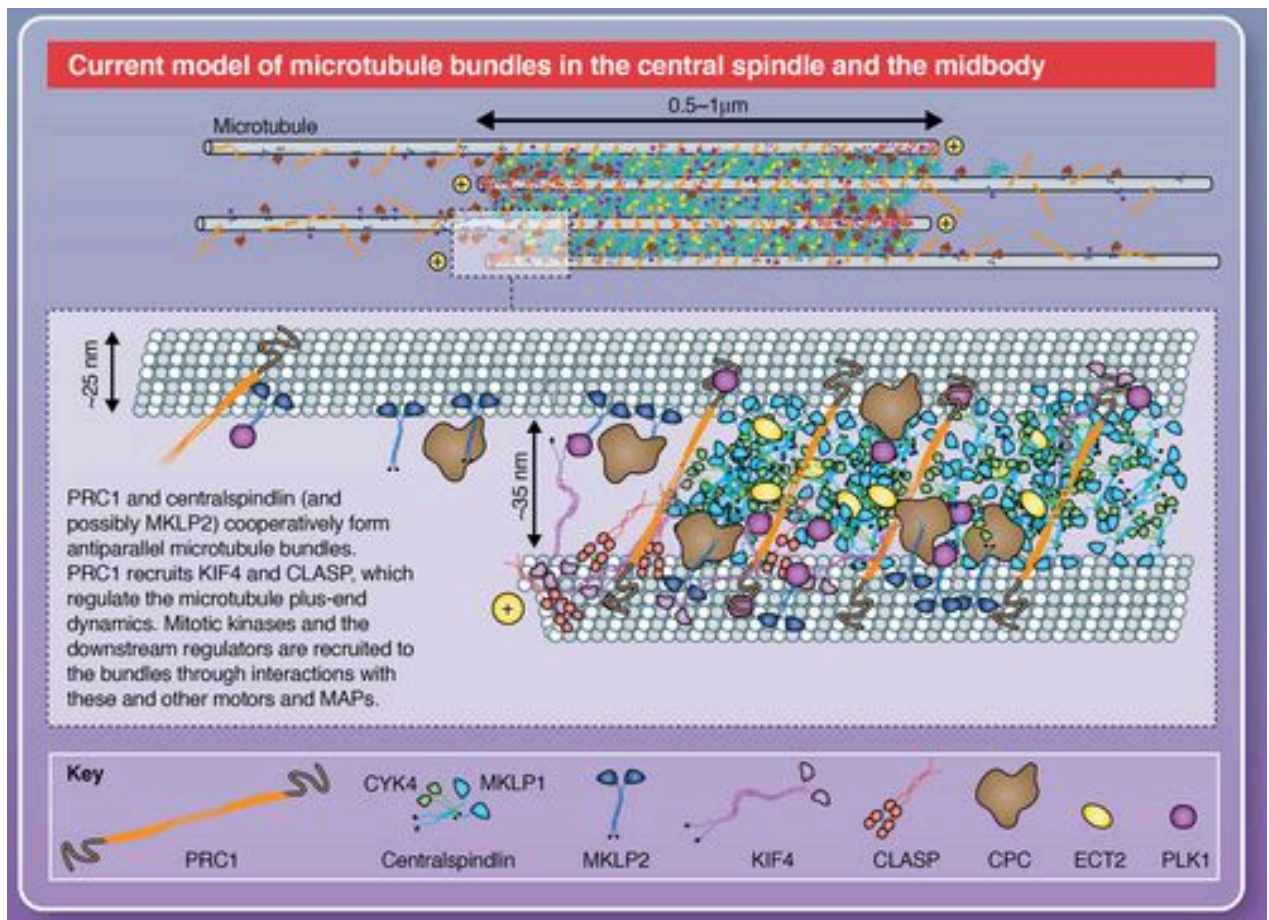


**Figure 17. Spindle midzone is complex multi-component system with PRC1 as main bundler and primary scaffold protein.** Spindle midzone is organised by PRC1 protein which bundles two antiparallel MTs forming tight central spindle during late anaphase. PRC1 also brings multiple components within this region serving as a scaffold for complex regulator network involving multiple targets depicted. Note: The scheme shows CLASPs as dimers, while recent work demonstrated that mammalian CLASPs are monomers under physiological conditions (Girao et al., 2020). Taken from Lee et al., 2012.



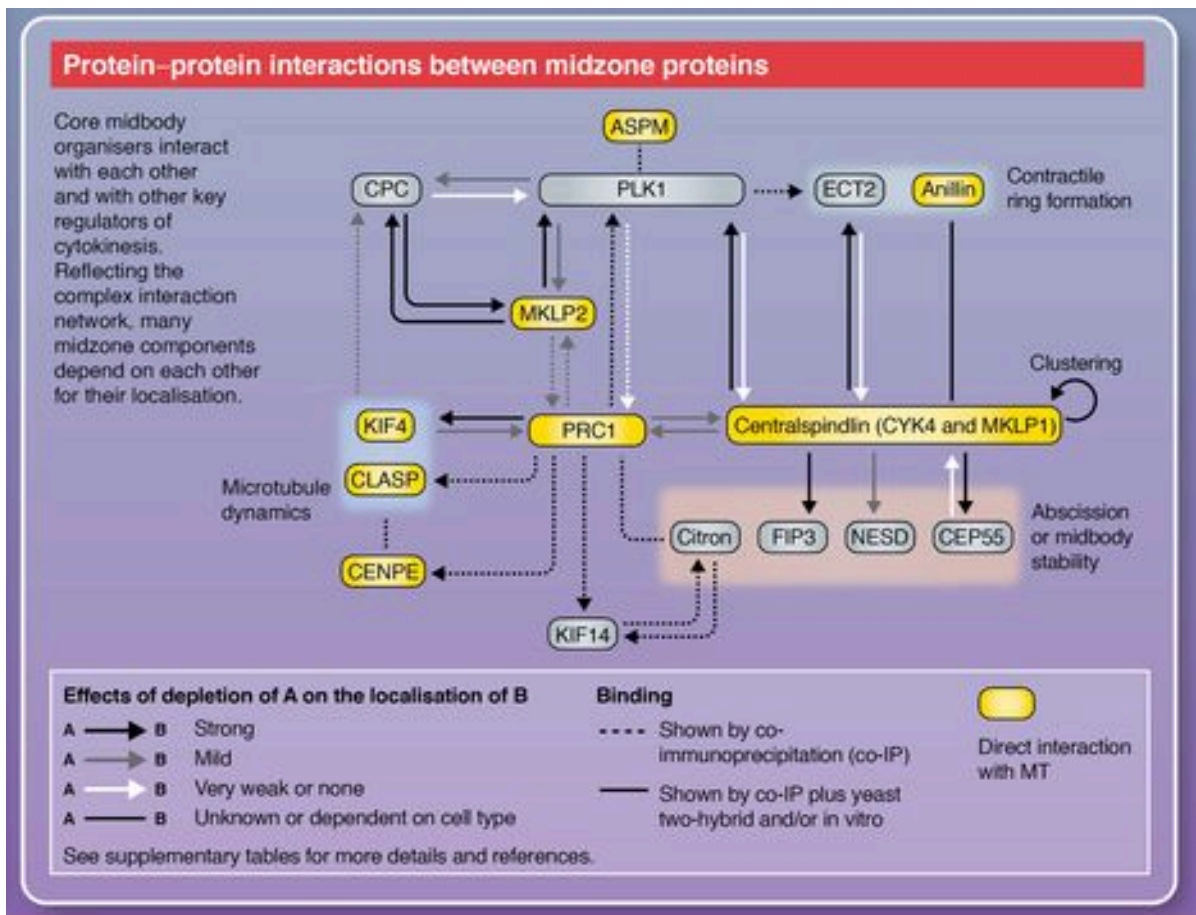


**Figure 18. PRC1-interacting partners in the spindle midzone and nature of their interactions.** Protein interactions between different midzone proteins and global interactions with MTs are depicted. Involvement of specific components during characteristic anaphase and cytokinesis events is noted. Strength of interaction between partners is represented by various styles of arrows as explained in the legend. The nature of binding is represented by line segmenting where full line indicates direct interactions, while segmented line indicates indirect binding of partners. Taken from Lee et al., 2012.

## 2.22 PRC1-interacting proteins

### 2.22.1 Kinesins-6 (MKLP1, MKLP2 and MPP1)

Centralspindlin is MT bundling multi-protein complex that is critical for the formation of the central spindle during anaphase and for connection of the mitotic spindle to the plasma membrane to secure the final cut during cytokinesis in animal cells (Lee et al., 2012). It is a stable 2:2 heterotetrameric complex of a kinesin-6 family of motor proteins, orthologous to

mammalian mitotic kinesin-like protein 1 (MKLP1) and a Rho-family GTPase-activating non-motor protein (RhoGAP) orthologous to *Caenorhabditis elegans* CYK-4 (CYK4) (Figure 17) (Mishima et al., 2002). In mitotic cells, the majority of MKLP1 and CYK4 are in the centralspindlin complex and free components are rarely observed. The motor domain of MKLP1 have the MT plus-end directed motor activity that can slide antiparallel MTs apart (Mishima et al., 2004; Nislow et al., 1992) which is essential for proper MT bundle formation and structure of midbody (Matuliene and Kuriyama, 2002) (Figure 17). The neck region of MKLP1, which links the motor domain to short coiled-coil stalk domain, is unusually long and contains the binding site for its partner CYK4 (Mishima et al., 2002). Both subunits of this complex are vital for MT bundling *in vitro* and central spindle formation *in vivo*.

Similar to PRC1, the interaction of centralspindlin with MTs is suppressed by CDK1 phosphorylation before anaphase onset (Mishima et al., 2004). The heterotetrameric centralspindlin forms higher-order clusters and this is strictly regulated by Aurora B kinase and 14-3-3 proteins (Douglas et al., 2010), as described earlier. This clustering activity is essential for its processive motility *in vitro* and for its sharp accumulation to the central position within the central spindle *in vivo* (Hutterer et al., 2009). PRC1 has been reported to interact with centralspindlin on the basis of coimmunoprecipitation experiments in HeLa cell lysates (Ban et al., 2004; Gruneberg et al., 2006; Kurasawa et al., 2004). PRC1 was also found to interact with the CYK4 subunit of centralspindlin in a yeast two-hybrid assay (Ban et al., 2004) (Figure 18). Also, when PRC1 is depleted, signal of centralspindlin components is lost and vice versa, which indicates that their respective localisations to the central spindle are interdependent (Verni et al., 2004) (Figure 18). However, the significance of interaction between PRC1 and centralspindlin for their recruitment to the spindle midzone and the formation of the central spindle is unclear because defects in either factor disrupt the central spindle structure as described in the previous sections.

On the other hand, mitotic kinesin-like protein 2 (MKLP2)/KIF20A is a less conserved member of the kinesin-6 family of motor proteins, which, in contrast to MKLP1, has not been reported to form a stable complex with other polypeptides (Lee et al., 2012). MKLP2 is crucial for the relocation of the CPC from the centromere to the central spindle (Gruneberg et al., 2004), for the appropriate localisation of PLK1 to the spindle midzone (Neef et al., 2003) and for regulation of KIF4A activity and localisation to the midzone region, probably through modulation of aurora B localisation (Nunes Bastos et al., 2013) (Figures 17 and 18). Lastly, vertebrates also have a third member of kinesin-6 family MPP1, which is also localised to the spindle midzone and is required for proper cytokinesis (Abaza et al., 2003).



### 2.22.2 Kinesin-4 (KIF4A)

Another PRC1-interacting midzone motor is the kinesin-4 family member KIF4A, which has an N-terminal motor domain followed by a long coiled-coil tail (~100 nm and longer than that of the conventional kinesin-1) that is responsible for its dimerization (Sekine et al., 1994) (Figure 17). It moves along the MTs towards their plus ends and upon its accumulation at the plus end, reduces MT polymerisation and depolymerisation dynamics (Bieling et al., 2010; Bringmann et al., 2004). KIF4 was the first kinesin found to associate with mitotic chromosomes and was thus termed chromokinesin. Few minutes after anaphase onset, a subpopulation of KIF4 accumulates at the central spindle and later on the midbody (Wang and Adler, 1995) (Figure 17). Reflecting this localisation pattern, KIF4 is involved in multiple steps of cell division, including the accurate formation of the central spindle (Kurasawa et al., 2004; Mazumdar et al., 2004; Zhu and Jiang, 2005) (Figure 16). KIF4 depletion causes abnormal elongation of the central spindle with unfocused MT overlaps (Hu et al., 2011).

The interaction between PRC1 and KIF4 is the best characterized interaction among midzone proteins (Lee et al., 2012). This interaction can be detected both by co-immunoprecipitation and yeast two-hybrid assays and is thus likely to be direct (Kurasawa et al., 2004) (Figure 18). CDK1 negatively regulates this interaction by phosphorylating PRC1 (Zhu and Jiang, 2005). Although the central spindle localisation of KIF4 is lost when PRC1 is depleted, PRC1 still localises to the central spindle and the midbody in the absence of KIF4, although in a broadened pattern, possibly reflecting the role of the PRC1-KIF4 interaction in transporting PRC1 to the plus ends of MTs (Zhu and Jiang, 2005) (Figure 18). However, aberrant PRC1 localisation in the absence of KIF4 can also be explained by an observed increase in the length of the MT overlaps (Hu et al., 2011), which is consistent with the *in vitro* observation that PRC1 and KIF4 have a combinatorial effect in regulating the length of the anti-parallel overlap (Bieling et al., 2010). Further study is needed to clarify the *in vivo* importance of their direct interaction because a KIF4 construct that lacks the C-terminal tail and thus does not bind PRC1 can still tightly focus itself and PRC1 to the centre of the spindle midzone (Hu et al., 2011).

Regarding KIF4A ability to slide *in vitro* (Bieling et al., 2010), as part of the already mentioned ‘end-tags’, that form at the plus-tip the of MT *in vitro* (Subramanian et al., 2013) and following its very low affinity for MTs when compared with other MT-binding proteins

(Wijeratne and Subramanian, 2018), it is speculated that fraction of KIF4A molecules, especially those at the very tip of the MT, can adopt a one-head bound state and collectively mediate MT sliding. Alternatively, high concentration of Kif4A at end-tags may stimulate intermolecular interactions between motors or binding between the Kif4A C-terminus and MT, despite low-affinity interactions among them. Authors speculate that it is more plausible to think that *in vitro* the C-terminus of KIF4A, which has low affinity for MTs, interacts with the N-terminus of PRC1 which has a higher affinity for MTs (Subramanian et al., 2013), and then these complexes within the untagged region of the antiparallel overlap drive antiparallel sliding of MTs (Wijeratne and Subramanian, 2018). Because we currently do not know if sliding of MTs by PRC1 and KIF4A contributes to the sliding and spindle elongation during anaphase it would be interesting to study relevance of this mechanism *in vivo* antiparallel overlaps.

### 2.22.3 Other motor proteins

Other kinesin-like motors, including kinesin-3 class member KIF14 (Gruneberg et al., 2006), the kinesin-7 class member CENP-E (also known as KIF10) (Liu et al., 2019), have also been reported to interact with PRC1 at the central spindle and the midbody, but their roles in organisation of the midzone MT bundles are scarcely studied, mainly revolving around structural or signalling roles within the midzone (Lee et al., 2012) (Figure 18).

## 2.23 Kinesin-5 as a major protein involved in sliding of antiparallel microtubules

Kinesin-5 protein EG5, one of the most studied kinesin members, is a motor protein with the motor domain located at the N-terminus which has a capacity to move toward MT plus-ends (Sawin et al., 1992) (Figure 19). Consistent with this, purified vertebrate EG5 walks processively toward the plus-ends of MTs with relatively short run lengths (~8 steps) (Kapitein et al., 2005; Valentine et al., 2006). Additionally, because they form bipolar homotetramers, Kinesin-5s use both their motor domains and non-motor tail domains to crosslink and simultaneously walk on two MTs, showing a preference for MTs in the antiparallel configuration (Kapitein et al., 2005) (Figure 18), effectively resulting in relative MTs sliding (Figure 8). The ability to move MTs relative to each other is thought to be the key feature of kinesin-5 motors that enables bipolar spindle formation (Mann and Wadsworth,

2019). This feature also distinguishes kinesin-5 from other kinesins, which typically transport vesicular cargos along the MT lattice. Regarding EG5 motor activity, the MT is both its cargo and track (Mann and Wadsworth, 2019). Despite the evidence that kinesin-5 is a plus-end directed motor, several groups recently made the surprising discovery that kinesin-5s from budding and fission yeast (Cin8, Kip1, Cut7) can move toward MT plus or minus ends, using the same motility mechanism, while their directionality is directed by different motor concentrations or ionic strength in solution (Gerson-Gurwitz et al., 2011; Roostalu et al., 2011). Furthermore, when engaged by two antiparallel MTs, motors switch direction and become less processive but the net overall movement is plus-end directed, regardless of ionic strength. These data suggested that when kinesin-5 is engaged between two antiparallel MTs plus-end directed motility is always triggered (Thiede et al., 2012), but relevance of this phenomenon for human EG5 *in vivo* is not known. Like many mitotic proteins, kinesin-5 localization and activation are controlled by cell cycle regulated phosphorylation (Yount et al., 2015). Although kinesin-5 phospho-regulation is common across organisms, the kinases and phosphatases, the phosphorylation sites, timing and consequences of phosphorylation vary greatly (Mann and Wadsworth, 2019).

In dividing cells, kinesin-5 binds to mitotic MTs important for spindle formation and this is regulated by phosphorylation within the tail domain (Mann and Wadsworth, 2019). In human cells phosphorylation of kinesin-5s' tail domain by CDK1 is required to localize the motors to centrosomes and spindle MTs early in mitosis (Blangy et al., 1997; Blangy et al., 1995; Cahu et al., 2008; Sawin and Mitchison, 1995). CDK1 also facilitates interactions of kinesin-5 with other proteins. For example, when CDK1 phosphorylates EG5 early in mitosis it localizes to centrosomes where it co-localizes and associates with the dynactin subunit p150 (Blangy et al., 1997). The tail domain of EG5 is also phosphorylated by Nek6/Nek7 and this is necessary for motor function and establishment of spindle bipolarity (Rapley et al., 2008). PLK1 kinase phosphorylates Nek9, which then activates Nek6/Nek7, ultimately resulting in phosphorylation of kinesin-5 at S1033 specifically at centrosomes (Bertran et al., 2011). Nek6/Nek7 phosphorylation does not affect the ability of EG5 to bind MTs, but regulates spindle pole localization where phosphorylation is needed for motor activity specifically to separate centrosomes during prophase (Rapley et al., 2008). It would be interesting to study how is this mechanism of regulation involved in anaphase localisation and activity of EG5 motor since CDK1 activity drops after onset of anaphase, as discussed above.

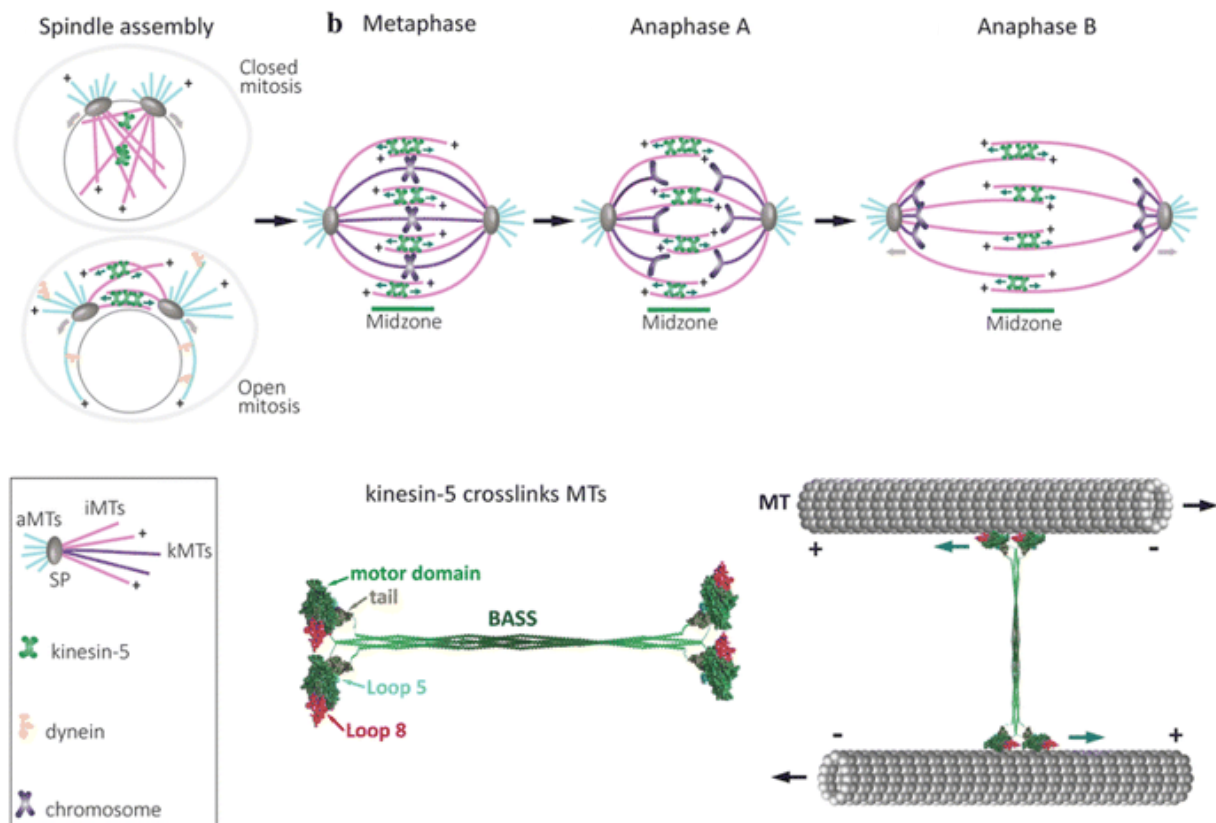


**Figure 19. Proposed roles of motor protein EG5 in mitosis.** Proposed roles of EG5 motor protein, localising in antiparallel midzone MTs, through mitotic stages are depicted on the top (see text for details). Structure of tetrameric EG5 motor with different domains and its interaction with antiparallel MTs both visualised on the bottom. Taken from Singh et al., 2018.

The most conserved role of kinesin-5 family members is to establish spindle bipolarity in early mitosis, as discussed above (Figure 19). Although some organisms do not require kinesin-5s for building a bipolar spindle, monopolar spindle formation is observed when kinesin-5 is mutated or inhibited in most organisms that have been studied thus far (Kapoor et al., 2000; Mayer et al., 1999; Sawin and Mitchison, 1995). Bi-directional motility has only been described for yeast kinesin-5 motors, but kinesin-5 is enriched at spindle poles in other cells (Gable et al., 2012; Sawin et al., 1992; Sawin and Mitchison, 1995), leaving the possible role of minus-end motility of EG5 open for investigation. On the other hand, previous work showed that EG5 is transported toward spindle poles in a dynein-dynactin dependent manner (Gable et al., 2012). In mammalian cells, the MT associated protein, TPX2, regulates EG5 motor stepping and localization to the spindle, and potentially couples EG5 to dynein-dynactin for minus-end directed transport (Eckerdt et al., 2008; Gable et al., 2012). Recently,

it was shown that TPX2 plays a role in localizing EG5 to centrosomes in prophase (Eibes et al., 2018) via an importin-independent cytoplasmic pool of TPX2 that localizes EG5 in a Nek6/Nek7 dependent manner. Moreover, *in vitro*, TPX2 slows down the MT-sliding activity of EG5 (Ma et al., 2011). Thus, in human cells both transport and interactions with specific binding partners contribute to kinesin-5 enrichment toward MT minus ends and despite differences in the mechanism of localization, it is speculated that poleward accumulation in prophase may serve to initiate MT sliding when antiparallel MTs are encountered, as in yeast spindles (Mann and Wadsworth, 2019).

Although much of the work on kinesin-5 has focused on its essential role in spindle formation, kinesin-5 is also needed to maintain spindle bipolarity in some organisms (Kapoor et al., 2000; Saunders and Hoyt, 1992; Sharp et al., 1999b) (Figure 19). In human cells of tumour origin, spindles remain bipolar following treatment with Eg5 inhibitors (Kapoor et al., 2000) due to action of kinesin-12 motor proteins (Sturgill and Ohi, 2013; Tanenbaum et al., 2009; Vanneste et al., 2009). On the other hand, non-transformed human cell lines are completely prone to EG5 inhibition and readily collapse to monopolar spindle, even after bipolar spindle has formed in metaphase (Gayek and Ohi, 2014) suggesting a possible gain of function of kinesin-12 in tumour-derived cell lines or general force balance issues between the motors. In tumour cell lines, after cells are depleted of kinesin-12, spindle shortening is observed, demonstrating that this motor also contributes to outward force production (Sturgill and Ohi, 2013). Additionally, overexpression of kinesin-12 (Kif15) can drive spindle formation in the absence of kinesin-5, although an alternate pathway for spindle formation is used (Sturgill et al., 2016). Interestingly, both kinesin-12 and kinesin-5 are regulated by TPX2 suggesting redundancy in motor regulation (Drechsler et al., 2014; Mann et al., 2017; Vanneste et al., 2009). Kinesin-12 has been reported to exist as a tetramer, although a dimeric form may also be functional (Drechsler et al., 2014; Mann et al., 2017). However, kinesin-12 tetramers crosslink only parallel MTs, aligning them into bundles (Drechsler and McAinsh, 2016) making this protein unlikely candidate for antiparallel MT sliding.

In some cells, kinesin-5 motors generate the force for spindle elongation (Figure 19). For example, in budding yeast, Cin8 and Kip1 drive antiparallel MT sliding and the contribution of each to anaphase is distinct. Kip1 plays a greater role in later anaphase events allowing the spindle to increase up to 5 times its initial length, and Cin8 is more important in early anaphase (Straight et al., 1998). In other cells, kinesin-5 activity is dispensable for anaphase B and in some cases, contributes even to antagonistic braking forces, probably by increasing friction in the overlap region thereby opposing other motor performing sliding or

opposing forces generated at the cell cortex (Collins et al., 2014). In *C. elegans*, cells lacking the kinesin-5 homolog, BMK1, show faster elongation than wild type cells (Saunders et al., 2007). Thus kinesin-5 in some systems is thought to act as a frictional brake, limiting the rate and extent of spindle elongation.

## 2.24 Spindle elongation by motor-driven sliding in human cells

What is the importance of motor proteins driving spindle elongation in human cells? First, one could test the sensitivity of spindle elongation to varying concentrations of ATP. Because of technical challenges, the data in human cells is scarce but in Ptk1 permeabilized cells, Cande has reported that the maximal rate of anaphase B was observed at the highest ATP concentration, while at a very low ATP concentration spindle elongation did not take place (Cande, 1982) and it was speculated that the ATP- and motor-dependence of anaphase B can be applied to human cells as well (Vukusic et al., 2019).

Thus far, spindle elongation in human cells was shown to be almost completely perturbed by inhibition of MT dynamics by addition of nocodazole (Canman et al., 2000) that non-specifically depolymerizes MTs, by addition of taxol (Afonso et al., 2014) that stabilizes MTs against depolymerisation, by perturbation of top signalling effectors that regulate multiple mitotic targets regulating both force-production by molecular motors and MT-dynamics, such as aurora kinases, PLK1, CDK1 or CyclinB (Afonso et al., 2019; Afonso et al., 2014; Brennan et al., 2007; Wolf et al., 2006), by inhibition of topoisomerase-II (Su et al., 2016) which resolves DNA supercoil threads and regulates activation of midzone pool of Aurora B (Coelho et al., 2008), by inducing a rigor-bound state of motors that localise to antiparallel region, such as Eg5 by treatment with FCPT (Afonso et al., 2014), thereby inhibiting MT sliding by increasing frictional forces in that region. However, none of these studies reported block in spindle elongation by active perturbation of direct force-producing proteins responsible for elongation itself.

On the other hand, the main motor candidate involved in the generation of outward forces through sliding of interpolar MTs is a plus-end directed motor from the kinesin-5 family EG5 whose homologues drives spindle elongation in yeast (Saunders et al., 1995; Straight et al., 1998), which has a capacity to slide antiparallel MTs *in vitro* (Kapitein et al., 2005) and during metaphase of human cells in cooperation with the kinesin-12 protein Kif15 is crucial for spindle length maintenance i.e. production of outward force (Tanenbaum et al., 2009; van Heesbeen et al., 2014). Second important candidate is the kinesin-6 protein

MKLP1/Kif23 that contributes to spindle elongation in yeast (Fu et al., 2009; Kruger et al., 2019) and *in vitro* has a capacity to slide antiparallel MTs apart (Nislow et al., 1992). However, inhibition of Eg5 combined with depletion of Kif15 did not affect sliding velocities in human cells in anaphase or spindle elongation velocities (Vukusic et al., 2017), similar to what is seen in *Drosophila* embryos (Brust-Mascher et al., 2009), although in both cases a large fraction of spindles collapsed in metaphase or showed delay in anaphase B onset. MKLP1, on the other hand, is involved in the regulation of midzone length in human cells (Hu et al., 2011), but has a minor effect on spindle elongation velocities, probably through regulation of the midzone stability (Vukusic et al., 2017). Thus, identity of motor proteins driving anaphase spindle elongation by sliding antiparallel MTs apart remains an open longstanding unanswered question in cell division. Furthermore, because of complex nature of mechanisms in spindle length regulation involving multi-layer signalling cascades, the exact mechanism behind regulation of mitotic spindle elongation through control of main force-producing proteins is not well understood. Elucidating both of these complex problems in anaphase of human cells will form a basis of this thesis.

### 3 MATERIALS AND METHODS

#### 3.1 Cell Lines

The cell lines used are: human U2OS cell lines (human osteosarcoma, female) both wild type and those permanently transfected and stabilized using CENP-A-GFP (protein of kinetochore complex) and mCherry-alpha-tubulin, were a gift from Marin Barišić and Helder Maiato (Institute for Molecular Cell Biology, University of Porto, Portugal) (developed in Barisic et al., 2015), human hTERT-RPE-1 (retinal pigmented epithelium, female) permanently transfected and stabilized using CENP-A-GFP and centrin1-GFP (protein of a centrosome complex), which was a gift from Alexey Khodjakov (Wadsworth Center, New York State Department of Health, Albany, NY) (developed in Magidson et al., 2011), human hTERT-RPE-1 permanently transfected and stabilized using PA-GFP- $\alpha$ -tubulin which was a gift from Patrick Meraldi (Faculty of Medicine, University of Geneva, Switzerland) (developed in (Jaqaman et al., 2010)), human hTERT-RPE-1 inducible CRISPR/Cas9/PRC1-G2.2 knock-out (KO) which was a gift from Iain Cheeseman (Massachusetts Institute of Technology, Cambridge, MA, USA) (developed and detailed in McKinley and Cheeseman, 2017), human HeLa cell line (human adenocarcinoma, female) separately permanently transfected and stabilized using BAC containing EG5-GFP which were a gift from Ina Poser and Tony Hyman (Max Planck Institute of Molecular Cell Biology and Genetics, Dresden, Germany) (developed in Poser et al., 2008). Cells were grown in flasks in Dulbecco's Modified Eagle's medium (DMEM) with Ultraglutamine (1 g/l D-glucose, pyruvate) (Lonza, Basel, Switzerland) supplemented with 10% of heat-inactivated Fetal Bovine Serum (FBS) (Sigma-Aldrich, St Louis, MO, USA), and penicillin/streptomycin solution (Lonza) to a final concentration of 100 I.U./mL penicillin and 100  $\mu$ g/mL streptomycin. Media was additionally supplemented for selection of some cell lines as follows: 50  $\mu$ g/ml geneticin G418 (Life Technologies, Waltham, MA, USA) was added in media for HeLa BAC cell line described above and 500  $\mu$ g/ml G418 was added in media for hTert-RPE-1 PA-GFP- $\alpha$ -tubulin cell line. The induction of RPE-1 PRC1 CRISPR cell line was performed using 1  $\mu$ g/mL doxycycline hyclate (Sigma) in DMEM media at 24 hr intervals for 4 days (with imaging and analysis on the fifth day), unless otherwise indicated. The cells were kept at 37°C and 5% CO<sub>2</sub> in a Galaxy 170s humidified incubator (Eppendorf, Hamburg, Germany). All used cell lines were confirmed to be mycoplasma free by monthly



checks using MycoAlert Mycoplasma Detection Kit (Lonza) and regular checks while imaging with DNA-stains.

### 3.2 Constructs, transfections and RNAi

U2OS cells were transiently transfected by electroporation using Nucleofector Kit R (Lonza, Basel, Switzerland) with the Nucleofector 2b Device (Lonza, Basel, Switzerland), using X-001 program. Transfection protocol provided by the manufacturer was followed. Cells were transfected with mCherry-PRC1 plasmid provided by Casper C. Hoogenraad (Utrecht University, Utrecht, Netherland).  $1 \times 10^6$  cells were electroporated with 1.5  $\mu\text{g}$  of plasmid DNA. Transfection of U2OS cells was performed 25–35 h before imaging. For all siRNA treatments,  $2 \times 10^5$  or  $3 \times 10^5$  cells were seeded and cultured in 1 ml DMEM medium with same supplements (as above) at 37°C and 5% CO<sub>2</sub> on 12-well cell culture plates (Greiner). After one-day growth, at ~70% confluency cells were transfected with 200 nM (except KIF15 siRNA: 100 nM and PRC1 siRNA 500 nM) raw targeting or non-targeting siRNA constructs diluted in a Opti-MEM medium (Life Technologies, Waltham, MA, USA). Transfection was performed using Lipofectamine RNAiMAX Reagent (Life Technologies) using protocol provided by the manufacturer. After 5h of treatment the medium was changed to regular DMEM medium described above. After 24h of treatment cells from one well were equally reseeded into glass bottom microwells with 4 compartments (Grainer), used later for imaging. 3h prior to imaging, the medium was replaced with Leibovit's (L-15) CO<sub>2</sub>-independent medium (Life Technologies), supplemented as above. The cells were imaged always 48 hours after transfection, unless otherwise indicated. The constructs used were as follows: human MKLP-1 siRNA (sc-35936, Santa Cruz Biotechnology), human KIF14 siRNA (sc-60882, Santa Cruz Biotechnology), human KIF4A siRNA (sc-60888, Santa Cruz Biotechnology), human KIF20A siRNA (sc-91657, Santa Cruz Biotechnology), control siRNA (sc-37007, Santa Cruz Biotechnology), human KIF15 siRNA (L-004960-00-0010, Dharmacon), human PRC1 siRNA (L-019491-00-0020, Dharmacon) and control siRNA (D001810-10-05) from Dharmacon. We observed that inhibition of MKLP1 blocked normal progression of cytokinesis that resulted in formation of binucleated cells. We have observed an increase of 81% in the number of binucleated/multinucleated cells in MKLP1 siRNA-treated samples (calculated from 88 cells) after 48h in comparison with the samples treated with control siRNA (calculated from 92 cells), similar to previous observations (Fontijn et al., 2001). Similarly, we have observed a significant increase in number of multinucleated cells

following 48h treatments with MKLP2 and PRC1 siRNA (Neef et al., 2003; Zhu and Jiang, 2005). Successful siRNA treatment was checked with immunocytochemistry using appropriate primary antibodies against same targets used in RNAi protocol. Cells were fixed using methanol protocol (described above) 48h after transfection with siRNA and imaged using protocol for imaging of fixed cells (described above).

### 3.3 Drugs

The stock solution of STLC was prepared in dimethyl sulfoxide (DMSO) to a final concentration of 25 mM. Drug was obtained from Sigma-Aldrich. The working solution was prepared in DMEM at 80  $\mu$ M (the half-maximal inhibitory concentration IC<sub>50</sub> for STLC in HeLa cells is 700 nM) (DeBonis et al., 2004). At the time of treatment, the working solution was added to cells at 1:1 volume ratio to obtain a final concentration of 40  $\mu$ M. To inhibit EG5 (kinesin-5), STLC was added in metaphase or early anaphase. Quick response was observed as most metaphase spindles collapsed into monopolar spindles in RPE-1 cells, minutes after STLC was added (Gayek and Ohi, 2014). For immunofluorescence and expansion microscopy of alpha-Tubulin, in treatments with STLC, drug was added to the cell culture media 5 min before fixation. Monastrol was obtained from Abcam and was used at a final concentration of 100  $\mu$ M. Similar to treatment with STLC, quick response was observed as a large fraction of metaphase spindles collapsed into monopolar spindles in RPE-1 cells, minutes after Monastrol was added. The half-maximal inhibitory concentration IC<sub>50</sub> for Monastrol is 14  $\mu$ M in cell-based assay (Mayer et al., 1999). The stock solution of GSK-923295 was prepared in dimethyl sulfoxide (DMSO) to a final concentration of 8 mM. GSK-923295 was obtained from MedChemExpress (MCE, NJ, USA). The working solution was prepared in DMEM at 200 nM. At the time of treatment, the working solution was added to cells at 1:1 volume ratio to obtain a final concentration of 100 nM (IC<sub>50</sub> value of compound is 3.2 nM) (Wood et al., 2010). To inhibit CENP-E, GSK-923295 was added in the late metaphase. Appearance of spindles blocked in prometaphase with fraction of kinetochores trapped around polar region of the spindle (Bennett et al., 2015) confirmed the effect of GSK-923295, imaged 30 min post-treatment with drug. The stock solution of ZM 447439 was prepared in dimethyl sulfoxide (DMSO) to a final concentration of 2 mM. ZM 447439 was obtained from Selleckchem (Munich, Germany). The working solution was prepared in DMEM at 8  $\mu$ M. At the time of treatment, the working solution was added to cells at 1:1 volume ratio to obtain a final concentration of 4  $\mu$ M (IC<sub>50</sub> value of compound is 110 nM for

Aurora A and 130 nM for Aurora B) (Ditchfield et al., 2003). To inhibit Aurora kinases, ZM 447439 was added at metaphase-to-anaphase transition. Specific Aurora A inhibitor I (TC-S 7010) was obtained from Selleckchem. The working solution was prepared in DMEM at 6  $\mu$ M. At the time of treatment, the working solution was added to cells at 1:1 volume ratio to obtain a final concentration of 3  $\mu$ M. IC<sub>50</sub> value of compound obtained from *in vitro* kinase assays is 3.4 nM (Aliagas-Martin et al., 2009). Upon treatment of metaphase cells with this inhibitor, quick metaphase spindle shortening is observed, similar to use of other Aurora A specific inhibitors, like MLN8237 (Courtheoux et al., 2018). Specific Aurora B inhibitor Barasertib (AZD1152-HQPA/AZD2) was obtained from Selleckchem. The working solution was prepared in DMEM at 120 nM. At the time of treatment, the working solution was added to cells at 1:1 volume ratio to obtain a final concentration of 60 nM. IC<sub>50</sub> value of compound obtained from *in vitro* kinase assays is 0.37 nM (Yang et al., 2007). In experiment where KIF15 was inhibited by siRNA treatment in U2OS cells, we observed rapid collapse of metaphase spindle upon 40  $\mu$ M STLC treatment, as reported previously (van Heesbeen et al., 2014).

### 3.4 Sample preparation

When cells reached 80% confluence, DMEM medium was removed from the flask and the cells were washed with 5 mL of 1% PBS. Afterward, 1 mL of 1% Trypsin/EDTA (Biochrom AG, Berlin, Germany) was added and the cells were incubated at 37 °C and 5% CO<sub>2</sub> in a humidified incubator (Eppendorf). After 5 min incubation, Trypsin was blocked by adding 2-5 mL of DMEM medium. Cells were counted using the Improved Neubauer chamber (BRAND GMBH + CO KG, Wertheim, Germany) and  $4.5 \times 10^5$  cells were seeded and cultured in 2ml DMEM medium with same supplements (as above) at 37°C and 5% CO<sub>2</sub> on 14 or 20 mm glass microwell uncoated 35mm dishes with 0.16-0.19mm (#1.5 coverglass) glass thickness (MatTek Corporation, Ashland, MA, USA). For siRNA experiments,  $1 \times 10^5$  cells were seeded in cell culture 35/10 mm glass bottom microwells with 4 compartments (Greiner, Frickenhausen, Germany) or  $2 \times 10^5$  in 12-well cell culture plates (Greiner) that were reseeded the day after into glass bottom microwells with 4 compartments. After one-day growth, 3h prior to imaging, the medium was replaced with Leibovit's (L-15) CO<sub>2</sub>-independent medium (Life Technologies), supplemented with 10% FBS (Life Technologies), 100 I.U./mL penicillin and 100  $\mu$ g/mL streptomycin. For live-cell staining of chromosomes 1 hour before imaging, silicon rhodamine (SiR)-DNA, also called SiR-Hoechst

(Lukinavicius et al., 2015) (Spirochrome AG, Stein am Rhein, Switzerland) was added to 1 mL of cells in a DMEM medium to a final concentration of 100 nM together with efflux pump inhibitor verapamil (Spirochrome AG), only in RPE-1 and U2OS cell lines, to a final concentration of 10  $\mu$ M.

### 3.5 Live cell imaging

HeLa cells expressing EG5-GFP were imaged using a Leica TCS SP8 X laser scanning confocal microscope with a HC PL APO  $\times$ 63/1.4 oil immersion objective (Leica, Wetzlar, Germany) heated with an objective integrated heater system (Okolab, Pozzuoli, NA, Italy). For excitation, a 488-nm line of a visible gas Argon laser and a visible white light laser at 575 nm were used for GFP and mRFP, respectively. GFP and mRFP emissions were detected with HyD (hybrid) detectors in ranges of 498–558 and 585–665 nm, respectively. Pinhole diameter was set to 0.8  $\mu$ m. Images were acquired at 30–60 focal planes with 0.5  $\mu$ m z-spacing, 30 nm xy-pixel size, and 400 Hz unidirectional xyz scan mode. The system was controlled with the Leica Application Suite X Software (1.8.1.13759, Leica, Wetzlar, Germany) and cells were maintained at 37 °C and in 5% CO<sub>2</sub> using Okolab stage top heating chamber (Okolab, Pozzuoli, NA, Italy). All RPE-1 and U2OS cells were imaged using Bruker Opterra Multipoint Scanning Confocal Microscope (detailed in (Buda et al., 2017)) (Bruker Nano Surfaces, Middleton, WI, USA). The system was mounted on a Nikon Ti-E inverted microscope equipped with a Nikon CFI Plan Apo VC  $\times$ 100/1.4 numerical aperture oil objective (Nikon, Tokyo, Japan). During imaging, cells were maintained at 37 °C and 5% CO<sub>2</sub> in Okolab Cage Incubator (Okolab, Pozzuoli, NA, Italy). A 60  $\mu$ m pinhole aperture was used and the xy-pixel size was 83 nm. For excitation of DAPI, GFP, mCherry or RFPa and SiR fluorescence, a 405, 488, 561 and 647 nm diode laser line was used, respectively. The excitation light was separated from the emitted fluorescence by using Opterra Dichroic and Barrier Filter Set 405/488/561/640 nm (DAPI/eGFP/TRITC/Cy5) (Chroma, USA). The brightfield imaging of RPE-1 PRC1 KO cells in different conditions was performed by illuminating sample with brightfield lamp (Nikon). Images were captured with an Evolve 512 Delta EMCCD Camera using 150 ms exposure time (Photometrics, Tucson, AZ, USA) with no binning performed. In experiments where whole spindle stack was imaged, z-stacks were acquired at 30-60 focal planes separated by 0.5  $\mu$ m with unidirectional xyz scan mode and with “Fast Acquisition” option in software enabled. Otherwise, one or few z-stacks were

imaged using 0.5  $\mu\text{m}$  spacing with unidirectional xyz scan mode. The system was controlled with the Prairie View Imaging Software (Bruker Nano Surfaces, Middleton, WI, USA).

### 3.6 Photoactivation (PA) stability and sliding assays

For photoactivation of fluorescence of PA-GFP, a 405-nm laser diode (Coherent, Santa Clara, CA, USA) was used. Photoactivation was performed using live photoactivation option in PrairieView software, with duration of pulse set to 400 ms for each point and laser power set to 40% for all experiments performed. Photoactivation was performed in a line pattern on an equally distributed 10 points, where each point represents one laser hit. The interval between the points was minimal, 0.05 ms, and photoactivation area was set to 0.5  $\mu\text{m}$  for each point. Photoactivation was performed after anaphase onset, perpendicular to spindle long axis, in between separating chromatids, visualized with 100 nM SiR-DNA stain and detected using maximum power of 0.5% of 647 diode laser. SiR-DNA was used to discriminate anaphase onset by perception of peripheral sister chromatids moving into characteristic anaphase “v-shape”, which was then used as a mark for start of the photoactivation assay. PA-GFP fluorescence was detected using 488 diode laser (on 30% of a maximum laser power), turned on just after onset of anaphase to minimize unwanted photoactivation. The excitation light was separated from the emitted fluorescence in both channels by using Opterra Dichroic and Barrier Filter Set 488/640 nm (eGFP/Cy5) (Chroma, USA). The interval between consecutive frames was set to 0.8 s, imaging one central z-plane and program was set to record 200 consecutive frames. Further details of this microscopy system and similar laser ablation and photoactivation assays were discussed elsewhere (Buda et al., 2017).

### 3.7 Immunofluorescence

Human RPE-1 cell line stably expressing centrin1-GFP and CENP-A-GFP were grown on glass-bottomed dishes (14 mm, No. 1.5, MatTek Corporation) and fixed by 1 mL of ice-cold methanol for 3 min at  $-20^{\circ}\text{C}$  for visualization of PRC1, EG5, KIF15, KIF4A, MKLP1, MKLP2 and KIF14. To visualize alpha-Tubulin in control cells and in the treatments, ice-cold methanol protocol was avoided because it destroys unstable MTs and cells were instead fixed by a mixture of 3.2% PFA (paraformaldehyde) and 0.25% GA (glutaraldehyde) in MT-stabilizing PEM buffer (0.1 M PIPES, 0.001 M  $\text{MgCl}_2 \times 6 \text{H}_2\text{O}$ , 0.001

M EDTA, 0.5 % Triton-X-100) for 10 min at room temperature (Heuser and Kirschner, 1980). After fixation with PFA and GA, for quenching, cells were incubated in 1mL of freshly prepared 0.1% borohydride in PBS (phosphate-buffered saline) for 7 min and after that in 1 mL of 100 mM NH<sub>4</sub>Cl and 100 mM glycine in PBS for 10 min at room temperature. Both methanol fixed cells and PFA and GA fixed cells were then washed with 1 mL of PBS, 3 times for 5 min. To block unspecific binding of antibodies, cells were incubated in 500 µL blocking/permeabilization buffer (2% normal goat serum (NGS) and 0.5% Triton-X-100 in water) for 45 min at room temperature. Cells were then incubated in 500 µL of primary antibody solution for 24h at 4 °C. The following primary antibodies were used: mouse monoclonal PRC1 (sc-376983, Santa Cruz Biotechnology), diluted 1:50; mouse monoclonal EG5 (sc-365681, Santa Cruz Biotechnology), diluted 1:50; mouse monoclonal KIF15 (sc-100948, Santa Cruz Biotechnology), diluted 1:50; mouse monoclonal KIF4A (sc-365144, Santa Cruz Biotechnology), diluted 1:50; rabbit polyclonal MKLP-1 (sc-867, Santa Cruz Biotechnology), diluted 1:50; mouse monoclonal KIF20A (sc-374508, Santa Cruz Biotechnology), diluted 1:50; rat anti-alpha Tubulin (Invitrogen), diluted 1:500. After primary antibody, cells were washed in PBS and then incubated in 500 µL of secondary antibody solution for 45 min at room temperature. Alexa Fluor 488, 594, and 647 (Invitrogen) were used as secondary antibodies (diluted 1:1000).

### 3.8 Expansion microscopy

Expansion microscopy protocol was a custom made as a combination of steps from of various previously developed protocols for expansion microscopy of human cells in culture (Chozinski et al., 2016; Tillberg et al., 2016; Truckenbrodt et al., 2019). Human RPE-1 cell line stably expressing centrin1-GFP and CENP-A-GFP were grown on glass-bottomed dishes (14 mm, No. 1.5, MatTek Corporation) and fixed by a mixture of 3.2 % PFA (paraformaldehyde) and 0.25 % GA (glutaraldehyde) in PEM buffer (0.1 M PIPES, 0.001 M MgCl<sub>2</sub> x 6 H<sub>2</sub>O, 0.001 M EDTA, 0.5 % Triton-X-100) for 10 min at room temperature. After fixation with PFA and GA, for quenching, cells were incubated in 1mL of freshly prepared 0.1% borohydride in PBS (phosphate-buffered saline) for 7 min and after that in 1 mL of 100 mM NH<sub>4</sub>Cl and 100 mM glycine in PBS for 10 min at room temperature. Cells were then washed with 1 mL of PBS, 3 times for 5 min. To block unspecific binding of antibodies, cells were incubated in 500 µL blocking/permeabilization buffer (2% normal goat serum (NGS) and 0.5% Triton-X-100 in water) for 45 min at room temperature. Cells were then incubated

in 500  $\mu$ L of primary antibody solution for 24h at 4 °C. Primary antibody that was used is rat anti-alpha Tubulin (Invitrogen). After primary antibody, cells were washed in PBS and then incubated in 500  $\mu$ L of secondary antibody solution for 45 min at room temperature. Secondary antibody is Alexa Fluor 594 (Invitrogen). To remove unbound secondary antibody from the sample, cells were washed three times with 1 ml of PBS for 5 min each, at room temperature. Acryloyl-X 1:100 (vol/vol) (Thermo Fisher Scientific) was diluted to 0.1 mg/mL in anchoring buffer. Sample was incubated with the anchoring solution for at least 6 h or overnight. The sample was washed two times in 1 ml of PBS, 5 min each, at room temperature, right before application of the gelation solution. Gel monomer components (8.6 wt% Sodium acrylate, 2.5 wt% Acrylamide, 0.15 wt% N,N'-Methylenebisacrylamide, 11.7 wt% Sodium chloride, 1x PBS and water) were mixed. The polymerization solution was applied to the sample and the gel was left to polymerize by 1 h incubation in a humidified chamber, at 37 °C. After that, sample was incubated in the digestion buffer (50 mM Tris pH 8.0, 1 mM EDTA, 0.5% Triton-X-100, 0.8 M guanidine HCl) with proteinase K added fresh every time the protocol was repeated (1:100, final concentration 8 units/mL) and was left for >8 h, or overnight in a humidified digestion chamber, at room temperature. After digestion, the remaining digestion buffer was removed from the dish and at least 2 mL ddH<sub>2</sub>O was added to the sample. ddH<sub>2</sub>O was removed after 10–20 min of incubation, using a Pipetboy or a vacuum pump and fresh ddH<sub>2</sub>O was added. The last step was repeated in sequence until no further expansion of the gel was observed, and this happened usually after four to five sequential water exchanges. Before the imaging, excess water was removed first by pipette and after that by a placing filter paper in the corners of the dish to minimize movement of the gel during imaging. Expansion factor was estimated from measured spindle length of the expanded metaphase spindle sample after dividing it with the spindle length of the non-expanded spindle in the same phase of the anaphase.

### 3.9 Imaging of fixed cells

All RPE-1 and U2OS cells fixed cells were imaged using Bruker Opterra Multipoint Scanning Confocal Microscope (Bruker) described above. In experiments where whole spindle stack was imaged, z-stacks were acquired at 30-60 focal planes for immunofluorescence images, and 60-120 focal planes for expanded samples, separated by 0.5  $\mu$ m with unidirectional xyz scan mode. A 60  $\mu$ m pinhole aperture was used and the xy-pixel size was 83 nm. For excitation of DAPI, GFP, mCherry or RFPa and SiR fluorescence, a

405, 488, 561 and 647 nm diode laser line was used, respectively. The excitation light was separated from the emitted fluorescence by using Opterra Dichroic and Barrier Filter Set 405/488/561/640 nm (DAPI/eGFP/TRITC/Cy5) (Chroma). Images were captured with an Evolve 512 Delta EMCCD Camera using 300 ms exposure time (Photometrics, Tucson, AZ, USA) with no binning performed. The frame average was performed 8 times for immunofluorescence images and 16 times for expansion microscopy images. All experiments were carried out using Nikon CFI Plan Apo VC  $\times 100/1.4$  numerical aperture oil objective (Nikon).

### 3.10 Parameters used to define metaphase-to-anaphase transition

The time of anaphase A onset for each individual cell was defined as the time point immediately prior to the separation of sister chromatid populations as annotated manually using visual inspection based on the increased distance between the sister kinetochore groups as cells transition from metaphase to anaphase. The onset of spindle elongation was defined as the time point immediately prior to the separation of two centrosomes as annotated by checking for continuous increase in the spindle length for two consecutive frames using custom made Matlab script (The MathWorks Inc., USA, R2018a) and double checked by visual inspection of original movies for possible errors.

### 3.11 Tracking of kinetochore, centrosome and chromosome motions

Kinetochores and centrosomes were tracked in time using Low Light Tracking Tool (LLTT), an ImageJ plugin (Krull et al., 2014). Tracking of kinetochores in the x, y plane was performed on individual imaging planes or on maximum-intensity projections of up to three planes. The position in z direction (3D) was ignored because it had a small contribution to the kinetochore movement. In order to obtain optimal tracking results, it was necessary to define good intensity offset in the channel with fluorescently labelled kinetochores. The intensity offset was defined by measuring the mean intensity around kinetochores in the first frame before start of tracking using 'freehand selection' tool in Fiji. Sometimes, when photobleaching was prominent, bleach correction using Histogram Matching Method in Fiji was done to compensate for a decrease in background intensity in time. Also, it was necessary to define EMCCD gain and Electrons per A/D count of the used EMCCD camera to correct the measured flux of the object and background noise. The EMCCD-GaussianML tracking



algorithm method was used (Krull et al., 2014) because it yielded more precise results compared with Gaussian-ML method, especially in situations when fast movement of the tracked object occurred (on a scale of micron per frame or more). All tracked objects were double checked by eye to ensure that tracking was accurate, because it was inaccurate in situations of an uneven intensity of tracked objects and in situations when multiple similar objects appeared in close proximity. If those cases were predominant, tracking was performed manually extracting xyz-coordinates of each kinetochore.  $\sigma$  value (standard deviation of the Gaussian used to approximate the Point Spread Function (PSF) of the tracked objects) was set to 1 to encompass just the tracked kinetochore. Detailed quantitative analysis of centrosome and kinetochore location was performed using custom made MATLAB scripts which determines the distance between the centroid of the sister kinetochores. Chromosomes were tracked using ImageJ line tool from a centromere region of a one sister chromosome to the same region of another sister. The velocities of kinetochore and centrosome separation were measured between 1 and 3 minutes after the onset of anaphase,  $(d_3-d_1)/(2t)$  where  $d$  is the distance between sister kinetochore centroids subtracted to the same distance in the last frame before anaphase or pole-to pole distance subtracted to the same distance in the last frame before anaphase (termed delta for all parameters defined this way) and  $t$  is the time period. This interval is chosen because these parameters are linearly increasing during this time period in untreated human cells (Afonso et al., 2014; Su et al., 2016).

### 3.12 Quantification of microtubule stability

MT stability was measured on single z-planes acquired in photoactivation assay. The onset of photoactivation was set as a first point of measurement, after all dots finished on predetermined photoactivation line, and second point of measurement was placed in a frame 30s after onset in all conditions imaged. Region between separated chromosomes in the last frame was used as a borderline for drawing a 100px thick line in ImageJ, horizontal to the spindle long axis, from which the fluorescence profile was extracted. The mean background fluorescent intensity measured in the same frame in cytoplasm (measured in ImageJ by drawing a 100px thick line), was subtracted from obtained intensities. The obtained values were plotted in SciDavis program (Free Software Foundation, Inc., Boston, MA, USA) and area under the peak was linearly integrated to obtain area of intensity for that frame. The same was performed for the frame defined as the onset of photoactivation using region of the same dimensions. The two values were divided to give estimation on how much of photoactivated-

$\alpha$ -tubulin fluorescence was lost following 30 s period in all conditions tested giving estimation of relative microtubule turn-over and stability.

### 3.13 Quantification of sliding velocity

The hTERT-RPE-1 permanently transfected and stabilized using PA-GFP- $\alpha$ -tubulin where imaged in a one middle z-plane using unidirectional xyz scan mode and with “Fast Acquisition” option in software enabled with interval of 0.8s between two frames. The width of photoactivated spot in the spindle midzone was measured using ImageJ by drawing a line segment along the photoactivated region, from the moment when photoactivation of tubulin finished for all dots on line segment used for photoactivation, across time frames separated by 0.8s, to the last frame frame of measurable photoactivation signal in the spindle midzone. The width was plotted as a function of time in Matlab home written script and on each curve linear regression was performed for points starting from 0, representing start of a measurement, to the 30s after. The velocities were calculated from a slope of a regression line. The position of a centrosome was determined only in those cells in which signal of photoactivated  $\alpha$ -tubulin could be discerned on both poles. Multiple bundles were tracked in single cell were appropriate but their velocities values were averaged for correlation graphs and bar plots.

### 3.14 Quantification of PRC1 overexpression

The fluorescence intensity signal of PRC1-mCherry was measured on the whole spindle region using ImageJ on sum-intensity projection of all z-stacks acquired. The background fluorescence intensity measured in the cytoplasm was subtracted from the mean value obtained, and this value was divided with number of z-stacks used in sum projection.

### 3.15 CRISPR KO cell scoring

CRISPR PRC1 KO cell were scored for successful knockout of PRC1 5dy post-induction with doxycycline by fixing cells with cold-methanol protocol (described above) and staining with mouse monoclonal PRC1 antibody (sc-376983, Santa Cruz Biotechnology), diluted 1:50, and Alexa Fluor 488 (Invitrogen) secondary antibody (diluted 1:1000). SiRNA, 100nM final concentration, was added post-fixation, 30 min before imaging, to stain DNA in order to identify anaphase cells. Successful KO without noticeable PRC1 signal in

the spindle midzone was observed in 90% of analysed cells (60 out of 68 cells) and 10% of the cells imaged had a normal PRC1 appearance, localising to the spindle midzone, similarly to all non-induced controls imaged.

### 3.16 Image processing and statistical analysis

Image processing was performed in ImageJ (National Institutes of Health, Bethesda, MD, USA). Quantification and statistical analysis were performed in MatLab. Figures were assembled in Adobe Illustrator CS5 and Adobe Photoshop CS5 (Adobe Systems, Mountain View, CA, USA). All kymographs were generated in ImageJ on maximum intensity projections of vertically rotated images by using a “Reslice” command and then performing maximum intensity projection and montage images were generated in ImageJ in single focal plane vertically oriented images using “Make Montage” command. The kymograph and montage images were rotated in every frame to fit the long axis of the spindle to be parallel with the central long axis of the box in ImageJ and spindle short axis to be parallel with the central short axis of the designated box in ImageJ. The designated box sizes were cut in the same dimensions for all panels in Figures where the same experimental setups were used across the treatments. When comparing different treatments in channels with same proteins labelled, minimum and maximum of the intensity in that channel was set to the values in the control treatment. When indicated, smoothing of images was done using Gaussian blur function in ImageJ ( $s=1.0-1.5$ ). Data are given as mean  $\pm$  s.t.d., unless otherwise stated. p values were obtained using unpaired two-sample Student’s t-test (significance level was 5%). When comparing the same parameters cell by cell, we used paired two-sample Student’s t-test (significance level was 5%).  $p < 0.05$  was considered statistically significant, very significant if  $0.001 < p < 0.01$  and extremely significant if  $p < 0.001$ . Values of all significant differences are given with degree of significance indicated (\* $0.01 < p < 0.05$ , \*\* $0.001 < p < 0.01$ , \*\*\* $p < 0.001$ , \*\*\*\* $< 0.0001$ ). For linear regression correlation measure between two parameters, nonparametric Spearman correlation coefficient, termed  $r_s$ , was used where  $p < 0.001$ . The number of analysed cells and specific parameters is given in the respective figure panel.

## 4 RESULTS AND DISCUSSION

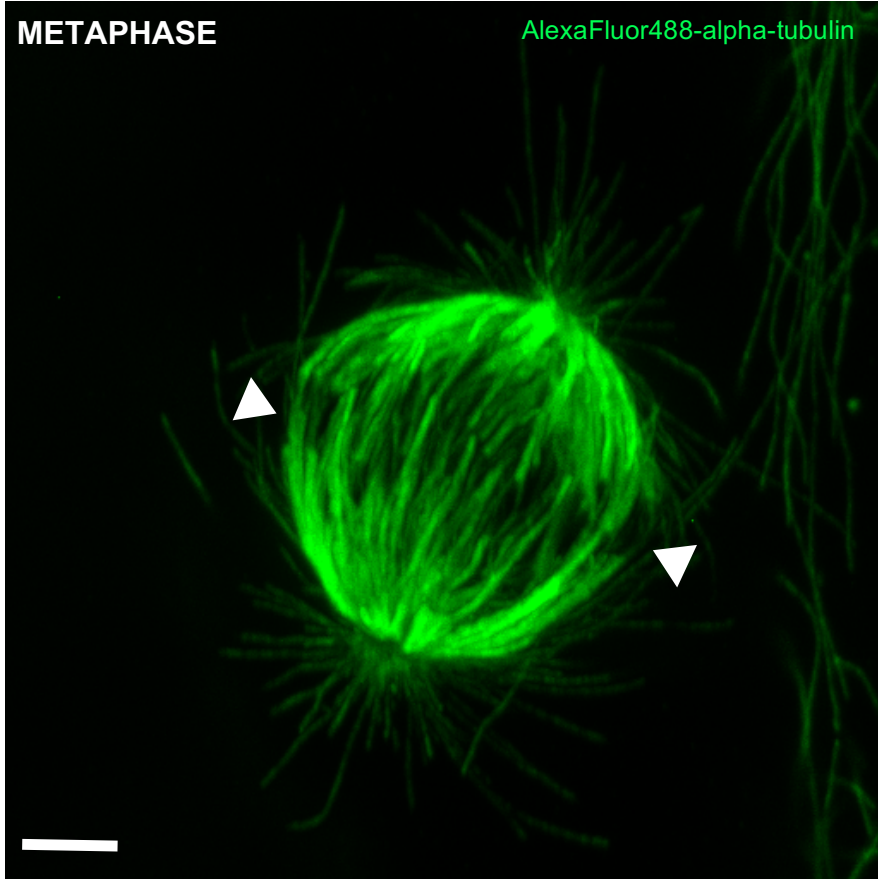
### 4.1 Motors that generate sliding forces during anaphase

#### 4.1.1 Expansion microscopy of mitotic spindles

First, to get a better insight into the structure of the anaphase spindle, expansion microscopy of the anaphase and metaphase spindles was performed, a new super-resolution technique based on physical isotropic expansion of the sample immersed in swellable polymer gel (Tillberg et al., 2016). The improved fixation techniques was also deployed, avoiding common fixation with cold methanol, where most unstable MTs are lost presumably because low temperatures generally tend to destroy unstable fraction of MTs within the spindles. In that regard, fixation with cytoskeletal extraction buffers was used, a somewhat forgotten concept based on preservation of the cytoskeleton structures during early *in vitro* fixation methods (Osborn and Weber, 1977). It was showed that anaphase mitotic spindle in human non-transformed RPE-1 cell line is composed of similar proportions of the main MT populations within the spindle, namely kinetochore, bridging and astral MTs, as seen in metaphase spindles of the same cells (Figure 20). Furthermore, bridging MTs were clearly visualised as discrete robust structures passing from one side of the spindle to the other, similar to metaphase spindle, encompassing a significant portion of the MTs within the anaphase spindle (Figure 20).

**METAPHASE**

AlexaFluor488-alpha-tubulin



**ANAPHASE**

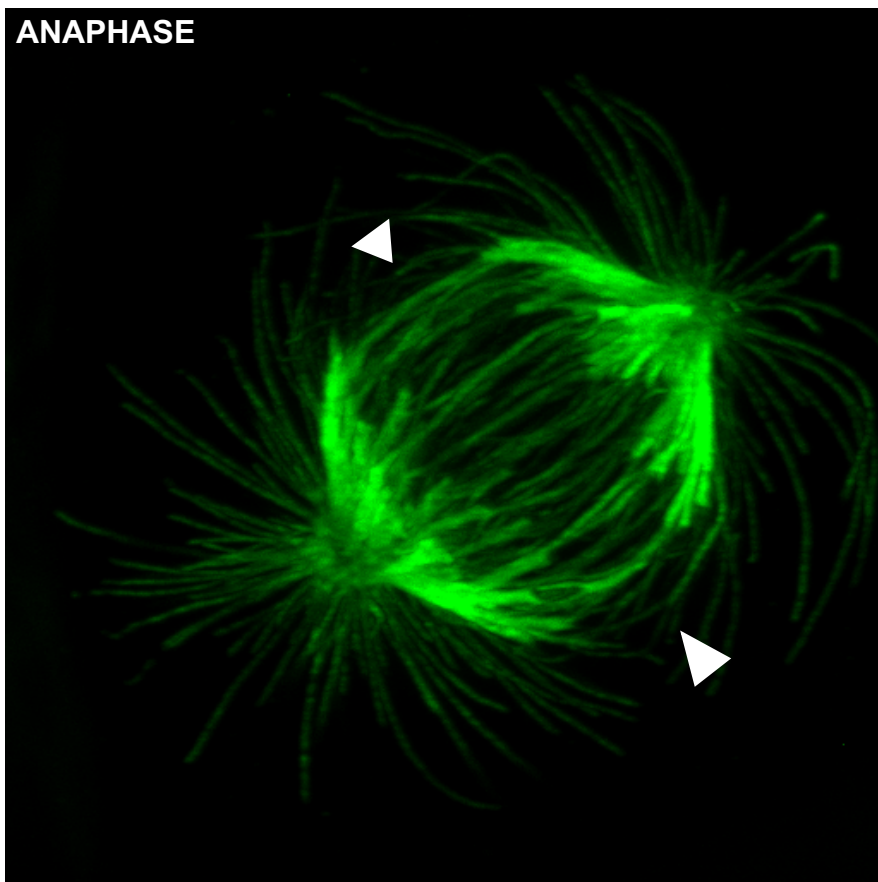


**Figure 20. Bridging microtubules are clearly visualised in both metaphase and anaphase spindles of human RPE-1 cells.** Maximum z-projection of the expanded metaphase (top) and anaphase (bottom) mitotic spindles of the human RPE-1 cells labelled with secondary AlexaFluor488 antibody targeted against  $\alpha$ -tubulin primary antibody. Region where bridging MTs are located is indicated with an arrowhead. Scale bar, 5  $\mu$ m.

#### 4.1.2 Role of EG5 and KIF15 redundancy during anaphase

Once it was established that bridging MTs are present as discrete structures in the anaphase spindle of human non-transformed cells the study turned to testing which motors are responsible for force-generation within the bridging MTs by sliding MTs apart. To test the role of different motor and non-motor proteins in spindle elongation a candidate-based assay was designed accordingly to specific protein localisation and functional patterns within anaphase midzone was developed (see Introduction section), with a main goal to find a combination of proteins that can completely abrogate anaphase B movements. As a primary approach, all force-producing proteins known to localise to the spindle midzone and all proteins known to slide antiparallel MTs apart from previous *in vitro* work (see Introduction section for more details) were depleted. Moreover, a minimal model system was used because extensive tubulin labelling with mCherry fluorophore in overexpression regime can adversely affect anaphase velocities, as seen in U2OS cells with stable expression of tubulin labelled with mCherry (Figure 21). The minimal model system used was a human non-transformed RPE-1 cell line stably expressing only two necessary components, CENP-A-GFP for labelling of kinetochores, and centrin1-GFP for labelling the centrioles as component of centrosomes. Also, the main quantitative measures resolved around tracking and quantification of kinetochore separation to observe a general effect of specific perturbation on anaphase, tracking of centrosomes to observe effect on spindle elongation and quantification of distance between kinetochore and its respective centrosome to observe the effect on poleward anaphase A movement (Vukusic et al., 2019). It was reasoned these would give the best measure of forces acting in anaphase on these important structures, since this is standard in the field (Scholey, 2016). As a measure of distance between anaphase parameters a *delta* value was used for measurements of distances between kinetochores and centrosomes (defined in Materials and methods) (Figure 22), because this approach nullifies effects from metaphase, like variable spindle sizes observed at the beginning of anaphase across multiple treatments (Figure 25). This approach was justified because peak-metaphase spindle size does

not correlate with spindle elongation velocities across the treatments in RPE-1 cells (Figure 26I). Moreover, use of this value did not affect the calculations of the velocities of kinetochore separation and spindle elongation, since these are calculated from anaphase onset only (see Material and methods).

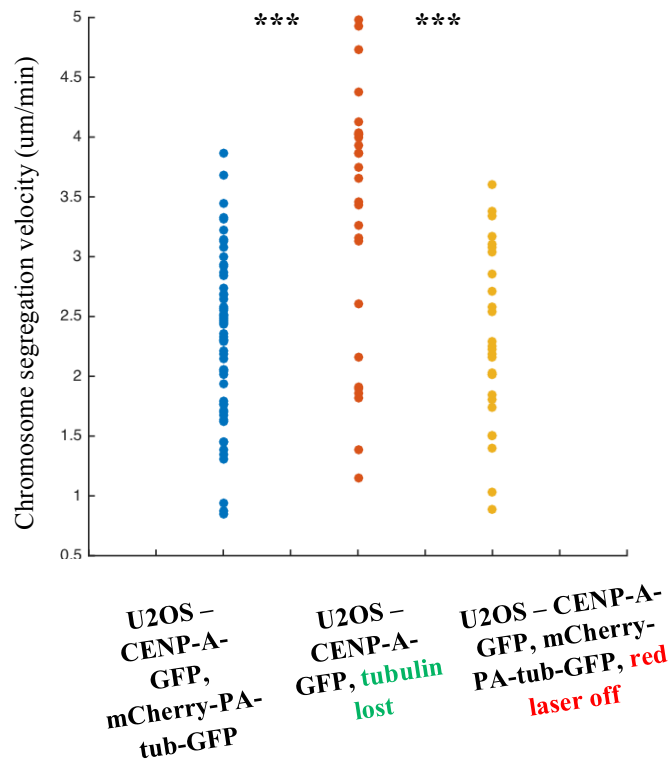


**Figure 21. Labelling of alpha-tubulin with mCherry alternate chromosome segregation rates.** Quantification (scatter plot) of velocity of separation of sister kinetochores measured from the onset of anaphase for different conditions as labelled. Note: lack of imaging of mCherry-alpha-tubulin (orange row) cannot restore the chromosome segregation values as loss off tubulin labelling can. Statistics: t-test (\*\*P < 0.001).

As a first step in study of molecular motors responsible for force-generation during spindle elongation, a complex storyline developed behind the most recognized sliding motor, kinesin-5 family member EG5 was explored, suggested by many to be a main sliding motor in different situations during mitosis (see detailed review by Mann and Wadsworth, 2019). To check if EG5 is indeed crucial for anaphase spindle elongation EG5 small molecule drug inhibitor S-trityl-L-cysteine (STLC) (Skoufias et al., 2006) was added to the late metaphase cells, trying to get close to the metaphase-to-anaphase transition. STLC was used because it

quickly inhibits Eg5-driven MT sliding velocity by targeting the catalytic domain of Eg5 and inhibiting Eg5 basal and MT-activated ATPase activity as well as mant-ADP release of the motor (Skoufias et al., 2006). This approach was used because adding the STLC earlier in mitosis leads to immediate spindle collapse into monopolar spindle (Gayek and Ohi, 2014) (Figure 24) and adding STLC in anaphase was complicated because anaphase duration is very short and while adding the drug cells can pass through large fraction of anaphase, complicating the conclusions.

Although plus-end directed motor kinesin-5 has been implicated as a major candidate for spindle elongation in budding yeast (Straight et al., 1998), its inhibition by STLC in RPE-1 human cells, shortened metaphase spindle immediately after addition of the drug (Figures 23, 24, 25), but after anaphase onset did not perturb spindle elongation velocities nor chromosome segregation velocities (Figure 24). Also, a fraction of cells did not respond to STLC treatment by reducing metaphase spindle length as some spent few minutes in unperturbed metaphase in STLC medium (Figures 23 and 24), before they entered anaphase with normal velocities. As can be seen in Figure 25, all other conditions where STLC was used, alone or in combination with some other perturbation, significantly shortened metaphase spindles of those cells that eventually entered anaphase, and no combination showed obvious additive effect to this inhibition.

Furthermore, in RPE-1 cells depleted of PRC1 and KIF8A, metaphase spindle length was longer when compared to controls, and these are the only treatments tested that increased the length of metaphase spindles significantly compared to controls, while depletion of NuMa, combined depletion of CLASP1 and CLASP2 proteins and Kif15 significantly shortened the metaphase spindle length (Figure 25), but in these conditions spindle collapse was never observed during metaphase.

On the other hand, a significant fraction of cells treated with STLC in metaphase collapsed into monopolar spindles, as reported previously (Gayek and Ohi, 2014) (Figure 24), meaning that EG5-outward force generation is crucial during metaphase in this system, but dispensable during anaphase when inward-forces acting on poles, that are balancing the outward EG5-generated force, are turned down (Su et al., 2016). It was noticed that addition of STLC to more prometaphase spindles, with uncongressed chromosomes, caused almost certain spindle collapse (data not shown), while in metaphase three distinct phenotypes can be observed, as noticed above. When added in metaphase, addition of STLC led to either spindle collapse into practical monopole, when spindle length shortened below 8  $\mu\text{m}$  (data not shown), representing point of no return (Figure 25) or to a new steady state spindle length



achieved on the somewhat shorter or significantly shorter spindle length values (Figure 23B), where last two categories always enter anaphase after variable times (Figures 23B and 24D).

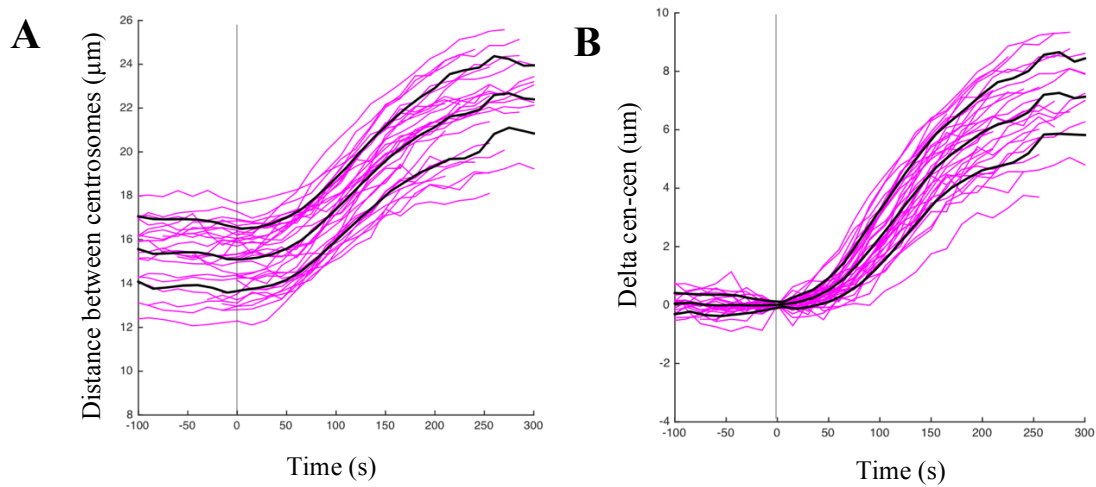


**Figure 22. Delta value as a measure of centrosome separation. (A)** Centrosome distance plotted as a function of time where zero represents onset of anaphase. Black lines indicate mean and standard deviation from a mean value for control RPE-1 cells. **(B)** Plot of relative centrosome separation distance (delta) defined as the centrosome-to-centrosome (cen-cen) distance at time  $t$  minus the cen-cen distance at  $t = 0$ , over time. Time 0 represents onset of centrosome separation (vertical black line). Black lines indicate mean (middle) and standard deviation from a mean value for the same pool of control RPE-1 cells as in A.

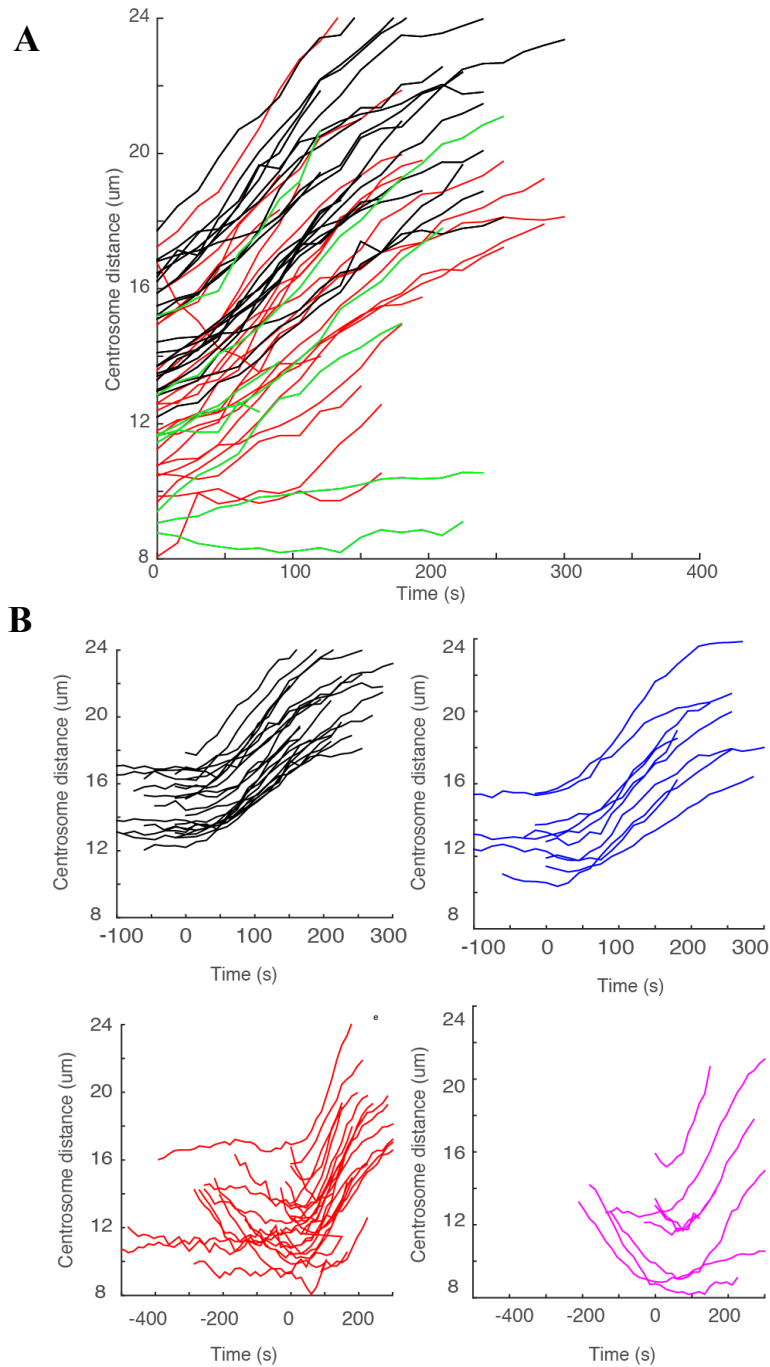


**Figure 23. Inhibition of STLC, with or without combined depletion of KIF15, is dispensable for anaphase spindle elongation. (A)** Centrosome distance plotted as a function of time where zero represent onset of centrosome separation. Black lines indicate control cells, red lines indicate STLC-treated cells and green lines indicate KIF15-depleted cells combined with inhibition of EG5 by STLC. **(B)** Centrosome distance plotted as a function of time where zero represent onset of kinetochore separation. Black lines; control cells, red lines;

STLC-treated cells, magenta lines; KIF15-depleted cells combined with inhibition of EG5 by STLC, blue lines; KIF15 depleted cells.

Next, to explore whether redundancy between kinesin-5 EG5 motor and kinesin-12 KIF5 motor could explain lack of effect on spindle elongation seen after STLC treatment, similar to what was observed in metaphase of human tumour cell lines where kinesin-12 is acting redundantly with EG5 in control of the metaphase spindle length (van Heesbeen et al., 2014; Vanneste et al., 2009), both proteins were perturbed in the same cells. In that regard, spindles were treated with STLC, as described above, but this time in combination with a depletion of kinesin-12 (KIF15) motor protein (Tanenbaum et al., 2009) using a small interfering RNA (siRNA) approach (Figure 26).

Surprisingly, this combination yielded similar results when compared with control and STLC-treated cells, both in regard of chromosome segregation, and spindle elongation velocities (Figure 26). Besides, a significant delay in anaphase B start respective to start of anaphase A was observed, after STLC treatment, and in the first minute or more after onset of chromosome segregation spindle poles frequently continue to collapse, or halt, while kinetochores moved poleward to them (Figures 24 and 36). Nevertheless, in almost all cases of STLC addition, in combination with KIF15 depletion or not, spindles collapsed or eventually entered anaphase and completed spindle elongation with unperturbed velocities (Figures 24, 26 and 36). Also, the depletion of KIF5 alone did not affect anaphase velocities (Figure 26), although shorter metaphase spindles were observed after this treatment (Figure 25), as published previously (Sturgill and Ohi, 2013). This suggested that other redundant pathways may be acting during generation of outward forces during anaphase in human cells, and accordingly, main metaphase force generators, acting dominantly on spindle length during that phase, cannot perturb spindle elongation during anaphase.

Moreover, since spindles depleted of KIF15 and treated with STLC tend to shorten their lengths drastically (up to 8  $\mu\text{m}$ , Figure 23) but can still enter anaphase with unperturbed elongation velocities (Figure 26), it was tested whether bridging interpolar microtubules are preserved in such spindles and whether sliding within those microtubules can be observed, as was predicted to be the case. For this purpose, U2OS cell line expressing kinetochore marker CENP-A-GFP, photoactivatable (PA)-GFP-alpha-tubulin and mCherry-alpha-tubulin was used in which KIF15 protein was depleted by siRNA approach and then STLC was added during late metaphase, just as in RPE-1 cells. As can be seen from Figure 27, such spindles possessed bridging fibers between sister kinetochores, even though spindle length is

considerably shorter than in control spindles, which is around 13 microns for this cell line (data not shown) (Vukusic et al., 2017). Furthermore, sliding within bridging microtubules was observed during anaphase after photoactivation of PA-alpha-tubulin within these bundles (Figure 27), indicating that bridging microtubules remained functional even though spindle length shortened drastically after inhibition of EG5 protein and depletion of KIF15 protein.

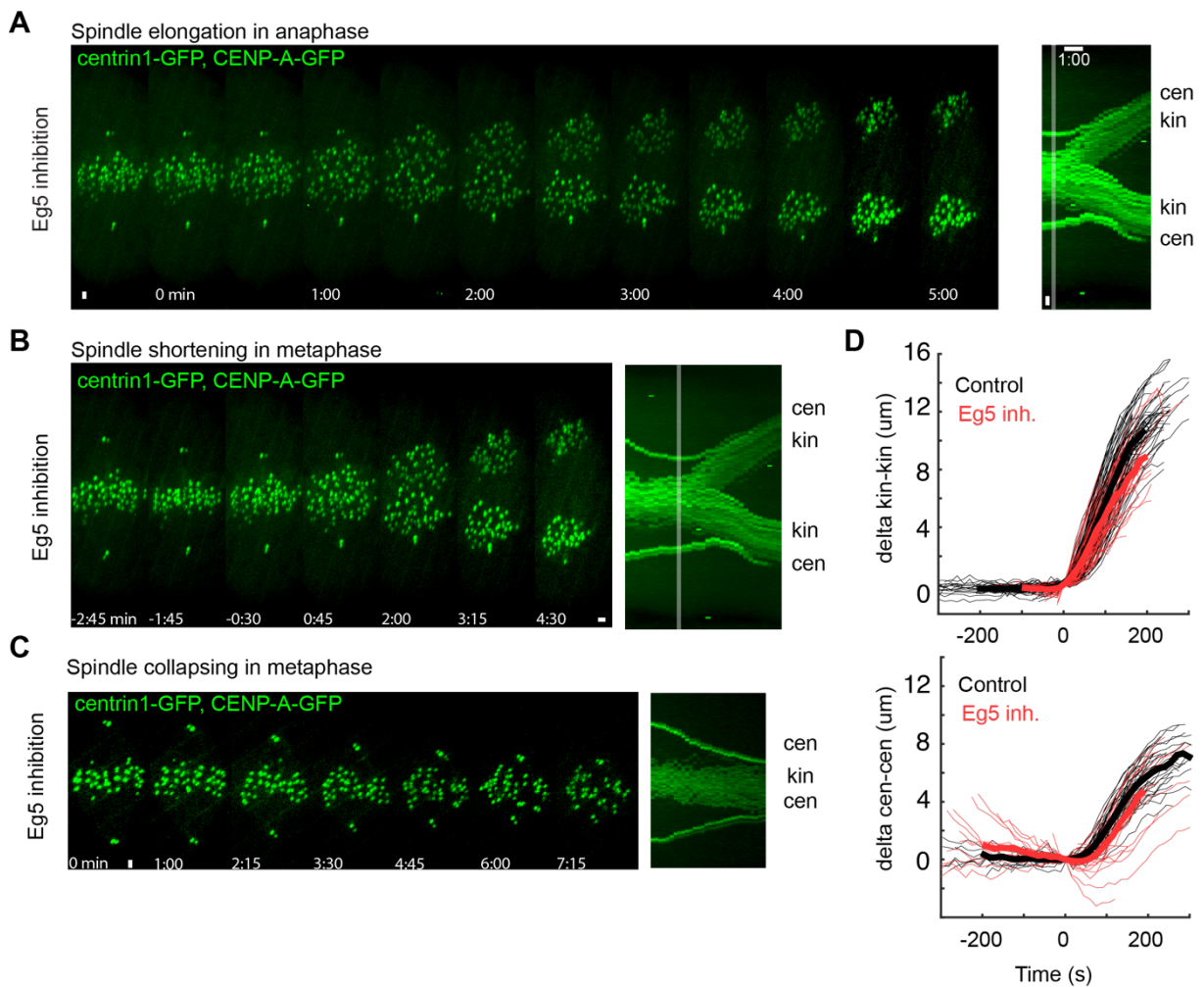


**Figure 24. Inhibition of EG5 is crucial for maintenance of metaphase spindle length but dispensable for anaphase spindle elongation.** (A) Live cell images of S-trityl-L-cysteine (STLC)-treated RPE-1 cell stably expressing CENP-A-GFP and centrin1-GFP. kin-kinetochore and cen-centrosome. (B) Live cell images of STLC-treated RPE-1 cell show shortening of spindle in metaphase and normal spindle elongation in anaphase. Time 0 represents anaphase onset. (C) Live cell images of RPE-1 cell show spindle collapsing during metaphase after STLC treatment. (D) Plots of relative kinetochore and centrosome separation distance (delta) defined as the kinetochore-to-kinetochore (kin-kin) and centrosome-to-centrosome (cen-cen) distance at time t minus the kin-kin and cen-cen distance at t = 0, over

time. Individual kinetochore and centrosome pairs (thin lines), mean (thick lines). Time zero represents start of STLC treatment. Images are maximum projection of acquired z-stack. Time shown as minutes:seconds. Vertical scale bars, 1  $\mu\text{m}$ . Horizontal scale bar, 1min.

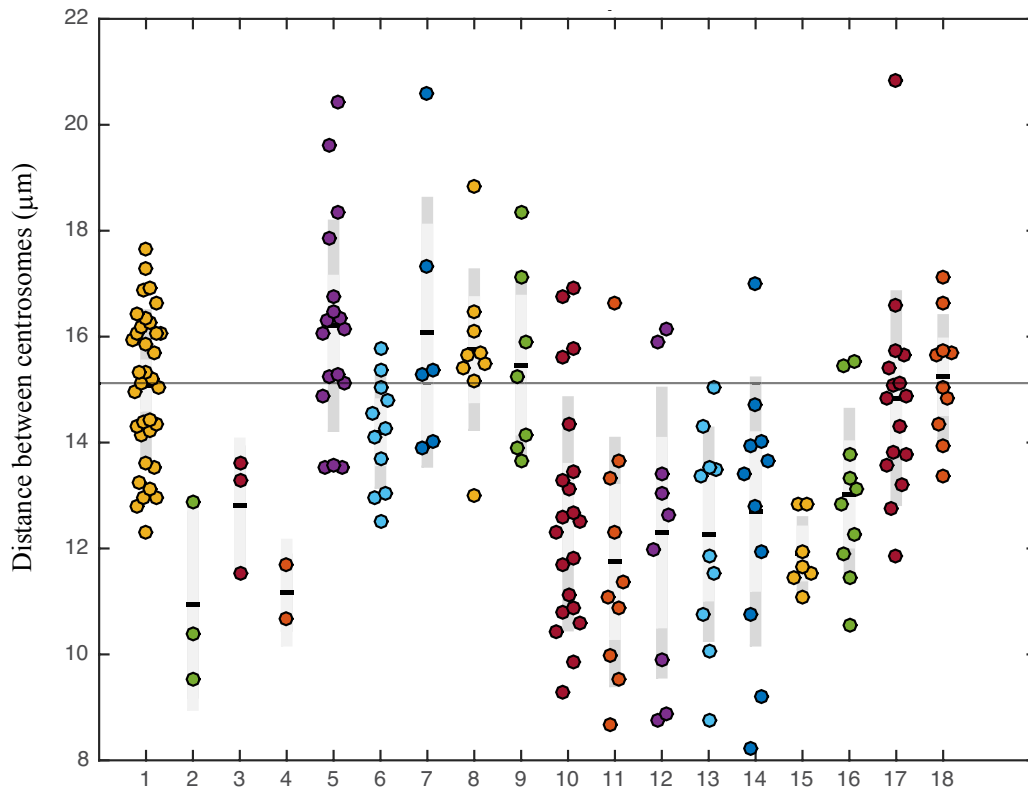


**Figure 25. Multiple factors influence maintenance of metaphase spindle length in RPE-1 cells with Eg5 motor being the dominant player.** Quantification (univariate scatter plot) of peak metaphase spindle length across different conditions in RPE-1 cells. Horizontal grey line indicates mean value for the control population of cells. Legend: 1-control, 2-CLASP1 depletion, 3-CLASP+CLASP2 depletion, 4-NuMa depletion. 5-PRC1 depletion, 6- KIF4A depletion, 7-KIF18A depletion, 8-EB3 depletion, 9-KIF18A+PRC1 depletion, 10-EG5 inhibition, 11-PRC1 depletion+EG5 inhibition, 12-KIF15 depletion+EG5 inhibition, 13-MKP1 depletion+EG5 inhibition, 14-MKLP1+KI15 depletion+EG5 inhibition, 15-MKLP1+MKLP2 depletion+EG5 inhibition, 16-KIF15 depletion, 17-MKLP1 depletion, 18-MKLP1+KIF15 depletion.

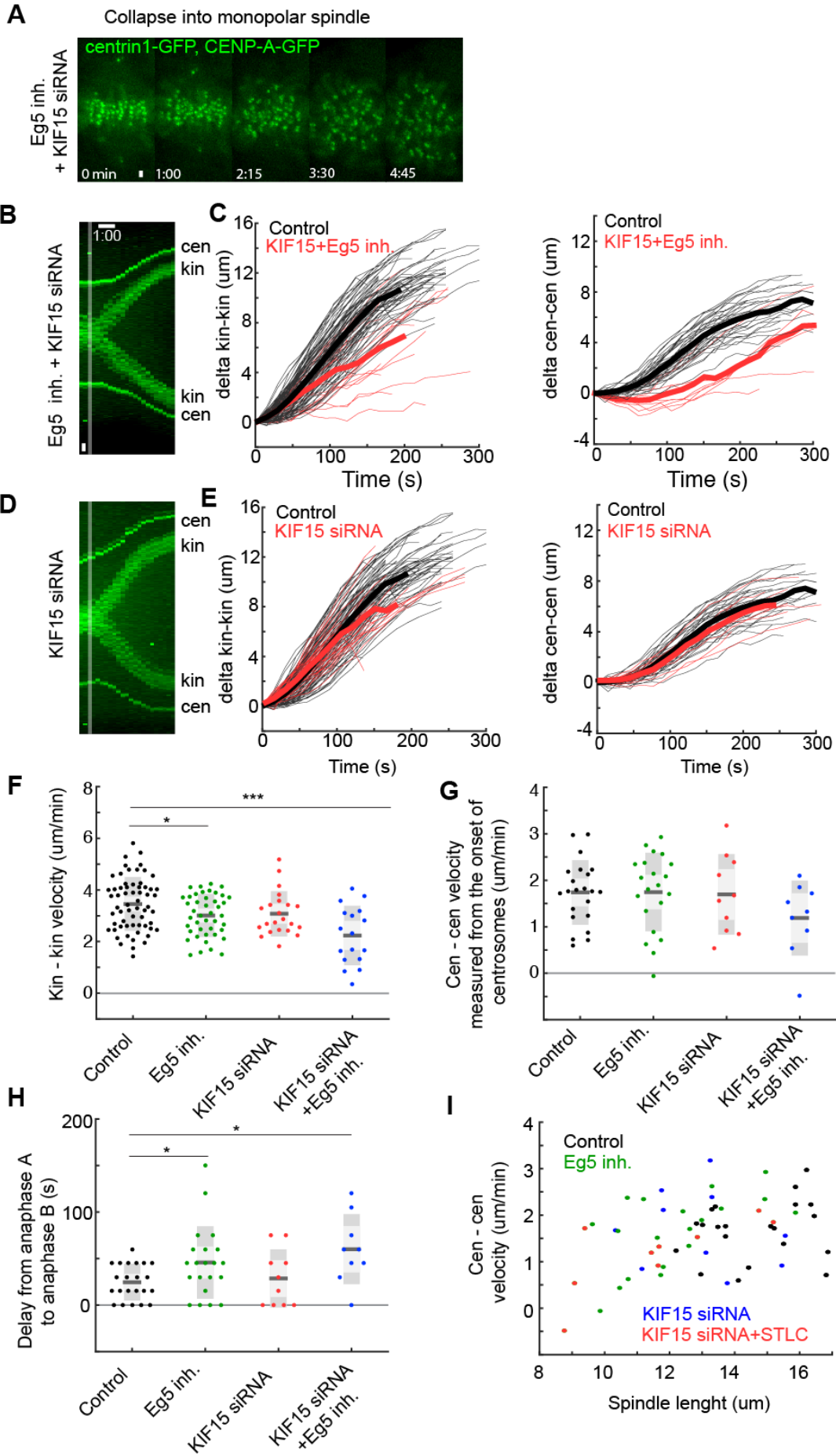
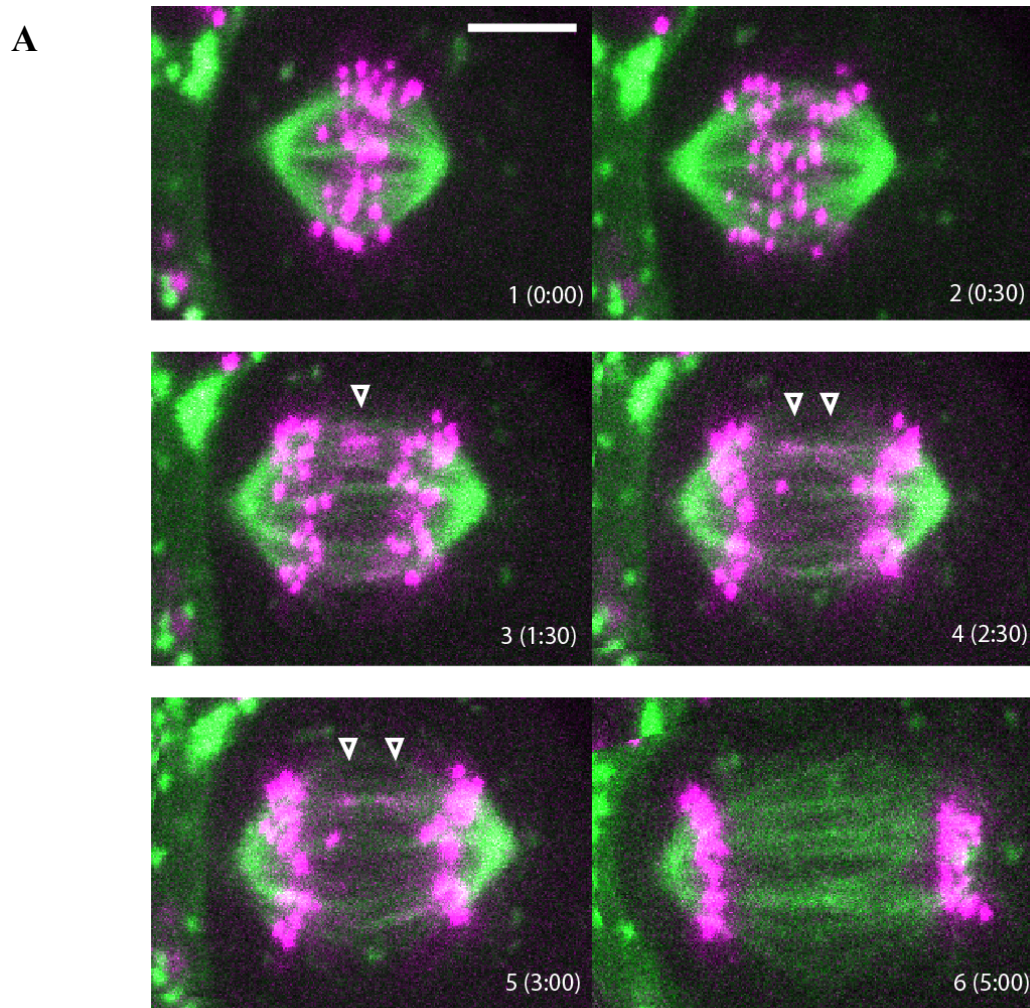


**Figure 26. Depletion of KIF15 and inhibition of EG5 combined with KIF15 depletion does not affect anaphase spindle elongation.** (A) Live cell images of KIF15 siRNA depleted and S-trityl-L-cysteine (STLC)-treated RPE-1 cell stably expressing CENP-A-GFP and centrin1-GFP showing metaphase spindle collapse and monopolar spindle formation. kin-kinetochore and cen-centrosome. Time zero represents start of STLC treatment. (B) Kymograph (consecutive maximal intensity projections onto the x-axis) of the live cell images of KIF15 siRNA depleted and S-trityl-L-cysteine (STLC)-treated RPE-1 cell stably expressing CENP-A-GFP and centrin1-GFP. (C) Plots of relative kinetochore and centrosome separation distance ( $\Delta$ ) defined as the kinetochore-to-kinetochore (kin-kin) and centrosome-to-centrosome (cen-cen) distance at time  $t$  minus the kin-kin and cen-cen distance at  $t = 0$ , over time. Individual kinetochore and centrosome pairs (thin lines), mean (thick lines). (D) Kymograph of the live cell images of KIF15 siRNA depleted RPE-1 cell. (E) Plots of relative kinetochore and centrosome separation distance over time. (F) Quantification (univariate scatter plot) of velocity of separation of sister kinetochores measured from the onset of anaphase. Boxes represent standard deviation (dark grey), 95% standard error of the mean (light grey) and mean value (black). Statistics: t test ( $***P < 0.001$ ;  $****P < 0.0001$ ). (G) Quantification of velocity of separation of spindle elongation measured from the onset of centrosome separation. (H) Quantification of spindle elongation delay (anaphase B) calculated as the difference between spindle elongation onset and kinetochore separation onset (anaphase A). Statistics: t test ( $*P < 0.05$ ). Note: EG5 inhibition by STLC treatment, with or without depletion of KIF15, induces a small delay in spindle elongation start compared to controls. (I) Linear regression and distribution of spindle elongation velocity (cen-cen) versus initial spindle length, measured at the beginning of anaphase, in indicated conditions. Note: initial spindle length and spindle elongation velocities are not correlated across conditions. Images are maximum projection of acquired z-stack. Time shown as minutes:seconds. Time 0 represents anaphase onset. Vertical scale bars, 1  $\mu$ m. Horizontal scale bar, 1min.





**B**

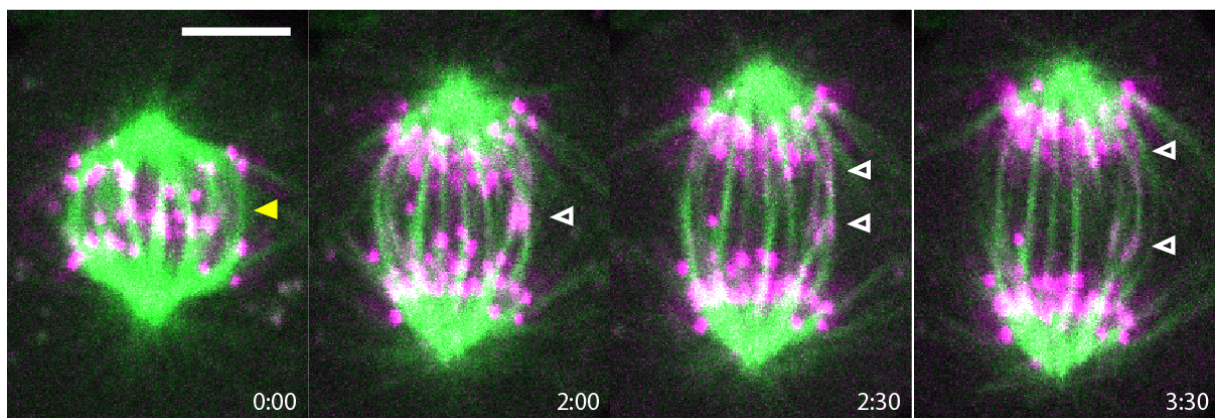


**Figure 27. Short spindles observed after depletion of KIF15 and inhibition of EG5 by STLC are able to elongate the spindle and possess interpolar microtubules capable of sliding during anaphase. (A)** Time-lapse images of the spindle in a U2OS cell stably expressing CENP-A-GFP, PA-alpha-tubulin (both magenta) and mCherry-alpha-tubulin (green), during anaphase and after photoactivation of PA-GFP-tubulin at time 1:30 within



bridging fibers after depletion of KIF15 by siRNA and inhibition of EG5 by 80  $\mu$ M STLC. White open arrowheads indicate the central part of the photoactivated spot, as it separates during anaphase. Time zero represents the onset of anaphase. **(B)** Time-lapse images of the spindles in U2OS cell line stably expressing CENP-A-GFP, PA-alpha-tubulin (both magenta) and mCherry-alpha-tubulin (green), during anaphase and after photoactivation of PA-GFP-tubulin at time 2:00 within bridging fibers after depletion of KIF15 by siRNA and inhibition of EG5 by 80  $\mu$ M STLC. Time zero represents the start of imaging. Yellow full arrowhead indicates the presence of bridging fibers within short spindle. Time zero represents the onset of anaphase. Scale bar; 5  $\mu$ m.

#### 4.1.3 Depletion of PRC1 does not affect velocity of spindle elongation

To test other candidates known to localise to spindle midzone region, the study turned to PRC1 protein, main bundler of antiparallel MTs (She et al., 2019). First, to explore how dynamics of overlap length, marked by PRC1 protein, changes during anaphase, U2OS cell line with kinetochores labelled with CENP-A-GFP and PRC1 labelled with mCherry transiently expressed from an introduced plasmid was used (see Materials and methods for details). As can be seen from Figure 28, length of PRC1 labelled overlaps tended to decrease during very early anaphase, as published by others (Pamula et al., 2019), and as expected from system in which MT sliding is present within overlaps, but extent of sliding did not follow the extent of spindle elongation (Figure 28B). This suggested that MTs must polymerize at the plus-ends in order to balance the nearly constant overlap length seen on Figure 28 after initial shortening during early anaphase. Similar dynamics has been observed recently by others (Pamula et al., 2019), but interpretation of these results lead us to different conclusions (see Concluding discussion for details).

Alternatively, the force required for spindle elongation could be generated in the interpolar region by a plus-end directed motor other than EG5 and KIF15. To test this assumption, the main crosslinker of antiparallel MTs and scaffold for recruitment of multiple motors, protein regulator of cytokinesis 1 (PRC1) (Lee et al., 2012) was depleted, with an siRNA approach. A high concentration of siRNA for the PRC1 depletion protocol must be used (see section Material and Methods for details) since this is a main bundler of antiparallel MTs in the mitotic spindle, and these are, as was envisioned in my hypothesis, the main structures responsible for force-generation during spindle elongation (Vukušić et al., 2019).

As seen in Figure 29, the depletion of PRC1 by this approach obtained almost complete removal of PRC1 protein from a spindle after 48h treatment with siRNA when compared to control cells. Interestingly, PRC1 depletion sometimes led to excessive spindle and cell elongation, as reported previously (Pamula et al., 2019) (Figure 30), while not affecting rates of spindle elongation and chromosome segregation in early anaphase (Figure 29), which ends in a point of time where in most control cells spindle elongation usually stops (Vukusic et al., 2019). Also, depletion of PRC1 in RPE-1 cells affected metaphase spindle length, by increasing it significantly compared to control cells treated with non-targeting siRNA (Figures 25 and 29).

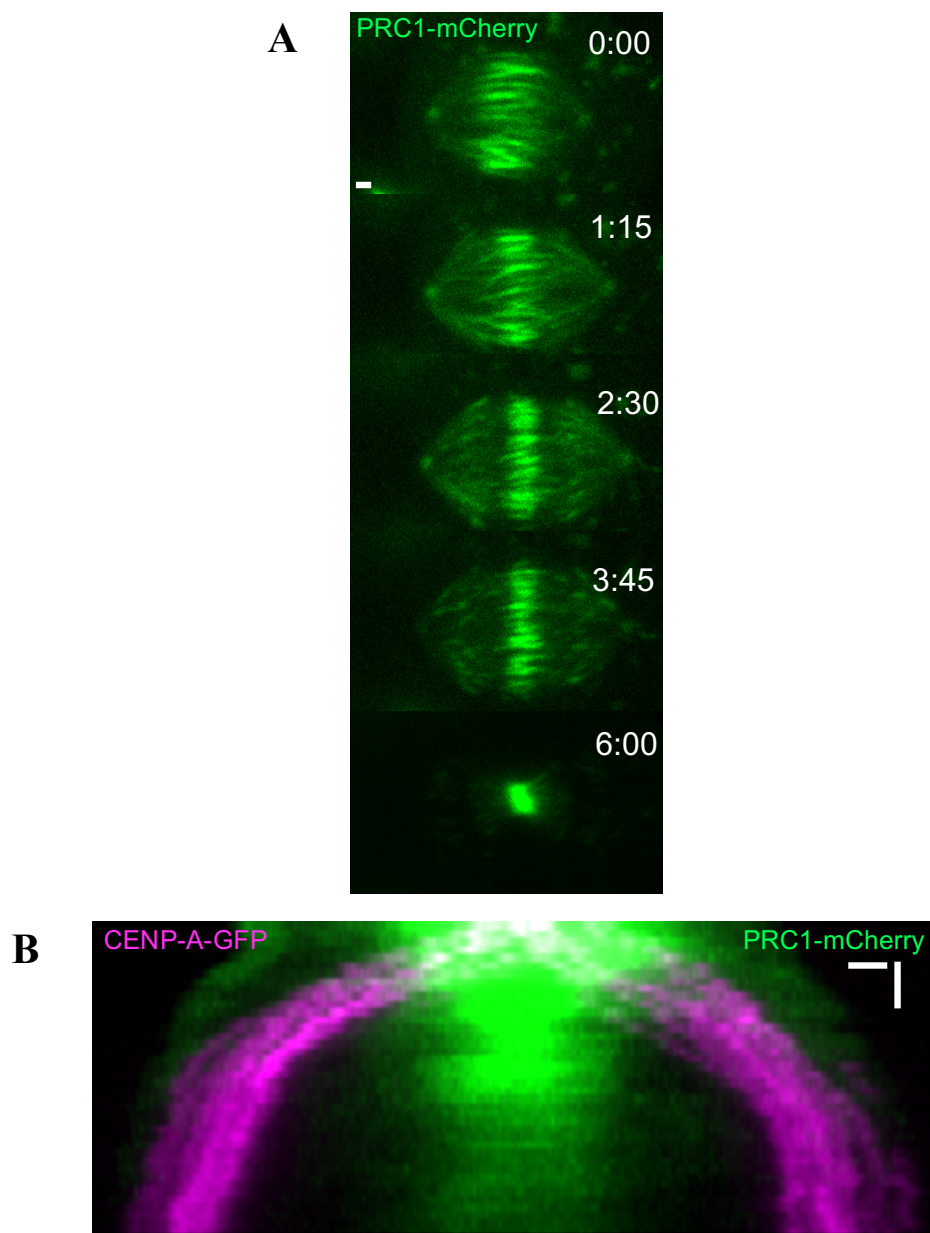


**Figure 28. Dynamics of PRC1-labelled overlaps during anaphase. (A)** Live cell images of U2OS cells during anaphase stably expressing CENP-A-GFP (channel not shown) and transiently expressing PRC1-mCherry. Time 0 represents onset of anaphase. Images are maximum projections. **(B)** Kymograph (consecutive maximum-intensity projection onto the y axis) of the U2OS cell (different then in A) stably expressing CENP-A-GFP (magenta) and transiently expressing PRC1-mCherry (green). Time shown as minutes:seconds. Vertical scale bars, 1  $\mu$ m. Horizontal scale bar, 1 min.

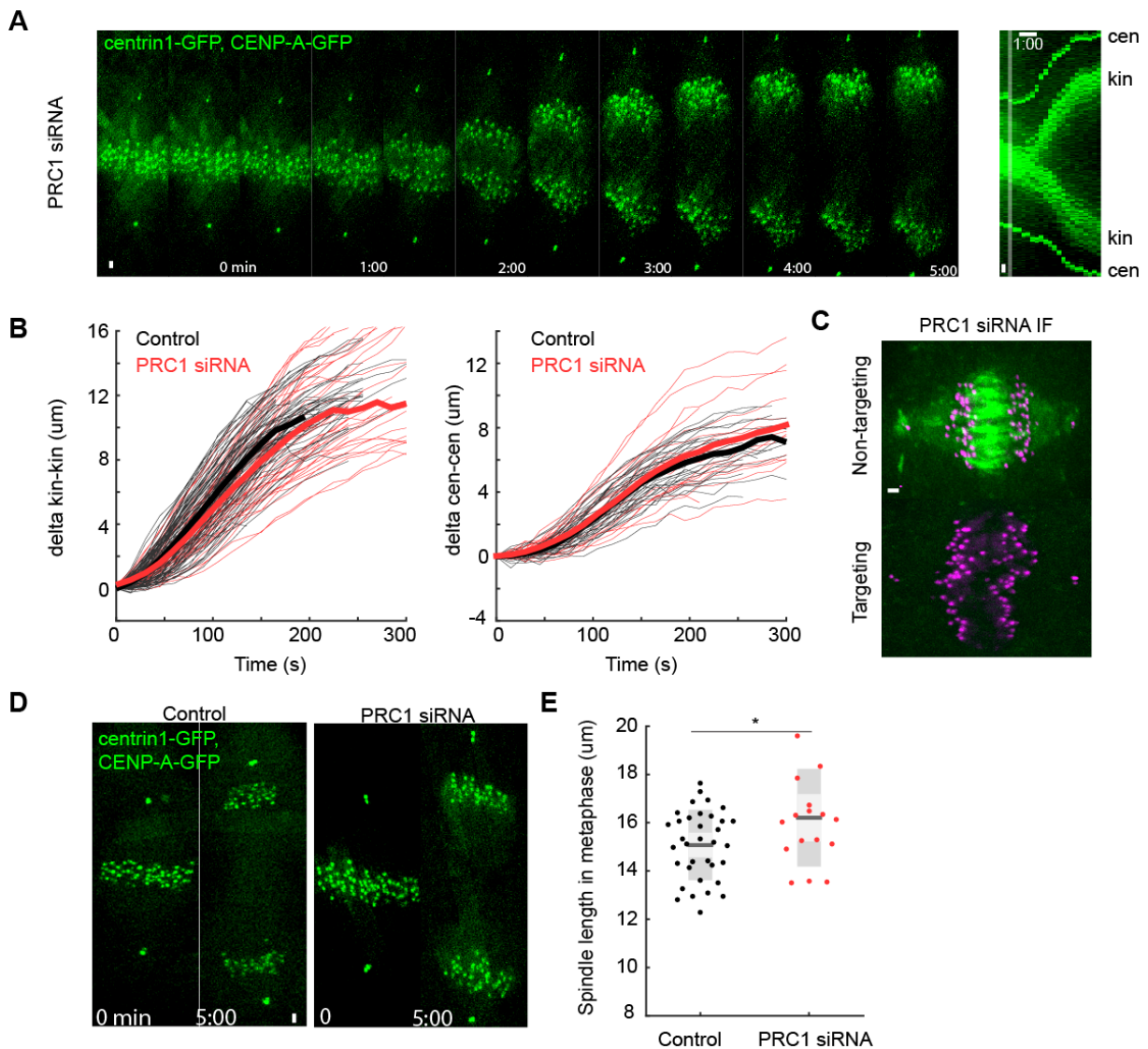
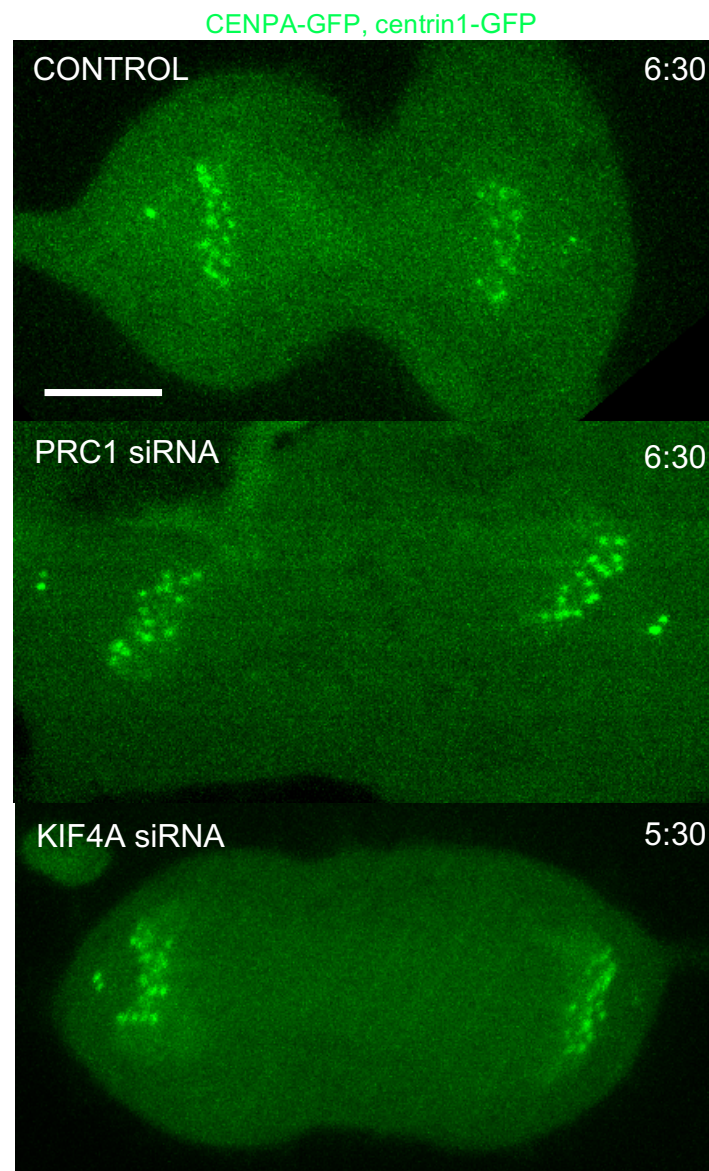


**Figure 29. Depletion of PRC1 does not affect anaphase spindle elongation. (A)** Live cell images of PRC1 siRNA depleted RPE-1 cell stably expressing CENP-A-GFP and centrin1-GFP show unperturbed spindle elongation. kin-kinetochore and cen-centrosome. **(B)** Plots of relative kinetochore and centrosome separation distance (delta) defined as the kinetochore-to-kinetochore (kin-kin) and centrosome-to-centrosome (cen-cen) distance at time t minus the

kin-kin and cen-cen distance at  $t = 0$ , over time. Individual kinetochore and centrosome pairs (thin lines), mean (thick lines). **(C)** Immunofluorescence (IF) images of fixed non-targeting treated and PRC1 siRNA-depleted RPE-1 cells stably expressing CENP-A-GFP and centrin1-GFP (magenta) stained with AlexaFluor594 conjugated with PRC1 antibody (green). **(D)** Live cell images of control and PRC1 siRNA depleted RPE-1 cell show longer metaphase and anaphase spindles after PRC1 depletion. **(E)** Quantification (univariate scatter plot) of spindle length in metaphase in treatments as in (D). Boxes represent standard deviation (dark grey), 95% standard error of the mean (light grey) and mean value (black). Statistics: t test ( $*P <$



0.05). Images are maximum projection of acquired z-stack. Time shown as minutes:seconds. Time 0 represents anaphase onset. Vertical scale bars, 1  $\mu\text{m}$ . Horizontal scale bar, 1 min.

**Figure 30. Depletion of PRC1 or KIF4A can cause excessive spindle elongation during late anaphase. (A)** Maximum z-projection live cell images of control (top) and PRC1 siRNA depleted (bottom) RPE-1 cells stably expressing CENP-A-GFP and centrin1-GFP. Time shown as minutes:seconds. Time is measured from the anaphase onset. Scale bar; 5  $\mu$ m.

Since PRC1 can induce excessive spindle elongation when compared to control cells (Figure 30), that suggested PRC1 is an important player in the regulation of spindle elongation halting at the end of the anaphase, and it was envisioned that this could happen either because PRC1 is inducing a strong frictional force in the spindle midzone during anaphase when overlap length is greatly reduced, as proposed by others (Pamula et al., 2019) or PRC1 is recruiting some factors responsible for maintenance of opposing force that hinders spindle elongation. Interestingly, depletion of PRC1-interacting partner KIF4A (Zhu and Jiang, 2005) resulted in a similar phenomenon (Figure 30), as reported previously (Hu et al., 2011), meaning that second possibility is probably more relevant for inducing break on spindle elongation in human cells (see Concluding Discussion for more details).

#### 4.1.4 Depletion of PRC1 does not influence spindle elongation velocities

In support of these results, revealing PRC1 itself is not required for early anaphase spindle elongation, individual depletions by siRNA approach (Figure 32) or inhibitions with small molecule inhibitors, where applicable, of all known PRC1-interacting motor proteins, KIF4A/Kinesin-4 (Kurasawa et al., 2004), KIF23/MKLP-1/Kinesin-6, KIF20A/MKLP-2/Kinesin-6 (Gruneberg et al., 2006), centromere-associated protein E (CENP-E)/Kinesin-7 (inhibited by small molecule allosteric inhibitor GSK-923295, see Materials and methods for details) and KIF14/Kinesin-3 (Kurasawa et al., 2004), did not strongly impact spindle elongation velocities nor chromosome segregation velocities during early anaphase (Figure 31). Therefore, single perturbation experiments of almost all molecular motors that were implicated in regulation of spindle midzone function during anaphase and cytokinesis (Lee et al., 2012), failed to stop anaphase spindle elongation, although some of them had a strong modulatory effect on elongation velocities.

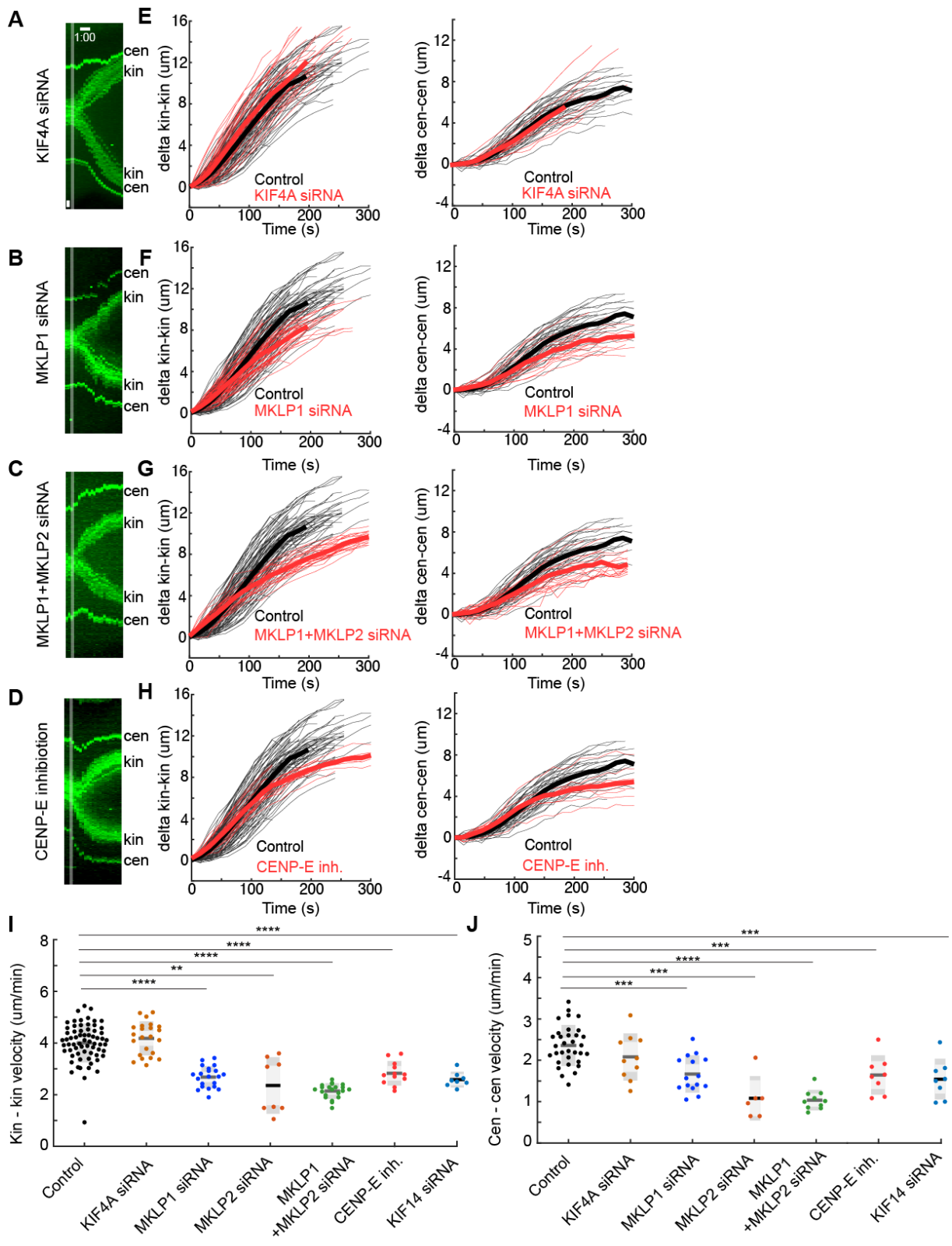




**Figure. 31. Depletion of PRC1-interacting partners has a minor effect on anaphase spindle elongation.** (A-D) Kymographs (consecutive maximal intensity projections onto the x-axis) of the live cell images of RPE-1 cells stably expressing CENP-A-GFP and centrin1-GFP in the siRNA depletions of KIF4A, MKLP1, MKLP1 + MKLP2 and CENP-E inhibition. (E-H) Plots of relative kinetochore and centrosome separation distance (delta) defined as the kinetochore-to-kinetochore (kin-kin) and centrosome-to-centrosome (cen-cen) distance at time t minus the kin-kin and cen-cen distance at t = 0, over time. Individual kinetochore and centrosome pairs (thin lines), mean (thick lines) for each condition from (A). Time 0 represents anaphase onset. (I, J) Quantification (univariate scatter plot) of velocity of separation of sister kinetochores (kin-kin) and spindle elongation (cen-cen) velocity. Boxes represent standard deviation (dark grey), 95% standard error of the mean (light grey) and mean value (black) for each condition from (A). Statistics: t test (\*\* P < 0.01, \*\*\*P < 0.001; \*\*\*\*P < 0.0001). Time shown as minutes:seconds. Vertical scale bars, 1  $\mu$ m. Horizontal scale bar, 1min.

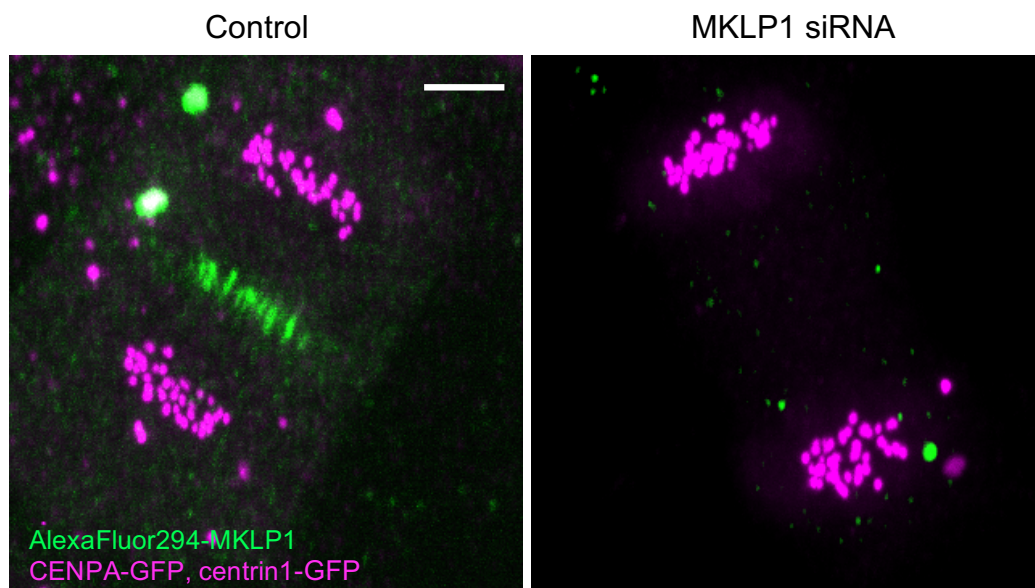


**Figure 32. MKLP1 motor protein can be successfully depleted using specific siRNAs.** Immunofluorescence (IF) images of fixed non-targeting RNA treated (right) and MKLP1 siRNA-depleted (left) RPE-1 cells stably expressing CENP-A-GFP and centrin1-GFP (green) stained with AlexaFluor594 conjugated with MKLP1 antibody (red). Scale bar, 5  $\mu$ m.

#### 4.1.5 PRC1 depletion and EG5 inhibition induce a complete block in spindle elongation

Next, the unknown redundant mechanisms between plus-end directed molecular motors, that could operate during spindle elongation in human cells were explored. As a first approach, the redundancy between EG5 motor and all PRC1-dependant motors (see previous section) was examined. To investigate this possible redundancy between EG5 and PRC1-dependent motors PRC1 was depleted by siRNA approach along with EG5 inhibition at metaphase-to-anaphase transition by STLC. Surprisingly, this perturbation resulted in completely impaired chromosome segregation by total block in spindle elongation and cell arrest in early anaphase for a significant amount of time (Figures 33, 34, and 36). This phenotype was not dependent on whether STLC was added in metaphase, like in original protocol described above, or in early anaphase (Figure 34), meaning that observed block was not a consequence of STLC treatment during metaphase when significant spindle shortening was observed (Figures 25, 33 and 36). This implicates that some PRC1-dependant protein or PRC1 itself was able to rescue spindle pole collapsing seen after STLC treatment following anaphase start, and after its depletion, this rescue mechanism was clearly abolished (Figure 36). The poleward motion of chromosomes started but their velocity was slower when compared to controls (Figure 35), probably reflecting the notion that in some cells, as the chromosomes started to separate, the spindle poles still collapsed toward each other, reducing the velocity of poleward kinetochore movement. Therefore, it was speculated that spindle elongation and poleward chromosome movement are largely independent processes in human cells, as shown before by others (Brennan et al., 2007), but final conclusion will merit future experiments.



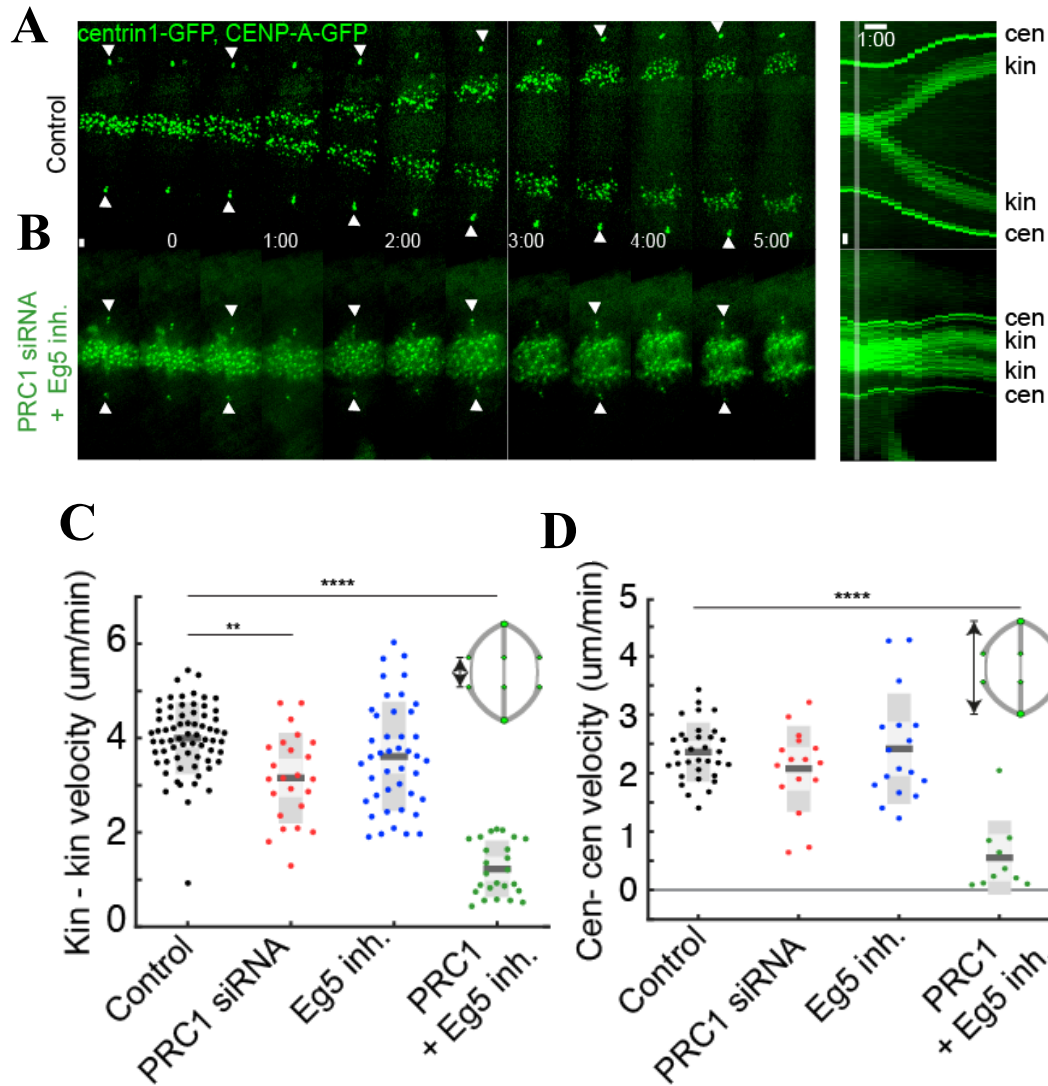


**Figure 33. Loss of PRC1 and inactivation of EG5 blocks spindle elongation during anaphase.** (A, B) Live cell images of control and protein regulator of cytokinesis 1 (PRC1) siRNA depleted and S-trityl-L-cysteine (STLC)-treated RPE-1 cell stably expressing CENP-A-GFP and centrin1-GFP. kin-kinetochore and cen-centrosome. White arrowheads indicate centrioles. (C, D) Quantification (univariate scatter plot) of velocity of separation of sister kinetochores and spindle elongation velocity (see schemes). Boxes represent standard deviation (dark grey), 95% standard error of the mean (light grey) and mean value (black). Statistics: t test (\*\*P < 0.01, \*\*\*\*P < 0.0001). (F) Statistics: t test (\*\*P < 0.01; \*\*\*\*P < 0.0001). Time shown as minutes:seconds. Images are maximum projection of acquired z-stack. Time 0 represents anaphase onset. Vertical scale bars, 1  $\mu$ m. Horizontal scale bar, 1min.

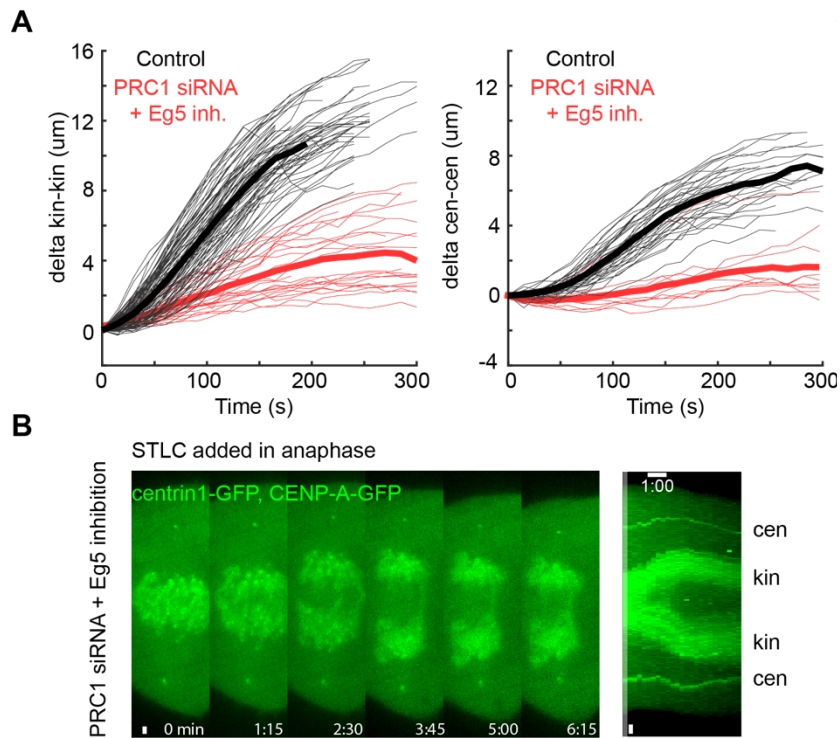


**Figure 34. Depletion of PRC1 combined with EG5 inhibition blocks spindle elongation in anaphase.** (A) Plots of relative kinetochore and centrosome separation distance (delta) defined as the kinetochore-to-kinetochore (kin-kin) and centrosome-to-centrosome (cen-cen) distance at time  $t$  minus the kin-kin and cen-cen distance at  $t = 0$ , over time in RPE-1 cells stably expressing CENP-A-GFP and centrin1-GFP. Individual kinetochore and centrosome pairs (thin lines), mean (thick lines). Time 0 represents anaphase onset. (B) Live cell images of PRC1 siRNA depleted and S-trityl-L-cysteine (STLC)-treated RPE-1 cell show unperturbed spindle elongation. kin-kinetochore and cen-centrosome. Time shown as minutes:seconds. Time 0 represents STLC addition.

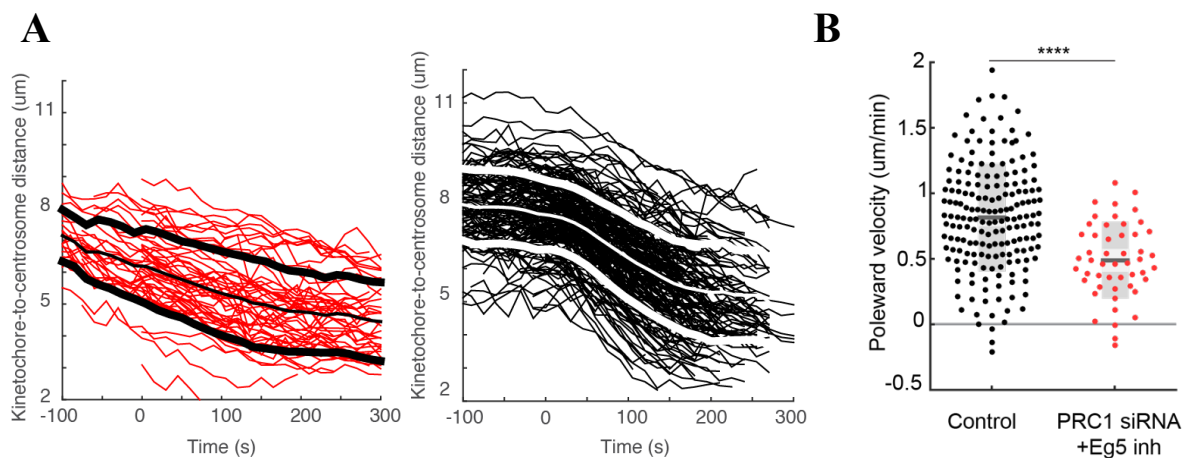


**Figure 35. Depletion of PRC1 combined with EG5 inhibition impacts poleward velocity rates during anaphase. (A)** Plots of distances between kinetochores and their respective poles, over time in RPE-1 cells stably expressing CENP-A-GFP and centrin1-GFP depleted of PRC1 by siRNA and treated with STLC (left) and control cells (right). Black and white lines indicate mean and standard deviation from a mean value. Time 0 represents onset of anaphase. **(B)** Quantification (univariate scatter plot) of kinetochore to pole distances for STLC-treated and PRC1 depleted (red) and control cells (black). Boxes represent standard deviation (dark grey), 95% standard error of the mean (light grey) and mean value (black). Statistics: t test (\*\*\*\*P < 0.0001). Images are maximum projection of acquired z-stack. Vertical scale bars, 1  $\mu$ m. Horizontal scale bar, 1 min.

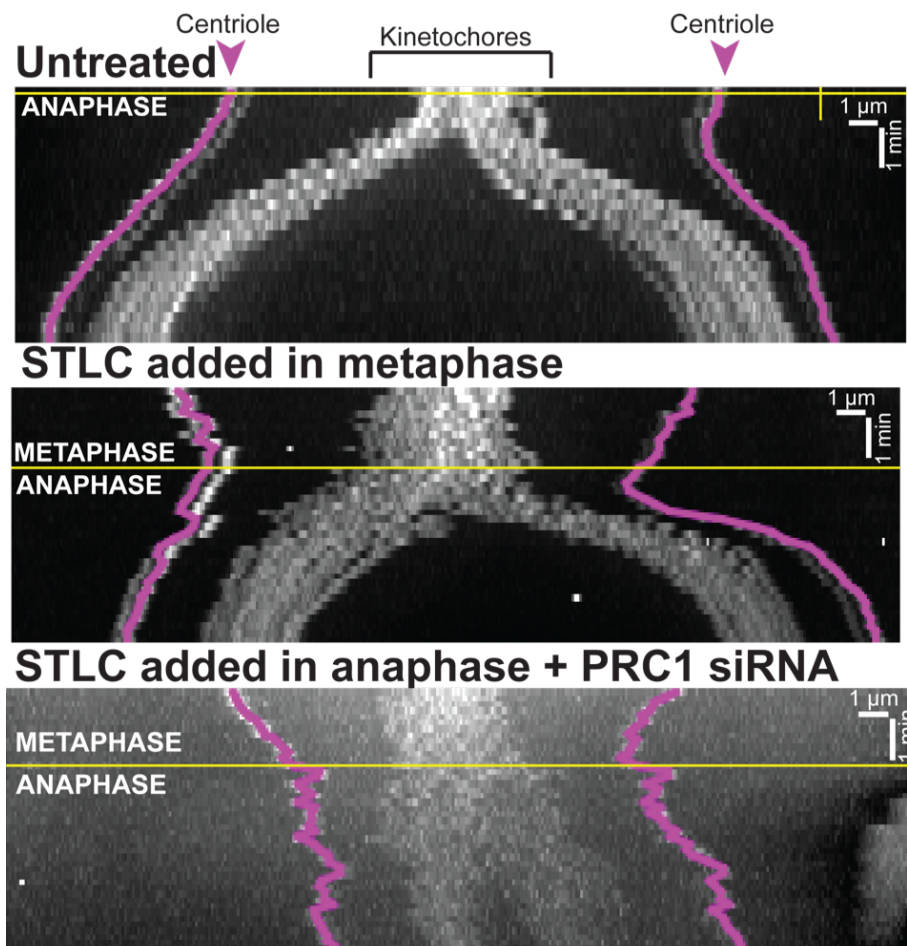


**Figure 36. Outward forces powering spindle elongation in the absence of EG5 activity are driven by KIF4A motor protein.** Kymographs (consecutive maximum-intensity projections onto the y axis) of the RPE-1 cells stably expressing CENP-A-GFP (grey) and centrin1-GFP (grey but its manual track overlaid in magenta) in indicated conditions during metaphase and anaphase. Yellow horizontal lines indicate onset of anaphase.

To check whether this major effect on anaphase was a consequence of PRC1-depletion by siRNA a novel CRISPR technology approach was used in which the total knock-outs (KO) of specific genes are achieved (see Introduction and Materials and methods section) (McKinley and Cheeseman, 2017). I took advantage of published base of inducible CRISPR-KOs in RPE-1 human cell line (<http://cellcycleknockouts.wi.mit.edu/>), and used an inducible PRC1-KO cell line, in which PRC1 could not be detected after 78h induction by doxycycline (Figure 38) (see Material and methods for details) (McKinley, 2018). Interestingly, the similar strong block of spindle elongation seen after depletion of PRC1 by siRNA combined with STLC treatment (Figure 33) was also observed by using inducible KO of PRC1 by CRISPR/Cas9 system combined with the STLC treatment, using the similar protocol of STLC treatment as before (Figures 37 and 38). The only difference was that, in condition of CRISPR KO, the chromosomes were labelled with DNA-specific stain SiR-DNA, instead of kinetochore labelling used in previous experiments, but this disparity did not influence the experimental setup since similar total block phenotype was observed in unlabelled CRISPR PRC1-KO cells combined with STLC treatment imaged only by wide-field microscopy (Figure 38C). Thus, the redundant activity of independent EG5 and PRC1 protein modules is crucial for spindle elongation in human cells. The total block of spindle elongation, on the other hand, was never observed in induced PRC1-KO cells or in non-induced control cells (Figures 37 and 38).

Moreover, when imaging cells where PRC1-KO was induced but STLC was not added in metaphase, spindle overelongation could be observed when compared with non-induced controls, with chromosomes mass distances surpassing 20  $\mu\text{m}$  at the end of anaphase (Figure 38B), similar to what is sometimes observed after depletion of PRC1 by siRNA (Figure 30). In non-induced control cells, the distance between chromosome masses reached stationary period after early anaphase at distances of around 12  $\mu\text{m}$ , as reported previously (Su et al., 2016). Also, chromosome segregation velocities were slightly but consistently elevated during early anaphase in the same condition when compared to non-induced controls (Figure 37B). This was contrary to situation when PRC1 was depleted by siRNA protocol where kinetochore velocities were similar in the same time period when compared to controls (Figure 28 and 33), probably reflecting the differences in PRC1 perturbation approaches.

Two described protein sliding modules, one composed of EG5 and other of PRC1 and its multiple interactors, are independent from each other since one is not required for spindle localisation of other (Figure 39), except for general effect of PRC1 depletion on spindle midzone structure by reducing the number of bundled MTs during late anaphase (Mollinari et

al., 2002), which consequentially reduced signal of EG5 staining in that region (Figure 39). This PRC1 depletion and imaging were done on HeLa BAC EG5-GFP cell line (see Materials and methods for details). Moreover, since PRC1 is a passive MT bundler (She et al., 2019), it was hypothesized that its necessity for spindle elongation is due to recruitment of active motor proteins involved in spindle elongation, rather than performing active sliding by itself, because this phenomenon was never reported in the literature for PRC1 protein (She et al., 2019).

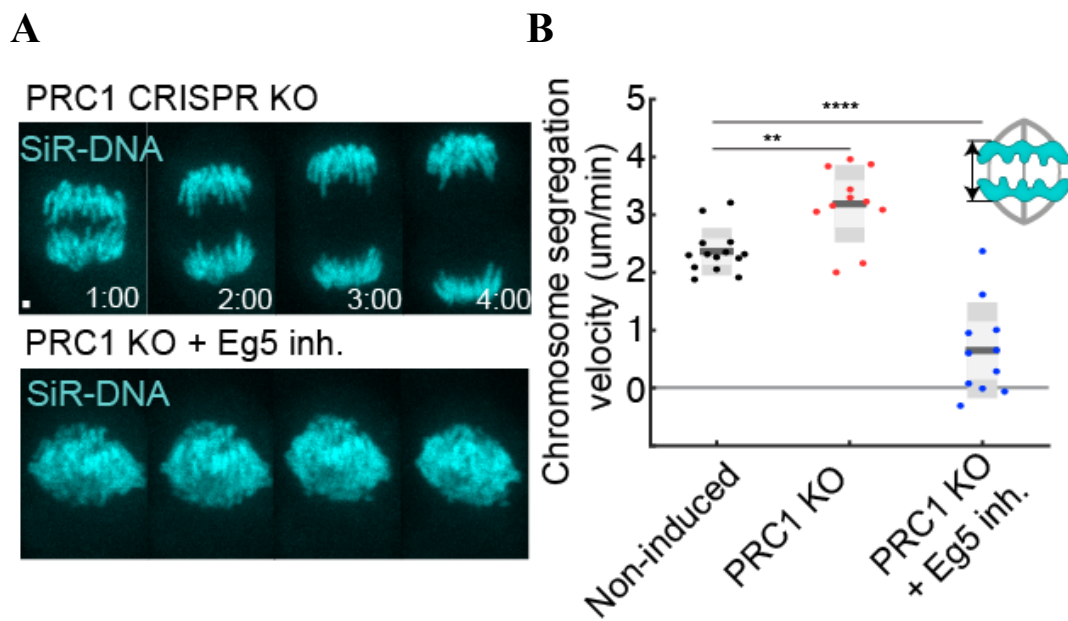


**Figure 37. Loss of PRC1 and inactivation of EG5 blocks spindle elongation during anaphase.** (A) Live cell images of induced RPE-1 PRC1 CRISPR knock-out (KO) and PRC1 KO treated with STLC. Silicon rhodamine (SiR)-DNA was used for chromosome staining. (B) Quantification of chromosome segregation velocity (see scheme) in CRISPR experiments. Statistics: t test (\*\*P < 0.01; \*\*\*\*P < 0.0001). Images are maximum projection of acquired z-stack. Time 0 represents anaphase onset. Scale bar, 1 µm.



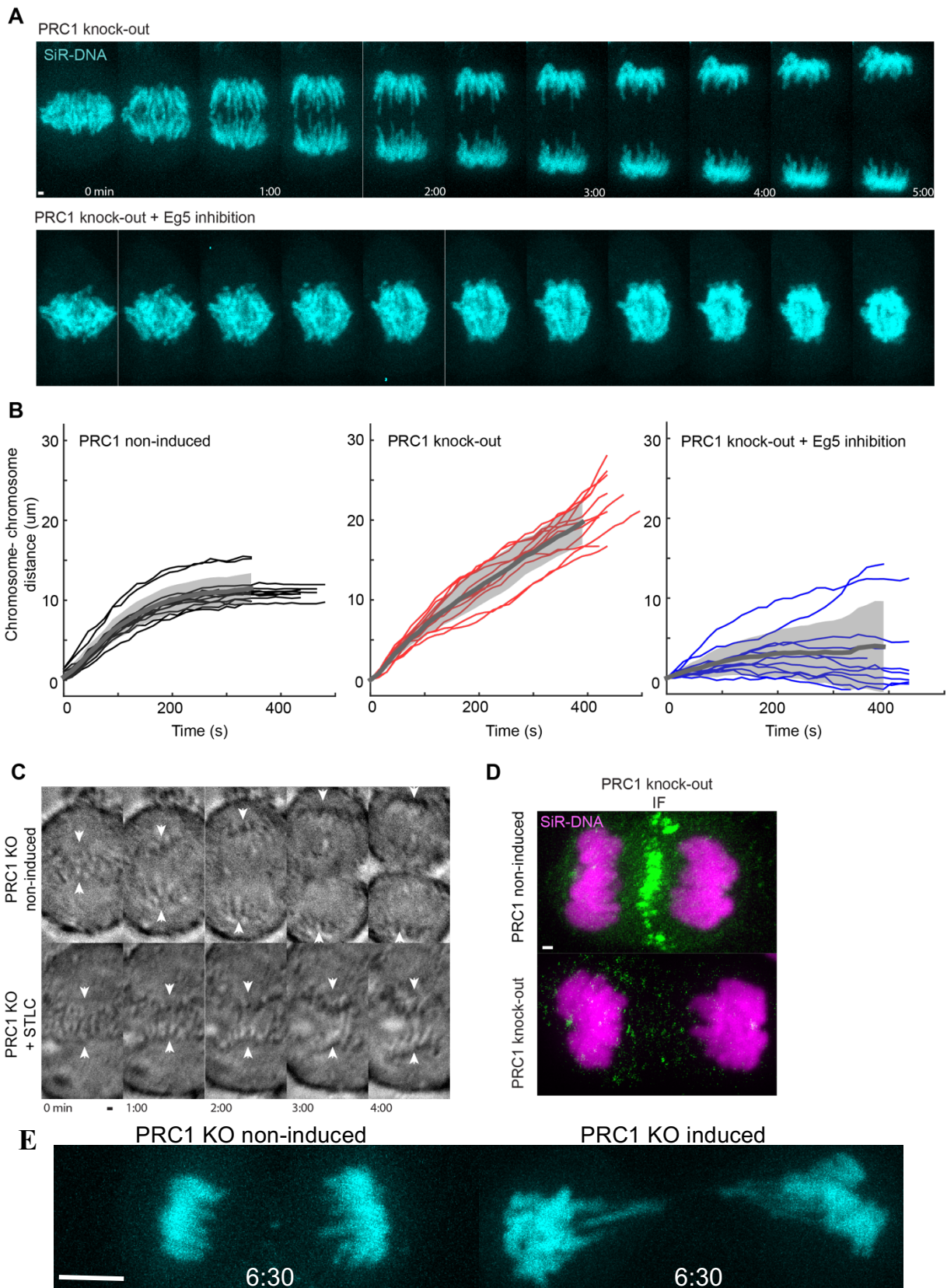


**Figure 38. PRC1 CRISPR knock-out (KO) combined with EG5 inhibition blocks spindle elongation in anaphase. (A)** Live cell images of induced RPE-1 PRC1 CRISPR KO and PRC1 KO treated with STLC imaged 4 days after doxycycline induction. Silicon rhodamine (SiR)-DNA (cyan) was used for chromosome staining. **(B)** Plots of relative chromosome segregation distance ( $\Delta$ ) defined as the chromosome-to-chromosome distance at time  $t$  minus the chromosome-chromosome distance at  $t = 0$ , over time. Individual chromosome pairs (thin lines), mean (thick grey lines) and SD (grey region) for indicated conditions. **(C)** Live cell brightfield images of induced RPE-1 PRC1 CRISPR KO and PRC1 CRISPR KO treated with STLC imaged 4 days after doxycycline induction. Note: chromosome segregation defects after STLC treatment are similar to ones observed in the same treatment but with chromosomes labelled with SiR-DNA. White arrowheads indicate position of chromosomes. **(D)** Immunofluorescence (IF) images of fixed non-induced PRC1 CRISPR KO and PRC1 CRISPR induced KO RPE-1 cells stained with AlexaFluor594 conjugated with PRC1 antibody (green) and silicon rhodamine (SiR)-DNA (magenta). **(E)** Live cell images of induced RPE-1 PRC1 CRISPR KO and PRC1 KO treated with STLC imaged 4 days after doxycycline induction. Silicon rhodamine (SiR)-DNA (cyan) was used for chromosome staining. Images are maximum projection of acquired z-stack. Time shown as minutes:seconds. Time 0 represents anaphase onset. Scale bars, 1  $\mu\text{m}$ .

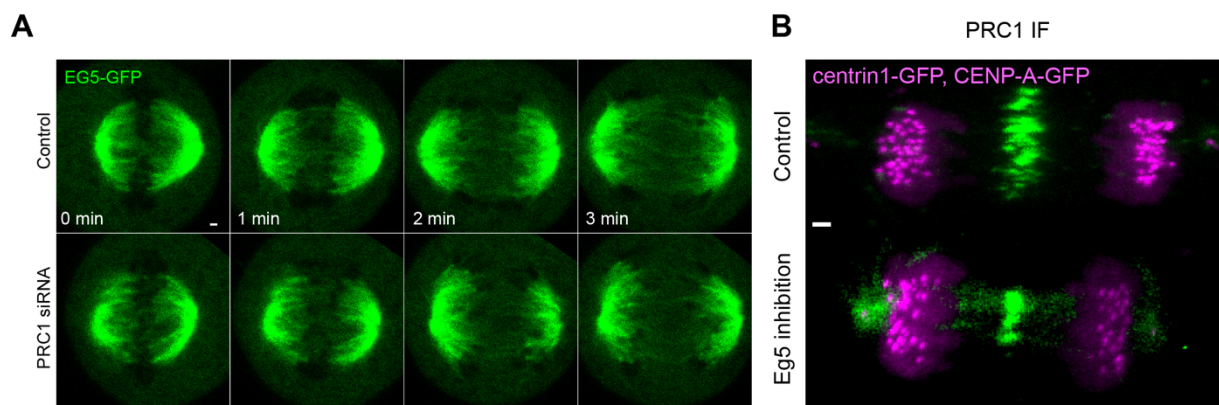


**Figure 39. Depletion of PRC1 does not affect EG5 localization on the spindle and *vice versa*.** **(A)** Live cell images of control and PRC1 siRNA depleted HeLa cells stably expressing EG5- GFP from a BAC. Images are single z-planes. This experiment was done by Patrik Risteski from Tolić group. **(B)** Immunofluorescence (IF) images of fixed control and 10 min STLC-treated RPE-1 cells stably expressing CENP-A-GFP and centrin1-GFP (magenta) stained with AlexaFluor594 conjugated with PRC1 antibody (green). Images are maximum projection of acquired z-stack. Time 0 represents anaphase onset. Scale bars, 1  $\mu\text{m}$ .

#### 4.1.6 EG5 motor protein and PRC1-interacting motor protein KIF4A are crucial for spindle elongation in human cells

To test this redundancy idea furthermore, all known PRC1-interacting partners (see above) were depleted, one by one, in combination with the same approach of EG5 inhibition by STLC. Similar approach was used for every target protein as for PRC1 depletion, establishing strong siRNA protocol that yielded complete loss of studied protein from a spindle midzone (Figures 29 and 32). As a first candidate, the KIF4A protein was explored as the best characterized PRC1 partner (Lee et al., 2012), known to slide MTs *in vitro* (Bieling et al., 2010). Surprisingly, depletion of KIF4A motor protein together with EG5 inhibition completely mirrored the long-term anaphase arrest seen after PRC1 depletion and EG5 inhibition with cells that completely lacked spindle elongation (Figures 40 and 41). This was, as in case of PRC1 depletion combined with EG5 inhibition, independent of STLC addition before or after anaphase onset (Figures 40 and 41). Effect on poleward chromosome velocity was also apparent and statistically significant, like in the case of PRC1 depletion combined with STLC treatment (Figure 41). This indicated that molecular motors EG5 and KIF4 are acting in redundant pathways during spindle elongation and are both crucial for this process in human cells. Also, because KIF4A is not brought immediately after anaphase onset to midzone region (Nunes Bastos et al., 2013), this might explain why delay in spindle elongation start is observed in cells treated with STLC compared with anaphase onset that eventually elongated their spindles with unperturbed velocities (Figures 26H and 36).

Furthermore, to observe if this strong spindle elongation block is specific to EG5 inhibition specifically by STLC drug, alternative small molecule drug inhibitor of EG5, monastrol (Kapoor et al., 2000; Mayer et al., 1999), was used. One recent study (Kim et al., 2019), suggested that, although both inhibitors are characterized by similar allosteric mode of EG5 inhibition, they differ in the capacity to inhibit EG5 microtubule depolymerising activity, where monastrol cannot inhibit this activity whereas STLC is very potent inhibitor of this activity. Regarding our results, this could suggest that observed anaphase block is induced because EG5 depolymerising activity is inhibited and not its sliding capacity via its motor activity, as it was predicted to be the case. However, as can be seen on Figure 42, there is no difference regarding both total spindle elongation block and reduced kinetochore segregation velocities, in cells depleted of KIF4A and with EG5 inhibited by either STLC or monastrol. Thus, it was concluded that perturbed EG5 depolymerising activity is not crucial for



observation of spindle elongation block seen after perturbation of two sliding motors EG5 and KIF4A.

4.1.7 Depletion of both kinesins-6, when combined with EG5 inhibition, can mimic the effect of KIF4A and EG5 perturbations

Next, the possible roles of kinesins-6 during spindle elongation were explored by combining their depletions with the STLC treatment. Unexpectedly, RNAi-mediated co-depletion of MKLP1 and MKLP2 together with EG5 inhibition was also reminiscent of EG5 inhibition and KIF4A depletion with cells lacking spindle elongation (Figures 40 and 43) that were in most cases also arrested in early anaphase (Figure 43). Surprisingly, neither depletions of MKLP1 or MKLP2, when individually combined with STLC treatment in metaphase, were able to affect anaphase velocities in similar way (Figure 44), meaning that their combination had an important redundant effect on spindle elongation. This suggests that both human kinesins-6 are required for anaphase spindle elongation, most probably as regulators of KIF4A in the spindle midzone, since MKLP2 does not have a capacity to slide antiparallel MTs apart (Lee et al., 2012). Therefore, it was suggested that MKLP1 and MKLP2 cooperatively regulate KIF4A in the spindle midzone, probably through Aurora B mediated pathway (Douglas et al., 2010; Gruneberg et al., 2004; Nunes Bastos et al., 2013; Ozlu et al., 2010), which then, together with EG5, drive anaphase spindle elongation in human cells.

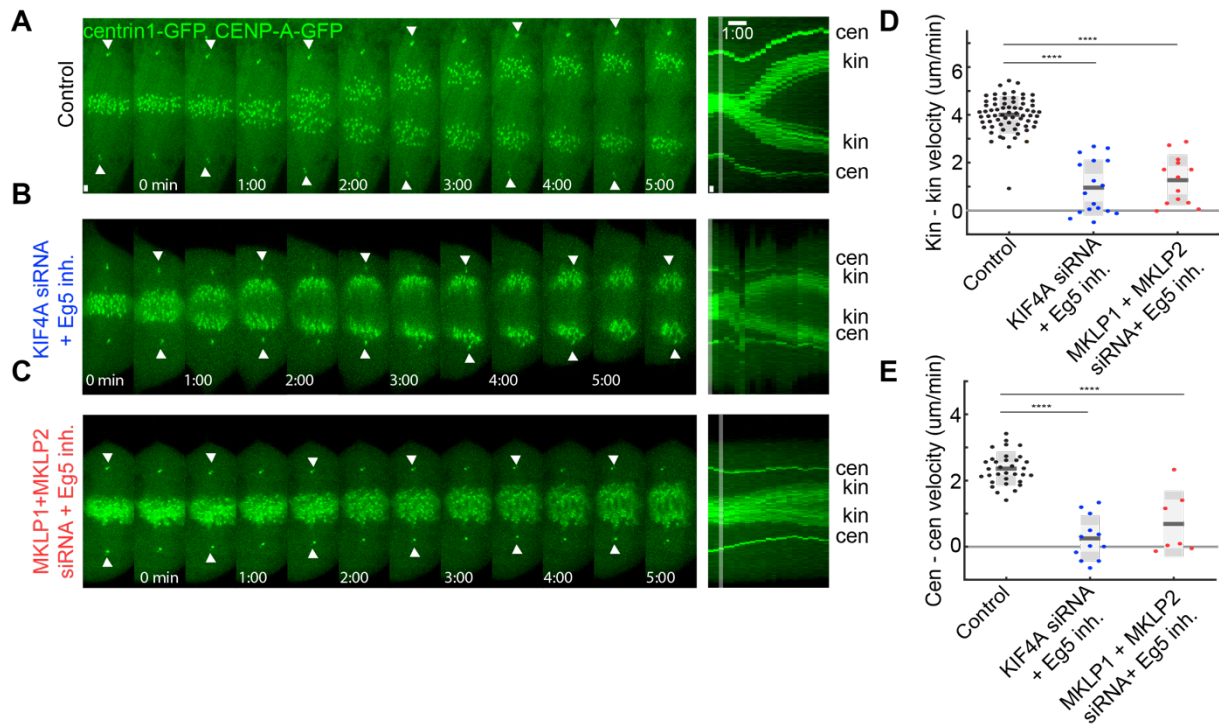


**Figure 40. Loss of KIF4A or both kinesins-6 with inactivation of EG5 induces anaphase arrest by blocking spindle elongation.** (A, B, C) Live cell images of control, KIF4A siRNA depleted and STLC-treated and mitotic kinesin-like protein 1 and 2 (MKLP1 and MKLP2) siRNA depleted and STLC-treated RPE-1 cells stably expressing CENP-A-GFP and centrin1-GFP. kin-kinetochore and cen-centrosome. White arrowheads indicate centrioles. (D, E) Quantification of velocity of separation of sister kinetochores and spindle elongation velocity. Statistics: t test (\*\*\*\*P < 0.0001). Time shown as minutes:seconds. Images are maximum projection of acquired z-stack. Time 0 represents anaphase onset. Vertical scale bars, 1  $\mu$ m. Horizontal scale bar, 1min.

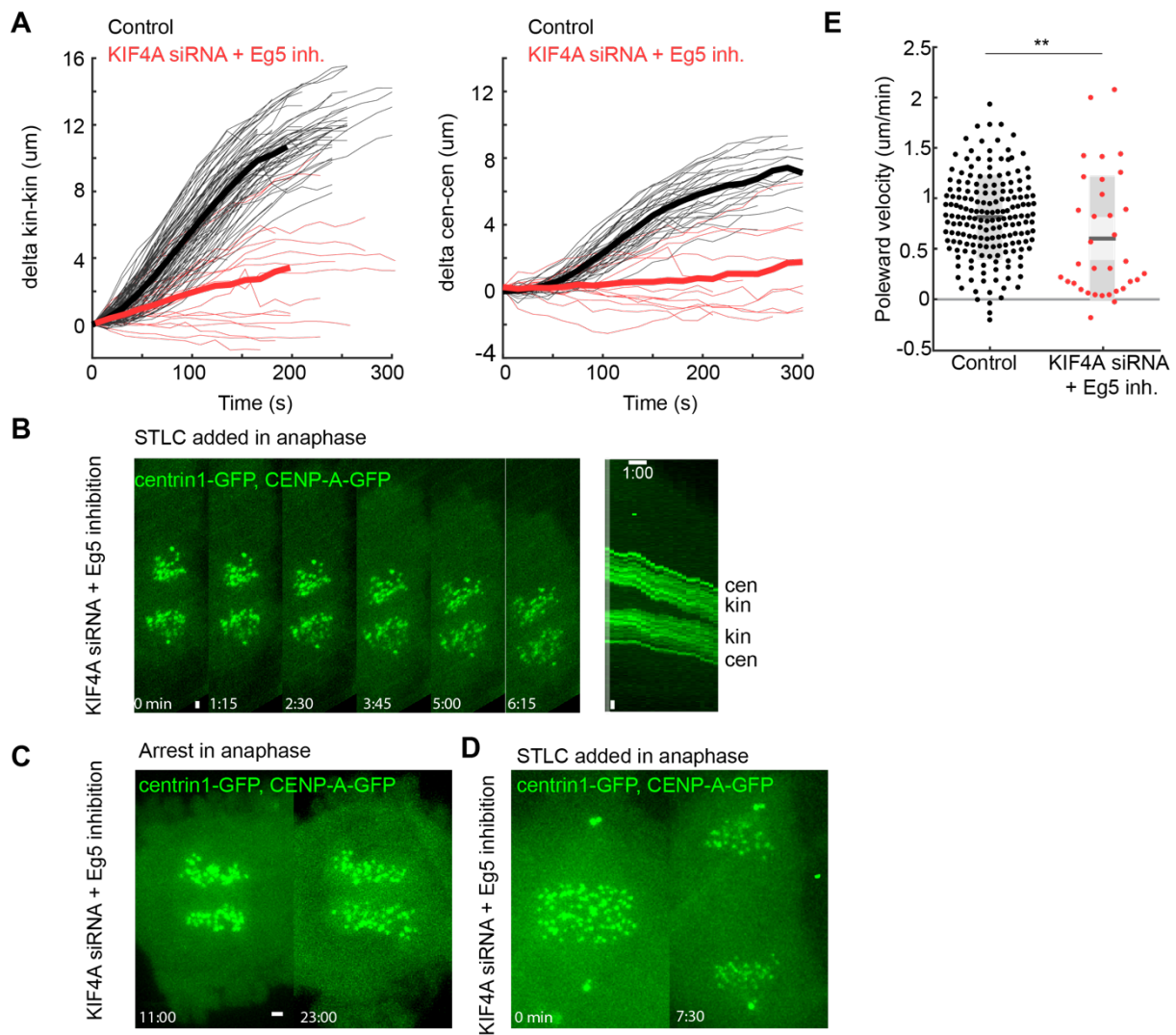


**Figure 41. Depletion of KIF4A combined with EG5 inhibition blocks spindle elongation in anaphase.** (A) Plots of relative kinetochore and centrosome separation distance (delta) defined as the kinetochore-to-kinetochore (kin-kin) and centrosome-to-centrosome (cen-cen) distance at time  $t$  minus the kin-kin and cen-cen distance at  $t = 0$ , over time in KIF4A siRNA depleted and S-trityl-L-cysteine (STLC)-treated RPE-1 cells stably expressing CENP-A-GFP and centrin1-GFP. Individual kinetochore and centrosome pairs (thin lines), mean (thick lines). (B) Live cell images of a cell from (A) show perturbed spindle elongation when STLC is added in anaphase. kin-kinetochore and cen-centrosome. (C) Live cell images of KIF4A siRNA depleted and STLC-treated RPE-1 cell show long-term anaphase arrest phenotype when STLC is added in anaphase. (D) Live cell images of KIF4A siRNA depleted and STLC-treated RPE-1 cell, with addition of STLC in anaphase, show small rate of spindle elongation. Note: in few examples, if STLC was added in early anaphase, spindle elongation could be observed but to lesser degree when compared to controls. Time 0 represents start of STLC treatment. (E) Quantification (univariate scatter plot) of kinetochore to pole velocities

(poleward velocity). Boxes represent standard deviation (dark grey), 95% standard error of the mean (light grey) and mean value (black). Statistics: t test (\*\* P < 0.01). Images are maximum projection of acquired z-stack. Time shown as minutes:seconds. Vertical scale bars, 1  $\mu$ m. Horizontal scale bar, 1min.

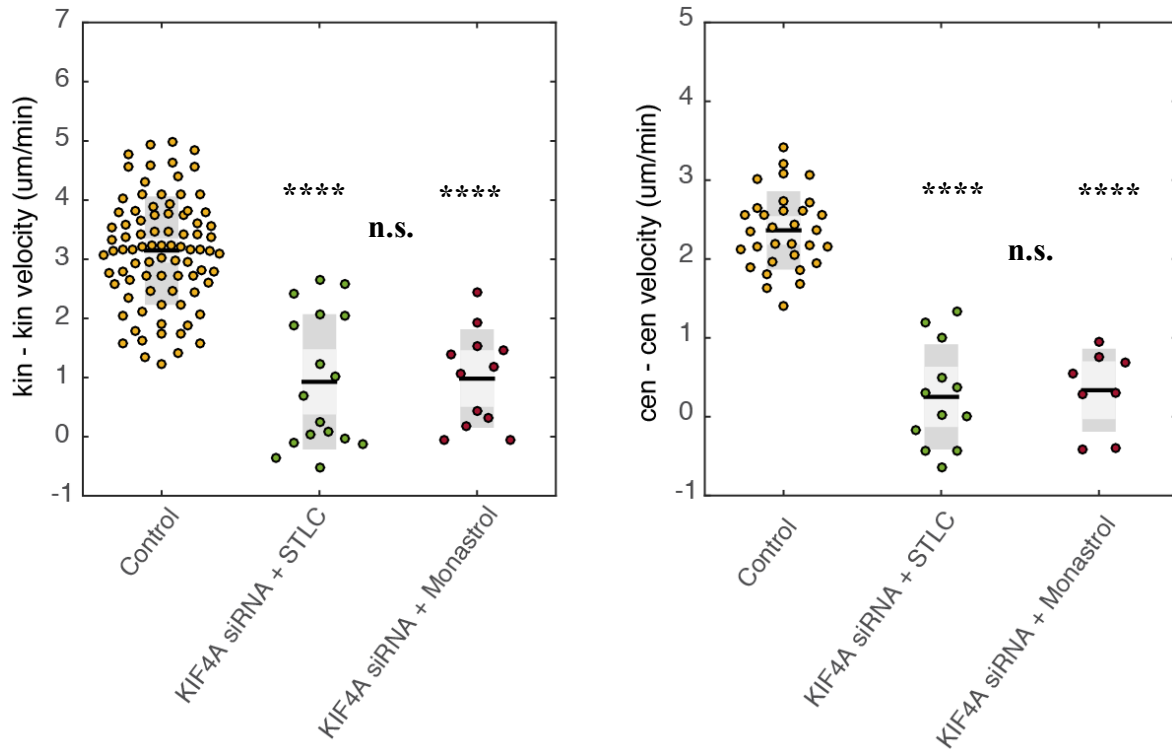


**Figure 42. Spindle elongation block observed after perturbation of KIF4A and EG5 is not specific to inhibition of EG5 by STLC drug.** Quantification (univariate scatter plot) of velocity of separation of sister kinetochores (kin-kin, left) and spindle elongation (cen-cen, right) velocity in indicated treatments. Boxes represent standard deviation (dark grey), 95% standard error of the mean (light grey) and mean value (black) for each condition, as indicated. Statistics: t test (n.s., not significant, \*\*\*\*P < 0.0001).

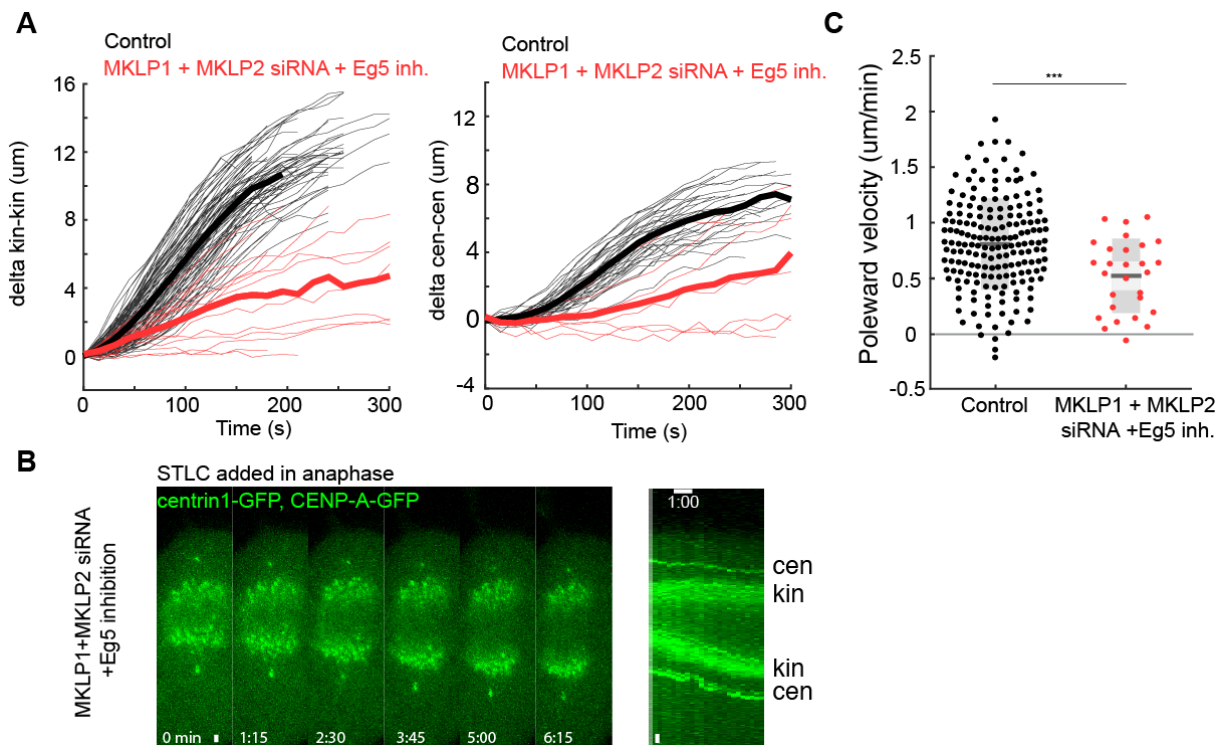


**Figure 43. Depletion of both kinesins-6 with inactivation of EG5 induces anaphase arrest.** (A) Plots of relative kinetochore and centrosome separation distance (delta) defined as the kinetochore-to-kinetochore (kin-kin) and centrosome-to-centrosome (cen-cen) distance at time  $t$  minus the kin-kin and cen-cen distance at  $t = 0$ , over time in MKLP1 and MKLP2 siRNA depleted and S-trityl-L-cysteine (STLC)-treated RPE-1 cells stably expressing CENP-A-GFP and centrin1-GFP. Individual kinetochore and centrosome pairs (thin lines), mean (thick lines). (B) Live cell images of a cell from (A) show blocked spindle elongation. kin-kinetochore and cen-centrosome. Time 0 represents start of STLC treatment. Time 0 represents anaphase onset. (C) Quantification (univariate scatter plot) of kinetochore to pole velocities (poleward velocity). Boxes represent standard deviation (dark grey), 95% standard error of the mean (light grey) and mean value (black). Statistics: t test ( $***P < 0.001$ ). Images are maximum projection of acquired z-stack. Time shown as minutes:seconds. Vertical scale bars, 1  $\mu\text{m}$ . Horizontal scale bar, 1min.

#### 4.1.8 CENP-E and KIF14 cannot mimic the observed block in spindle elongation

Among other PRC1-interacting partners, inhibition of CENP-E and depletion of KIF14, when combined with EG5 inhibition, were not able to mimic the strong effect on

spindle elongation and chromosome segregation observed after attenuation of EG5 activity and PRC1 depletion (Figure 44), meaning they are not essential for spindle elongation during early anaphase in human cells.

Also, at this point, I would like to note that the various other regulatory proteins in RPE-1 cells were tested to find their possible link to spindle elongation. Among these, KIF18A protein, from a family of kinesins-8, molecular motor known to regulate MT dynamics at plus-end of kinetochore MTs (Stumpff et al., 2008) and EB3, a plus-end tracking protein, who can track growing MTs, and recruit different factors to plus-ends important for their stability (Akhmanova and Steinmetz, 2008) were tested. Depletion of these candidates, EB3 by 48h treatment with siRNA and KIF18A by 24h treatment, did not impose a strong impact on spindle elongation rates, while effect on chromosome segregation rates was more prominent after these perturbations (Figure 45). This indicates that their effect is probably exerted on chromosome poleward velocity rates. KIF18A depletion led to highly disarranged orientation of chromosomes along the whole metaphase spindle (data not shown), as reported previously (Stumpff et al., 2008), but these cells after long metaphase delay eventually entered and finished anaphase with unperturbed elongation velocities. Cells treated with KIF18A siRNA for 48h, on the other hand, never entered anaphase, when imaged for more than 1 hour in single cases (data not shown), as already reported (Stumpff et al., 2008). It was concluded that these proteins probably exert most of their effects on anaphase through regulation of plus-ends of k-fibers. Interestingly, when PRC1 was co-depleted with KIF18A, a small effect was observed on spindle elongation velocity (Figure 45). Moreover, the redundancy between kinesin-6 MKLP1 and main metaphase outward force-generators KIF15 and EG5 was tested, trying to elucidate if failure to stop anaphase after depletion of KIF15 and inhibition of EG5 (Figure 26) is due to MKLP1 being brought to the midzone after onset of anaphase (Kurasawa et al., 2004). Interestingly, while this combination is capable of reducing both spindle elongation and chromosome segregation rates in RPE-1 cells (Figure 45), an additive effect to MKLP1 depletion combined with EG5 inhibition (Figure 44) or MKLP1 depletion was not observed, either when combined with KIF15 depletion or not (Figures 31, 44 and 45).

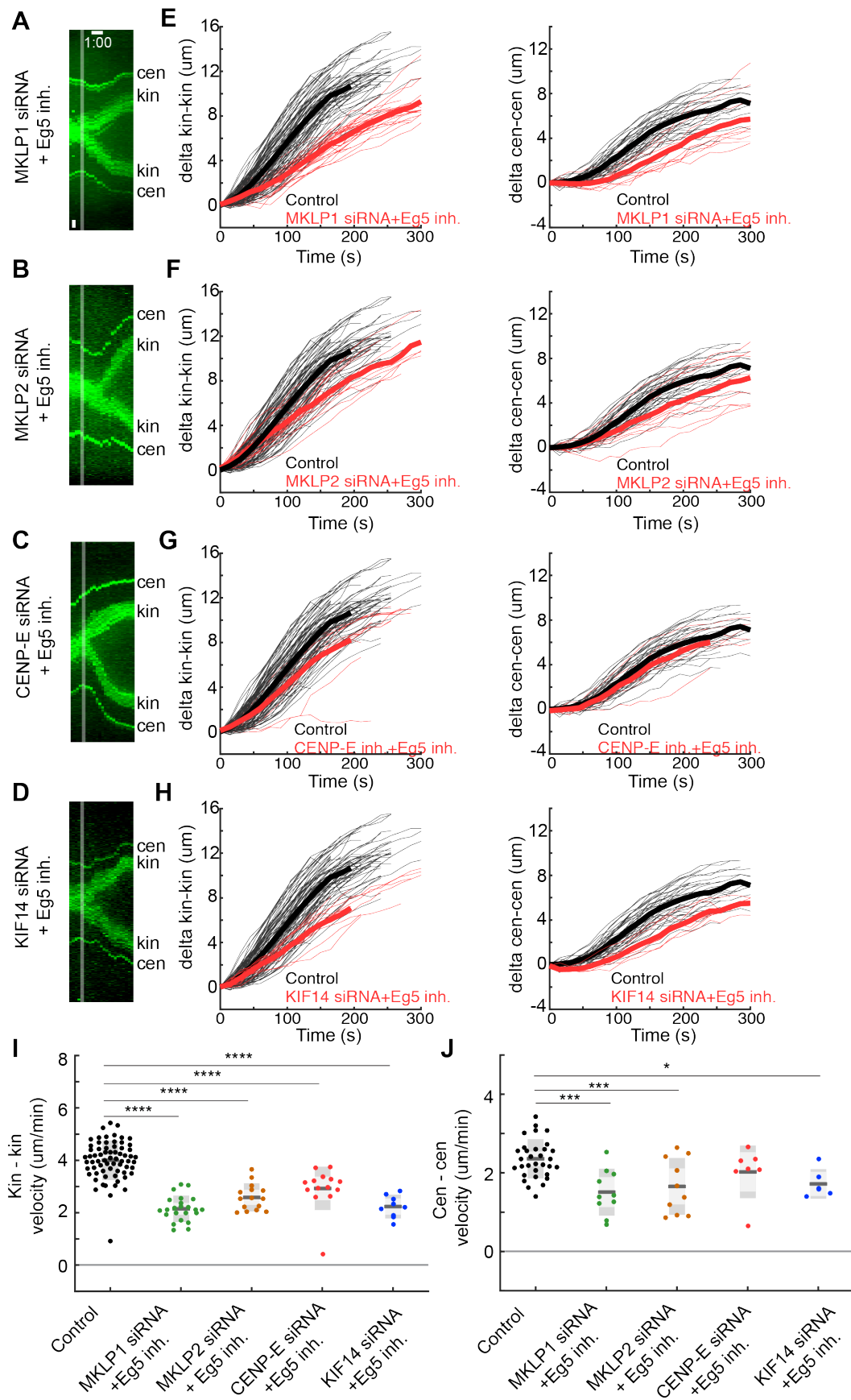




**Figure 44. Depletion of PRC1 interacting partners with inactivation of EG5 has a minor effect on anaphase spindle elongation.** (A-D) Kymographs (consecutive maximal intensity projections onto the x-axis) of the live cell images of RPE-1 cells stably expressing CENP-A-GFP and centrin1-GFP in the siRNA depletions of KIF4A, MKLP1, MKLP1 + MKLP2 and CENP-E inhibition combined with S-trityl-L-cysteine (STLC)-treatment. (E-H) Plots of relative kinetochore and centrosome separation distance (delta) defined as the kinetochore-to-kinetochore (kin-kin) and centrosome-to-centrosome (cen-cen) distance at time t minus the kin-kin and cen-cen distance at t = 0, over time. Individual kinetochore and centrosome pairs (thin lines), mean (thick lines) for each condition from (A). Time 0 represents anaphase onset. (I, J) Quantification (univariate scatter plot) of velocity of separation of sister kinetochores (kin-kin) and spindle elongation (cen-cen) velocity. Boxes represent standard deviation (dark grey), 95% standard error of the mean (light grey) and mean value (black) for each condition from (A). Statistics: t test (\*\*P < 0.01; \*\*\*P < 0.001). Vertical scale bars, 1  $\mu$ m. Horizontal scale bar, 1 min.

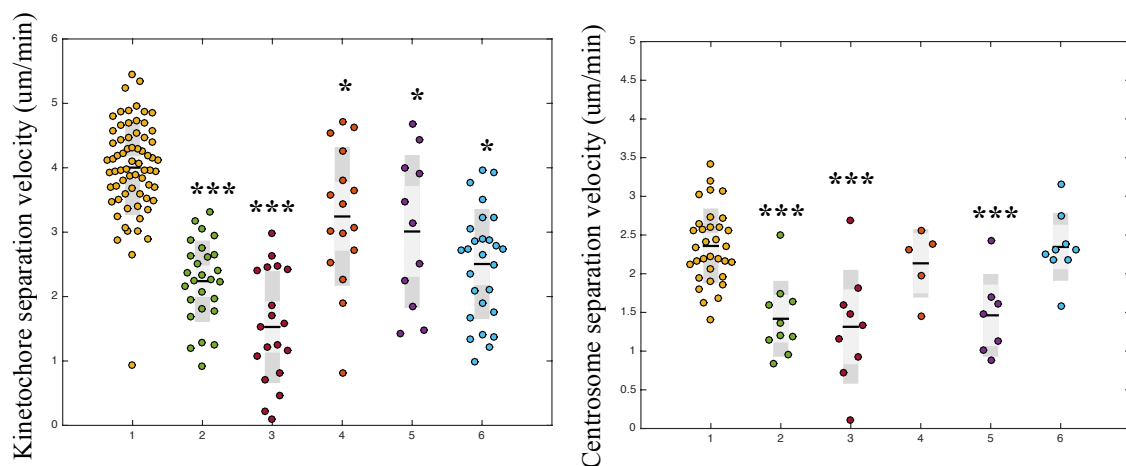


**Figure 45. Depletions of different regulatory proteins do not strongly impact anaphase velocities or display additive effects in comparison with single inhibitions.** Quantification (univariate scatter plot) of velocity of separation of sister kinetochores (left) and spindle elongation (right) velocity. Boxes represent standard deviation (dark grey), 95% standard error of the mean (light grey) and mean value (black) for each condition. Statistics: t test (\* < 0.05; \*\*\*P < 0.001). Conditions: 1-Control, 2-MKLP1+KIF15 depletion, 3-MKLP1+KIF15 depletion combined with EG5 inhibitions, 4-KIF18A depletion 5-KIF18A+PRC1 depletion, 6-EB3 depletion.



#### 4.1.9 Both Auroras are regulating spindle elongation

After it was have established that EG5 and PRC1-interacting partner KIF4A are crucial for spindle elongation, the study turned to regulation of this process by studying the role of Aurora kinases, main downstream regulators of multiple components important during anaphase (Afonso et al., 2017). Surprisingly, inhibition of both Aurora kinases at anaphase onset by small molecule inhibitor ZM-447439 (Ditchfield et al., 2003) also completely blocked anaphase spindle elongation (Figure 46), as reported previously (Afonso et al., 2014), and co-inhibition of Aurora kinases and EG5 obtained similar results (Figure 46). This suggested that Aurora kinases might separately regulate both sliding modules acting as a major regulators of spindle elongation in human cells, but that hypothesis awaits further studies (see Concluding discussion section for more details).

To establish that Auroras are indeed crucial for spindle elongation, and to test whether Aurora B is controlling KIF4A module while Aurora A controls EG5 module, as it was predicted, both kinases were inhibited with their specific inhibitors, Barasertib (AZD1152-HQPA) for Aurora B and Aurora A Inhibitor I (TC-S 7010) for Aurora A (see Materials and methods for details), and then combine these inhibitors with KIF4A depletion and EG5 inhibition with STLC. However, it was observed that while inhibition of both kinases separately can impact the spindle elongation and kinetochore segregation velocities, as observed previously (Reboutier et al., 2013, Hegarat et al., 2011), the inhibition of both kinases by mixing the drugs up did not produced the expected additive effect and did not induce spindle elongation block (Figure 47). This was unexpected and contrary to inhibition of both kinases by ZM-447439 inhibitor which induced strong spindle elongation block (see above, compare Figures 46 and 47), which suggested that this inhibitor was probably acting non-specifically on other mitotic kinases (see Concluding discussion for more details) or these inhibitors are not inhibiting Auroras as well as ZM drug. However, spindles treated with Aurora A inhibitor I exhibited fast shortening of the metaphase spindle, before entry into anaphase (data now shown), similarly to previous studies (Courtheoux et al., 2018), indicating that concentration of inhibitor was sufficient to inhibit kinase activity. Besides, spindle elongation block was not observed after combining EG5 inhibition with inhibition of Aurora B (Figure 47), predicted to control KIF4A protein localisation (Nunes-Bastos et al., 2013), and neither by combining KIF4A depletion with inhibition of Aurora A (Figure 47), known to depend on interaction with TPX2 (Kufer et al., 2002), protein regulator of EG5 motor (Ma et al., 2011). Moreover, as Aurora B is completely dependent on kinesin-6 MKLP2 to localise to

midzone MTs (Gruneberg et al., 2004), this result is consistent with the observation that depletion of MKLP2 when combined with EG5 inhibition did not induce spindle elongation block phenotype (Figure 44). To conclude, Aurora kinases are involved in control of spindle elongation, probably by controlling the length and stability of midzone MTs (Afonso et al., 2017), but their co-inhibition cannot specifically block this process in human cells, meaning that additional mechanisms are probably required, such is control by other mitotic kinases (see Concluding discussion for more details).

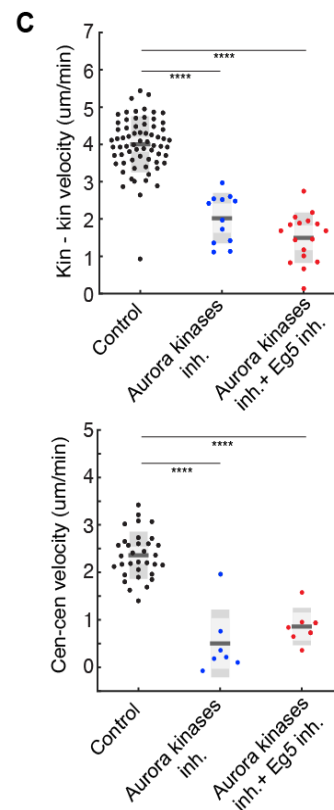
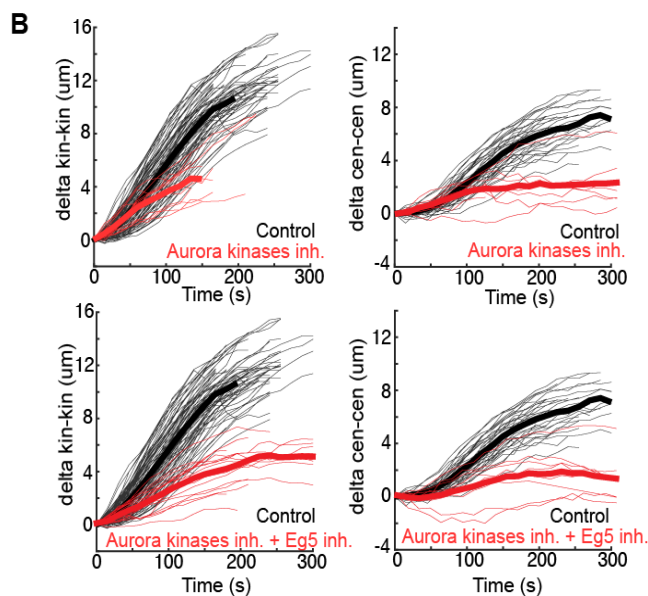
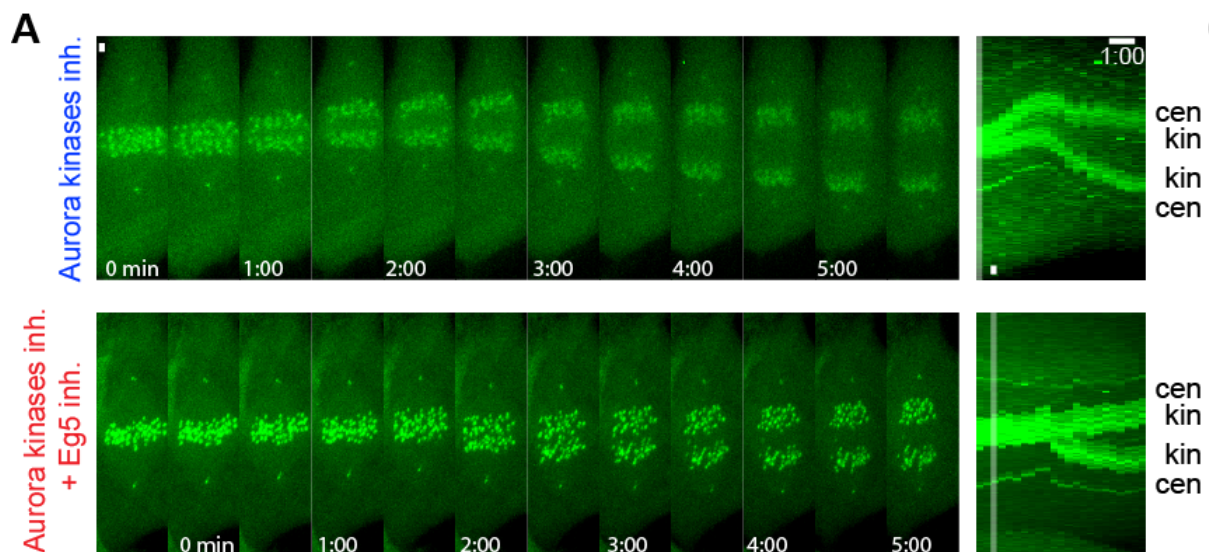


**Figure 46. Inhibition of both Aurora kinases by ZM-447439 blocks spindle elongation.**

**(A)** Live cell images of RPE-1 cells stably expressing CENP-A-GFP and centrin1-GFP treated with ZM-447439 and co-treated with ZM-447439 and STLC that show blocked spindle elongation. kin-kinetochore and cen-centrosome. Time 0 represents anaphase onset.

**(B)** Plots of relative kinetochore and centrosome separation distance ( $\Delta$ ) defined as the kinetochore-to-kinetochore (kin-kin) and centrosome-to-centrosome (cen-cen) distance at time  $t$  minus the kin-kin and cen-cen distance at  $t = 0$ , over time in ZM-447439 treated and S-trityl-L-cysteine (STLC) co-treated RPE-1 cells. Individual kinetochore and centrosome pairs (thin lines), mean (thick lines).

**(C)** Quantification (univariate scatter plot) of velocity of separation of sister kinetochores (left) and spindle elongation (right) velocity. Boxes represent standard deviation (dark grey), 95% standard error of the mean (light grey) and mean value (black) for each condition. Statistics: t test (\*\*\* $P < 0.001$ , \*\*\*\* $P < 0.0001$ ). Images are maximum projection of acquired z-stack. Time shown as minutes:seconds. Vertical scale bars, 1  $\mu\text{m}$ . Horizontal scale bar, 1min.

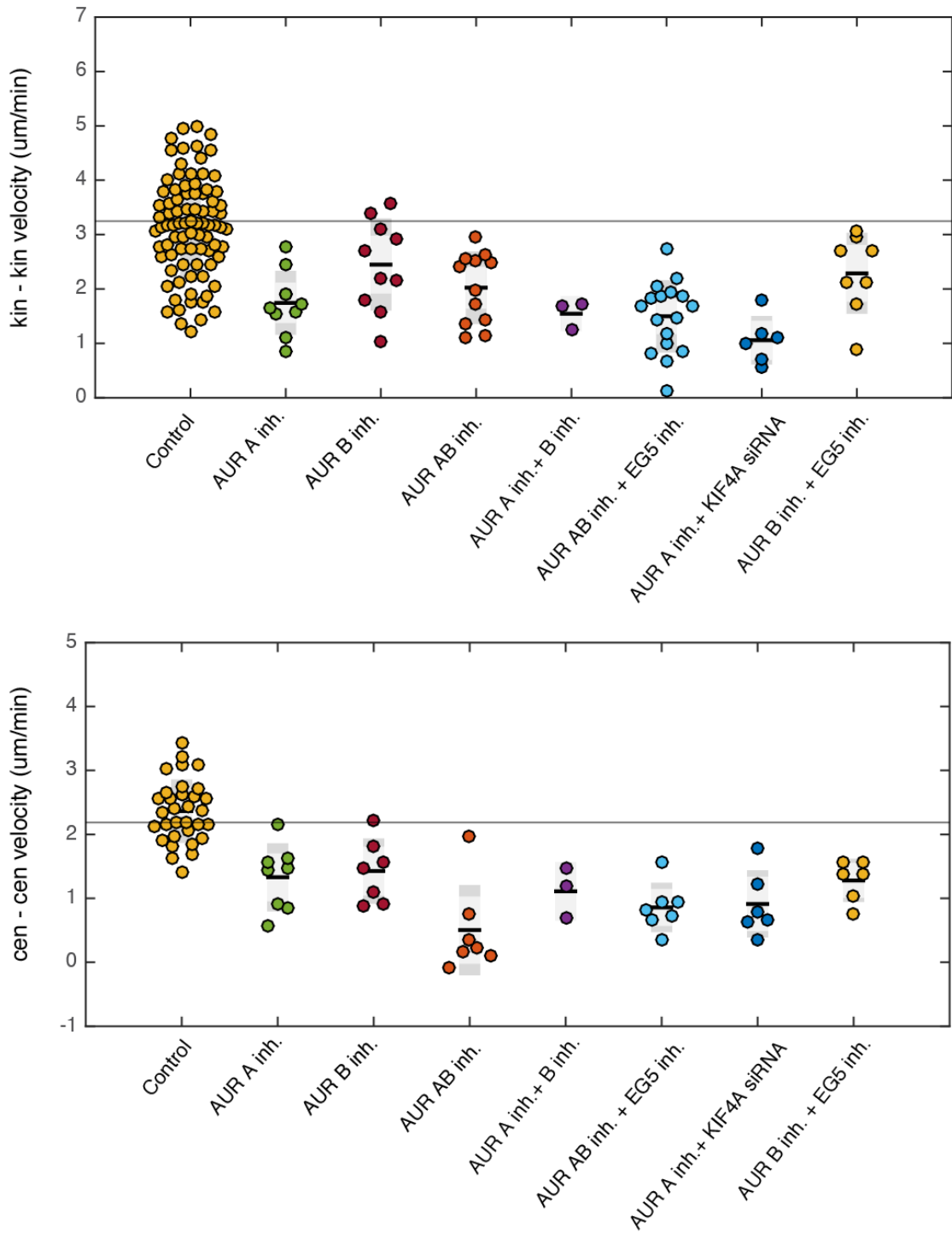


**Figure 47. Inhibition of Aurora kinases by differential inhibitors cannot induce spindle elongation block.** Quantification (univariate scatter plot) of velocity of separation of sister kinetochores (kin-kin, left) and spindle elongation (cen-cen, right) velocity across indicated conditions. Boxes represent standard deviation (dark grey), 95% standard error of the mean (light grey) and mean value (black) for each condition indicated. Horizontal black line represents mean value of the control population. Statistics: t test (\* < 0.05; \*\*\*P < 0.001).

#### 4.1.10 All tested perturbations have a little effect on structure of midzone microtubules

Next, the study turned to structural studies concerning spindle midzone MTs after important protein perturbations established thus far. To investigate whether complete lack of midzone MTs, reported by some to happen after depletion of PRC1 protein (Mollinari et al., 2002; Mollinari et al., 2005), could explain the observed anaphase arrest the  $\alpha$ -tubulin was immunolabeled, using a MT-preserving protocol (see Materials and methods section), after different treatments including depletion of PRC1, inhibition of EG5 by STLC treatment, combined depletion of PRC1 and inhibition of EG5 and combined depletion of KIF4A and inhibition of EG5. Using this approach, it was shown that midzone MT organization is similar in control and across the different treatments (Figure 48), some of which have a great impact on spindle elongation (see previous sections), meaning that midzone MTs were present in all conditions during early anaphase and no obvious structural differences could be detected using this assay. Also, no apparent effect can be detected on structural composition of astral MTs as well (Figure 48), as they were present in all conditions studied. Importantly, depletion of PRC1 often caused the global changes in midzone MT organization during late anaphase and telophase, where reduced signal of midzone MTs was sometimes observed and central spindle was not established in extreme examples when compared to controls (Figures 49 and 50), as reported in previous studies (Mollinari et al., 2002; Pamula et al., 2019). This suggested that PRC1 bundling of midzone MTs is important for establishment of central spindle during late anaphase, but is dispensable for maintaining structure of midzone antiparallel MTs during early anaphase, where most of spindle elongation takes place (Vukusic et al., 2019). Thus, global changes in midzone MT organization cannot explain the anaphase arrest phenotype observed after depletion of PRC1 or KIF4A when combined with inhibition of EG5 by STLC treatment.

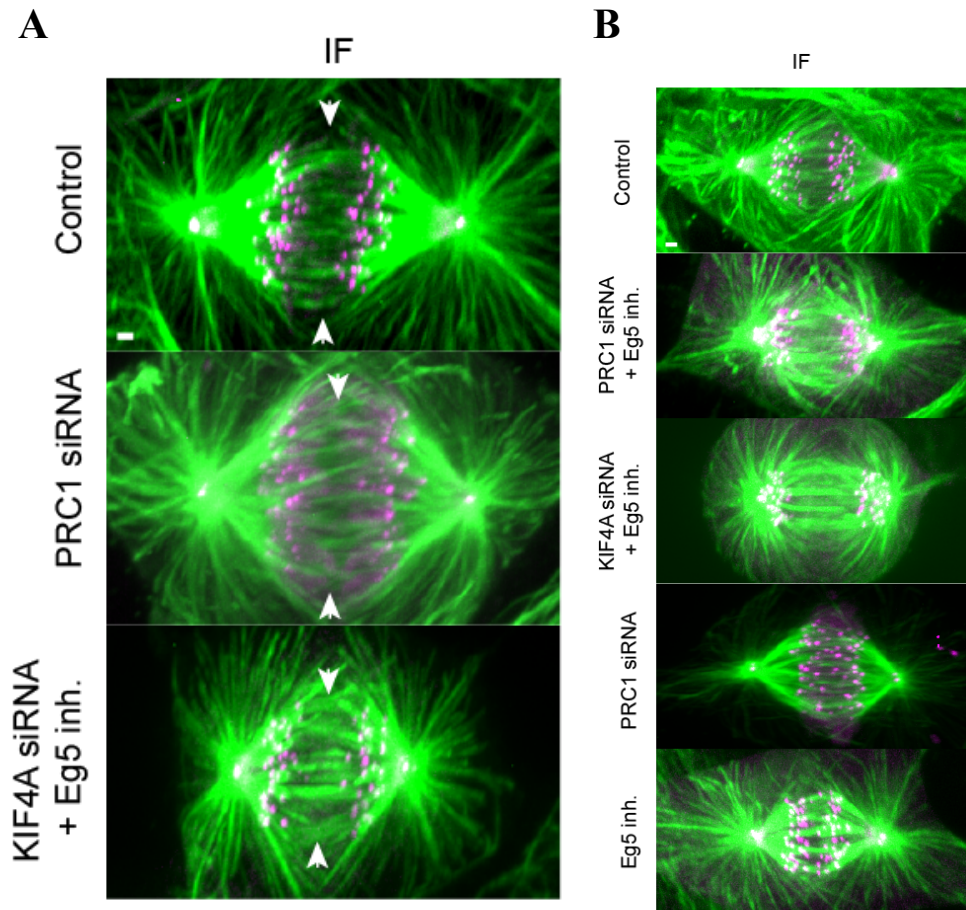


**Figure 48. Lack of spindle elongation and anaphase arrest cannot be explained by the lack of midzone microtubules. (A)** Immunofluorescent (IF) images of fixed control, PRC1 siRNA-depleted and Kif4A siRNA-depleted and STLC-treated RPE-1 cells stably expressing CENP-A-GFP and centrin1-GFP (magenta) and stained with AlexaFluor594 conjugated with  $\alpha$ -tubulin antibody (green). **(B)** Immunofluorescence (IF) images of fixed RPE-1 cells stably expressing CENP-A-GFP and centrin1-GFP (magenta) stained with AlexaFluor594 conjugated with  $\alpha$ -tubulin antibody in indicated conditions. Scale bars, 1  $\mu$ m.



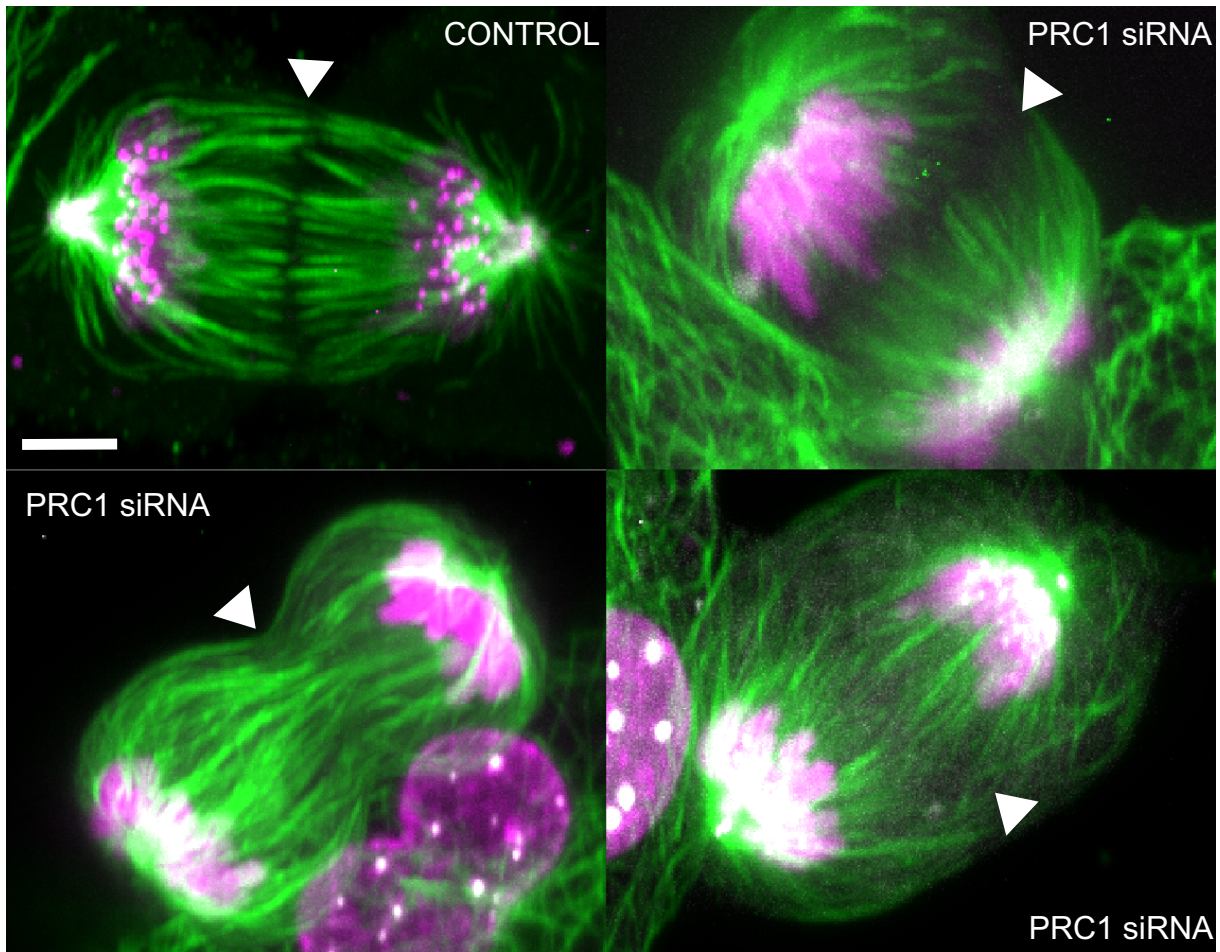


**Figure. 49. Depletion of PRC1 is disrupting central spindle structure in the late anaphase cells.** Maximum z-projection images of control (top left) and PRC1 siRNA depleted RPE-1 cells stably expressing CENP-A-GFP and centrin1-GFP labelled with secondary antibody AlexaFluor488 targeted against  $\alpha$ -tubulin primary antibody. Arrowheads point to the spindle midzone region. Scale bar; 5  $\mu$ m.

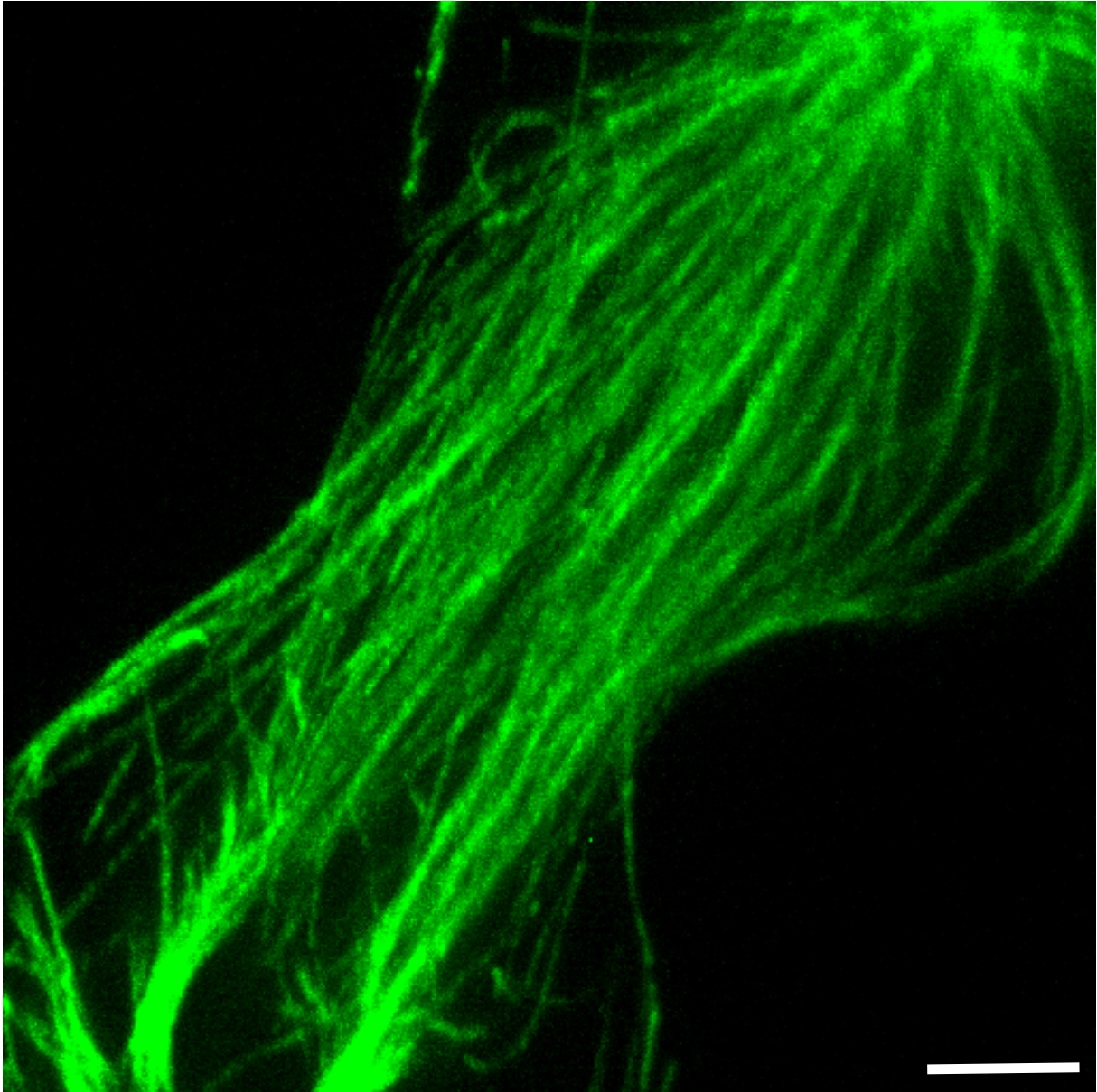


**Figure. 50. Expansion microscopy of the central spindle after depletion of PRC1.** Maximum z-projection expanded image of and PRC1 siRNA depleted RPE-1 cell labelled with secondary antibody AlexaFluor488 targeted against  $\alpha$ -tubulin primary antibody. Scale bar; 5  $\mu$ m.

To further confirm these results, the expansion microscopy technique was employed (Chozinski et al., 2016, see previous sections), in which the sample is mechanically expanded in a swellable polymer gel to obtain much better resolution on standard confocal microscopes when compared with the classical immunofluorescence protocols (Tillberg et al., 2015). By using this technique, it was observed that midzone MTs were indeed present in central part of the spindle in all conditions studied, including STLC treatment only, combination of KIF4A



depletion and STLC treatment and control untreated cells (Figures 51 and 52). In all conditions bridging midzone MTs were present in discrete filamentous pattern, and no obvious structural aberrations could be detected (Figures 51 and 52).

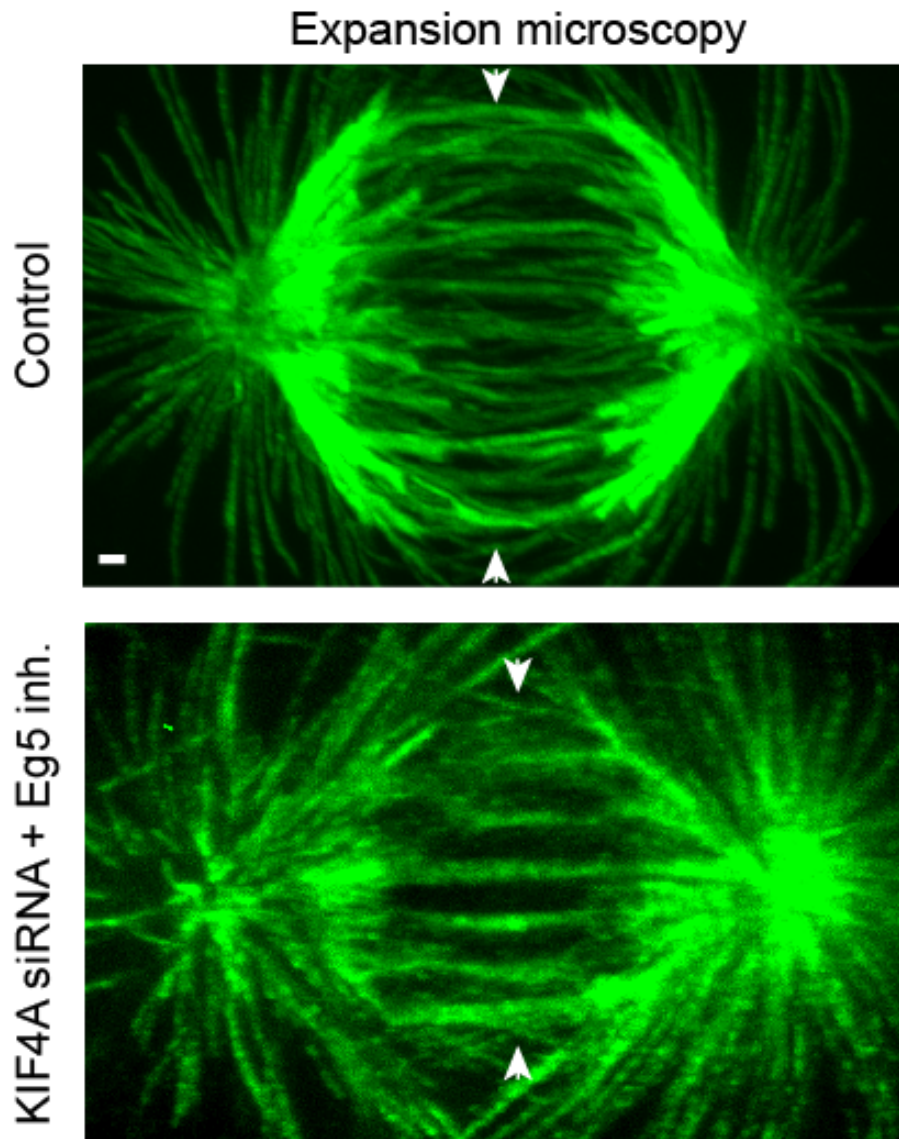


**Figure 51. Spindle midzone microtubules are not lost after combined depletion of KIF4A and inhibition of EG5 by STLC.** Expansion microscopy images of fixed control (top) and Kif4A siRNA-depleted and STLC-treated RPE-1 (bottom) cells stained with AlexaFluor594 conjugated with  $\alpha$ -tubulin antibody. Expansion factor is estimated from spindle length to be 2.3x. Images are maximum projection of acquired z-stack. Scale bar, 1  $\mu$ m.

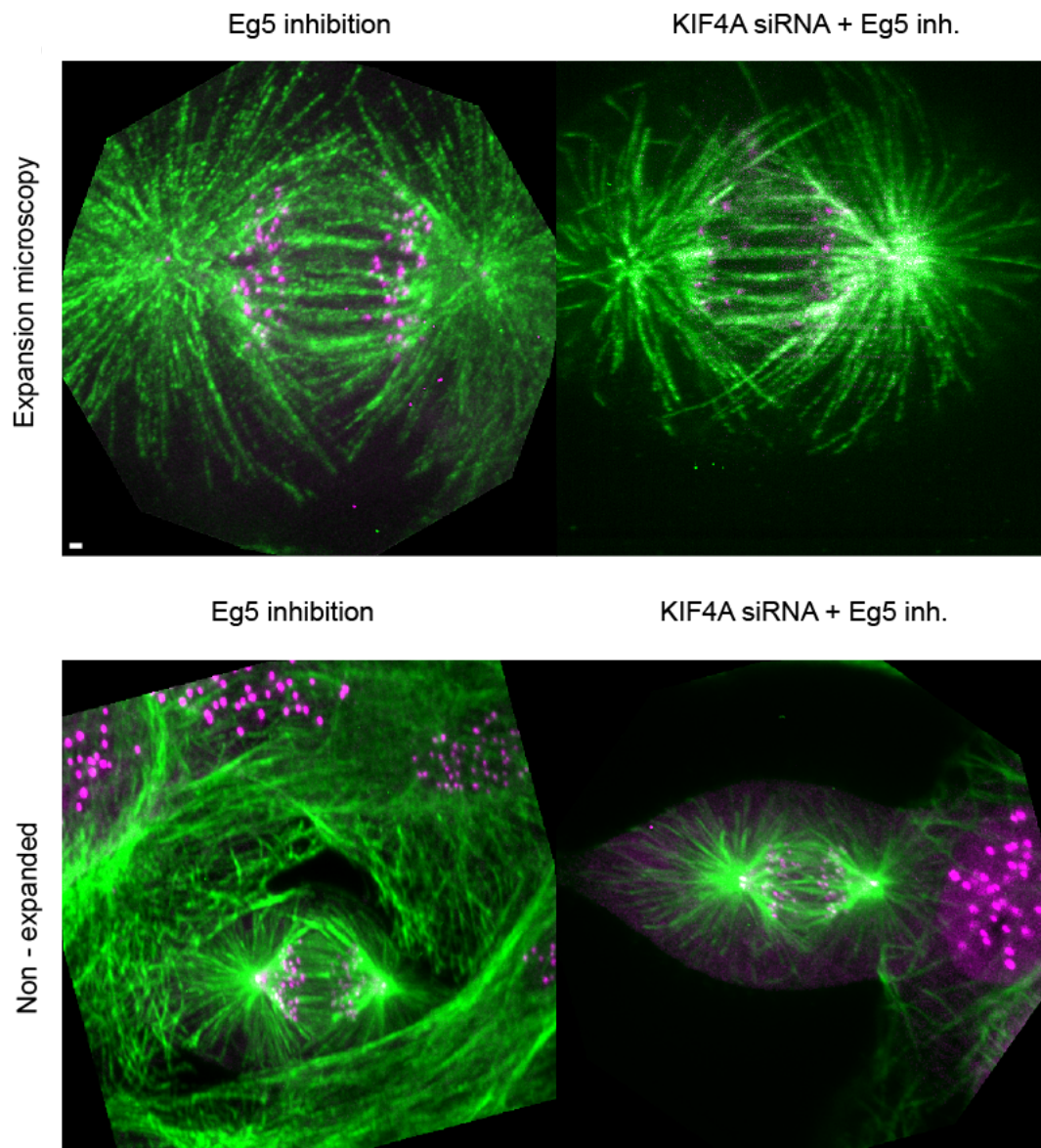


**Figure 52. Lack of spindle elongation observed after depletion of KIF4A and inhibition of EG5 cannot be explained by loss of midzone microtubules.** Expanded and non-expanded images of fixed STLC-treated and KIF4A siRNA-depleted and STLC-treated RPE-1 cells stably expressing CENP-A-GFP and centrin1-GFP (magenta) stained with AlexaFluor594 conjugated with  $\alpha$ -tubulin antibody (green). Expansion factor is estimated from measured spindle length to be 2.3x. Images are maximum projection of acquired z-stack. Scale bar, 1  $\mu$ m.

#### 4.1.11 Decrease in protein stability cannot explain the block in spindle elongation

Afterwards, the study turned to dynamic studies of deviations in MT stability that could possibly be a result of different treatments presented above, to answer if this

mechanism explains the anaphase arrest phenotype observed. This approach was done because it was previously reported that depletions of PRC1 or MKLP1 can affect MT stability (Hu et al., 2012; Vukusic et al., 2017) and changes in MT stability are known to impact anaphase movements in general (Hegarar et al., 2011; Hu et al., 2011; Hu et al., 2012). Furthermore, to check the effect of increased midzone MT stability on anaphase movements PRC1 protein was overexpressed in the U2OS cells by transient expression of PRC1 protein from a plasmid with a constitutive promoter (see Material and methods for details). After imaging spindles in anaphase with various PRC1 levels on the spindle (Figure 53) the total PRC1 signal on the spindle in each cell was quantified (see Materials and methods) and compared with mean separation velocities, regarding key anaphase parameters, in the same cell (Figure 53). By using this approach, it was showed that over-bundling of midzone MTs by means of overexpressing PRC1 in U2OS cells can greatly reduce spindle elongation velocity, chromosome segregation velocity and even poleward chromosome velocity (Figure 53). This implicated that increased stability of MTs in the antiparallel region by over-bundling of these MTs can reduce spindle elongation velocities and moreover, increasing the level of PRC1 protein on the spindle lowered the spindle elongation velocities, probably through large increase in frictional forces that oppose the outward forces exerted by molecular motors in the overlaps (Wijeratne and Subramanian, 2018) (see Concluding Discussion for more details).

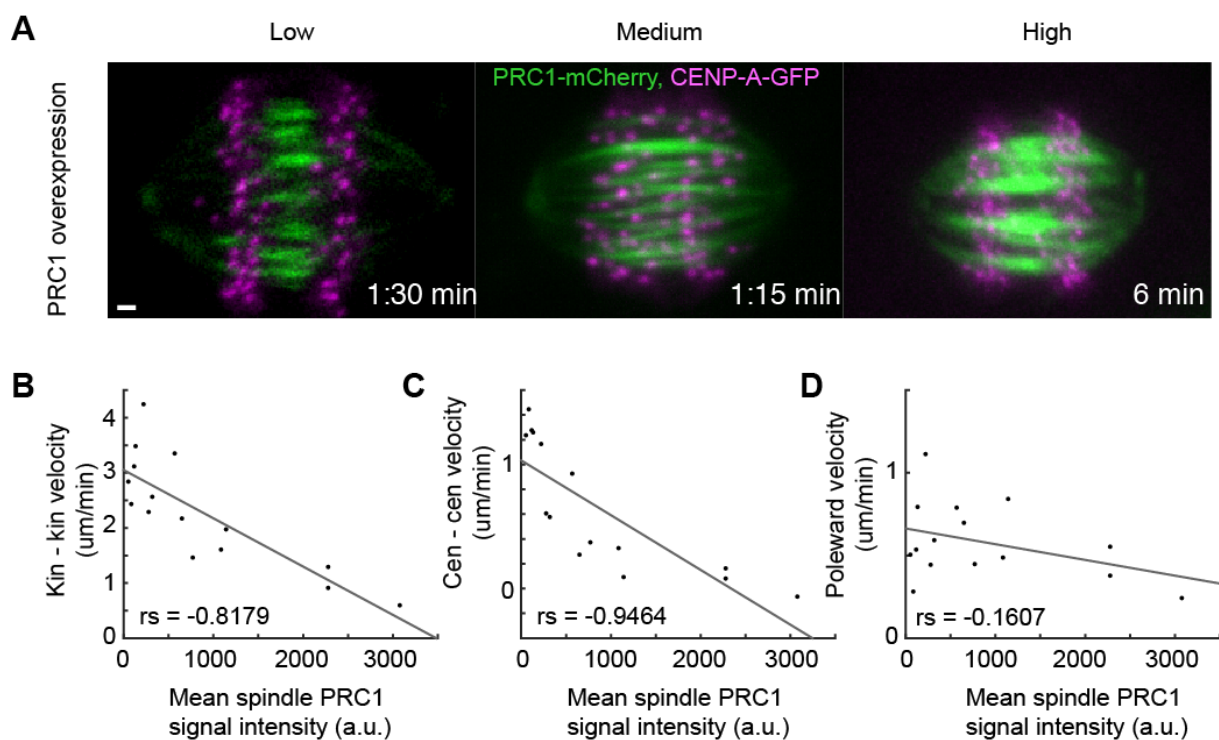


**Figure 53. PRC1 overexpression decreases spindle elongation velocities in U2OS cells.**

(A) Live cell images of U2OS cells stably expressing CENP-A-GFP and transiently



expressing various levels of PRC1-mCherry as indicated. **(B-D)** Linear regression and distribution of kinetochore separation (kin-kin), centrosome separation (cen-cen) and kinetochore-to-centrosome (poleward) velocity versus mean PRC1 signal intensity.  $r_s$ , Spearman correlation coefficient,  $P < 0.001$ . Images are maximum projection of acquired z-stack. Time 0 represents anaphase onset. Time shown as minutes:seconds. Scale bar, 1  $\mu\text{m}$ .

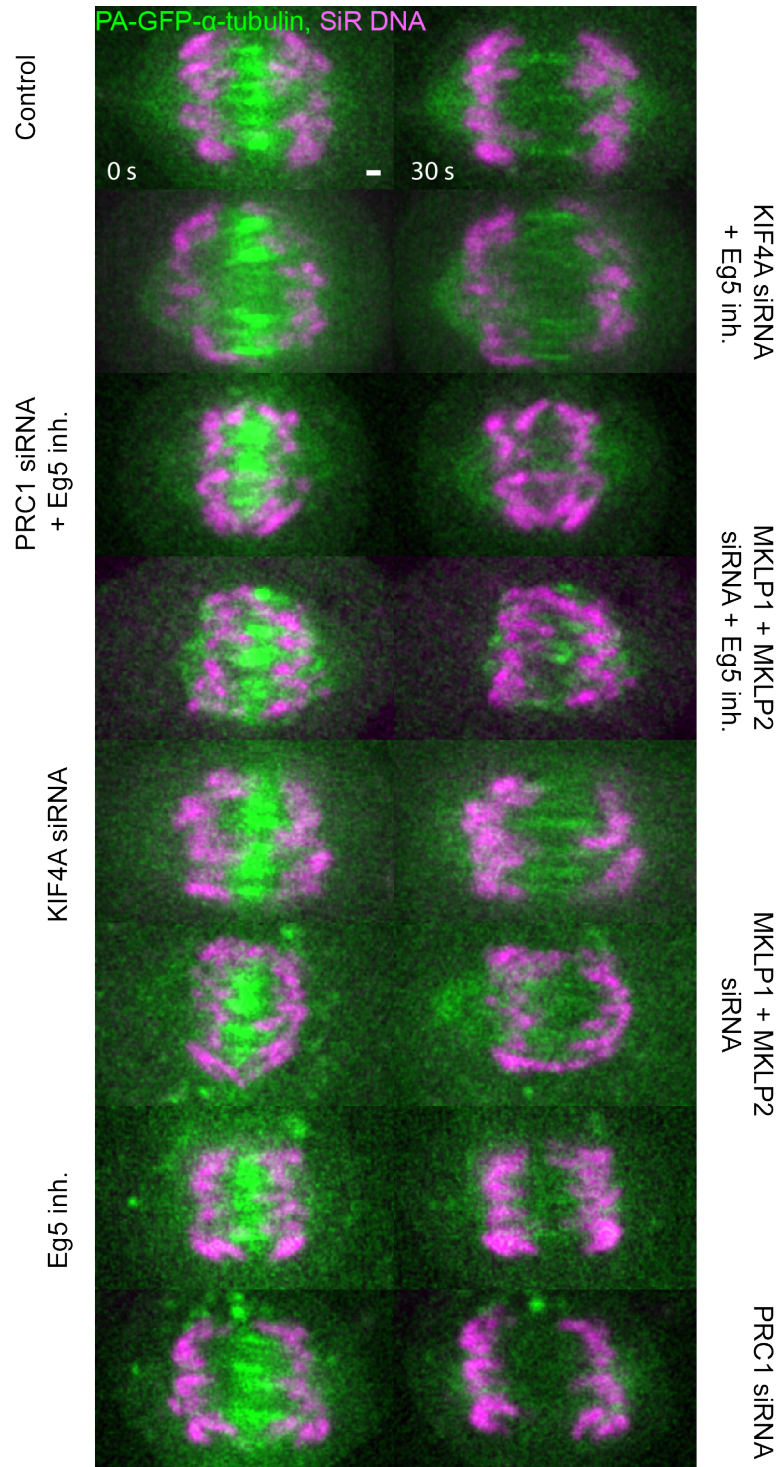


**Figure 54. Characterization of midzone stability in RPE-1 cells after different treatments using midzone photoactivation assay.** Smoothed live cell images of RPE-1 cells after photoactivation of photoactivatable (PA)-GFP- $\alpha$ -tubulin in indicated conditions. Silicon rhodamine (SiR)-DNA (magenta) was used for chromosome staining. Time 0 represents photoactivation onset. Images are single z-planes. Time shown in seconds (s). Scale bars, 1  $\mu$ m.

Because stability can negatively influence spindle elongation, it was investigated whether the anaphase arrest phenotype of afore mentioned RNA interference (RNAi) combinations, when combined with EG5 inhibition (see previous sections), is due to disrupted MT stability. To do so, the fluorescence dissipation after photoactivation (FDAPA) of photoactivatable(PA)-GFP- $\alpha$ -tubulin was used to measure MT stability in various conditions (Figures 54 and 55) (see Material and methods for details). An assay in which midzone MTs were photoactivated after onset of anaphase in a line pattern (see Materials and methods for details) was used and chromosomes were additionally labelled using SiR-DNA stain (Figures 54 and 55). MT stability was reduced significantly only in combinations that included depletion of PRC1 protein, as shown previously (Hu et al., 2011), while in the remaining conditions MT stability was not greatly impaired (Figures 54 and 55). Somewhat surprisingly reduced stability was also observed in STLC-treatment only (Figures 54 and 55), but this trend was not followed in other combinations where EG5 was inhibited by the same drug together with depletion of other proteins (Figures 54 and 55).

Besides, to test the connection between degree of stability of midzone MTs and anaphase velocities across conditions, it was tested whether chromosome segregation and spindle elongation velocities depend on the MT stability across the treatments (Figure 55). Surprisingly, these velocities were not correlated with MT stability across conditions (Figure 55), demonstrating that the strong effect seen after modulating kinesin EG5 together with KIF4A or MKLP1 and MKLP2 or PRC1 does not depend on the lowered midzone MT turnover rates. Spindle elongation during early anaphase is thus, contrary to earlier suggestions (Pamula et al., 2019), independent of midzone MT stability provided primarily by MT bundling protein PRC1.

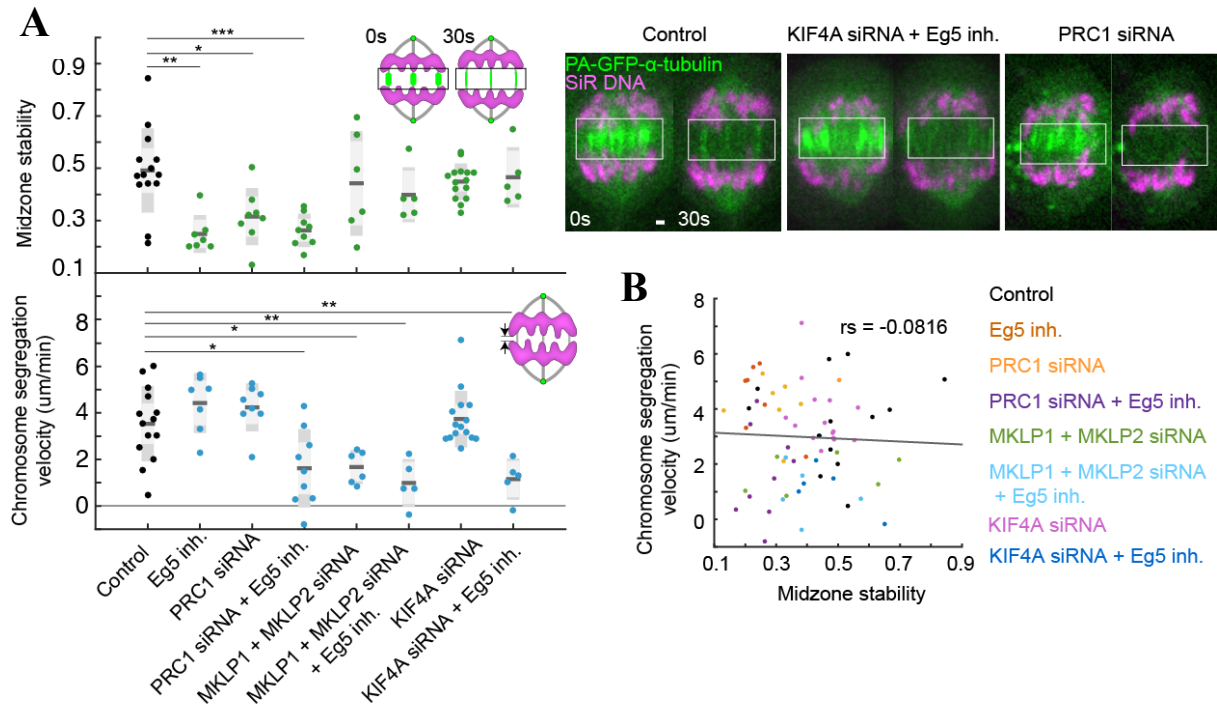


**Figure 55. Decreased midzone stability does not affect chromosome segregation velocities during anaphase.** (A) Smoothed live cell images of RPE-1 cells after photoactivation of photoactivatable (PA)-GFP- $\alpha$ -tubulin in indicated conditions. SiR-DNA (magenta) was used for chromosome staining. Time 0 represents photoactivation onset. Integrated area of intensity was measured using region indicated with a box, along short axis of a box (right). Quantification of ratio of integrated photoactivated signal at time 30s and 0s from onset of photoactivation and chromosome segregation velocity in same time frame in indicated treatments (see schemes). Statistics: t test (\* $P < 0.05$ ; \*\*  $P < 0.01$ ; \*\*\* $P < 0.001$ ) (left). (B) Linear regression and distribution of chromosome segregation velocity versus midzone stability in the different conditions.  $r_s$ , Spearman correlation coefficient,  $P < 0.001$ . Scale bar, 1  $\mu\text{m}$ .

#### 4.1.12 Sliding is greatly perturbed in conditions that block spindle elongation

Finally, the study turned to dynamic study of MT sliding using the same assay as in experiments when MT stability was measured to investigate whether EG5 and KIF4A exert anaphase arrest through defective antiparallel MT sliding, as was predicted. The sliding of midzone MTs after photoactivation of PA-GFP- $\alpha$ -tubulin was quantified by measuring the width of photoactivated spot on midzone MTs over time (Figures 56 and 57), using that as a

readout of sliding force since width of photoactivated spot is increasing during sliding of antiparallel MTs (Vukusic et al., 2017) (Figures 56 and 57). Because some treatments greatly reduced the stability of midzone MTs (Figures 54 and 55), the imaging parameters were adjusted to achieve very fast imaging, with 0.8s interval between two consecutive frames (see Materials and methods). This approach enabled the high-quality imaging of MT dynamics in conditions where midzone MT stability was very low.



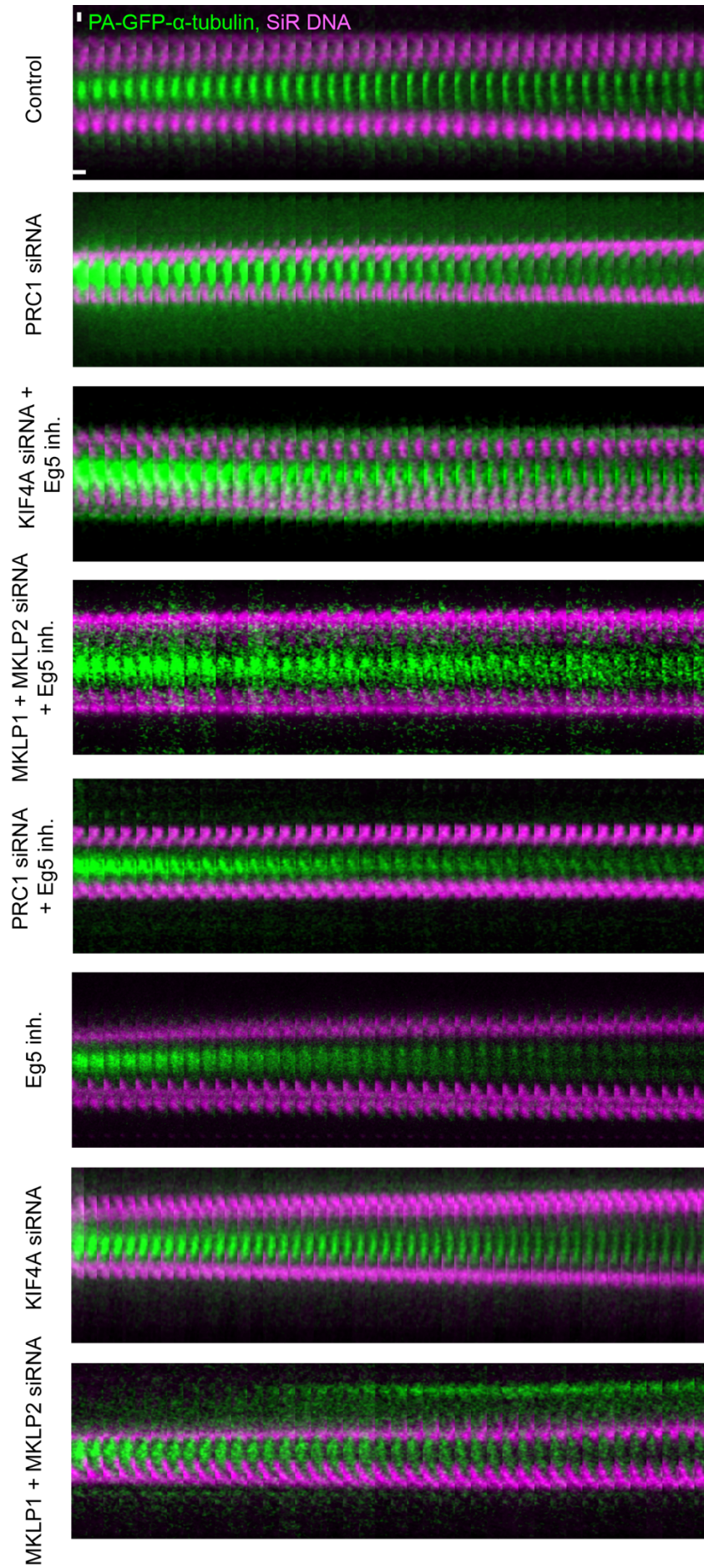




**Figure 56. Characterization of sliding in RPE-1 cells after different treatments using midzone photoactivation assay.** Smoothed time-lapse live images of mitotic spindle midzone region in RPE-1 cells after photoactivation of photoactivatable (PA)-GFP- $\alpha$ -tubulin in indicated treatments. Silicon rhodamine (SiR)-DNA (magenta) was used for chromosome staining. Horizontal scale bar, 0.8s. Vertical scale bar, 1  $\mu$ m.

Surprisingly, the sliding velocity was significantly reduced compared to controls after simultaneous depletion of KIF4A and EG5 inhibition (Figures 56, 57 and 58). In line with this data, all other conditions impacting KIF4A activity (see previous sections), combined with EG5 inhibition, mimicked this phenotype strongly affecting sliding velocities (Figures 56, 57 and 58). Unexpectedly, sliding could be observed and measured in conditions that had a great impact on stability of midzone MTs (Figures 54 and 55), like after depletion of PRC1 protein (Figure 57), meaning that stable antiparallel MTs bundled by PRC1 are not prerequisite for MT sliding during anaphase in human cells (See Concluding discussion for details). On the other hand, one consequence of decreased MT stability was that MT sliding could not be observed after 40s of photoactivation in those conditions, lasting approximately 20s in most photoactivated bundles (data not shown) (see Materials and methods for details).

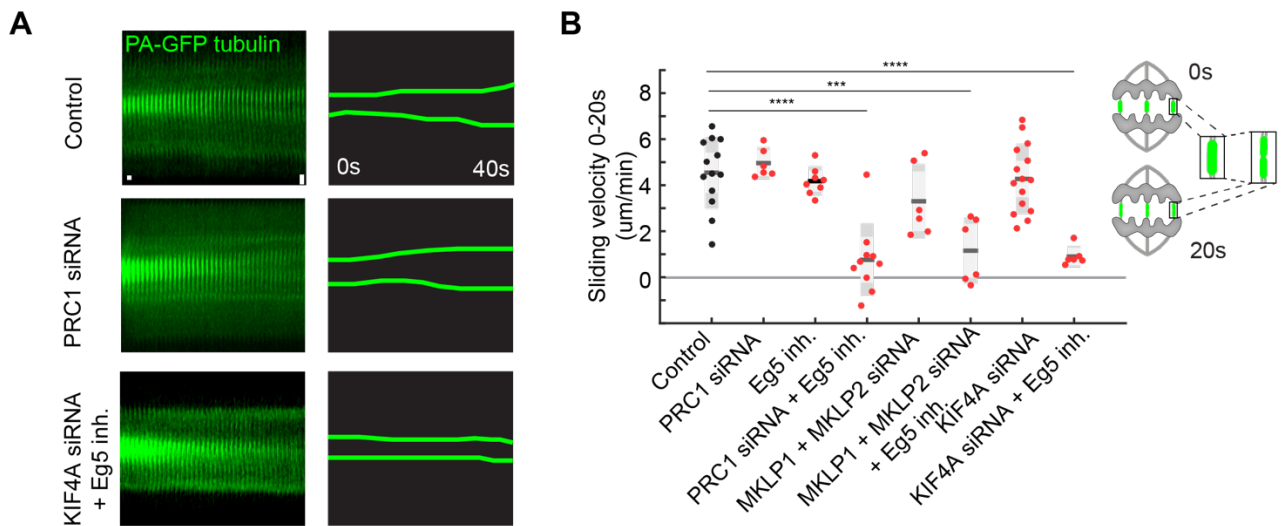


**Figure 57. Chromosome segregation and spindle elongation are dependent upon KIF4A and EG5-generated sliding.** (A) Montage time-lapse live images of mitotic spindle midzone region after photoactivation of photoactivatable (PA)-GFP- $\alpha$ -tubulin in indicated treatments. Note that photoactivated spot does not spread in time after KIF4A siRNA depletion and STLC

treatment compared with control and PRC1 siRNA depletion (see scheme generated from kymographs on the left). Horizontal scale bar, 0.8s. Vertical scale bar, 1  $\mu\text{m}$ . **(B)** Quantification of velocity of photoactivated spot spreading (sliding velocity, see scheme) in the different conditions. Statistics: t test (\*\*P < 0.01; \*\*\*\*P < 0.0001).

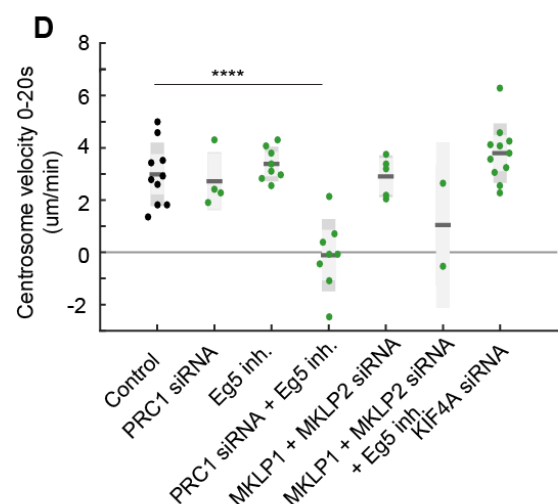
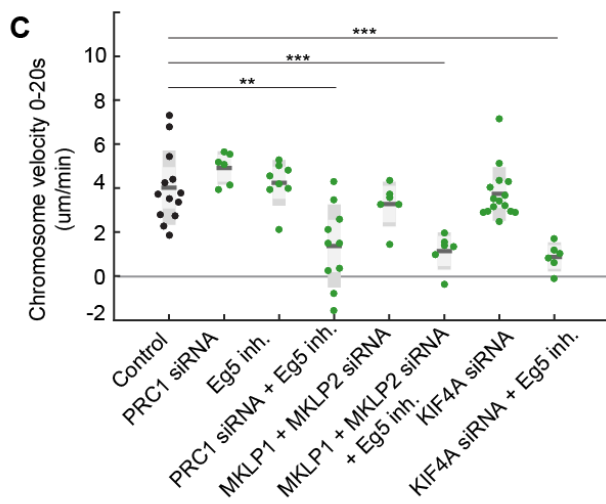
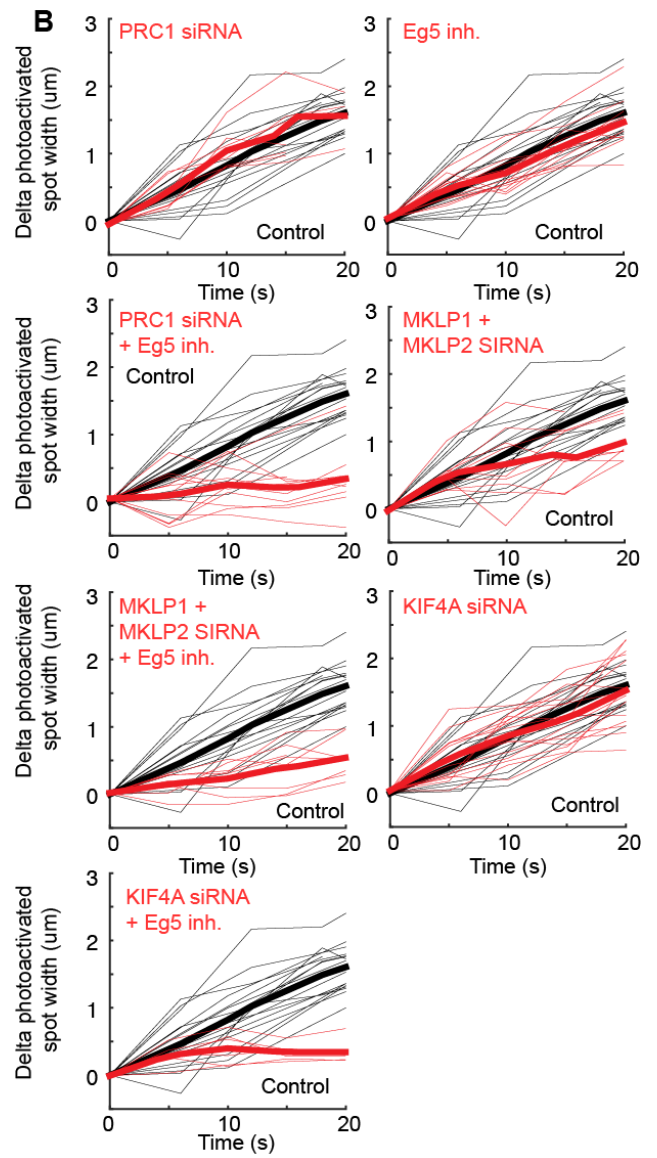
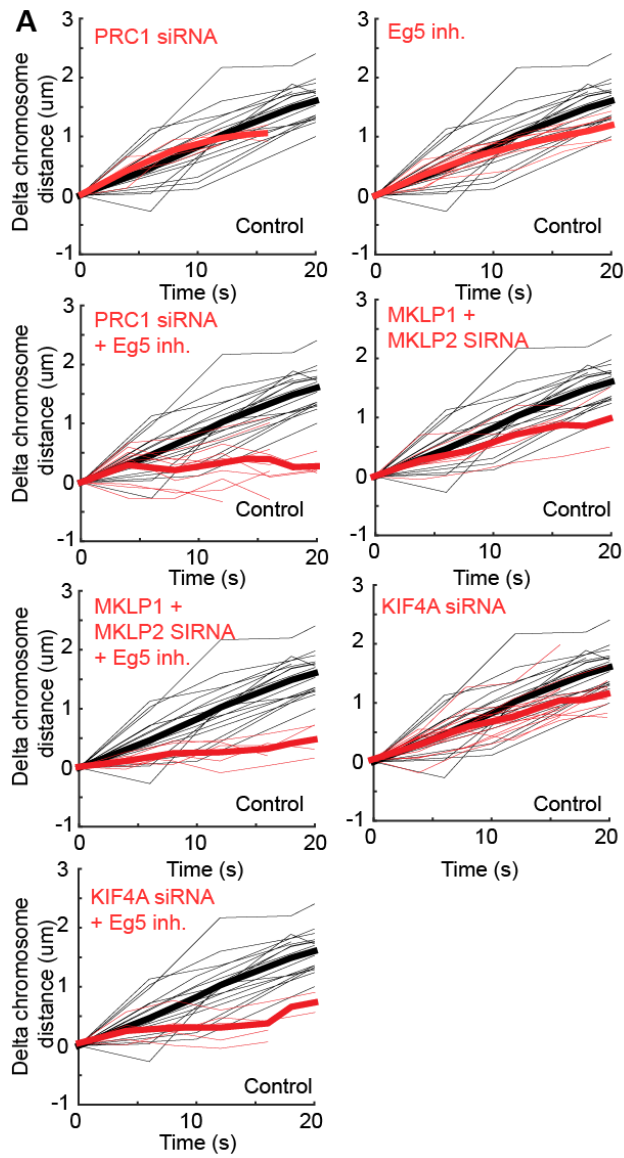


**Figure 58. Sliding of midzone microtubules and anaphase velocities are impaired after EG5 inhibition when combined with conditions perturbing KIF4A motor protein. (A)** Plots of relative chromosome segregation distance ( $\Delta$ ) defined as the chromosome-to-chromosome distance at time  $t$  minus the chromosome-to-chromosome distance at  $t = 0$ , over time in RPE-1 cells stably expressing CENP-A-GFP and centrin1-GFP in indicated conditions. Individual kinetochore and centrosome pairs (thin lines), mean (thick lines). **(B)** Plots of relative photoactivated spot length ( $\Delta$ ) defined as the photoactivated spot length at time  $t$  minus the photoactivated spot length at  $t = 0$ , over time in RPE-1 cells in indicated conditions. Time 0 represents photoactivation onset. **(C, D)** Quantification (univariate scatter plot) of velocity of chromosome segregation and centrosome separation. Boxes represent standard deviation (dark grey), 95% standard error of the mean (light grey) and mean value (black) for indicated conditions. Statistics: t test (\*\*  $P < 0.01$ ; \*\*\* $P < 0.001$ ; \*\*\*\* $P < 0.0001$ ).

Finally, to test the possible relationship between degree of MT sliding in midzone MTs and anaphase velocities across conditions, it was tested whether chromosome segregation and spindle elongation velocities depend on the degree of midzone MT sliding. Surprisingly, chromosome segregation and spindle elongation velocities were strongly correlated with sliding rates across conditions (Figure 59), which suggested that the origin of anaphase arrest is a result of defective MT sliding. Consequently, it could be said that MT sliding is thus a good predictor of whether anaphase will result in successful or unsuccessful separation of chromosomes (Figures 56, 57, 58 and 59). Taken together, it was concluded that KIF4A and EG5 are major plus-end directed sliding motors in anaphase crucial for faithful chromosome segregation in human cells.

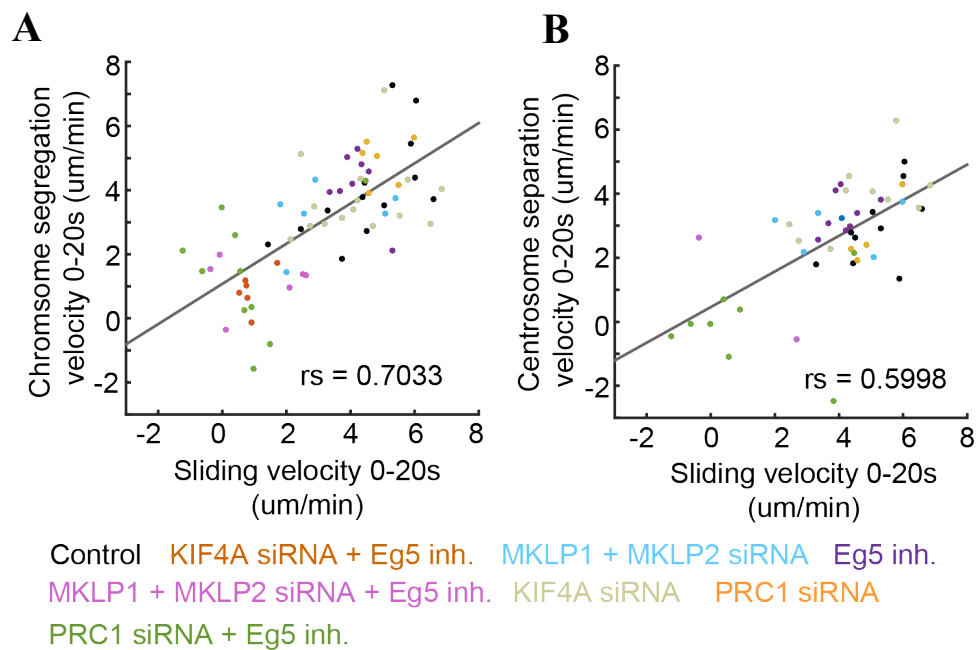


**Figure 59. Chromosome segregation and spindle elongation are correlated with sliding velocities across conditions.** (A, B) Linear regression and distribution of chromosome segregation velocity and centrosome separation velocity versus sliding velocity in the different conditions as indicated. Original data on Figure 52. rs, Spearman correlation coefficient,  $P < 0.001$ .

## 4.2 Additional experiments on U2OS cells

The set of depletion or inhibition experiments on human tumour osteosarcoma U2OS cell line was also performed to get a better insight into force-generating mechanisms of anaphase in that model cell line. The cell line that was used had a stable expression of kinetochore marker CENP-A-GFP, photoactivatable (PA)-GFP-alpha-tubulin and mCherry-alpha-tubulin (see Materials and methods for details). As was already noted, it was noticed that this cell line was characterized by decreased chromosome separation velocities when compared to non-transformed RPE-1 cells (compare Figures 21 and 26F), and what is more important to values for U2OS cells found in the literature (Ganem et al., 2005), or to the same cell line after complete loss of alpha-tubulin-mCherry expression (Figure 21). The problem was traced to alpha-tubulin labelling with mCherry fluorophore or constant overexpression of

alpha-tubulin in these cells, first one being more plausible explanation (see Concluding discussion for details).

By performing multiple perturbation experiments, however, it was observed that individual siRNA depletions of spindle midzone components PRC1 and its partner MKLP1 lowered chromosome segregation rates in these cells when compared to controls (Figure 61), probably reflecting their role in MT stabilization by extensive MT bundling during anaphase (Hu et al., 2011; Vukusic et al., 2017) (see Concluding discussion for more details). Interestingly, these results did not follow ones on RPE-1 cells where these two individual depletions did not alter chromosome segregation rates to similar degree (Figures 29, 30 and 31), although MKLP1 depletion was following the same overall trend in both cell lines, as reported already in the literature (Abaza et al., 2003). Also, these depletions similarly influenced spindle elongation rates and also poleward velocity rates in U2OS cells (Figures 60 and 62), pointing they might be operating on the same pathway, as predicted before (Hu et al., 2011).

Also, confirming the results obtained on RPE-1 cells (Figure 26), STLC treatment and STLC treatment combined with depletion of KIF15 by siRNA, did not impact spindle elongation rates (Figure 60), nor other two anaphase parameters measured (Figures 61 and 62). Experiments involving treatment with STLC were always performed on late metaphase spindles, as was described for RPE-1 cells. Only difference between these cells was that in U2OS cells, the spindle did not shorten in metaphase after addition of STLC, as in RPE-1 cells (Figure 24), but did after combined depletion with KIF15 (Figure 27), as reported previously (van Heeseben et al., 2014). Moreover, individual KIF15 depletion by siRNA did not impact rates of measured anaphase parameters (Figures 60, 61 and 62).

On the other hand, KIF4A depletion with siRNA obtained interesting results in which chromosome segregation and spindle elongation rates were increased significantly compared to control U2OS cells with alpha-tubulin labelled with mCherry (Figures 60 and 62). This is interesting because when same experiments were performed in U2OS cells that had lost tubulin labelling with mCherry, this phenomenon was not observed, implicating that all other rates regarding anaphase parameters might be similar to control cells (Figure 61). Similarly, no significant effect of this depletion on spindle elongation velocity was observed in RPE-1 cells, when compared to control cells (Figure 31) and also in literature using HeLa cells expressing GFP- $\beta$ -tubulin (Hu et al., 2011). There are multiple possible explanations for this complex phenomenon that was observed but these will be considered in Concluding discussion section. Interestingly, KIF4A depletion increased not only spindle elongation and

chromosome segregation rates, but also sliding rates within the spindle midzone (measured as in RPE-1 cells, see Materials and methods for details) (Figure 63) and sliding rates were inversely correlated with sister kinetochore distance at the start of photoactivation (Figure 63), meaning that sliding rate is decreasing over time, as anaphase progresses.

Moreover, since KIF4A cells were hyperelongating (Figure 63D), just like in RPE-1 cells (Figure 30), in this context sliding could be observed above 10  $\mu\text{m}$  distances between separating chromosomes, whereas in control cells there was no observable sliding above these kinetochore distances, because spindle elongation and kinetochore velocity drastically stopped at that point (Figure 63). This suggested that sliding can nicely follow the overelongation phenotype and that this phenotype could be a consequence of changed MT sliding parameters (see Concluding discussion for more details). Moreover, sliding seemed to be more stable and discrete in KIF4A depleted cells when compared with controls (Figure 63), visualised also by much more defined midzone bundles in this context (Figure 63), all pointing to increased stability of bridging MTs. This was not the case in RPE-1 cell line, where depletion of KIF4A does not impact stability of midzone MTs (Figure 55), probably reflecting different labelling of tubulin between these cells (see Concluding Discussion for more details).

Interestingly, a fraction of KIF4A depleted U2OS cells (20%), often exhibited extensive buckling of midzone MTs in some point during anaphase, followed by spindle pole rotation and midzone MT splaying (Figure 63), whereas other cells exhibited defined MT bundles within the midzone, capable of fast spindle elongation that lasted longer than in controls (Figure 63). Interestingly, buckling of midzone MTs was also observed in a study that combined depletion of KIF4A, with a depletion of MKLP1 that perturbs cell elongation, where the cell elongation could not follow the excessive spindle elongation (Hu et al., 2011), thereby opposing this movement, ultimately leading to buckling of MTs at the site of force-generation. Authors speculated this is one point in favour of sliding filament mechanism in human cells which proposes that forces required for spindle elongation come from inside a spindle (McIntosh et al., 1969; Hu et al., 2011). This is the case because in this situation MTs within the spindle produce the force that is transmitted by other MT structures that eventually hit a barrier of a cell wall MTs resulting in a buckling of MTs at the primary force-generation site.

Finally, similarly to individual depletion of KIF4A in cells labelled with mCherry-alpha-tubulin, depletion of plus-end tracking protein EB3 by siRNA in cells without alpha-tubulin labelled, significantly increased rates for all measured anaphase parameters when compared to controls (Figures 60, 61 and 62). This is also contrary to RPE-1 cells, where such

phenomenon was not observed after depletion of EB3 protein (Figure 45). The possible mechanisms are conferred in detail in Concluding discussion part of the thesis.

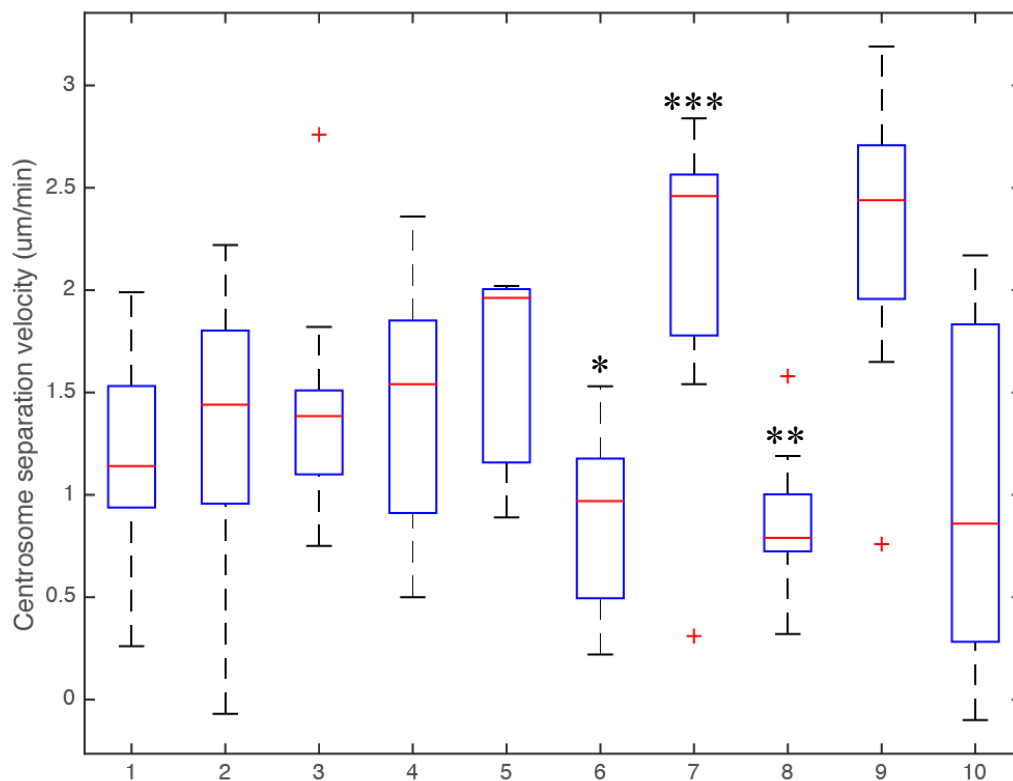


**Figure 60. MKLP1 and PRC1 depletions are reducing spindle elongation rates while KIF4A depletion and EB3 depletion increase these rates in U2OS cells.** Box plot of centrosome separation velocities in different treatments in U2OS cells labelled with CENPA-GFP and mCherry-alpha-tubulin. In the box plot, the central mark indicates the median, with the bottom and top edges of the box indicating the 25th and 75th percentiles, respectively. The whiskers extend to the most extreme data points, with exception of the outliers that are marked individually with the plus symbol. Statistics: t test (\* $P < 0.05$ ; \*\* $P < 0.01$ ; \*\*\* $P < 0.001$ ). Legend: 1-STLC-control, 2-STLC treatment, 3-non-targeting RNA, 4-KIF15 siRNA, 5-KIF15 siRNA+STLC, 6-MKLP1 siRNA, 7- KIF4A siRNA, 8-PRC1 siRNA, 9-EB3 siRNA in CENPA-GFP only cells, 10-PRC1 overexpression in CENPA-GFP only cells.



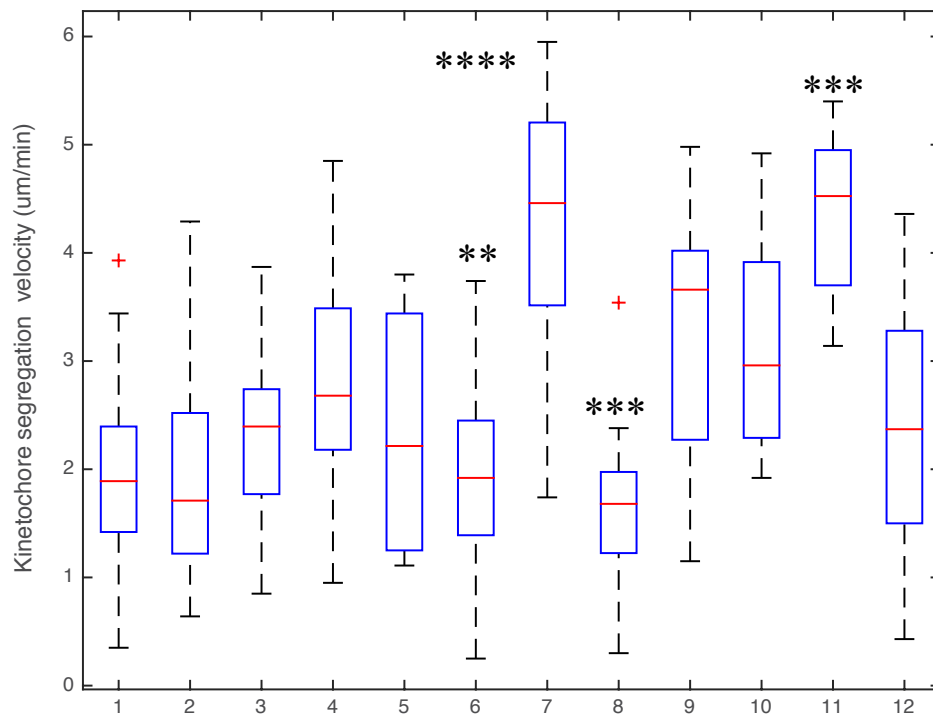


**Figure 61. MKLP1 and PRC1 depletions are reducing chromosome segregation rates while KIF4A depletion and EB3 depletion increase these rates in U2OS cells.** Box plot of kinetochore separation velocities in different treatments in U2OS cells labelled with CENPA-GFP and mCherry-alpha-tubulin. In the box plot, the central mark indicates the median, with the bottom and top edges of the box indicating the 25th and 75th percentiles, respectively. The whiskers extend to the most extreme data points, with exception of the outliers that are marked individually with the plus symbol. Statistics: t test (\*\*P < 0.01; \*\*\*P < 0.001; \*\*\*\*P < 0.0001). Legend: 1-STLC-control, 2-STLC treatment, 3-non-targeting RNA, 4-KIF15 siRNA, 5-KIF15 siRNA+STLC, 6-MKLP1 siRNA, 7- KIF4A siRNA, 8-PRC1 siRNA, 9- control CENPA-GFP only cells, 10- KIF4A siRNA in CENPA-GFP only cells, 11-EB3 SiRNA in CENPA-GFP only cells, 12-PRC1 overexpression in CENPA-GFP only cells.

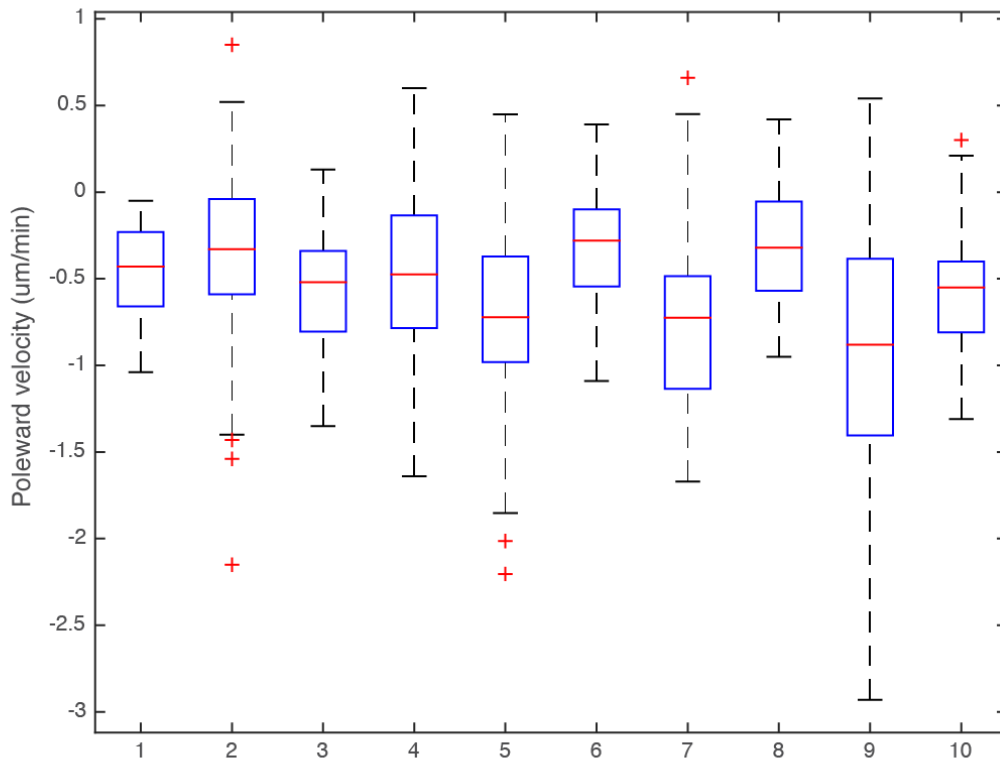


**Figure 62. Poleward velocities in U2OS cells are mainly unaffected upon perturbations of various mitotic regulators.** Box plot of poleward kinetochore separation velocities after different treatments in U2OS cells labelled with CENPA-GFP and mCherry-alpha-tubulin. In the box plot, the central mark indicates the median, with the bottom and top edges of the box indicating the 25th and 75th percentiles, respectively. The whiskers extend to the most extreme data points, with exception of the outliers that are marked individually with the plus symbol. Legend: 1-STLC-control, 2-STLC treatment, 3-non-targeting RNA, 4-KIF15 siRNA, 5-KIF15 siRNA+STLC, 6-MKLP1 siRNA, 7-KIF4A siRNA, 8-PRC1 siRNA, 9-EB3 siRNA in CENPA-GFP only cells, 10-PRC1 overexpression in CENPA-GFP only cells.

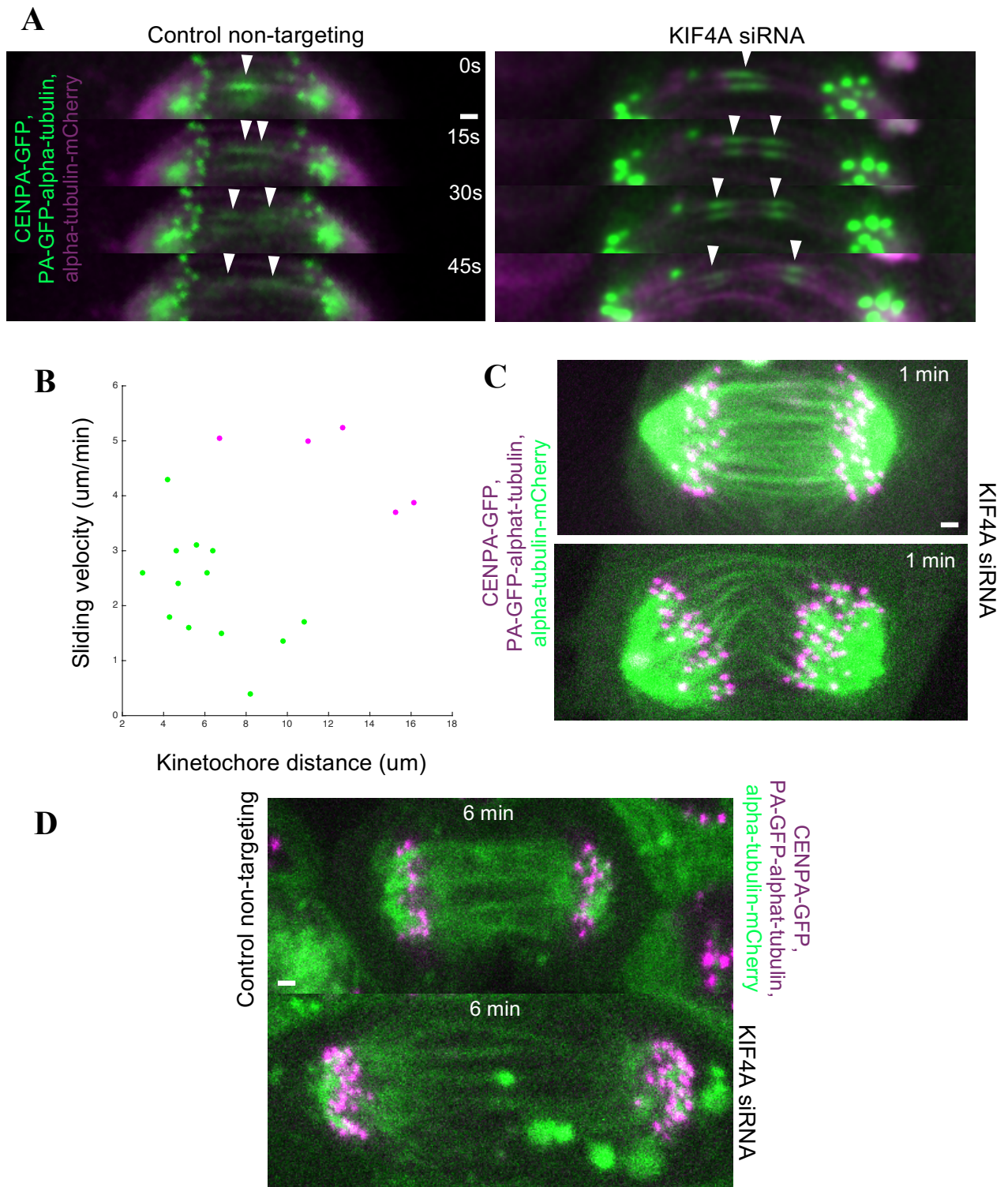


**Figure 63. Sliding is faster and more stable in U2OS cell line after depletion of KIF4A protein.** (A) Smoothed time-lapse images of the half anaphase spindles in U2OS cell line stably expressing CENP-A-GFP, PA-alpha-tubulin and mCherry-alpha-tubulin, after photoactivation of PA-GFP-tubulin at time 0 within bridging fibers in indicated conditions. Arrowhead indicate the central part of the photoactivated spot, as it separates during anaphase. (B) Quantification (scatter plot) of sliding velocity versus initial kinetochore distance, measured at the first frame of photoactivation, in controls (green) and KIF4A-depleted (magenta) U2OS cells. (C, D) Time-lapse images of the anaphase spindles in U2OS

cell line stably expressing CENP-A-GFP, PA-alpha-tubulin and mCherry-alpha-tubulin treated with KIF4A siRNA. Time zero represents the onset of anaphase. Scale bar; 1  $\mu\text{m}$ .

## 5 CONCLUDING DISCUSSION

### 5.1 Regulation of spindle length and main motors involved

Chromosomes must be faithfully segregated to maintain genome integrity during multiple cell divisions. The dynamic mitotic spindle, a macromolecular machine, drives this process (Pavin and Tolić, 2016). The mitosis itself is subdivided into different phases, and during anaphase chromosomes segregate to opposite sides of the cell by depolymerization-driven k-fiber shortening and spindle elongation (Maiato and Lince-Faria, 2010). During anaphase A, it is thought that direct force producer is MT depolymerisation itself, and proteins are merely a regulators or couplers of that process (Asbury et al., 2017). However, little is known about direct force-producing proteins required for chromosome segregation during anaphase B in human cells (Vukusic et al., 2019). Interestingly, shorter or longer metaphase spindles, due to deletion or inhibition of a single molecular motor or non-motor MAP, display chromosome segregation defects later in anaphase (Goshima and Scholey, 2010). On the other hand, these single perturbation experiments of multiple motors and MT regulators rarely can impact anaphase movements globally, mostly affecting only single chromosomes, pointing to possible redundant mechanisms operating during this phase of mitosis where outward generated forces play a dominant role (Goshima and Scholey, 2010; Zhu et al., 2005).

To date, spindle elongation in human cells has been envisioned as a process that could involve two possible mechanisms, cortical pulling by astral MTs connected to spindle poles and the cell cortex (force generated outside the spindle) and outward pushing of interpolar MTs, connected to two spindle halves, by sliding filament mechanisms (force generated inside the spindle) (Scholey et al., 2016). Our group has recently found that most interpolar MTs within human spindles are laterally connected with sister k-fibers in form of an antiparallel bridging MTs (Kajtez et al., 2016; Polak et al., 2017), and these MTs are playing an important role during chromosome segregation in these cells (Vukusic et al., 2017). Also, we and others have shown that these MTs are sliding apart as anaphase progresses and their destruction significantly abrogates normal anaphase movements (Vukusic et al., 2017; Yu et al., 2019). This arguments that in human cells, the force required for spindle elongation is generated within the spindle, where sliding of bridging MTs is pushing k-fibers apart by a friction of passive crosslinks between them (Vukusic et al., 2017). This force is then transmitted to spindle poles by connections between k-fibers, that are itself connected to

structure of the spindle pole (McDonald et al., 1992; McIntosh and Landis, 1971; Nixon et al., 2017; Yu et al., 2019). Moreover, since laser ablation of astral MTs (Vukusic et al., 2017) and depletion of dynein cortical adaptors (Kiyomitsu and Cheeseman, 2013), are not affecting chromosome segregation during early anaphase in human cells, this rules out cortical pulling mechanisms as a possible force-generator for spindle elongation, while its role as a main regulator of spindle orientation is well-established in this system (Lu and Johnston, 2013). On the other hand, dynein impacts chromosome segregation during late anaphase (Kiyomitsu and Cheeseman, 2013), where overall movement of chromosomes is minor compared to early anaphase, leaving this mechanism open to detailed characterization.

However, despite extensive knowledge gathered on *in vitro* sliding capacity of multiple motors (Bieling et al., 2010; Kapitein et al., 2005; Su et al., 2013), motor proteins required for sliding filament mechanism (McIntosh et al., 1969) during anaphase in human cells are not known (Vukusic et al., 2019). To understand this problem, we must first look at regulation of metaphase spindle length, since one could imagine these two processes are connected, both concerning spindle length regulation, only difference being metaphase is a steady state and during anaphase spindle is constantly elongating, meaning outward forces are predominating (Goshima and Scholey, 2010). Metaphase steady-state constant length is thought to be maintained by a force-balance model between antagonistic pushing outward and pulling inward forces (Figure 64). Remarkably, removal of any single, or combination of force contributors results in a new steady-state length. The most renowned antagonism in human spindles is achieved in metaphase between EG5 as a dominant outward motor, and dynein as a dominant inward motor (Goshima and Scholey, 2010). Recently, the kinesin-14 KIFC3 has been identified as a counteracting motor to EG5 in prophase centrosome separation (Hata et al., 2019).

It was observed that such force-balancing phenomenon exists in RPE-1 model system, in which EG5 is obviously dominant outward exerting motor since, after its inhibition with STLC, spindles usually tend to collapse very quickly into practically monopolar spindles where two centrosomes are very close to each other, as described earlier by others (Sturgill and Ohi, 2014) (Figure 64). This collapse is presumably mediated by forces exerted by inward directed minus-end motors, primarily dynein, since its depletion restores spindle collapse seen after EG5 inhibition (van Heesbeen et al., 2014) (Figure 64). Depletion of the minus-end directed kinesin-14 family member HSET (KIFC1) cannot restore the spindle collapse observed upon EG5 inhibition in human cells (van Heesbeen et al., 2014). On the other hand, in tumour cell lines, story is more complex because KIF15 can maintain the spindle bipolar

shape and constant metaphase spindle length without EG5, but their simultaneous perturbations collapse spindle in metaphase (Figure 64), as published by others (Tanenbaum et al., 2009; van Heesbeen et al., 2014; Vanneste et al., 2009). However, it is still not clear what is exact mechanism behind this redundant phenomenon and whether KIF15 exert outward force on poles through sliding of antiparallel microtubules (Reinemann et al., 2017), similarly to EG5, or it can slide parallel microtubules, establishing divergent mechanism of outward force production (Drechsler and McAinsh, 2016).

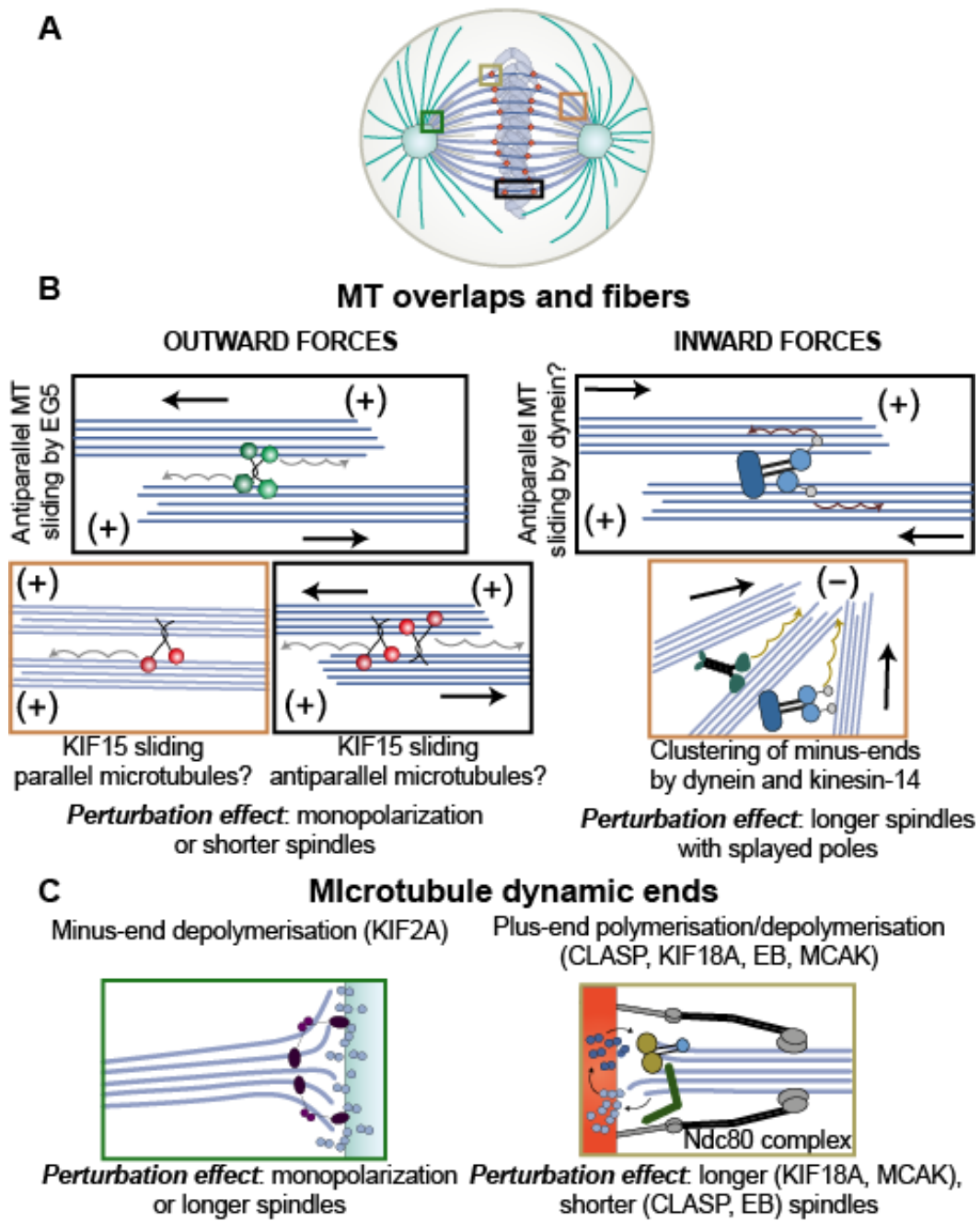


**Figure 64. Main mechanisms that regulate steady-state length of the metaphase mitotic spindle.** (A) Scheme of the human metaphase spindle with main force-producing regions depicted that are involved in regulation of steady state length balance. (B) Antagonism between inward and outward forces during metaphase include multiple possible mechanisms exerted by molecular motors and depicted on schemes of main regions within spindle where force-production takes place. (C) Regulation of dynamic properties of both microtubule ends can also impact metaphase length regulation as depicted on schemes. Black bold arrows point to direction of overall MT motion as a result of forces produced by motors walking on microtubules (grey and yellow arrows).

On the other hand, fraction of RPE-1 cells treated with STLC, alone or in combination with other motors, obviously can enter anaphase and proceed with spindle elongation, some even after spindle is shortened drastically with minimum length being around 7-8  $\mu\text{m}$  that was observed through experiments reported here. What is even more interesting, this spindle length at the beginning of anaphase is not correlated with anaphase spindle elongation velocities meaning that this system is having low and possibly high boundaries of spindle length in which the system is behaving similarly regarding spindle elongation. This is contrary to yeast spindles, where sliding filament mechanism also drives spindle elongation (Scholey et al., 2016), since in this system overlap and spindle length are scaling with elongation velocities (Kruger et al., 2019). This is not a trivial problem, because it points out to the fact that spindle overlap length might be quite similar between small spindles of 8  $\mu\text{m}$  and large spindles of 25  $\mu\text{m}$ , since their elongation velocities are similar, but that awaits further studies. On the other hand, initial overlap length may not be important for velocity of motor sliding, contrary to *in vitro* studies done for EG5 and KIF4-PRC1 complexes (Shimamoto et al., 2015, Wijeratne and Subramanian, 2018), but it could be important for extent of sliding *in vivo*, since longer spindles in metaphase tend to be longer in telophase.

Regarding that phenomenon, it would be interesting to study the exact dynamics of the spindle collapse, after inhibition of EG5, to see if the spindle is collapsing from the inside-out or the other way around. I expect that spindle is probably collapsing from the poles inward, because poles are most likely the place where dominant minus-end directed motors, like dynein and to a lesser extent kinesin-14 family member KIFC1, that are driving the collapse (Mountain et al., 1999; van Heesbeen et al., 2014), exert their forces (She and Yang, 2017) (Figure 64). However, other groups have proposed that dynein can mediate the antiparallel



MT inward sliding in overlap regions, thus opposing the outward force generated by EG5 (Ferenz et al., 2009; Tanenbaum et al., 2013) (Figure 64). On the other hand, as shown in this thesis and by others, proteins regulators of microtubule dynamic ends, both plus and minus, can also greatly contribute to steady state spindle length regulation during metaphase (Goshima and Scholey, 2010). Those include members of kinesin-13 family of protein depolymerases KIF2A and MCAK (KIF2C) (not studied in this thesis), localised either at poles or at the kinetochore (Goshima and Scholey, 2010), EB family of plus-end tracking proteins that stabilise microtubule tips, CLASP family members known to induce polymerization at plus-ends and kinesin-8 family member KIF18A, recognized regulator of depolymerisation at microtubule plus-end (Akhmanova and Steinmetz, 2015).

To conclude, even though EG5-generated motor is crucial for spindle length maintenance during metaphase, by generating the critical fraction of outward force, it is not experimentally proven that EG5 is indeed producing force through antiparallel MT sliding mechanism for establishment of this maintenance *in vivo*, as predicted by most researchers from *in vitro* studies (Kapitein et al., 2005), since large fraction of this motor in human cells is located around spindle poles (Mann and Wadsworth, 2019). Moreover, the nature of force-production by counteracting motor dynein is also not clear in human spindles (Ferenz et al., 2009) and the same stands for nature of force-production of KIF15 plus-end generated motor, with multiple mechanisms proposed that are under debate (Drechsler and McAnish, 2016, Reinemann et al., 2017) (Figure 64).

## 5.2 Kinesins KIF4A and Eg5 drive elongation of the anaphase spindle

On the other hand, EG5 seems to be dispensable for anaphase chromosome segregation and spindle elongation in human cells since its inhibition is not affecting rates of these phenomena when compared to control untreated RPE-1 cells. Similar findings were also reported in *Drosophila* embryo mitosis after injection of antibodies against kinesin-5 (Brust-Mascher et al., 2009). This points out that some other plus-end directed motors might be operating within the overlaps, or at the other site within the spindle, that act redundantly with EG5 in term of outward force production that is consequently moving spindle poles from each other during anaphase. Moreover, the fact that spindles are able to shorten their length after EG5 inhibition during metaphase, but soon after anaphase onset, elongate them, points to the fact that additional outward force-generating mechanisms are turned on at this point. In this thesis I show, using combined depletion and inactivation assays to explore redundancy

between multiple force-generating motors, together with CRISPR technology, that PRC1-dependent motor KIF4A/kinesin-4, together with EG5/kinesin-5 motor is essential for spindle elongation in human cells. After this double perturbation, no spindle elongation is observed and cells are arrested in anaphase for significant amount of time.

Additionally, it is interesting that spindles do not collapse in anaphase after this combined perturbation abrogating them of major proteins generating outward force during this phase of mitosis. This is probably due to the fact that most minus-end directed motors that produce inward force, like spindle-bound dynein and kinesin-14 KIFC1, are downregulated or removed from their spindle sites after anaphase onset (Pfarr et al., 1990; Su et al., 2016), similar to some alternative outward force producers like chromosome-bound chromokinesins KID and KIF4A (Su et al., 2016), and I speculate that spindle achieves the new steady-state length in anaphase without major outward and inward force-producers.

Regarding long-term anaphase arrest that I observed, I speculate this is a result of abrogated spindle elongation I achieved by perturbation of force-producing proteins EG5 and KIF4A, and there is possibility that top signalling effectors, like CyclinB, AuroraB, CDK1 or PLK1, are also affected by this because their perturbations can sometimes lead to similar phenotypes in human cells (Afonso et al., 2019; Afonso et al., 2014; Brennan et al., 2007; Su et al., 2016; Vazquez-Novelle et al., 2014; Wolf et al., 2006). Some of these reported anaphase B block phenotypes, sometimes called pseudoanaphases, work by inducing either a metaphase-like phosphorylation state during anaphase, by keeping CDK1 activity high during anaphase, as imposed by non-degradable forms of Cyclin B or by deregulation of MT dynamic properties through deregulation of PRC1 phosphorylation imposed by inhibiting PLK1 activity, thereby inducing a telophase-like state in anaphase. Only in the case of Aurora kinases, it is not clear how both kinases induce anaphase block phenotype in human cells (Afonso et al., 2014; Hegarat et al., 2011). Interestingly, inhibition of phosphatases, that are hallmark of mitotic exit, do not induce an anaphase B block phenotype (Afonso et al., 2014; Su et al., 2016). I propose that most potent anaphase B block phenotypes seen in our experiments are a consequence of blocked spindle elongation, by means of perturbation of force-producing proteins. Similar phenotypes, on the other hand, can be seen also by perturbation of their potential regulators, including PLK1 or CDK1 kinases, as discussed above, but for establishment of exact link between concrete force-producing proteins and their regulators, additional experiments must be performed.

### 5.3 Regulation of KIF4A and EG5 sliding modules

What is interesting about EG5 and KIF4A combination is that EG5 is apparently exerting force through mitosis, from the onset of prophase, when CDK1 activity, being a master regulator of EG5 motor, is upregulated thereby increasing its affinity to MTs (Mann and Wadsworth, 2019), to late anaphase, when CDK1 is gradually degraded (Afonso et al., 2017), thereby reducing EG5 phosphorylation state (Blangy et al., 1997) (Figures 65 and 66). This is supported by EG5-GFP fluorescence recovery from photobleaching (FRAP) and total internal reflection fluorescence (TIRF) microscopy experiments (Gable et al., 2012) in which EG5 was very dynamic through mitosis, motion of EG5 puncta in the midzone was similar throughout mitosis, and motion velocities were comparable in each direction, except in late anaphase spindles when these values significantly differ. However, this concept merits additional experimental approaches to prove its major points.

Also, while I observed that MT sliding is perturbed after combined depletion of KIF4A and inhibition of EG5 by STLC during anaphase, in previous phases EG5 role in antiparallel MT sliding is only inferred from its *in vitro* capacity to slide antiparallel MTs (Kapitein et al., 2005), since this was never experimentally proven in live cells. KIF4A is also capable of sliding antiparallel MTs apart *in vitro*, especially when in complex with PRC1 protein (Bieling et al., 2010; Wijeratne and Subramanian, 2018). However, KIF4A is during pre-anaphase stages located on the chromosome arms as chromoskinesin protein (Mazumdar and Misteli, 2005), where it exerts outward forces on spindle by walking on MTs while being connected to chromosome arm with the other domain (Figures 65 and 66). Few minutes after anaphase onset, by a mechanism involving MKLP2 and Aurora B (Nunes Bastos et al., 2013), KIF4A is brought to antiparallel MTs in the spindle midzone, where it obviously can slide MTs apart, since its depletion combined with STLC treatment strongly influence this phenomenon during anaphase, as shown in this thesis (Figures 65 and 66). Interestingly, in cells treated with STLC, where EG5 activity is inhibited, there was a consistent delay in start of the spindle elongation relative to anaphase onset compared with controls. I speculate this delay might include the time needed for sufficient amount of KIF4A to accumulate in the antiparallel overlaps to drive sliding mechanism, since this is regulated by signalling at metaphase-to-anaphase transition, but this point requires additional experiments to be performed.

Mitotic regulation of this motor is rather complex and awaits further studies. For example, Aurora B regulates this protein by direct phosphorylation, thereby promoting its association with MTs, but KIF4A can localise on MTs even in the absence of Aurora B activity, but tends to dissociate faster, as shown using FRAP experiments (Nunes Bastos et al., 2013). Also, KIF4A C-terminal MT binding domain is weak interactor with MTs, and it tends to dissociate fast, when not in complex with PRC1 protein which binds MTs much more tightly than KIF4A (Wijeratne and Subramanian, 2018). Thus, it is not clear whether KIF4A can exert force on antiparallel MTs in the absence of PRC1 protein and absence of function mutants of KIF4A could potential answer this question in the future studies. Interestingly, one study showed that KIF4A is able to suppress midzones from growing continually even when its PRC1 binding domain is absent (Hu et al., 2011), but it should be noted that this motor is not only characterized by MT sliding activity, but also by capacity to regulate MT dynamics at the plus-ends of interpolar MTs, where it increases catastrophe frequency of single MTs (Bringmann et al., 2004), and these two functions could be differently regulated.

Therefore, it is possible that KIF4A function in driving antiparallel MT sliding in the center of antiparallel overlap is dependent on PRC1 protein while its function in growth inhibition on the plus-end of interpolar MTs is largely PRC1-independent. This is a reasonable assumption because in these regions, *in vitro* called “end tips”, KIF4A proteins can oligomerize due to very high concentration of the protein, thereby increasing their MT binding affinity (Wijeratne and Subramanian, 2018). Also, there is possibility that one-head bound motors can perform the function of MT growth suppression (Wijeratne and Subramanian, 2018), while interaction with PRC1 is needed for antiparallel sliding role of the motor in the overlap center. This is supported by our experiments in which spindle elongation is completely blocked by depletion of PRC1 protein combined with EG5 inhibition implicating PRC1-KIF4A interaction as crucial for this process to occur in human cells.

Moreover, KIF4A regulation with MKLP2 and Aurora B is also not clearly defined, since MKL2 depletion combined with STLC treatment cannot mimic the affect observed after KIF4A depletion combined with STLC treatment, as should be the case according to literature models (Gruneberg et al., 2004; Nunes Bastos et al., 2013) especially given the fact that inhibition of Aurora B can greatly perturb spindle elongation (Afonso et al., 2014) (Figure 65). Interestingly, as I have shown in this thesis, Aurora B inhibition alone can mimic the MKLP2 depletion phenotype regarding spindle elongation, as predicted by literature models (Gruneberg et al., 2004), but it cannot induce the spindle block depletion phenotype when combined with EG5 inhibition. Since combined depletion of MKLP1 and MKLP2 combined

with STLC treatment is far better at mimicking the spindle elongation block of KIF4A depletion combined with STLC treatment, I speculate that MKLP1 plays important, but still undefined role in regulation of KIF4A protein, probably through regulation of some mitotic kinase, but that awaits further studies (Figure 65). Moreover, it is interesting how non-discriminatory inhibition of both Aurora kinases can block spindle elongation, as shown in this thesis, and by others (Afonso et al., 2014), similar to inhibition of direct force producers EG5 and KIF4A, implicating them as strong regulators of spindle elongation. However, inhibition of both Auroras using this non-discriminatory inhibitor cannot be reproduced by mix of two specific inhibitors of Aurora kinases, as shown in this thesis, suggesting that ZM inhibitor might inhibit some other mitotic kinases (Ditchfield et al., 2003), which are known to induce the total spindle elongation block phenotype as discussed above.

This Aurora mechanism might not act through direct force-producing proteins however, since it is known that both Aurora kinases are phosphorylating target proteins important for regulation of midzone length, stability and nucleation, including KIF4A, KIF2A, p150Glued and TACC3 (Afonso et al., 2017), but I speculate that this is not crucial during early anaphase, where spindle elongates the most, since I showed that decreased midzone stability cannot explain the anaphase B block phenotype of KIF4A depletion and EG5 inhibition by STLC. On the other hand, most of these published effects have some impact on spindle elongation movements, similarly to what is observed in this thesis for depletion of kinesins-6 MKLP1 and MKLP2, kinesin-7 CENP-E and kinesin-3 KIF14 but this impact is not major effect as total block I reported after perturbing the direct force-producing proteins kinesin-4 KIF4A and kinesin-5 EG5.

To conclude, I speculated that both Auroras might separately regulate both sliding modules, where Aurora B is probably important for KIF4A sliding module since it is a known regulator of this protein (Nunes Bastos et al., 2013), and Aurora A might be important for regulation of EG5 protein, because EG5 regulatory partner TPX2 is phosphorylated by this kinase (Waitzman and Rice, 2014) (Figure 65). This is interesting because it is observed that TPX2, and consequently Aurora A, are not present in the spindle midzone during anaphase, while EG5 is present at that location (Mann and Wadsworth, 2018), but how Aurora A influences spindle midzone while being located mainly on centrosomes, transitioning to spindle midzone in telophase cells, is not clear (Afonso et al., 2017) (Figure 65). However, as shown in this thesis, although perturbation of Aurora kinases had a strong impact on spindle elongation and chromosome segregation, the total block of spindle elongation was not observed in multiple combinations of Aurora kinases and motor proteins found to be essential

for spindle elongation in this thesis. This suggests that Auroras are probably involved as non-direct modulators of important aspects of anaphase, such as midzone MT dynamics and length, but they are not exclusively important for localisation of key motor components of both sliding modules. It is probably more plausible that CDK1 is involved in some part of this regulation, since it is a known positive regulator of EG5 during earlier stages of mitosis (Blangy et al., 1995), it is a master negative regulator of PRC1-KIF4A midzone complex (Zhu and Jiang, 2005) and perturbation of this kinase can greatly impact spindle elongation in human cells (Afonso et al., 2019), but that assumption awaits further studies. Regarding this point, one study reported that cohesin cleavage, and subsequent drop in CDK1 activity are sufficient to promote proper segregation of chromosomes during anaphase in human cells (Oliveira et al., 2010).

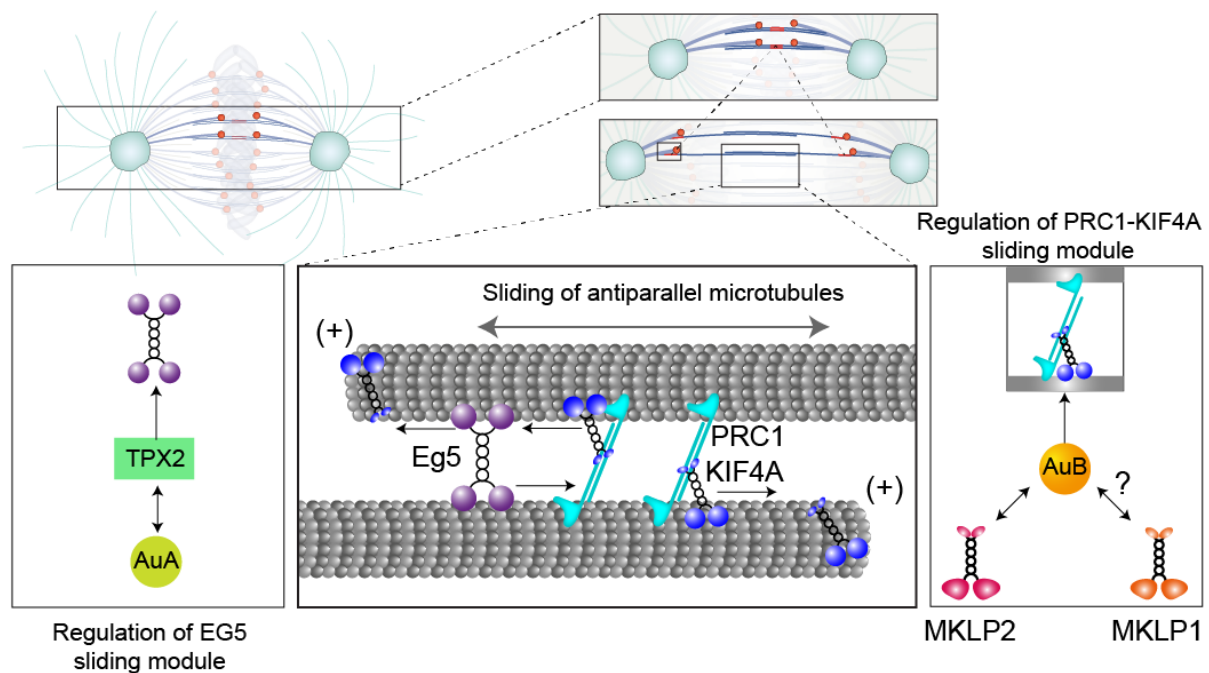


**Figure 65. Proposed model for the sliding in the antiparallel region of anaphase mitotic spindle including two independent sliding modules.** One module is composed of plus-end directed motor tetramer EG5 and other is composed of PRC1-dependent plus-end directed motor KIF4A. The first is, as I suggested, regulated by Aurora A kinase phosphorylating TPX2 protein, which is important for EG5 localisation on MTs. The latter is probably regulated by Aurora B kinase (AuB) whose midzone localization is dependent on both kinesins-6, MKLP1 and MKLP2. On the plus-ends of interpolar MTs, KIF4A protein is also suppressing MT dynamics, probably independently of PRC1. Grey double-headed arrows point

to direction of overall MT motion sliding over each other as a result of forces produced by motors walking on antiparallel MTs (black arrows).

## 5.4 Role of microtubule stability during early and late anaphase

One interesting observation from this thesis is that reduced midzone stability, provided primarily by midzone MT bundler PRC1, does not impact spindle elongation rates, as stability is suggested by some researchers to be very important part of anaphase segregation and spindle elongation (Pamula et al., 2019). In that regard, it is known for some time that compared with unbundled growing MTs, which have a half-life of tens of seconds, a subset of midzone MTs is stabilized ~10-fold (Salmon et al., 1984; Saxton et al., 1984). Today, we know that this function is primarily mediated by PRC1 and its interacting partner MKLP1, both being the potent bundlers of antiparallel MTs important for mechanical resilience of central spindle (Lee et al., 2012). However, it remained unclear if this increase in MT stability, mediated by decrease in PRC1 phosphorylation state after anaphase onset, is important for all stages during anaphase, as suggested by some researchers (Pamula et al., 2019). Here I show that central spindle MT stability provided by MT bundler PRC1 is not crucial for anaphase spindle elongation during early anaphase, encompassing first 5 minutes after anaphase onset, where spindle elongates the most (Vukusic et al., 2019). This is evident from the fact that reduced MT stability is not following the trend of reduced spindle elongation velocities across conditions, meaning that perturbed elongation is a result of defects in some other process, and I show in this thesis that this is a result of defective MT sliding mediated by combined action of EG5 and KIF4A motor proteins.

Moreover, this suggests that these motors are capable of exerting similar amount of force required for spindle elongation by sliding antiparallel MTs that are not as stable as those bundled by PRC1 protein in unperturbed situation. In that regard, I observed that propagation of sliding in control cells is usually very ordered and follows the direction of the main spindle axis while in PRC1 depleted cells this propagation of sliding, seen through separation of two spots of photoactivated tubulin, is following this pattern for a short amount of time, around 20s, and then splits in directions that are often not on the main spindle axis, probably indicating detachment of MTs.

This phenomenon brings us to the mechanism behind braking action induced by PRC1 protein in the spindle midzone during late anaphase, the most studied phenomenon within spindle midzone (Bieling et al., 2010; Braun et al., 2011; Lansky et al., 2015; Mollinari et al.,

2002; Pamula et al., 2019; She et al., 2019; Subramanian et al., 2013; Subramanian et al., 2010; Wijeratne and Subramanian, 2018). I also observed that during late anaphase, spindles depleted of PRC1 and spindles in CRISPR PRC1 KO do not stop spindle elongation in same time as control spindles do, and this lead to phenomenon of spindle overelongation, implying PRC1 as important player in inducing braking at this point in anaphase, thereby opposing the forces driving spindle elongation. One possibility, suggested by some authors (Pamula et al., 2019), is that PRC1 can induce frictional forces within the spindle midzone to oppose cortical pulling by astral MTs mediated by cytoplasmic dynein on the cortex (Scholey et al., 2016). However, as mentioned previously, depletion of dynein adaptors on the cortex does not impact chromosome segregation during early anaphase in human cells (Kiyomitsu and Cheeseman, 2013), meaning this mechanisms of spindle elongation impeding is unlikely. I speculate that this mechanism instead involves braking imposed to sliding of midzone located plus-end generating motors KIF4A and EG5, whose redundancy I discovered in this thesis. I imagine this braking could happen in multiple ways.

First, it is known that overelongation phenotype is also observed after depletion of PRC1-interacting partner KIF4A (Hu et al., 2011), whose role is not only to slide antiparallel MTs, but also to inhibit their length controlling dynamics of their plus-ends (Bringmann et al., 2004), as already noted. Moreover, it is known that PRC1 bundles increase drastically in length after KIF4A depletion (Hu et al., 2011; Zhu and Jiang, 2005), implying longer overlaps within those bundles. Regarding this phenomenon, if KIF4A is depleted from the spindle midzone, more EG5 motors could bind to longer antiparallel overlaps and exert their forces for longer times, since balance of overlap length is switched to favouring polymerization of interpolar MTs, ultimately leading to overelongation phenotype. That means that in normal spindles, KIF4A is restricting length of antiparallel overlap leading to steady-state overlap length seen in telophase spindles where net movement of spindle poles is negligible (Vukusic et al., 2019).

Also, PRC1 is probably by itself taking part in this braking because *in vitro* experiments have shown that yeast Ase1 accumulates in overlap regions as a direct result of the reduction of their length and resists further filament movement due to increase in entropic forces (Braun et al., 2011). Because PRC1 signal increases in the region of the central spindle during late anaphase in human cells (Zhu and Jiang, 2005), this mechanism is not ruled out. This possibility is not supported by recent FRAP experiments demonstrating that turnover of PRC1 in the midzone of early anaphase spindles is relatively fast,  $\sim 10\times$  faster than that of



GFP-Ase1 in the budding yeast midzone (Pamula et al., 2019), but I speculate that turnover of PRC1 would be much closer to yeast spindles when measured during late anaphase, as overelongation, due to lack of braking mechanisms, takes place during that period, but that awaits further research. To conclude, braking is probably induced in late anaphase by KIF4A inhibiting the growth of the MTs in the overlaps thereby compressing the PRC1 molecules in the narrow overlap zone, increasing the entropic force opposing midzone sliding motors.

Moreover, I have shown that spindles tend to elongate with very high velocities after depletion of KIF4A, but only in U2OS cells labelled with mCherry-alpha tubulin, that also have lower chromosome segregation velocities when compared with controls. What I think is special about these cells is their increased MT stability that is probably happening due to labelling of alpha-tubulin specifically with mCherry fluorophore or because alpha-tubulin is overexpressed in this system. Second possibility is not favoured because percentage of tubulin labelled in comparison with total tubulin within the cell is very low and it is known that use of a large protein tag is prone to produce measurement artefacts as it may affect the dynamics and ultrastructural organization of the protein studied (van de Linde et al., 2012). Moreover, one recent study (Ferreira et al., 2019) has shown that human cells labelled with mCherry-alpha-tubulin have higher MT stability during metaphase, measured by MT turn-over rates, when compared with cells labelled with mEoS-alpha-tubulin. Therefore, KIF4A depletion can result in fast spindle elongation, even during early anaphase, but only when interpolar MTs are hyperstabilised. Interestingly, increased stabilisation of MTs in cell line with tubulin labelled with mCherry also leads to decrease in chromosome poleward rates when compared to unlabelled cells, probably reflecting the fact that k-fibers rely on depolymerisation to shrink during anaphase A (Vukusic et al., 2019). On the other hand, I hypothesised that this stabilization is favoured by molecular motors located within spindle midzone, such is EG5, and moreover, this implies that force can be transmitted to spindle poles more efficiently, probably because connections that propagate the forces from the spindle midzone to the spindle poles, do not detach as often as in controls.

Contrary, it is interesting that increased stability can also have opposite effect on spindle elongation when done by overexpression of PRC1 protein, as I have shown in this thesis. In this case, spindle midzone is unnaturally stabilized by increase in number of PRC1 molecules present, inferred from PRC1-mCherry signal in that region, which leads to blocked spindle elongation by a mechanism similar to PLK1 inhibition. This treatment is known to induce premature midzone formation in early anaphase cells by increase in PRC1 bundling

activity (Brennan et al., 2007; Hu et al., 2012), thereby increasing both stability of MTs and frictional forces in the midzone, opposing midzone motors that try to slide antiparallel MTs apart in order to elongate the spindle, as I have shown in this thesis. This means that spindle stability is important for spindle elongation, but this is highly dependent on cellular context regarding protein levels present in the specific location during specific point in time. Regarding that, I hypothesize that hyperstabilization and friction induced by extensive PRC1 bundling produce a far greater effect on spindle dynamics than stabilization done by labelling alpha-tubulin with mCherry.

Regarding transmission of force generated within the spindle midzone, recent study has shown that most midzone MTs, that pass from one half-spindle to other during anaphase, are nucleated probably within the k-fibers, and they are not in direct contact with the spindle poles (Yu et al., 2019). This means that force generated by spindle midzone sliding is transmitted by connections between these bridging fibers and their respective k-fibers connected to spindle poles. These lateral connections are known to be important for force transmission during metaphase and anaphase in human cells (Kajtez et al., 2016; Vukusic et al., 2017).

## 5.5 Regulation of antiparallel overlap length

On the other hand, regarding importance of polymerization of interpolar MTs during anaphase, one recent study pointed that ends of MTs in overlap regions are nondynamic in human cells and supported a model in which the change in overlap length within MT bundles during anaphase is directly related to the extent of MT sliding (Pamula et al., 2019). However, as shown in this thesis, velocity of MT sliding is strongly correlated with spindle elongation velocity, which is additionally always smaller in value in human cells. That suggests that explanation in which cortical pulling forces can pull the spindle poles, thereby pulling the interpolar MTs with them (Aist et al., 1991), is ruled out because in that situation one would expect sliding rates to be equal or smaller than rates of centrosomes separation. Similar phenomenon as in this thesis regarding spindle elongation and sliding correlations were observed in *Drosophila* embryo mitosis (Brust-Mascher et al., 2004; Brust-Mascher et al., 2009; Wang et al., 2011). Moreover, the peak-metaphase overlap length, measured to be around 5  $\mu\text{m}$  in human cells inferred from PRC1 signal length (Pamula et al., 2019; Polak et al., 2017), cannot explain the extent of spindle elongation since spindle elongates in anaphase

by 6-9 microns and if theory of nondynamic ends is correct, spindle could elongate to maximum extent of 5  $\mu\text{m}$  after which midzone MTs would completely slide apart, phenomenon never observed in anaphase of normal human cells as overlap length in central spindle during late anaphase is around 2  $\mu\text{m}$  (Lee et al., 2012).

Moreover, after depletion of KIF4A, spindle overlaps measured by extent of PRC1 signal, increase in length, and spindles tend to elongate over much larger distances, meaning that spindle overlap length might be the key feature that defines final length of the spindle at telophase. To conclude, regarding theory of nondynamic ends, I postulate it is more plausible that interpolar MTs polymerize at the midzone as the anaphase B spindle elongates, as reported previously in Ptk1 cells (Saxton et al., 1994), possibly assisted by the augmin- $\gamma$ -TuRC-dependent branching polymerization of ipMT plus-ends in human cells (Uehara et al., 2013). The dynamics of ipMTs plus-ends is then probably regulated by PRC1-dependent CLASP proteins, known to localise to spindle midzone (Liu et al., 2009) where they can control plus-end dynamics (Maiato et al., 2005), PRC1-dependent protein KIF4A (Kurasawa et al., 2004), known regulator of interpolar MTs plus-ends (Zhu and Jiang, 2005), possibly MT-depolymerizing kinesin KIF18A that localise to central spindle in late telophase, and various members of kinesin-13 family of MT-depolymerases like KIF2A (Uehara et al., 2013)

## 5.6 Transmission of sliding force to chromosomes and poles

Also, one interesting notion is that MT sliding velocity within spindle midzone tends to correlate perfectly with chromosome segregation velocity, both in overall direction of movement and also in values for individual cases studied. Interestingly, one recent study also observed similar phenomenon (Yu et al., 2019), implying that force transmission from the spindle midzone region to the chromosome region is very efficient process. On the other hand, how is this coordinated with depolymerisation of k-fiber MTs at kinetochores, that also contributes to chromosome segregation velocities (Vukusic et al., 2017), remains unknown, but it is possible that at small intervals, this k-fiber movement is not easily observable, because of its stochastic nature (Su et al, 2016).

Interestingly, sliding velocities also tend to correlate with spindle elongation velocities, but only in the overall direction of the movement while values for individual cases are always lower for spindle elongation, in almost all cases studied. Similar phenomenon was

reported for anaphase B in *Drosophila* embryos (Wang et al., 2011). This suggests that fraction of the force generated within the spindle midzone is lost, probably by MT minus-end depolymerisation, seen as poleward flux of tubulin subunits, and only some fraction of it is efficiently transmitted all the way to the spindle poles. This prediction was favoured by some authors trying to explain similar observations in *Drosophila* embryos (Wang et al., 2011; Wang et al., 2013) making it plausible model especially since in human spindles, similar to *Drosophila* embryo, degradation of cyclin B, thought to control extent of minus-end depolymerisation (Cheerambathur et al., 2007), is prerequisite for spindle elongation (Afonso et al., 2017). This model of spindle length regulation is known in the literature as “slide-flux-or-elongate”, developed mainly based on data obtained in *Drosophila* spindles (Scholey et al., 2016). I think this observation is due to the fact that nature of crosslinking in the area between  $\sim 1 \mu\text{m}$  from the chromosomes, where junction point between bridging MTs and k-fiber is located (Kajtez et al., 2016), and spindle poles, is much more dynamic in attachment and detachment, then in region close to chromosomes, reflecting unstable nature of this connections. This suggests that crosslinking proteins between parallel MTs are differentially located or regulated at these locations along k-fiber.

However, since observed slowing down of sliding rates in the poleward direction in human system is a main limit of “slide-flux-or-elongate” model, an alternative possibility is that plus-end generated motors located within MTs overlap in an anti-parallel orientation, give rise to rapid MT sliding rates in this region, while these motors are antagonized by minus-end directed motors at increasing distances away from the spindle equator where MTs overlap in a parallel orientation, giving rise to a gradual slowing down of MT sliding to eventually stalling at the poles. This theory of spindle length control is known as “slide-and-cluster” model, developed mainly based on data obtained in *Xenopus* spindles (Burbank et al., 2007; Dumont and Mitchinson, 2009). Observation of gradual stalling phenomenon in MT sliding is similar in nature to rate of transport of  $\gamma\text{TuRC}$ -capped MTs which is faster near the equator ( $\sim 0.04 \mu\text{m s}^{-1}$ , similar to the rate of kinesin-5 motility) than the poles ( $\sim 0.006 \mu\text{m s}^{-1}$ ) in the metaphase spindle of human cells (Lecland and Luders, 2014) and to flux velocity decrease near spindle poles by  $\sim 20\%$  in *Xenopus* spindles (Yang et al., 2008). However, details of molecular nature of connections between k-fibers and bridging fibers in human cells, and dynamic nature of their interactions, awaits further studies.

Here, I would like to comment on possible role of interpolar bridging MTs during anaphase A movement that is driven by k-fiber depolymerisation (Vukusic et al., 2019).

Chromosomes, in human monopolar spindles that are result of EG5 inhibition by STLC, are capable of entering anaphase-like poleward movement after inhibition of MPS1 kinase by AZ3146 inhibitor and their velocities are highly similar to those in bipolar spindles, arguing that Eg5 and antiparallel MTs are non-essential for anaphase A (Su et al., 2016). However, it was recently shown that kinetochore MTs are strongly linked with interpolar bridging MTs during anaphase by measuring the similar sliding and flux velocities between these fibers (Vukusic et al., 2017) in bipolar spindles, suggesting that bridging fibers may somehow impact k-fiber depolymerization. Curiously, one recent study has shown that cutting of all midzone MTs during early anaphase can stop chromosome motion for a short time period (Yu et al., 2019), while k-fibers depolymerization continued during that period, moving poles to chromosomes, and not the other way around. This suggests that in the bipolar spindle, interpolar MTs could be a structural prerequisite for synchronous poleward movement of sister chromosomes to occur concomitantly with spindle elongation during anaphase B, like predicted by some authors (McIntosh et al., 2012), but that awaits further research.

## 5.7 Rethinking the anaphase movements

Taken together, our findings answer a long-standing question in cell division field. It was unclear what motor proteins drive chromosome segregation and spindle elongation in human cells through sliding mechanism (Vukusic et al., 2019). Our data reveal that sliding is operated through two independent modules, one composed of EG5 motor protein which generates outward forces throughout cell division (Blangy et al., 1995), and the other composed of KIF4A which turns on after anaphase onset (Kurasawa et al., 2004), when KIF4A is brought to midzone MTs by its interaction with PRC1 (Figures 65 and 66). KIF4A is then probably regulated by a cascade involving Kinesins-6, Aurora B and possibly CDK1. Sliding forces generated in the midzone antiparallel region by these modules are then transmitted to spindle poles most probably through their lateral connections to k-fibers (Vukusic et al., 2017; Yu et al., 2019). It would be interesting to study the details of signalling cascade that regulates spindle elongation in human cells where multiple mitotic kinases are promising candidates that could separately regulate both sliding modules (Afonso et al., 2017; Blangy et al., 1995; Hegarat et al., 2011).

Conclusively, as we have learned from this thesis, anaphase is a very robust phase of mitosis that relies on multiple motor proteins to accomplish the crucial tasks behind

chromosome segregation, including spindle elongation. I reason this is due to the fact that anaphase represents final point in the mitotic process, where after extensive expenditure of cell energy to check that chromosomes are properly attached to spindle MTs (Meraldi et al., 2004), the cell must ensure that chromosomes are separated enough for chromosome decondensation and nuclear envelope reformations to ensue (Afonso et al., 2014), resulting finally in two daughter cells with equal number of chromosomes. In that regard, anaphase is not only adapted to precision rather than to speed (Maiato and Lince-Faria, 2010; Nicklas, 1983), but also anaphase is highly robust and characterized by redundancy to achieve effective separation of sister chromatids in order to adapt to ever changing environment of the cell.

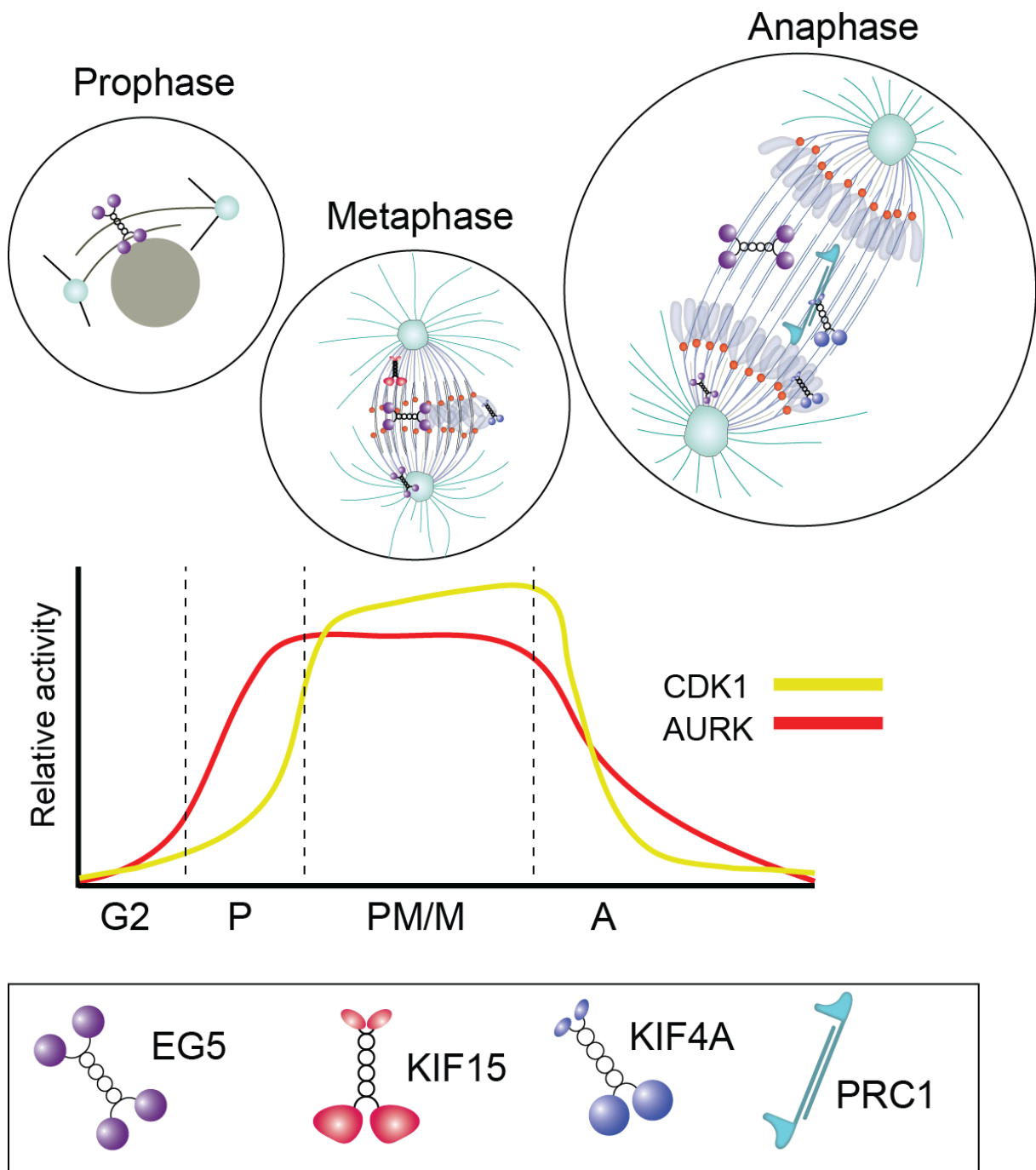


**Figure 66. Simplified model for force production involving most important players in region of antiparallel overlaps and relative activity of their main regulators during mitosis in human cells.** During prophase, as activity of CDK1 is increasing, EG5 pushes two poles apart, probably by sliding antiparallel MTs apart. During prometaphase, as the spindle elongates after initial capture of chromosomes, and metaphase, when spindle is in a dynamic steady state, EG5 is exerting outward force on spindle poles probably by sliding MTs apart, assisted by KIF15 motor bound to parallel MTs, and counteracted by minus-end directed motors (these not shown for simplicity). During this period, KIF4A is located mainly on

chromosome arms. As anaphase starts, and Aurora B is transferred to the spindle midzone, EG5 continues to exert outward pushing force on the spindle poles, but during this phase it is assisted by KIF4A motor, who also transferred to antiparallel MTs making complex with PRC1 MT bundler. As cells approaches telophase, and CDK1 and Aurora B drops, sliding activity of these motors is probably suppressed. G2, gap two; P, prophase; PM/M, prometaphase/metaphase; A, anaphase. Middle part graph is adapted from Nasa and Kettenbach, 2018.



## 6 CONCLUSIONS

Mitosis is a crucial biological process that ensures equal transmission of copied genetic material from a parent cell into two daughter cells. Mitosis as such has fascinated researchers from the first drawings of mitotic spindle done 150 years ago by Walter Flemming. Since then we discovered that mitotic spindle is a very complex structure encompassing various MT populations behaving very differently and exhibiting both dynamic and robust properties depending on the context behind specific phases of mitosis. Moreover, numerous proteins have been described that associate directly or indirectly with mitotic spindle in various organisms and, supported by *in vitro* studies and theoretical modelling, many basic principles behind various mitotic spindle functions have been described.

One of the renowned mechanisms in the field of mitosis is called sliding filament mechanism, proposed in 1969 by McIntosh and co-workers, which postulates that sliding of the antiparallel MTs in relation to one another, powered by plus-end generated motor, can produce sufficient outward force to push different structures within the spindle from each other, similar to myosin muscle contraction mechanisms. This mechanism has been proposed to participate in spindle pole separation during prophase, spindle elongation during prometaphase, spindle length balance during metaphase and finally in spindle elongation during anaphase (Figure 67). On the other hand, a competing hypothesis, termed cortical pulling mechanism, has been proposed in which force for movement within the spindle is produced at a cell cortex and is then transmitted by astral MTs resulting in pull of the spindle poles. Consequentially, proposition of these mechanisms has encouraged numerous structural and functional studies that tried to elucidate their principles. These structural studies established that mitotic spindle is, among other things, composed of MTs that grow from one half-spindle to the other where in the central region of the spindle MTs from the opposite sides assemble into an antiparallel overlap. Such structure is obviously the perfect candidate for sliding filament mechanism.

Additionally, our group has recently found that these interpolar overlap MTs are strongly crosslinked to k-fibers into single mechanical unit, and can thus balance the forces of tension and compression within k-fibers during metaphase. Also, by performing laser cutting of k-fibers, we find that kinetochores can segregate when not in direct or indirect contact with spindle poles, and thus astral MTs, establishing bridging fibers as important contributors to chromosome segregation during anaphase. Also, we showed that, during anaphase, as

chromosomes segregate to opposite sides of the cell by kinetochore fiber shortening and spindle elongation, in between separating chromosomes, antiparallel bridging MTs slide apart. Additionally, we and others have shown that disruption of bridging MT sliding by mechanical perturbations like laser ablation, results in perturbed chromosome segregation and spindle elongation, while disruption of astral MTs does not. These results suggested old debate can finally be settled in human cells where cortical pulling mechanism is obviously taking a minor part in spindle elongation and where sliding filament is a dominant mechanism. Likewise, perturbation of cortical localisation of dynein, main motor responsible for force generation at the cell cortex, by depletion of its adaptors, does not impact chromosome segregation during early anaphase.

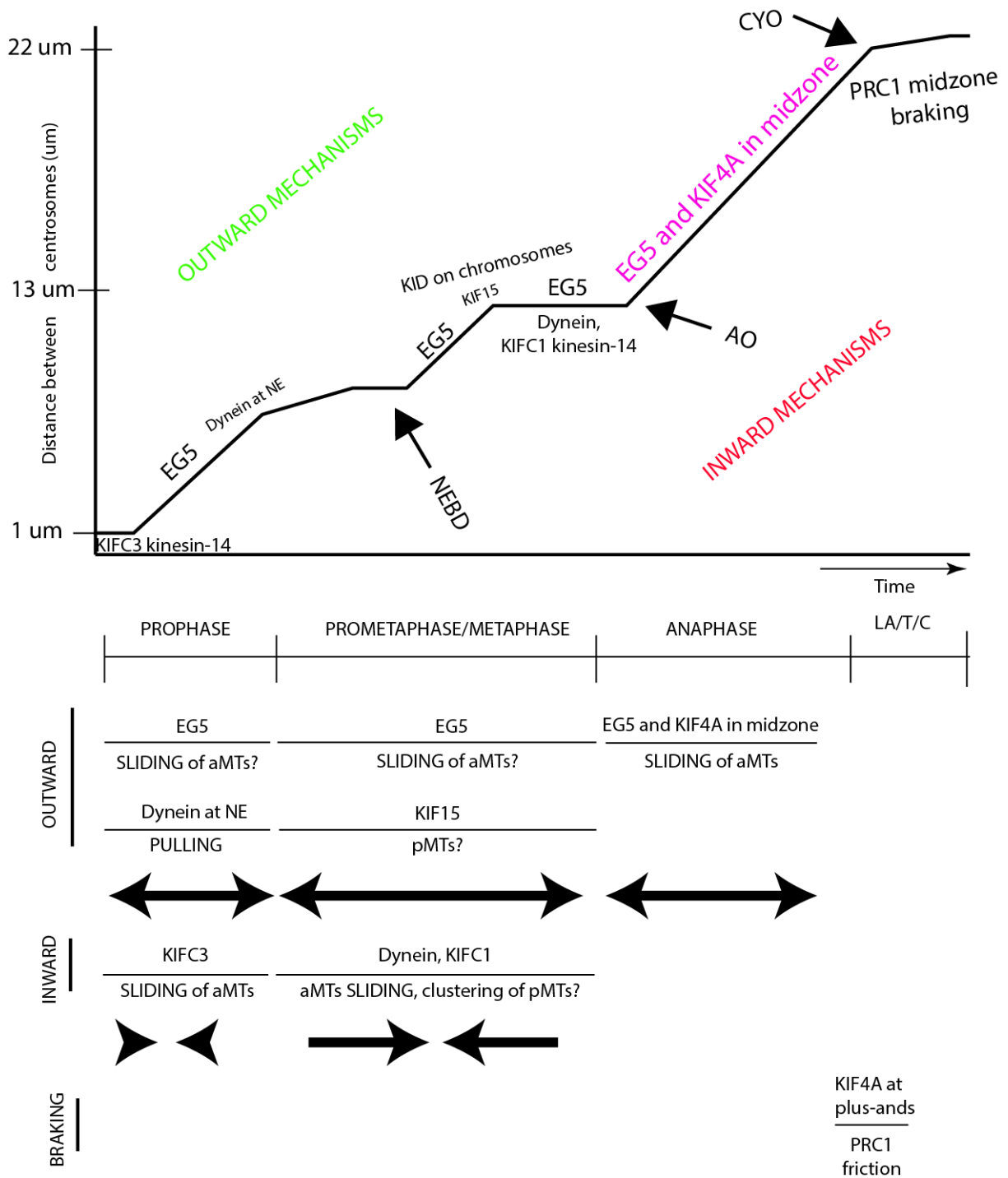
Still, one question remained unanswered, what proteins generate force in sliding filament mechanism? Numerous studies conducted thus far have tried to answer this question, and during spindle assembly it is thought that EG5 is solely responsible for this force production, while in metaphase it can be supported by kinesin-12 protein KIF15 in tumour cell lines. However, if EG5 is inhibited in late metaphase cells, that eventually enter anaphase, spindle elongation is not affected, regardless of KIF15 protein being perturbed or not. Also, *in vitro* experiments demonstrated that other plus-end generated motors like KIF4A, MKLP-1 and yeast kinesin-8 Kip3, can slide antiparallel MTs apart, but when inhibited they cannot stop anaphase spindle elongation, moreover all of them are having a minor impact on this process. This can lead to conclusion that effects on anaphase, observed upon mechanical perturbation of bridging MTs, are probably nonspecific, or some third unknown mechanism may be at action.

In this thesis, I tried to answer this perplexing question by using redundancy approach with ultimate goal to find a combination of motor proteins that could stop anaphase spindle elongation, if such exists. This means that proteins must be inhibited not only individually during anaphase, because most of them already were in numerous studies done to date, but they must be perturbed in multiple combinations of motors and their regulators. I hypothesized that multiple motors operate during sliding of antiparallel MTs in human cells. In that regard, it was surprising when I found that anaphase spindle elongation can be specifically and reproducibly blocked by inhibition of motor EG5 and perturbation of passive antiparallel MT crosslinker PRC1, using various techniques. This suggested that either some unknown mechanism is at place or PRC1 is recruiting some motor to the antiparallel MTs, which then can substitute for EG5 activity. Therefore, I attempted to deplete all PRC1-

interacting proteins, one by one, in combination with EG5 inhibition to find a right mixture of crucial motors. I think I succeeded at this because depletion of PRC1-interacting partner KIF4A and inhibition of EG5 completely mimicked the anaphase arrest observed after PRC1 depletion combined with EG5 inhibition. This means that PRC1 was merely a platform important for localisation of KIF4A to the antiparallel MTs, where this protein is then exerting force by sliding antiparallel MTs apart.

Furthermore, I showed that this combined perturbation is directly impeding sliding by measuring the growth of photoactivated tubulin within antiparallel overlaps. Also, this sliding rate is strongly correlated with both spindle elongation and chromosome segregation rates across all conditions tested, making it a very good predictor of a successful anaphase. I also suggested that these two sliding modules, as I called it, are independent from each other during anaphase, and KIF4A module is probably regulated by action of both kinesins-6, since their combined depletion together with EG5 inhibition is partially mimicking KIF4A depletion combined with EG5 inhibition. I also reasoned that Aurora kinases are regulating some parts of this process, because inhibition of both kinases can greatly effect spindle elongation during anaphase, but for exact mechanism additional experiments must be performed. Finally, I discovered that these molecular motors can slide MTs even when these are highly unstable, after depletion of main crosslinking protein PRC1, and when their interactions, and consequentially sliding itself, is not lasting long as in control spindles.

To conclude this thesis, our findings resolve one perplexing problem in cell division field. It was unclear what motor proteins drive chromosome segregation and spindle elongation in human cells through sliding filament mechanism and our data reveal that sliding of antiparallel MTs during anaphase is operated through two independent modules, one centered around EG5 motor protein, and other where key protein is KIF4A motor. Lastly, these findings complete a missing anaphase puzzle in the general model of regulation of spindle length in human cells (Figure 67).



## STOP

**Figure 67. Simplified model of spindle length regulation by motor proteins in human cells including new anaphase force-generating mechanisms discovered in this thesis.** Distance between centrosomes during mitosis as a function of time in human cells taking prophase pathway in which centrosomes separate already in prophase, opposed to prometaphase pathway of centrosome separation in which most of the pre-anaphase centrosome separation is observed during prometaphase, detailed in Kaseda et al., 2012. Main

force-generators are depicted, those producing outward forces on spindle poles above the line, and those contributing to inward forces below the line. Anaphase force-generating mechanism discovered in this thesis is labelled in magenta. Key transition events during mitosis are noted by an arrow. NEBD, nuclear envelope breakdown; AO, anaphase onset, CYO, cytokinesis onset, NE, nuclear envelope, aMTs, antiparallel MTs and LA/T/C, late anaphase/telophase/cytokinesis. Data for Figure is gathered from various sources mentioned through the thesis, mainly including original data from: this thesis, Su et al., 2016, Hata et al., 2019., Kaseda et al., 2012; Magidson et al., 2011; Raaijmakers et al., 2012; Vukusic et al., 2017 and Young et al., 2014. Model does not include important non-motor regulators of MTs. Time axis is not to scale.

## 7 REFERENCES

- Abaza, A., Soleilhac, J.M., Westendorf, J., Piel, M., Crevel, I., Roux, A., and Pirollet, F. (2003). M phase phosphoprotein 1 is a human plus-end-directed kinesin-related protein required for cytokinesis. *J Biol Chem* 278, 27844-27852.
- Adams, R.R., Wheatley, S.P., Gouldsworthy, A.M., Kandels-Lewis, S.E., Carmena, M., Smythe, C., Gerloff, D.L., and Earnshaw, W.C. (2000). INCENP binds the Aurora-related kinase AIRK2 and is required to target it to chromosomes, the central spindle and cleavage furrow. *Curr Biol* 10, 1075-1078.
- Afonso, O., Castellani, C.M., Cheeseman, L.P., Ferreira, J.G., Orr, B., Ferreira, L.T., Chambers, J.J., Morais-de-Sa, E., Maresca, T.J., and Maiato, H. (2019). Spatiotemporal control of mitotic exit during anaphase by an aurora B-Cdk1 crosstalk. *Elife* 8.
- Afonso, O., Figueiredo, A.C., and Maiato, H. (2017). Late mitotic functions of Aurora kinases. *Chromosoma* 126, 93-103.
- Afonso, O., Matos, I., Pereira, A.J., Aguiar, P., Lampson, M.A., and Maiato, H. (2014). Feedback control of chromosome separation by a midzone Aurora B gradient. *Science* 345, 332-336.
- Aist, J.R., Bayles, C.J., Tao, W., and Berns, M.W. (1991). Direct experimental evidence for the existence, structural basis and function of astral forces during anaphase B in vivo. *J Cell Sci* 100 (Pt 2), 279-288.
- Aist, J.R., Liang, H., and Berns, M.W. (1993). Astral and spindle forces in PtK2 cells during anaphase B: a laser microbeam study. *J Cell Sci* 104 (Pt 4), 1207-1216.
- Akhmanova, A., and Steinmetz, M.O. (2008). Tracking the ends: a dynamic protein network controls the fate of microtubule tips. *Nat Rev Mol Cell Biol* 9, 309-322.
- Aliagas-Martin, I, Burdick, D., Corson, L., Dotson, J., Drummond, J., Fields, C., Huang O.W., Hunsaker, T., Kleinheinz, T., Krueger, E., Liang, J., Moffat, J., Phillips, G., Pulk R, Rawson, T.E., Ultsch, M., Walker, L., Wiesmann, C., Zhang, B., Zhu, B.Y., and Cochran, A.G. A class of 2,4-bisanilinopyrimidine Aurora A inhibitors with unusually high selectivity against Aurora B. *J Med Chem* 28, 3300-3307.
- Alvarez-Fernandez, M., and Medema, R.H. (2013). Novel functions of FoxM1: from molecular mechanisms to cancer therapy. *Front Oncol* 3, 30.
- Ananthanarayanan, V., Schattat, M., Vogel, S.K., Krull, A., Pavin, N., and Tolic-Norrelykke, I.M. (2013). Dynein motion switches from diffusive to directed upon cortical anchoring. *Cell* 153, 1526-1536.
- Asbury, C.L. (2017). Anaphase A: Disassembling Microtubules Move Chromosomes toward Spindle Poles. *Biology (Basel)* 6.
- Auckland, P., and McAinsh, A.D. (2019). CENP-F controls force generation and the dynein-dependent stripping of CENP-E at kinetochores. *BioRxiv* 627380; doi: <https://doi.org/10.1101/627380>
- Bader, J.R., and Vaughan, K.T. (2010). Dynein at the kinetochore: Timing, Interactions and Functions. *Semin Cell Dev Biol* 21, 269-275.
- Ban, R., Irino, Y., Fukami, K., and Tanaka, H. (2004). Human mitotic spindle-associated protein PRC1 inhibits MgcRacGAP activity toward Cdc42 during the metaphase. *J Biol Chem* 279, 16394-16402.
- Bannigan, A., Lizotte-Waniewski, M., Riley, M., and Baskin, T.I. (2008). Emerging molecular mechanisms that power and regulate the anastral mitotic spindle of flowering plants. *Cell Motil Cytoskeleton* 65, 1-11.

Barisic, M., Silva e Sousa, R., Tripathy, S.K., Magiera, M.M., Zaytsev, A.V., Pereira, A.L., Janke, C., Grishchuk, E.L., and Maiato, H. (2015). Mitosis. Microtubule detyrosination guides chromosomes during mitosis. *Science* *348*, 799-803.

Barr, A.R., and Gergely, F. (2007). Aurora-A: the maker and breaker of spindle poles. *J Cell Sci* *120*, 2987-2996.

Barton, N.R., and Goldstein, L.S. (1996). Going mobile: microtubule motors and chromosome segregation. *Proc Natl Acad Sci U S A* *93*, 1735-1742.

Bastos, R.N., Cundell, M.J., and Barr, F.A. (2014). KIF4A and PP2A-B56 form a spatially restricted feedback loop opposing Aurora B at the anaphase central spindle. *J Cell Biol* *207*, 683-693.

Belar, K. (1929). Beitrage zur Kausalanalyse der Mitose : II. Untersuchungen an den Spermatozyten von Chorthippus (Stenobothrus) lineatus Panz. *Wilhelm Roux Arch Entwickl Mech Org* *118*, 359-484.

Ben-David, U., Ha, G., Khadka, P., Jin, X., Wong, B., Franke, L., and Golub, T.R. (2016). The landscape of chromosomal aberrations in breast cancer mouse models reveals driver-specific routes to tumorigenesis. *Nat Commun* *7*, 12160.

Bennett, A., Bechi, B., Tighe, A., Thompson, S., Procter, D.J., and Taylor, S.S. (2015). Cenp-E inhibitor GSK923295: Novel synthetic route and use as a tool to generate aneuploidy. *Oncotarget* *6*, 20921-20932.

Bertran, M.T., Sdelci, S., Regue, L., Avruch, J., Caelles, C., and Roig, J. (2011). Nek9 is a Plk1-activated kinase that controls early centrosome separation through Nek6/7 and Eg5. *EMBO J* *30*, 2634-2647.

Betterton, M.D., and McIntosh, J.R. (2013). Regulation of chromosome speeds in mitosis. *Cell Mol Bioeng* *6*, 418-430.

Bieling, P., Telley, I.A., and Surrey, T. (2010). A minimal midzone protein module controls formation and length of antiparallel microtubule overlaps. *Cell* *142*, 420-432.

Blangy, A., Arnaud, L., and Nigg, E.A. (1997). Phosphorylation by p34cdc2 protein kinase regulates binding of the kinesin-related motor HsEg5 to the dynactin subunit p150. *J Biol Chem* *272*, 19418-19424.

Blangy, A., Lane, H.A., d'Herin, P., Harper, M., Kress, M., and Nigg, E.A. (1995). Phosphorylation by p34cdc2 regulates spindle association of human Eg5, a kinesin-related motor essential for bipolar spindle formation in vivo. *Cell* *83*, 1159-1169.

Braun, M., Lansky, Z., Fink, G., Ruhnnow, F., Diez, S., and Janson, M.E. (2011). Adaptive braking by Ase1 prevents overlapping microtubules from sliding completely apart. *Nat Cell Biol* *13*, 1259-1264.

Brennan, I.M., Peters, U., Kapoor, T.M., and Straight, A.F. (2007). Polo-like kinase controls vertebrate spindle elongation and cytokinesis. *PLoS One* *2*, e409.

Bringmann, H., Skiniotis, G., Spilker, A., Kandels-Lewis, S., Vernos, I., and Surrey, T. (2004). A kinesin-like motor inhibits microtubule dynamic instability. *Science* *303*, 1519-1522.

Brinkley, B.R., and Cartwright, J., Jr. (1971). Ultrastructural analysis of mitotic spindle elongation in mammalian cells in vitro. Direct microtubule counts. *J Cell Biol* *50*, 416-431.

Brinkley, B.R., and Cartwright, J., Jr. (1975). Cold-labile and cold-stable microtubules in the mitotic spindle of mammalian cells. *Ann N Y Acad Sci* *253*, 428-439.

Brust-Mascher, I., Civelekoglu-Scholey, G., Kwon, M., Mogilner, A., and Scholey, J.M. (2004). Model for anaphase B: role of three mitotic motors in a switch from poleward flux to spindle elongation. *Proc Natl Acad Sci U S A* *101*, 15938-15943.

Brust-Mascher, I., Sommi, P., Cheerambathur, D.K., and Scholey, J.M. (2009). Kinesin-5-dependent poleward flux and spindle length control in *Drosophila* embryo mitosis. *Mol Biol Cell* *20*, 1749-1762.

Buda, R., Vukusic, K., and Tolic, I.M. (2017). Dissection and characterization of microtubule bundles in the mitotic spindle using femtosecond laser ablation. *Methods Cell Biol* 139, 81-101.

Burbank, K.S., Mitchison T.J., and Fisher, D.S. (2007). Slide-and-cluster models for spindle assembly. *Curr Biol* 17, 1373–1383.

Cahu, J., Olichon, A., Hentrich, C., Schek, H., Drinjakovic, J., Zhang, C., Doherty-Kirby, A., Lajoie, G., and Surrey, T. (2008). Phosphorylation by Cdk1 increases the binding of Eg5 to microtubules in vitro and in *Xenopus* egg extract spindles. *PLoS One* 3, e3936.

Cai, S., O'Connell, C.B., Khodjakov, A., and Walczak, C.E. (2009). Chromosome congression in the absence of kinetochore fibres. *Nat Cell Biol* 11, 832-838.

Cande, W.Z. (1982). Nucleotide requirements for anaphase chromosome movements in permeabilized mitotic cells: anaphase B but not anaphase A requires ATP. *Cell* 28, 15-22.

Canman, J.C., Hoffman, D.B., and Salmon, E.D. (2000). The role of pre- and post-anaphase microtubules in the cytokinesis phase of the cell cycle. *Curr Biol* 10, 611-614.

Cassimeris, L.U., Walker, R.A., Pryer, N.K., and Salmon, E.D. (1987). Dynamic instability of microtubules. *Bioessays* 7, 149-154.

Charnley, M., Anderegg, F., Holtackers, R., Textor, M., and Meraldi, P. (2013). Effect of Cell Shape and Dimensionality on Spindle Orientation and Mitotic Timing. *PLoS One* 8, e66918.

Cheeseman, I.M., and Desai, A. (2008). Molecular architecture of the kinetochore-microtubule interface. *Nat Rev Mol Cell Biol* 9, 33-46.

Cheerambathur, D.K., Civelekoglu-Scholey, G., Brust-Mascher, I., Sommi, P., Mogilner, A., Scholey, J.M. (2007). Quantitative analysis of an anaphase B switch: predicted role for a microtubule catastrophe gradient. *J Cell Biol* 177, 995–1004.

Chozinski, T.J., Halpern, A.R., Okawa, H., Kim, H.J., Tremel, G.J., Wong, R.O., and Vaughan, J.C. (2016). Expansion microscopy with conventional antibodies and fluorescent proteins. *Nat Methods* 13, 485-488.

Cimini, D., Cameron, L.A., and Salmon, E.D. (2004). Anaphase spindle mechanics prevent mis-segregation of merotelically oriented chromosomes. *Curr Biol* 14, 2149-2155.

Civelekoglu-Scholey, G., and Scholey, J.M. (2010). Mitotic force generators and chromosome segregation. *Cell Mol Life Sci* 67, 2231-2250.

Coelho, P.A., Queiroz-Machado, J., Carmo, A.M., Moutinho-Pereira, S., Maiato, H., and Sunkel, C.E. (2008). Dual role of topoisomerase II in centromere resolution and aurora B activity. *PLoS Biol* 6, e207.

Collins, E., Mann, B.J., and Wadsworth, P. (2014). Eg5 restricts anaphase B spindle elongation in mammalian cells. *Cytoskeleton (Hoboken)* 71, 136-144.

Courtheoux, T., Diallo, A., Damodaran, A.P., Rebutier, D., Watrin, E. and Prigent, C. (2018). Aurora A kinase activity is required to maintain an active spindle assembly checkpoint during prometaphase. *J Cell Sci* 131.

Cross, R.A., and McAinsh, A. (2014). Prime movers: the mechanochemistry of mitotic kinesins. *Nat Rev Mol Cell Biol* 15, 257-271.

DeBonis, S., Skoufias, D.A., Lebeau, L., Lopez, R., Robin, G., Margolis, R.L., Wade, R.H., and Kozielski, F. (2004). In vitro screening for inhibitors of the human mitotic kinesin Eg5 with antimitotic and antitumor activities. *Mol Cancer Ther* 3, 1079-1090.

DeLuca, J.G., Howell, B.J., Canman, J.C., Hickey, J.M., Fang, G., and Salmon, E.D. (2003). Nuf2 and Hec1 are required for retention of the checkpoint proteins Mad1 and Mad2 to kinetochores. *Curr Biol* 13, 2103-2109.

DeLuca, J.G., Moree, B., Hickey, J.M., Kilmartin, J.V., and Salmon, E.D. (2002). hNuf2 inhibition blocks stable kinetochore-microtubule attachment and induces mitotic cell death in HeLa cells. *J Cell Biol* 159, 549-555.



Desai, A., Maddox, P.S., Mitchison, T.J., and Salmon, E.D. (1998). Anaphase A chromosome movement and poleward spindle microtubule flux occur at similar rates in *Xenopus* extract spindles. *J Cell Biol* *141*, 703-713.

Desai, A., and Mitchison, T.J. (1997). Microtubule polymerization dynamics. *Annu Rev Cell Dev Biol* *13*, 83-117.

Ding, R., McDonald, K.L., and McIntosh, J.R. (1993). Three-dimensional reconstruction and analysis of mitotic spindles from the yeast, *Schizosaccharomyces pombe*. *J Cell Biol* *120*, 141-151.

Ditchfield, C., Johnson, V.L., Tighe, A., Ellston, R., Haworth, C., Johnson, T., Mortlock, A., Keen, N., and Taylor, S.S. (2003). Aurora B couples chromosome alignment with anaphase by targeting BubR1, Mad2, and Cenp-E to kinetochores. *J Cell Biol* *161*, 267-280.

Douglas, M.E., Davies, T., Joseph, N., and Mishima, M. (2010). Aurora B and 14-3-3 coordinately regulate clustering of central spindle during cytokinesis. *Curr Biol* *20*, 927-933.

Downing, K.H., and Nogales, E. (1998). Tubulin and microtubule structure. *Curr Opin Cell Biol* *10*, 16-22.

Drechsler, H., and McAinsh, A.D. (2016). Kinesin-12 motors cooperate to suppress microtubule catastrophes and drive the formation of parallel microtubule bundles. *Proc Natl Acad Sci U S A* *113*, E1635-1644.

Drechsler, H., McHugh, T., Singleton, M.R., Carter, N.J., and McAinsh, A.D. (2014). The Kinesin-12 Kif15 is a processive track-switching tetramer. *Elife* *3*, e01724.

Dudka, D., Noatynska, A., Smith, C.A., Liaudet, N., McAinsh, A.D., and Meraldi, P. (2018). Complete microtubule-kinetochore occupancy favours the segregation of merotelic attachments. *Nat Commun* *9*, 2042.

Dumont, J., Oegema, K., and Desai, A. (2010). A kinetochore-independent mechanism drives anaphase chromosome separation during acentrosomal meiosis. *Nat Cell Biol* *12*, 894-901.

Dumont, S., and Mitchison, T.J. (2009). Force and length in the mitotic spindle. *Curr Biol* *19*, R749-761.

Dumont, S., Salmon, E.D., and Mitchison, T.J. (2012). Deformations within moving kinetochores reveal different sites of active and passive force generation. *Science* *337*, 355-358.

Eckerdt, F., Eyers, P.A., Lewellyn, A.L., Prigent, C., and Maller, J.L. (2008). Spindle pole regulation by a discrete Eg5-interacting domain in TPX2. *Curr Biol* *18*, 519-525.

Eibes, S., Gallisa-Sune, N., Rosas-Salvans, M., Martinez-Delgado, P., Vernos, I., and Roig, J. (2018). Nek9 Phosphorylation Defines a New Role for TPX2 in Eg5-Dependent Centrosome Separation before Nuclear Envelope Breakdown. *Curr Biol* *28*, 121-129 e124.

Elting, M.W., Hueschen, C.L., Udy, D.B., and Dumont, S. (2014). Force on spindle microtubule minus ends moves chromosomes. *J Cell Biol* *206*, 245-256.

Ferreira, L.T., Orr, B., Rajendraprasad, G., Pereira, A.J., Lemos, C., Lima, J.T., Guasch Boldú, C., Ferreira, J.G., Barisic, M., and Maiato, H. (2019). Microtubule tyrosination/detyrosination specifies a mitotic error code. *BioRxiv* 801977; doi: <https://doi.org/10.1101/801977>

Ferenz, N.P., Paul, R., Fagerstrom, C., Mogilner, A., and Wadsworth, P. (2009). Dynein antagonizes eg5 by crosslinking and sliding antiparallel microtubules. *Curr Biol* *19*, 1833-1838.

Fernandez, P., Maier, M., Lindauer, M., Kuffer, C., Storchova, Z., and Bausch, A.R. (2011). Mitotic spindle orients perpendicular to the forces imposed by dynamic shear. *PLoS One* *6*, e28965.

Fink, G., Hajdo, L., Skowronek, K.J., Reuther, C., Kasprzak, A.A., and Diez, S. (2009). The mitotic kinesin-14 Ncd drives directional microtubule-microtubule sliding. *Nat Cell Biol* *11*, 717-723.

Fink, G., Schuchardt, I., Colombelli, J., Stelzer, E., and Steinberg, G. (2006). Dynein-mediated pulling forces drive rapid mitotic spindle elongation in *Ustilago maydis*. *EMBO J* 25, 4897-4908.

Fisher, K.H., Deane, C.M., and Wakefield, J.G. (2008). The functional domain grouping of microtubule associated proteins. *Commun Integr Biol* 1, 47-50.

FitzHarris, G. (2012). Anaphase B precedes anaphase A in the mouse egg. *Curr Biol* 22, 437-444.

Fontijn, R.D., Goud, B., Echard, A., Jollivet, F., van Marle, J., Pannekoek, H., and Horrevoets, A.J. (2001). The human kinesin-like protein RB6K is under tight cell cycle control and is essential for cytokinesis. *Mol Cell Biol* 21, 2944-2955.

Fu, C., Ward, J.J., Loiodice, I., Velve-Casquillas, G., Nedelec, F.J., and Tran, P.T. (2009). Phospho-regulated interaction between kinesin-6 Klp9p and microtubule bundler Ase1p promotes spindle elongation. *Dev Cell* 17, 257-267.

Gable, A., Qiu, M., Titus, J., Balchand, S., Ferenz, N.P., Ma, N., Collins, E.S., Fagerstrom, C., Ross, J.L., Yang, G., *et al.* (2012). Dynamic reorganization of Eg5 in the mammalian spindle throughout mitosis requires dynein and TPX2. *Mol Biol Cell* 23, 1254-1266.

Ganem, N.J., Upton, K., and Compton, D.A. (2005). Efficient mitosis in human cells lacking poleward microtubule flux. *Curr Biol* 15, 1827-1832.

Gatlin, J.C., and Bloom, K. (2010). Microtubule motors in eukaryotic spindle assembly and maintenance. *Semin Cell Dev Biol* 21, 248-254.

Gayek, A.S., and Ohi, R. (2014). Kinetochore-microtubule stability governs the metaphase requirement for Eg5. *Mol Biol Cell* 25, 2051-2060.

Gerson-Gurwitz, A., Thiede, C., Movshovich, N., Fridman, V., Podolskaya, M., Danieli, T., Lakamper, S., Klopfenstein, D.R., Schmidt, C.F., and Gheber, L. (2011). Directionality of individual kinesin-5 Cin8 motors is modulated by loop 8, ionic strength and microtubule geometry. *EMBO J* 30, 4942-4954.

Girão H., Okada N., Rodrigues T.A., Silva A.O., Figueiredo A.C., Garcia Z., Moutinho-Santos T., Hayashi I., Azevedo J.E., Macedo-Ribeiro S., and Maiato H. (2020). CLASP2 binding to curved microtubule tips promotes flux and stabilizes kinetochore attachments. *J Cell Biol* 219. pii: e201905080.

Glotzer, M. (2009). The 3Ms of central spindle assembly: microtubules, motors and MAPs. *Nat Rev Mol Cell Biol* 10, 9-20.

Godinho, S.A., and Pellman, D. (2014). Causes and consequences of centrosome abnormalities in cancer. *Philos Trans R Soc Lond B Biol Sci* 369.

Gorbsky, G.J., Sammak, P.J., and Borisy, G.G. (1987). Chromosomes move poleward in anaphase along stationary poleward chromosome motion in fission yeast. *EMBO J* 25, 4888-4896.

Grishchuk, E.L., Molodtsov, M.I., Ataulakhanov, F.I., and McIntosh, J.R. (2005). Force production by disassembling microtubules. *Nature* 438, 384-388.

Gruneberg, U., Neef, R., Honda, R., Nigg, E.A., and Barr, F.A. (2004). Relocation of Aurora B from centromeres to the central spindle at the metaphase to anaphase transition requires MKlp2. *J Cell Biol* 166, 167-172.

Gruneberg, U., Neef, R., Li, X., Chan, E.H., Chalamalasetty, R.B., Nigg, E.A., and Barr, F.A. (2006). KIF14 and citron kinase act together to promote efficient cytokinesis. *J Cell Biol* 172, 363-372.

Hata, S., Pastor Peidro, A., Panic, M., Liu, P., Atorino, E., Funaya, C., Jakle, U., Pereira, G., and Schiebel, E. (2019). The balance between KIFC3 and EG5 tetrameric kinesins controls the onset of mitotic spindle assembly. *Nat Cell Biol* 21, 1138-1151.

Hauf, S., Waizenegger, I.C., and Peters, J.M. (2001). Cohesin cleavage by separase required for anaphase and cytokinesis in human cells. *Science* 293, 1320-1323.

Hegarar, N., Smith, E., Nayak, G., Takeda, S., Eyers, P.A., and Hocheegger, H. (2011). Aurora A and Aurora B jointly coordinate chromosome segregation and anaphase microtubule dynamics. *J Cell Biol* *195*, 1103-1113.

Helmke, K.J., Heald, R., and Wilbur, J.D. (2013). Interplay between spindle architecture and function. *Int Rev Cell Mol Biol* *306*, 83-125.

Hentrich, C., and Surrey, T. (2010). Microtubule organization by the antagonistic mitotic motors kinesin-5 and kinesin-14. *J Cell Biol* *189*, 465-480.

Heuser, J.E., and Kirschner, M.W. (1980). Filament organization revealed in platinum replicas of freeze-dried cytoskeletons. *J Cell Biol* *86*, 212-234.

Hocheegger, H., Takeda, S., and Hunt, T. (2008). Cyclin-dependent kinases and cell-cycle transitions: does one fit all? *Nat Rev Mol Cell Biol* *9*, 910-916.

Howard, J., and Hyman, A.A. (2009). Growth, fluctuation and switching at microtubule plus ends. *Nat Rev Mol Cell Biol* *10*, 569-574.

Hsia, K.C., Wilson-Kubalek, E.M., Dottore, A., Hao, Q., Tsai, K.L., Forth, S., Shimamoto, Y., Milligan, R.A., and Kapoor, T.M. (2014). Reconstitution of the augmin complex provides insights into its architecture and function. *Nat Cell Biol* *16*, 852-863.

Hu, C.K., Coughlin, M., Field, C.M., and Mitchison, T.J. (2011). KIF4 regulates midzone length during cytokinesis. *Curr Biol* *21*, 815-824.

Hu, C.K., Ozlu, N., Coughlin, M., Steen, J.J., and Mitchison, T.J. (2012). Plk1 negatively regulates PRC1 to prevent premature midzone formation before cytokinesis. *Mol Biol Cell* *23*, 2702-2711.

Hummer, S., and Mayer, T.U. (2009). Cdk1 negatively regulates midzone localization of the mitotic kinesin Mklp2 and the chromosomal passenger complex. *Curr Biol* *19*, 607-612.

Hutterer, A., Glotzer, M., and Mishima, M. (2009). Clustering of centralspindlin is essential for its accumulation to the central spindle and the midbody. *Curr Biol* *19*, 2043-2049.

Inoue, S. (1952). The effect of colchicine on microscopic and submicroscopic structure of the mitotic spindle. *Exp Cell Res (Suppl)* *2*, 305-318.

Inoue, S., and Ritter, H., Jr. (1975). Dynamics of mitotic spindle organization and function. *Soc Gen Physiol Ser* *30*, 3-30.

Inoue, S., and Sato, H. (1967). Cell motility by labile association of molecules. The nature of mitotic spindle fibers and their role in chromosome movement. *J Gen Physiol* *50*, Suppl:259-292.

Janisch, K.M., McNeely, K.C., Dardick, J.M., Lim, S.H., and Dwyer, N.D. (2018). Kinesin-6 KIF20B is required for efficient cytokinetic furrowing and timely abscission in human cells. *Mol Biol Cell* *29*, 166-179.

Jaqaman, K., King, E.M., Amaro, A.C., Winter, J.R., Dorn, J.F., Elliott, H.L., McHedlishvili, N., McClelland, S.E., Porter, I.M., Posch, M., *et al.* (2010). Kinetochore alignment within the metaphase plate is regulated by centromere stiffness and microtubule depolymerases. *J Cell Biol* *188*, 665-679.

Jensen, C.G. (1982). Dynamics of spindle microtubule organization: kinetochore fiber microtubules of plant endosperm. *J Cell Biol* *92*, 540-558.

Jiang, W., Jimenez, G., Wells, N.J., Hope, T.J., Wahl, G.M., Hunter, T., and Fukunaga, R. (1998). PRC1: a human mitotic spindle-associated CDK substrate protein required for cytokinesis. *Mol Cell* *2*, 877-885.

Joglekar, A.P. (2016). A Cell Biological Perspective on Past, Present and Future Investigations of the Spindle Assembly Checkpoint. *Biology (Basel)* *5*.

Jongerius, A. (2017). Control mechanisms of microtubule overlap regions (Wageningen University), pp. 134.

Kajtez, J., Solomatina, A., Novak, M., Polak, B., Vukusic, K., Rudiger, J., Cojoc, G., Milas, A., Sumanovac Sestak, I., Risteski, P., *et al.* (2016). Overlap microtubules link sister k-fibres and balance the forces on bi-oriented kinetochores. *Nat Commun* 7, 10298.

Kamasaki, T., O'Toole, E., Kita, S., Osumi, M., Usukura, J., McIntosh, J.R., and Goshima, G. (2013). Augmin-dependent microtubule nucleation at microtubule walls in the spindle. *J Cell Biol* 202, 25-33.

Kapitein, L.C., Peterman, E.J., Kwok, B.H., Kim, J.H., Kapoor, T.M., and Schmidt, C.F. (2005). The bipolar mitotic kinesin Eg5 moves on both microtubules that it crosslinks. *Nature* 435, 114-118.

Kapoor, T.M., Mayer, T.U., Coughlin, M.L., and Mitchison, T.J. (2000). Probing spindle assembly mechanisms with monastrol, a small molecule inhibitor of the mitotic kinesin, Eg5. *J Cell Biol* 150, 975-988.

Kaseda, K., McAinsh, A.D., and Cross, R.A. (2012). Dual pathway spindle assembly increases both the speed and the fidelity of mitosis. *Biol Open* 1, 12-18.

Khodjakov, A., La Terra, S., and Chang, F. (2004). Laser microsurgery in fission yeast; role of the mitotic spindle midzone in anaphase B. *Curr Biol* 14, 1330-1340.

Kim, D.C., Kim, E.D., Liu, L., Buckley, R.S., Parameswaran, S., Kim, S., Wojcik, E.J. (2019). Small molecule allosteric uncoupling of microtubule depolymerase activity from motility in human Kinesin-5 during mitotic spindle assembly. *Sci Rep* 9, 19900.

Kinoshita, K., Habermann, B., and Hyman, A.A. (2002). XMAP215: a key component of the dynamic microtubule cytoskeleton. *Trends Cell Biol* 12, 267-273.

Kirschner, M., and Mitchison, T. (1986). Beyond self-assembly: from microtubules to morphogenesis. *Cell* 45, 329-342.

Kitagawa, M., Fung, S.Y., Hameed, U.F., Goto, H., Inagaki, M., and Lee, S.H. (2014). Cdk1 coordinates timely activation of MKlp2 kinesin with relocation of the chromosome passenger complex for cytokinesis. *Cell Rep* 7, 166-179.

Kiyomitsu, T., and Cheeseman, I.M. (2012). Chromosome- and spindle-pole-derived signals generate an intrinsic code for spindle position and orientation. *Nat Cell Biol* 14, 311-317.

Kiyomitsu, T., and Cheeseman, I.M. (2013). Cortical dynein and asymmetric membrane elongation coordinately position the spindle in anaphase. *Cell* 154, 391-402.

Kops, G.J., Saurin, A.T., and Meraldi, P. (2010). Finding the middle ground: how kinetochores power chromosome congression. *Cell Mol Life Sci* 67, 2145-2161.

Koshland, D.E., Mitchison, T.J., and Kirschner, M.W. (1988). Polewards chromosome movement driven by microtubule depolymerization in vitro. *Nature* 331, 499-504.

Kotak, S. (2019). Mechanisms of Spindle Positioning: Lessons from Worms and Mammalian Cells. *Biomolecules* 9.

Kotak, S., Busso, C., and Gonczy, P. (2013). NuMA phosphorylation by CDK1 couples mitotic progression with cortical dynein function. *EMBO J* 32, 2517-2529.

Kotak, S., and Gonczy, P. (2014). NuMA phosphorylation dictates dynein-dependent spindle positioning. *Cell Cycle* 13, 177-178.

Kozlowski, C., Srayko, M., and Nedelec, F. (2007). Cortical microtubule contacts position the spindle in *C. elegans* embryos. *Cell* 129, 499-510.

Kruger, L.K., Sanchez, J.L., Paoletti, A., and Tran, P.T. (2019). Kinesin-6 regulates cell-size-dependent spindle elongation velocity to keep mitosis duration constant in fission yeast. *Elife* 8.

Krull, A., Steinborn, A., Ananthanarayanan, V., Ramunno-Johnson, D., Petersohn, U., and Tolic-Norrellykke, I.M. (2014). A divide and conquer strategy for the maximum likelihood localization of low intensity objects. *Opt Express* 22, 210-228.

Kurasawa, Y., Earnshaw, W.C., Mochizuki, Y., Dohmae, N., and Todokoro, K. (2004). Essential roles of KIF4 and its binding partner PRC1 in organized central spindle midzone formation. *EMBO J* 23, 3237-3248.

Laan, L., Pavin, N., Husson, J., Romet-Lemonne, G., van Duijn, M., Lopez, M.P., Vale, R.D., Julicher, F., Reck-Peterson, S.L., and Dogterom, M. (2012). Cortical dynein controls microtubule dynamics to generate pulling forces that position microtubule asters. *Cell* 148, 502-514.

Laband, K., Le Borgne, R., Edwards, F., Stefanutti, M., Canman, J.C., Verbavatz, J.M., and Dumont, J. (2017). Chromosome segregation occurs by microtubule pushing in oocytes. *Nat Commun* 8, 1499.

Lampson, M.A., and Cheeseman, I.M. (2011). Sensing centromere tension: Aurora B and the regulation of kinetochore function. *Trends Cell Biol* 21, 133-140.

Lampson, M.A., and Kapoor, T.M. (2006). Unraveling cell division mechanisms with small-molecule inhibitors. *Nat Chem Biol* 2, 19-27.

Lansky, Z., Braun, M., Ludecke, A., Schlierf, M., ten Wolde, P.R., Janson, M.E., and Diez, S. (2015). Diffusible crosslinkers generate directed forces in microtubule networks. *Cell* 160, 1159-1168.

Lawo, S., Bashkurov, M., Mullin, M., Ferreria, M.G., Kittler, R., Habermann, B., Tagliaferro, A., Poser, I., Hutchins, J.R., Hegemann, B., *et al.* (2009). HAUS, the 8-subunit human Augmin complex, regulates centrosome and spindle integrity. *Curr Biol* 19, 816-826.

Lecland, N., and Luders, J. (2014). The dynamics of microtubule minus ends in the human mitotic spindle. *Nat Cell Biol* 16, 770-778.

Lee, K.Y., Davies, T., and Mishima, M. (2012). Cytokinesis microtubule organisers at a glance. *J Cell Sci* 125, 3495-3500.

Leslie, R.J., and Pickett-Heaps, J.D. (1983). Ultraviolet microbeam irradiations of mitotic diatoms: investigation of spindle elongation. *J Cell Biol* 96, 548-561.

Lioutas, A., and Vernos, I. (2013). Aurora A kinase and its substrate TACC3 are required for central spindle assembly. *EMBO Rep* 14, 829-836.

Liu, J., Wang, Z., Jiang, K., Zhang, L., Zhao, L., Hua, S., Yan, F., Yang, Y., Wang, D., Fu, C., *et al.* (2009). PRC1 cooperates with CLASP1 to organize central spindle plasticity in mitosis. *J Biol Chem* 284, 23059-23071.

Liu, X., Xu, L., Li, J., Yao, P.Y., Wang, W., Ismail, H., Wang, H., Liao, B., Yang, Z., Ward, T., *et al.* (2019). Mitotic motor CENP-E cooperates with PRC1 in temporal control of central spindle assembly. *J Mol Cell Biol*.

Lodish, H.E.A. *et al.* (2014). *Molecular cell biology*, 7th ed. (W. H. Freeman and Company, New York).

Lu, M.S., and Johnston, C.A. (2013). Molecular pathways regulating mitotic spindle orientation in animal cells. *Development* 140, 1843-1856.

Lukinavicius, G., Blaukopf, C., Pershagen, E., Schena, A., Reymond, L., Derivery, E., Gonzalez-Gaitan, M., D'Este, E., Hell, S.W., Wolfram Gerlich, D., *et al.* (2015). SiR-Hoechst is a far-red DNA stain for live-cell nanoscopy. *Nat Commun* 6, 8497.

Ma, N., Titus, J., Gable, A., Ross, J.L., and Wadsworth, P. (2011). TPX2 regulates the localization and activity of Eg5 in the mammalian mitotic spindle. *J Cell Biol* 195, 87-98.

Maffini, S., Maia, A.R., Manning, A.L., Maliga, Z., Pereira, A.L., Junqueira, M., Shevchenko, A., Hyman, A., Yates, J.R., 3rd, Galjart, N., *et al.* (2009). Motor-independent targeting of CLASPs to kinetochores by CENP-E promotes microtubule turnover and poleward flux. *Curr Biol* 19, 1566-1572.

Magidson, V., O'Connell, C.B., Loncarek, J., Paul, R., Mogilner, A., and Khodjakov, A. (2011). The spatial arrangement of chromosomes during prometaphase facilitates spindle assembly. *Cell* 146, 555-567.

Maiato, H., Gomes, A.M., Sousa, F., and Barisic, M. (2017). Mechanisms of Chromosome Congression during Mitosis. *Biology (Basel)* 6.

Maiato, H., Khodjakov, A., and Rieder, C.L. (2005). *Drosophila* CLASP is required for the incorporation of microtubule subunits into fluxing kinetochore fibres. *Nat Cell Biol* 7, 42-47.

Maiato, H., and Lince-Faria, M. (2010). The perpetual movements of anaphase. *Cell Mol Life Sci* 67, 2251-2269.

Mallavarapu, A., Sawin, K., and Mitchison, T. (1999). A switch in microtubule dynamics at the onset of anaphase B in the mitotic spindle of *Schizosaccharomyces pombe*. *Curr Biol* 9, 1423-1426.

Mann, B.J., Balchand, S.K., and Wadsworth, P. (2017). Regulation of Kif15 localization and motility by the C-terminus of TPX2 and microtubule dynamics. *Mol Biol Cell* 28, 65-75.

Mann, B.J., and Wadsworth, P. (2018). Distribution of Eg5 and TPX2 in mitosis: Insight from CRISPR tagged cells. *Cytoskeleton (Hoboken)* 75, 508-521.

Mann, B.J., and Wadsworth, P. (2019). Kinesin-5 Regulation and Function in Mitosis. *Trends Cell Biol* 29, 66-79.

Martin-Lluesma, S., Stucke, V.M., and Nigg, E.A. (2002). Role of Hec1 in spindle checkpoint signaling and kinetochore recruitment of Mad1/Mad2. *Science* 297, 2267-2270.

Mastrorarde, D.N., McDonald, K.L., Ding, R., and McIntosh, J.R. (1993). Interpolar spindle microtubules in PTK cells. *J Cell Biol* 123, 1475-1489.

Matuliene, J., and Kuriyama, R. (2002). Kinesin-like protein CHO1 is required for the formation of midbody matrix and the completion of cytokinesis in mammalian cells. *Mol Biol Cell* 13, 1832-1845.

Mayer, T.U., Kapoor, T.M., Haggarty, S.J., King, R.W., Schreiber, S.L., and Mitchison, T.J. (1999). Small molecule inhibitor of mitotic spindle bipolarity identified in a phenotype-based screen. *Science* 286, 971-974.

Mayr, M.I., Hummer, S., Bormann, J., Gruner, T., Adio, S., Woehlke, G., and Mayer, T.U. (2007). The human kinesin Kif18A is a motile microtubule depolymerase essential for chromosome congression. *Curr Biol* 17, 488-498.

Mazumdar, M., and Misteli, T. (2005). Chromokinesins: multitasking players in mitosis. *Trends Cell Biol* 15, 349-355.

Mazumdar, M., Sundareshan, S., and Misteli, T. (2004). Human chromokinesin KIF4A functions in chromosome condensation and segregation. *J Cell Biol* 166, 613-620.

McClelland, M.L., Gardner, R.D., Kallio, M.J., Daum, J.R., Gorbsky, G.J., Burke, D.J., and Stukenberg, P.T. (2003). The highly conserved Ndc80 complex is required for kinetochore assembly, chromosome congression, and spindle checkpoint activity. *Genes Dev* 17, 101-114.

McDonald, K., Pickett-Heaps, J.D., McIntosh, J.R., and Tippit, D.H. (1977). On the mechanism of anaphase spindle elongation in *Diatoma vulgare*. *J Cell Biol* 74, 377-388.

McDonald, K.L., O'Toole, E.T., Mastrorarde, D.N., and McIntosh, J.R. (1992). Kinetochore microtubules in PTK cells. *J Cell Biol* 118, 369-383.

McEwen, B.F., Chan, G.K., Zubrowski, B., Savoian, M.S., Sauer, M.T., and Yen, T.J. (2001). CENP-E is essential for reliable bioriented spindle attachment, but chromosome alignment can be achieved via redundant mechanisms in mammalian cells. *Mol Biol Cell* 12, 2776-2789.

McEwen, B.F., Heagle, A.B., Cassels, G.O., Buttle, K.F., and Rieder, C.L. (1997). Kinetochore fiber maturation in PtK1 cells and its implications for the mechanisms of chromosome congression and anaphase onset. *J Cell Biol* 137, 1567-1580.

McIntosh, J.R. (1994). The roles of microtubules in chromosome movement. In *Microtubules* (New York: Wiley-Liss), pp. 413-434.

McIntosh, J.R., Grishchuk, E.L., Mophew, M.K., Efremov, A.K., Zhudenkov, K., Volkov, V.A., Cheeseman, I.M., Desai, A., Mastrorarde, D.N., and Ataullakhanov, F.I. (2008). Fibrils

connect microtubule tips with kinetochores: a mechanism to couple tubulin dynamics to chromosome motion. *Cell* *135*, 322-333.

McIntosh, J.R., and Hays, T. (2016). A Brief History of Research on Mitotic Mechanisms. *Biology (Basel)* *5*.

McIntosh, J.R., Hepler, P.K., and van Wie, D.G. (1969). Model for mitosis. *Nature* *224*, 659-663.

McIntosh, J.R., and Landis, S.C. (1971). The distribution of spindle microtubules during mitosis in cultured human cells. *J Cell Biol* *49*, 468-497.

McIntosh, J.R., Molodtsov, M.I., and Ataullakhanov, F.I. (2012). Biophysics of mitosis. *Q Rev Biophys* *45*, 147-207.

McIntosh, J.R., Volkov, V., Ataullakhanov, F.I., and Grishchuk, E.L. (2010). Tubulin depolymerization may be an ancient biological motor. *J Cell Sci* *123*, 3425-3434.

McKinley, K.L. (2018). Employing CRISPR/Cas9 genome engineering to dissect the molecular requirements for mitosis. *Methods Cell Biol* *144*, 75-105.

McKinley, K.L., and Cheeseman, I.M. (2017). Large-Scale Analysis of CRISPR/Cas9 Cell-Cycle Knockouts Reveals the Diversity of p53-Dependent Responses to Cell-Cycle Defects. *Dev Cell* *40*, 405-420 e402.

McNeill, P.A., and Berns, M.W. (1981). Chromosome behavior after laser microirradiation of a single kinetochore in mitotic PtK2 cells. *J Cell Biol* *88*, 543-553.

Meraldi, P., Draviam, V.M., and Sorger, P.K. (2004). Timing and checkpoints in the regulation of mitotic progression. *Dev Cell* *7*, 45-60.

Milas, A., and Tolić, I.M. (2016). Relaxation of interkinetochore tension after severing of a k-fiber depends on the length of the k-fiber stub. *Matters Select*.

Mishima, M., Kaitna, S., and Glotzer, M. (2002). Central spindle assembly and cytokinesis require a kinesin-like protein/RhoGAP complex with microtubule bundling activity. *Dev Cell* *2*, 41-54.

Mishima, M., Pavicic, V., Gruneberg, U., Nigg, E.A., and Glotzer, M. (2004). Cell cycle regulation of central spindle assembly. *Nature* *430*, 908-913.

Mitchison, T., Evans, L., Schulze, E., and Kirschner, M. (1986). Sites of microtubule assembly and disassembly in the mitotic spindle. *Cell* *45*, 515-527.

Mitchison, T., and Kirschner, M. (1984). Dynamic instability of microtubule growth. *Nature* *312*, 237-242.

Mitchison, T.J. (1989). Polewards microtubule flux in the mitotic spindle: evidence from photoactivation of fluorescence. *J Cell Biol* *109*, 637-652.

Mitchison, T.J., and Salmon, E.D. (1992). Poleward kinetochore fiber movement occurs during both metaphase and anaphase-A in newt lung cell mitosis. *J Cell Biol* *119*, 569-582.

Mogilner, A., and Craig, E. (2010). Towards a quantitative understanding of mitotic spindle assembly and mechanics. *J Cell Sci* *123*, 3435-3445.

Mohri, H. (1968). Amino-acid composition of "Tubulin" constituting microtubules of sperm flagella. *Nature* *217*, 1053-1054.

Mollinari, C., Kleman, J.P., Jiang, W., Schoehn, G., Hunter, T., and Margolis, R.L. (2002). PRC1 is a microtubule binding and bundling protein essential to maintain the mitotic spindle midzone. *J Cell Biol* *157*, 1175-1186.

Mollinari, C., Kleman, J.P., Saoudi, Y., Jablonski, S.A., Perard, J., Yen, T.J., and Margolis, R.L. (2005). Ablation of PRC1 by small interfering RNA demonstrates that cytokinetic abscission requires a central spindle bundle in mammalian cells, whereas completion of furrowing does not. *Mol Biol Cell* *16*, 1043-1055.

Mountain, V., Simerly, C., Howard, L., Ando, A., Schatten, G., and Compton, D.A. (1999). The kinesin-related protein, HSET, opposes the activity of Eg5 and cross-links microtubules in the mammalian mitotic spindle. *J Cell Biol* *147*, 351-366.

Mukherjee, S., Diaz Valencia, J.D., Stewman, S., Metz, J., Monnier, S., Rath, U., Asenjo, A.B., Charafeddine, R.A., Sosa, H.J., Ross, J.L., *et al.* (2012). Human Fidgetin is a microtubule severing the enzyme and minus-end depolymerase that regulates mitosis. *Cell Cycle* *11*, 2359-2366.

Muller-Reichert, T., Kiewisz, R., and Redemann, S. (2018). Mitotic spindles revisited - new insights from 3D electron microscopy. *J Cell Sci* *131*.

Musacchio, A., and Desai, A. (2017). A Molecular View of Kinetochore Assembly and Function. *Biology (Basel)* *6*.

Nagaoka, S.I., Hassold, T.J., and Hunt, P.A. (2012). Human aneuploidy: mechanisms and new insights into an age-old problem. *Nat Rev Genet* *13*, 493-504.

Nasa, I., and Kettenbach, A.N. (2018). Coordination of Protein Kinase and Phosphoprotein Phosphatase Activities in Mitosis. *Front Cell Dev Biol* *6*, 30.

Neef, R., Klein, U.R., Kopajtich, R., and Barr, F.A. (2006). Cooperation between mitotic kinesins controls the late stages of cytokinesis. *Curr Biol* *16*, 301-307.

Neef, R., Preisinger, C., Sutcliffe, J., Kopajtich, R., Nigg, E.A., Mayer, T.U., and Barr, F.A. (2003). Phosphorylation of mitotic kinesin-like protein 2 by polo-like kinase 1 is required for cytokinesis. *J Cell Biol* *162*, 863-875.

Nicklas, R.B. (1983). Measurements of the force produced by the mitotic spindle in anaphase. *J Cell Biol* *97*, 542-548.

Nicklas, R.B. (1989). The motor for poleward chromosome movement in anaphase is in or near the kinetochore. *J Cell Biol* *109*, 2245-2255.

Nicklas, R.B., Kubai, D.F., and Hays, T.S. (1982). Spindle microtubules and their mechanical associations after micromanipulation in anaphase. *J Cell Biol* *95*, 91-104.

Nislow, C., Lombillo, V.A., Kuriyama, R., and McIntosh, J.R. (1992). A plus-end-directed motor enzyme that moves antiparallel microtubules in vitro localizes to the interzone of mitotic spindles. *Nature* *359*, 543-547.

Nixon, F.M., Gutierrez-Caballero, C., Hood, F.E., Booth, D.G., Prior, I.A., and Royle, S.J. (2015). The mesh is a network of microtubule connectors that stabilizes individual kinetochore fibers of the mitotic spindle. *Elife* *4*.

Nixon, F.M., Honnor, T.R., Clarke, N.I., Starling, G.P., Beckett, A.J., Johansen, A.M., Brettschneider, J.A., Prior, I.A., and Royle, S.J. (2017). Microtubule organization within mitotic spindles revealed by serial block face scanning EM and image analysis. *J Cell Sci* *130*, 1845-1855.

Nunes Bastos, R., Gandhi, S.R., Baron, R.D., Gruneberg, U., Nigg, E.A., and Barr, F.A. (2013). Aurora B suppresses microtubule dynamics and limits central spindle size by locally activating KIF4A. *J Cell Biol* *202*, 605-621.

Oegema, K., Desai, A., Rybina, S., Kirkham, M., and Hyman, A.A. (2001). Functional analysis of kinetochore assembly in *Caenorhabditis elegans*. *J Cell Biol* *153*, 1209-1226.

Ohi, R., Coughlin, M.L., Lane, W.S., and Mitchison, T.J. (2003). An inner centromere protein that stimulates the microtubule depolymerizing activity of a KinI kinesin. *Dev Cell* *5*, 309-321.

Oliveira, R.A., Hamilton, R.S., Pauli, S., Davis, I., and Nasmyth, K. (2010). Cohesin cleavage and Cdk inhibition trigger formation of daughter nuclei. *Nat Cell Biol* *12*, 185-192.

Osborn, M., and Weber, K. (1977). The display of microtubules in transformed cells. *Cell* *12*, 561-571.

Ostergren, G. (1951). The mechanism of co-orientation in bivalents and multivalents. *Hereditas* *37*, 85-156.

O'Toole, E., Morphew, M., and McIntosh, J.R. (2020) Electron tomography reveals aspects of spindle structure important for mechanical stability at metaphase. *Mol Biol Cell* *31*, 184-195.



Ozlu, N., Monigatti, F., Renard, B.Y., Field, C.M., Steen, H., Mitchison, T.J., and Steen, J.J. (2010). Binding partner switching on microtubules and aurora-B in the mitosis to cytokinesis transition. *Mol Cell Proteomics* 9, 336-350.

Pamula, M.C., Carlini, L., Forth, S., Verma, P., Suresh, S., Legant, W.R., Khodjakov, A., Betzig, E., and Kapoor, T.M. (2019). High-resolution imaging reveals how the spindle midzone impacts chromosome movement. *J Cell Biol* 218, 2529-2544.

Pavin, N., and Tolic, I.M. (2016). Self-Organization and Forces in the Mitotic Spindle. *Annu Rev Biophys* 45, 279-298.

Pavin, N., and Tolic-Norrelykke, I.M. (2013). Dynein, microtubule and cargo: a menage a trois. *Biochem Soc Trans* 41, 1731-1735.

Paweletz, N. (2001). Walther Flemming: pioneer of mitosis research. *Nat Rev Mol Cell Biol* 2, 72-75.

Peterman, E.J., and Scholey, J.M. (2009). Mitotic microtubule crosslinkers: insights from mechanistic studies. *Curr Biol* 19, R1089-1094.

Petry, S., and Vale, R.D. (2015). Microtubule nucleation at the centrosome and beyond. *Nat Cell Biol* 17, 1089-1093.

Pfarr, C.M., Coue, M., Grissom, P.M., Hays, T.S., Porter, M.E., and McIntosh, J.R. (1990). Cytoplasmic dynein is localized to kinetochores during mitosis. *Nature* 345, 263-265.

Piehl, M., Tulu, U.S., Wadsworth, P., and Cassimeris, L. (2004). Centrosome maturation: measurement of microtubule nucleation throughout the cell cycle by using GFP-tagged EB1. *Proc Natl Acad Sci U S A* 101, 1584-1588.

Polak, B., Risteski, P., Lesjak, S., and Tolic, I.M. (2017). PRC1-labeled microtubule bundles and kinetochore pairs show one-to-one association in metaphase. *EMBO Rep* 18, 217-230.

Poser, I., Sarov, M., Hutchins, J.R., Heriche, J.K., Toyoda, Y., Pozniakovsky, A., Weigl, D., Nitzsche, A., Hegemann, B., Bird, A.W., *et al.* (2008). BAC TransgeneOmics: a high-throughput method for exploration of protein function in mammals. *Nat Methods* 5, 409-415.

Potapova, T.A., Daum, J.R., Pittman, B.D., Hudson, J.R., Jones, T.N., Satinover, D.L., Stukenberg, P.T., and Gorbsky, G.J. (2006). The reversibility of mitotic exit in vertebrate cells. *Nature* 440, 954-958.

Powers, A.F., Franck, A.D., Gestaut, D.R., Cooper, J., Gracyzk, B., Wei, R.R., Wordeman, L., Davis, T.N., and Asbury, C.L. (2009). The Ndc80 kinetochore complex forms load-bearing attachments to dynamic microtubule tips via biased diffusion. *Cell* 136, 865-875.

Raaijmakers, J.A., and Medema, R.H. (2014). Function and regulation of dynein in mitotic chromosome segregation. *Chromosoma* 123, 407-422.

Raaijmakers, J.A., van Heesbeen, R.G., Meaders, J.L., Geers, E.F., Fernandez-Garcia, B., Medema, R.H., and Tanenbaum, M.E. (2012). Nuclear envelope-associated dynein drives prophase centrosome separation and enables Eg5-independent bipolar spindle formation. *EMBO J* 31, 4179-4190.

Rapley, J., Nicolas, M., Groen, A., Regue, L., Bertran, M.T., Caelles, C., Avruch, J., and Roig, J. (2008). The NIMA-family kinase Nek6 phosphorylates the kinesin Eg5 at a novel site necessary for mitotic spindle formation. *J Cell Sci* 121, 3912-3921.

Rath, O., and Kozielski, F. (2012). Kinesins and cancer. *Nat Rev Cancer* 12, 527-539.

Reboutier, D., Troadec, M.B., Cremet, J.Y., Chauvin, L., Guen, V., Salaun, P., and Prigent, C. (2013). Aurora A is involved in central spindle assembly through phosphorylation of Ser 19 in P150Glued. *J Cell Biol* 201, 65-79.

Recouvreur, P., and Dogterom, M. (2012). Dissecting spindle architecture with a laser. *Cell* 149, 507-509.

Reinemann, D.N., Sturgill, E.G., Das, D.K., Degen, M.S., Vörös, S., Hwang, W., Ohi, R., and Lang, M.J. (2017). Collective Force Regulation in Anti-Parallel Microtubule Gliding by Dimeric Kif15 Kinesin Motors. *Curr Biol* 27, 2810-2820.

Rieder, C.L., and Khodjakov, A. (2003). Mitosis through the microscope: advances in seeing inside live dividing cells. *Science* 300, 91-96.

Rieder, C.L., and Salmon, E.D. (1994). Motile kinetochores and polar ejection forces dictate chromosome position on the vertebrate mitotic spindle. *J Cell Biol* 124, 223-233.

Ris, H. (1949). The anaphase movement of chromosomes in the spermatocytes of the grasshopper. *Biol Bull* 96, 90-106.

Rogers, G.C., Rogers, S.L., Schwimmer, T.A., Ems-McClung, S.C., Walczak, C.E., Vale, R.D., Scholey, J.M., and Sharp, D.J. (2004). Two mitotic kinesins cooperate to drive sister chromatid separation during anaphase. *Nature* 427, 364-370.

Rogers, G.C., Rogers, S.L., and Sharp, D.J. (2005). Spindle microtubules in flux. *J Cell Sci* 118, 1105-1116.

Roostalu, J., Hentrich, C., Bieling, P., Telley, I.A., Schiebel, E., and Surrey, T. (2011). Directional switching of the kinesin Cin8 through motor coupling. *Science* 332, 94-99.

Roostalu, J., Schiebel, E., and Khmelinskii, A. (2010). Cell cycle control of spindle elongation. *Cell Cycle* 9, 1084-1090.

Ruchaud, S., Carmena, M., and Earnshaw, W.C. (2007). Chromosomal passengers: conducting cell division. *Nat Rev Mol Cell Biol* 8, 798-812.

Salmon, E.D., Goode, D., Maugel, T.K., and Bonar, D.B. (1976). Pressure-induced depolymerization of spindle microtubules. III. Differential stability in HeLa cells. *J Cell Biol* 69, 443-454.

Salmon, E.D., Leslie, R.J., Saxton, W.M., Karow, M.L., and McIntosh, J.R. (1984). Spindle microtubule dynamics in sea urchin embryos: analysis using a fluorescein-labeled tubulin and measurements of fluorescence redistribution after laser photobleaching. *J Cell Biol* 99, 2165-2174.

Saunders, A.M., Powers, J., Strome, S., and Saxton, W.M. (2007). Kinesin-5 acts as a brake in anaphase spindle elongation. *Curr Biol* 17, R453-454.

Saunders, W.S., and Hoyt, M.A. (1992). Kinesin-related proteins required for structural integrity of the mitotic spindle. *Cell* 70, 451-458.

Saunders, W.S., Koshland, D., Eshel, D., Gibbons, I.R., and Hoyt, M.A. (1995). *Saccharomyces cerevisiae* kinesin- and dynein-related proteins required for anaphase chromosome segregation. *J Cell Biol* 128, 617-624.

Sawin, K.E., LeGuelllec, K., Philippe, M., and Mitchison, T.J. (1992). Mitotic spindle organization by a plus-end-directed microtubule motor. *Nature* 359, 540-543.

Sawin, K.E., and Mitchison, T.J. (1995). Mutations in the kinesin-like protein Eg5 disrupting localization to the mitotic spindle. *Proc Natl Acad Sci U S A* 92, 4289-4293.

Saxton, W.M., and McIntosh, J.R. (1987). Interzone microtubule behavior in late anaphase and telophase spindles. *J Cell Biol* 105, 875-886.

Saxton, W.M., Stemple, D.L., Leslie, R.J., Salmon, E.D., Zavortink, M., and McIntosh, J.R. (1984). Tubulin dynamics in cultured mammalian cells. *J Cell Biol* 99, 2175-2186.

Schmidt, J.C., Arthanari, H., Boeszoermyeni, A., Dashkevich, N.M., Wilson-Kubalek, E.M., Monnier, N., Markus, M., Oberer, M., Milligan, R.A., Bathe, M., *et al.* (2012). The kinetochore-bound Ska1 complex tracks depolymerizing microtubules and binds to curved protofilaments. *Dev Cell* 23, 968-980.

Scholey, J.M., Civelekoglu-Scholey, G., and Brust-Mascher, I. (2016). Anaphase B. *Biology* (Basel) 5.

Sekine, Y., Okada, Y., Noda, Y., Kondo, S., Aizawa, H., Takemura, R., and Hirokawa, N. (1994). A novel microtubule-based motor protein (KIF4) for organelle transports, whose expression is regulated developmentally. *J Cell Biol* 127, 187-201.

Sharp, D.J., McDonald, K.L., Brown, H.M., Matthies, H.J., Walczak, C., Vale, R.D., Mitchison, T.J., and Scholey, J.M. (1999a). The bipolar kinesin, KLP61F, cross-links

microtubules within interpolar microtubule bundles of *Drosophila* embryonic mitotic spindles. *J Cell Biol* *144*, 125-138.

Sharp, D.J., Rogers, G.C., and Scholey, J.M. (2000). Microtubule motors in mitosis. *Nature* *407*, 41-47.

Sharp, D.J., Yu, K.R., Sisson, J.C., Sullivan, W., and Scholey, J.M. (1999b). Antagonistic microtubule-sliding motors position mitotic centrosomes in *Drosophila* early embryos. *Nat Cell Biol* *1*, 51-54.

She, Z.Y., Wei, Y.L., Lin, Y., Li, Y.L., and Lu, M.H. (2019). Mechanisms of the Ase1/PRC1/MAP65 family in central spindle assembly. *Biol Rev Camb Philos Soc* *94*, 2033-2048.

She, Z.Y., and Yang, W.X. (2017). Molecular mechanisms of kinesin-14 motors in spindle assembly and chromosome segregation. *J Cell Sci* *130*, 2097-2110.

Shelden, E., and Wadsworth, P. (1990). Interzonal microtubules are dynamic during spindle elongation. *J Cell Sci* *97 (Pt 2)*, 273-281.

Shimamoto, Y., Maeda, Y.T., Ishiwata, S., Libchaber, A.J., and Kapoor, T.M. (2011). Insights into the micromechanical properties of the metaphase spindle. *Cell* *145*, 1062-1074.

Sikirzhyski, V., Magidson, V., Steinman, J.B., He, J., Le Berre, M., Tikhonenko, I., Ault, J.G., McEwen, B.F., Chen, J.K., Sui, H., *et al.* (2014). Direct kinetochore-spindle pole connections are not required for chromosome segregation. *J Cell Biol* *206*, 231-243.

Singh, S.K., Pandey, H., Al-Bassam, J., and Gheber, L. (2018). Bidirectional motility of kinesin-5 motor proteins: structural determinants, cumulative functions and physiological roles. *Cell Mol Life Sci* *75*, 1757-1771.

Skoufias, D.A., DeBonis, S., Saoudi, Y., Lebeau, L., Crevel, I., Cross, R., Wade, R.H., Hackney, D., and Kozielski, F. (2006). S-trityl-L-cysteine is a reversible, tight binding inhibitor of the human kinesin Eg5 that specifically blocks mitotic progression. *J Biol Chem* *281*, 17559-17569.

Spurck, T.P., and Pickett-Heaps, J.D. (1987). On the mechanism of anaphase A: evidence that ATP is needed for microtubule disassembly and not generation of polewards force. *J Cell Biol* *105*, 1691-1705.

Spurck, T.P., Pickett-Heaps, J.D., and Klymkowsky, M.W. (1986). Metabolic inhibitors and mitosis: II. Effect of dinitrophenol/deoxyglucose and nocodazole on the microtubule cytoskeleton. *Protoplasma* *131*, 60-74.

Straight, A.F., Sedat, J.W., and Murray, A.W. (1998). Time-lapse microscopy reveals unique roles for kinesins during anaphase in budding yeast. *J Cell Biol* *143*, 687-694.

Stumpff, J., von Dassow, G., Wagenbach, M., Asbury, C., and Wordeman, L. (2008). The kinesin-8 motor Kif18A suppresses kinetochore movements to control mitotic chromosome alignment. *Dev Cell* *14*, 252-262.

Sturgill, E.G., Norris, S.R., Guo, Y., and Ohi, R. (2016). Kinesin-5 inhibitor resistance is driven by kinesin-12. *J Cell Biol* *213*, 213-227.

Sturgill, E.G., and Ohi, R. (2013). Kinesin-12 differentially affects spindle assembly depending on its microtubule substrate. *Curr Biol* *23*, 1280-1290.

Su, K.C., Barry, Z., Schweizer, N., Maiato, H., Bathe, M., and Cheeseman, I.M. (2016). A Regulatory Switch Alters Chromosome Motions at the Metaphase-to-Anaphase Transition. *Cell Rep* *17*, 1728-1738.

Su, X., Arellano-Santoyo, H., Portran, D., Gaillard, J., Vantard, M., They, M., and Pellman, D. (2013). Microtubule-sliding activity of a kinesin-8 promotes spindle assembly and spindle-length control. *Nat Cell Biol* *15*, 948-957.

Subramanian, R., Ti, S.C., Tan, L., Darst, S.A., and Kapoor, T.M. (2013). Marking and measuring single microtubules by PRC1 and kinesin-4. *Cell* *154*, 377-390.

Subramanian, R., Wilson-Kubalek, E.M., Arthur, C.P., Bick, M.J., Campbell, E.A., Darst, S.A., Milligan, R.A., and Kapoor, T.M. (2010). Insights into antiparallel microtubule crosslinking by PRC1, a conserved nonmotor microtubule binding protein. *Cell* *142*, 433-443.

Sullivan, M., and Morgan, D.O. (2007). Finishing mitosis, one step at a time. *Nat Rev Mol Cell Biol* *8*, 894-903.

Tanaka, K., Kitamura, E., Kitamura, Y., and Tanaka, T.U. (2007). Molecular mechanisms of microtubule-dependent kinetochore transport toward spindle poles. *J Cell Biol* *178*, 269-281.

Tanenbaum, M.E., Macurek, L., Janssen, A., Geers, E.F., Alvarez-Fernandez, M., and Medema, R.H. (2009). Kif15 cooperates with eg5 to promote bipolar spindle assembly. *Curr Biol* *19*, 1703-1711.

Tanenbaum, M.E., Vale, R.D., and McKenney, R.J. (2013). Cytoplasmic dynein crosslinks and slides anti-parallel microtubules using its two motor domains. *Elife* *2*, e00943.

Telley, I.A., Gaspar, I., Ephrussi, A., and Surrey, T. (2012). Aster migration determines the length scale of nuclear separation in the *Drosophila* syncytial embryo. *J Cell Biol* *197*, 887-895.

Thiede, C., Fridman, V., Gerson-Gurwitz, A., Gheber, L., and Schmidt, C.F. (2012). Regulation of bi-directional movement of single kinesin-5 Cin8 molecules. *Bioarchitecture* *2*, 70-74.

Tillberg, P.W., Chen, F., Piatkevich, K.D., Zhao, Y., Yu, C.C., English, B.P., Gao, L., Martorell, A., Suk, H.J., Yoshida, F., *et al.* (2016). Protein-retention expansion microscopy of cells and tissues labeled using standard fluorescent proteins and antibodies. *Nat Biotechnol* *34*, 987-992.

Tolić, I.M. (2018). Mitotic spindle: Kinetochore fibers hold on tight to interpolar bundles. *Eur Biophys J.* *47*, 191-203.

Tolic, I.M., and Pavin, N. (2016). Bridging the gap between sister kinetochores. *Cell Cycle* *15*, 1169-1170.

Tolic-Norrelykke, I.M., Sacconi, L., Thon, G., and Pavone, F.S. (2004). Positioning and elongation of the fission yeast spindle by microtubule-based pushing. *Curr Biol* *14*, 1181-1186.

Truckenbrodt, S., Sommer, C., Rizzoli, S.O., and Danzl, J.G. (2019). A practical guide to optimization in X10 expansion microscopy. *Nat Protoc* *14*, 832-863.

Uehara, R., Kamasaki, T., Hiruma, S., Poser, I., Yoda, K., Yajima, J., Gerlich, D.W., and Goshima, G. (2016). Augmin shapes the anaphase spindle for efficient cytokinetic furrow ingression and abscission. *Mol Biol Cell* *27*, 812-827.

Uehara, R., Nozawa, R.S., Tomioka, A., Petry, S., Vale, R.D., Obuse, C., and Goshima, G. (2009). The augmin complex plays a critical role in spindle microtubule generation for mitotic progression and cytokinesis in human cells. *Proc Natl Acad Sci U S A* *106*, 6998-7003.

Uehara, R., Tsukada, Y., Kamasaki, T., Poser, I., Yoda, K., Gerlich, D.W., and Goshima, G. (2013). Aurora B and Kif2A control microtubule length for assembly of a functional central spindle during anaphase. *J Cell Biol* *202*, 623-636.

Uretz, R.B., Bloom, W., and Zirkle, R.E. (1954). Irradiation of parts of individual cells. II. Effects of an ultraviolet microbeam focused on parts of chromosomes. *Science* *120*, 197-199.

Valentine, M.T., Fordyce, P.M., Krzysiak, T.C., Gilbert, S.P., and Block, S.M. (2006). Individual dimers of the mitotic kinesin motor Eg5 step processively and support substantial loads in vitro. *Nat Cell Biol* *8*, 470-476.

van de Linde, S., Heilemann, M., and Sauer, M. (2012). Live-cell super-resolution imaging with synthetic fluorophores. *Annu Rev Phys Chem* *63*, 519-540.

van Heesbeen, R.G., Tanenbaum, M.E., and Medema, R.H. (2014). Balanced activity of three mitotic motors is required for bipolar spindle assembly and chromosome segregation. *Cell Rep* *8*, 948-956.

Vanneste, D., Takagi, M., Imamoto, N., and Vernos, I. (2009). The role of Hklp2 in the stabilization and maintenance of spindle bipolarity. *Curr Biol* *19*, 1712-1717.

Varma, D., Monzo, P., Stehman, S.A., and Vallee, R.B. (2008). Direct role of dynein motor in stable kinetochore-microtubule attachment, orientation, and alignment. *J Cell Biol* *182*, 1045-1054.

Varma, D., and Salmon, E.D. (2012). The KMN protein network--chief conductors of the kinetochore orchestra. *J Cell Sci* *125*, 5927-5936.

Vazquez-Novelle, M.D., Sansregret, L., Dick, A.E., Smith, C.A., McAinsh, A.D., Gerlich, D.W., and Petronczki, M. (2014). Cdk1 inactivation terminates mitotic checkpoint surveillance and stabilizes kinetochore attachments in anaphase. *Curr Biol* *24*, 638-645.

Verhey, K.J., and Hammond, J.W. (2009). Traffic control: regulation of kinesin motors. *Nat Rev Mol Cell Biol* *10*, 765-777.

Verni, F., Somma, M.P., Gunsalus, K.C., Bonaccorsi, S., Belloni, G., Goldberg, M.L., and Gatti, M. (2004). Feo, the *Drosophila* homolog of PRC1, is required for central-spindle formation and cytokinesis. *Curr Biol* *14*, 1569-1575.

Vladimirou, E., McHedlishvili, N., Gasic, I., Armond, J.W., Samora, C.P., Meraldi, P., and McAinsh, A.D. (2013). Nonautonomous movement of chromosomes in mitosis. *Dev Cell* *27*, 60-71.

Vleugel, M., Kok, M., and Dogterom, M. (2016). Understanding force-generating microtubule systems through in vitro reconstitution. *Cell Adh Migr* *10*, 475-494.

Volkov, V.A., Huis In 't Veld, P.J., Dogterom, M., and Musacchio, A. (2018). Multivalency of NDC80 in the outer kinetochore is essential to track shortening microtubules and generate forces. *Elife* *7*.

Vorozhko, V.V., Emanuele, M.J., Kallio, M.J., Stukenberg, P.T., and Gorbsky, G.J. (2008). Multiple mechanisms of chromosome movement in vertebrate cells mediated through the Ndc80 complex and dynein/dynactin. *Chromosoma* *117*, 169-179.

Vukusic, K., Buda, R., Bosilj, A., Milas, A., Pavin, N., and Tolic, I.M. (2017). Microtubule Sliding within the Bridging Fiber Pushes Kinetochore Fibers Apart to Segregate Chromosomes. *Dev Cell* *43*, 11-23 e16.

Vukusic, K., Buda, R., and Tolic, I.M. (2019). Force-generating mechanisms of anaphase in human cells. *J Cell Sci* *132*.

Waitzman, J.S., and Rice, S.E. (2014). Mechanism and regulation of kinesin-5, an essential motor for the mitotic spindle. *Biol Cell* *106*, 1-12.

Walczak, C.E., Cai, S., and Khodjakov, A. (2010). Mechanisms of chromosome behaviour during mitosis. *Nat Rev Mol Cell Biol* *11*, 91-102.

Walczak, C.E., and Heald, R. (2008). Mechanisms of mitotic spindle assembly and function. *Int Rev Cytol* *265*, 111-158.

Wandke, C., Barisic, M., Sigl, R., Rauch, V., Wolf, F., Amaro, A.C., Tan, C.H., Pereira, A.J., Kutay, U., Maiato, H., *et al.* (2012). Human chromokinesins promote chromosome congression and spindle microtubule dynamics during mitosis. *J Cell Biol* *198*, 847-863.

Wang, H., Brust-Mascher, I., Cheerambathur, D., and Scholey, J.M. (2011). Coupling between microtubule sliding, plus-end growth and spindle length revealed by kinesin-8 depletion. *Cytoskeleton (Hoboken)* *67*, 715-728.

Wang, H., Brust-Mascher, I., Civelekoglu-Scholey, G., and Scholey, J.M. (2013). Patronin mediates a switch from kinesin-13-dependent poleward flux to anaphase B spindle elongation. *J Cell Biol* *203*, 35-46.

Wang, S.Z., and Adler, R. (1995). Chromokinesin: a DNA-binding, kinesin-like nuclear protein. *J Cell Biol* *128*, 761-768.

Waterman-Storer, C.M., Desai, A., Bulinski, J.C., and Salmon, E.D. (1998). Fluorescent speckle microscopy, a method to visualize the dynamics of protein assemblies in living cells. *Curr Biol* 8, 1227-1230.

Waters, J.C., Cole, R.W., and Rieder, C.L. (1993). The force-producing mechanism for centrosome separation during spindle formation in vertebrates is intrinsic to each aster. *J Cell Biol* 122, 361-372.

Waters, J.C., Mitchison, T.J., Rieder, C.L., and Salmon, E.D. (1996). The kinetochore microtubule minus-end disassembly associated with poleward flux produces a force that can do work. *Mol Biol Cell* 7, 1547-1558.

Welburn, J.P., Grishchuk, E.L., Backer, C.B., Wilson-Kubalek, E.M., Yates, J.R., 3rd, and Cheeseman, I.M. (2009). The human kinetochore Ska1 complex facilitates microtubule depolymerization-coupled motility. *Dev Cell* 16, 374-385.

Wendell, K.L., Wilson, L., and Jordan, M.A. (1993). Mitotic block in HeLa cells by vinblastine: ultrastructural changes in kinetochore-microtubule attachment and in centrosomes. *J Cell Sci* 104 ( Pt 2), 261-274.

Wheatley, S.P., Hinchcliffe, E.H., Glotzer, M., Hyman, A.A., Sluder, G., and Wang, Y. (1997). CDK1 inactivation regulates anaphase spindle dynamics and cytokinesis in vivo. *J Cell Biol* 138, 385-393.

Wiese, C., and Zheng, Y. (2006). Microtubule nucleation: gamma-tubulin and beyond. *J Cell Sci* 119, 4143-4153.

Wijeratne, S., and Subramanian, R. (2018). Geometry of antiparallel microtubule bundles regulates relative sliding and stalling by PRC1 and Kif4A. *Elife* 7.

Winey, M., Mamay, C.L., O'Toole, E.T., Mastronarde, D.N., Giddings, T.H., Jr., McDonald, K.L., and McIntosh, J.R. (1995). Three-dimensional ultrastructural analysis of the *Saccharomyces cerevisiae* mitotic spindle. *J Cell Biol* 129, 1601-1615.

Wittmann, T., Hyman, A., and Desai, A. (2001). The spindle: a dynamic assembly of microtubules and motors. *Nat Cell Biol* 3, E28-34.

Wolf, F., Wandke, C., Isenberg, N., and Geley, S. (2006). Dose-dependent effects of stable cyclin B1 on progression through mitosis in human cells. *EMBO J* 25, 2802-2813.

Wood, K.W., Lad, L., Luo, L., Qian, X., Knight, S.D., Nevins, N., Brejc, K., Sutton, D., Gilmartin, A.G., Chua, P.R., *et al.* (2010). Antitumor activity of an allosteric inhibitor of centromere-associated protein-E. *Proc Natl Acad Sci U S A* 107, 5839-5844.

Wordeman, L. (2010). How kinesin motor proteins drive mitotic spindle function: Lessons from molecular assays. *Semin Cell Dev Biol* 21, 260-268.

Worrall, J.T., Tamura, N., Mazzagatti, A., Shaikh, N., van Lingen, T., Bakker, B., Spierings, D.C.J., Vladimirov, E., Fojer, F., and McClelland, S.E. (2018). Non-random Mis-segregation of Human Chromosomes. *Cell Rep* 23, 3366-3380.

Wurzenberger, C., and Gerlich, D.W. (2011). Phosphatases: providing safe passage through mitotic exit. *Nat Rev Mol Cell Biol* 12, 469-482.

Yang, G., Cameron, L.A., Maddox, P.S., Salmon, E.D., and Danuser, G. (2008). Regional variation of microtubule flux reveals microtubule organization in the metaphase meiotic spindle. *J Cell Biol* 182, 631-639.

Yang, Z., Tulu, U.S., Wadsworth, P., and Rieder, C.L. (2007). Kinetochore dynein is required for chromosome motion and congression independent of the spindle checkpoint. *Curr Biol* 17, 973-980.

Yang, J., Ikezoe, T., Nishioka, C., Tasaka, T., Taniguchi, A., Kuwayama, Y., Komatsu, N., Bandobashi, K., Togitani, K., Koeffler, H.P., Taguchi, H., and Yokoyama, A. (2007). AZD1152, a novel and selective aurora B kinase inhibitor, induces growth arrest, apoptosis, and sensitization for tubulin depolymerizing agent or topoisomerase II inhibitor in human acute leukemia cells in vitro and in vivo. *Blood* 110, 2034-2040.

- Young, S., Besson, S., and Welburn, J.P. (2014). Length-dependent anisotropic scaling of spindle shape. *Biol Open* 3, 1217-1223.
- Yount, A.L., Zong, H., and Walczak, C.E. (2015). Regulatory mechanisms that control mitotic kinesins. *Exp Cell Res* 334, 70-77.
- Yu, C.H., Redemann, S., Wu, H.Y., Kiewisz, R., Yoo, T.Y., Conway, W., Farhadifar, R., Muller-Reichert, T., and Needleman, D. (2019). Central-spindle microtubules are strongly coupled to chromosomes during both anaphase A and anaphase B. *Mol Biol Cell* 30, 2503-2514.
- Zhang, H., and Dawe, R.K. (2011). Mechanisms of plant spindle formation. *Chromosome Res* 19, 335-344.
- Zhu, C., and Jiang, W. (2005). Cell cycle-dependent translocation of PRC1 on the spindle by Kif4 is essential for midzone formation and cytokinesis. *Proc Natl Acad Sci U S A* 102, 343-348.
- Zhu, C., Zhao, J., Bibikova, M., Levenson, J.D., Bossy-Wetzel, E., Fan, J.B., Abraham, R.T., and Jiang, W. (2005). Functional analysis of human microtubule-based motor proteins, the kinesins and dyneins, in mitosis/cytokinesis using RNA interference. *Mol Biol Cell* 16, 3187-3199.

#### **Web sources**

1. <https://www.nature.com/scitable/content/drawing-of-mitosis-by-walther-flemming-43904/>
2. <http://cellcycleknockouts.wi.mit.edu/>

## 8 Author biography

Kruno Vukušić was born on June 12, 1991 in Split where he finished elementary and high schools. He graduated Molecular Biology in 2015 on Faculty of Science at University of Zagreb under the mentorship of prof. dr. sc. Iva Tolić on the theme “Organisation of microtubules and force-balance analysis in metaphase spindles of HeLa and Ptk1 cells”. Since 2015 he has been working in the Biophysics Laboratory at the Ruđer Bošković Institute (IRB) as an Associate on the ERC Project NewSpindleForce under the mentorship of prof. dr. sc. Iva Tolić. In the same time, he was enrolled in the Postgraduate Study of Biology at the Faculty of Science in Zagreb. As part of Tolić group he combined cell and molecular biology tools including confocal microscopy, molecular genetics, biophysical tools including laser microsurgery, optical engineering, computer quantifications and statistical analysis. His current research interests focus more on anaphase chromosome dynamics and resolving the force-generating mechanisms that occur during that process in human cells. During his work at the IRB, he participated in seven international conferences (Central European Genome Stability and Dynamics Meeting 2016, Zagreb (presentation), EMBL Symposia 2016 "Microtubules: From Atoms to Complex Systems", Heidelberg (poster), 12th International Congress of Cell Biology 2016, Prague (presentation), 17th International European Light Microscopy Initiative Meeting 2017, Dubrovnik (presentation), EMBO Conference on Meiosis 2017, Hvar (poster), Conference “Mitotic spindle: From living and synthetic systems to theory” 2019, Split (poster) and Biophysical Conference 2019, Hvar (presentation)) and 1 workshop (ESF workshop "Dynamics of the Cytoskeleton" 2017, Zagreb (poster)). In 2015, he spent 6 months as a guest scientist on Max Planck Institute of Molecular Cell Biology and Genetics, Dresden, Germany. To date, he has published 3 scientific papers in international scientific journals, one recent preprint, two book chapters and one review paper. He was awarded with Honour for special achievements as a student in 2013 from University of Zagreb, Scholarship from Croatian Ministry of education and sports in 2011, Scholarship from City of Split for especially talented students in 2014 and Annual award of the Ruđer Bošković Institute for the best scientific papers in 2017.

### **Publications:**

1. Kajtez, J. \*, Solomatina, A. \*, Novak, M. \*, Polak, B., **Vukušić, K.**, Rudiger, J., Cojoc, G., Milas, A., Šumanovac Šestak, I., Risteski, P., Tavano, F., Klemm, A. H., Roscioli, E., Welburn, J., Cimini, D., Glunčić, M., Pavin, N., Tolić, I. M. (2016). Overlap microtubules link sister k-fibers and balance the forces on bi-oriented kinetochores. *Nat. Commun.* 7, 10298



2. **Vukušić, K.**, Šikić, S., Balen, B. (2016). Recombinant therapeutic proteins produced in plants: towards engineering of human-type O-and N-glycosylation. *Periodicum biologicorum* 118, 2; 75-90.
3. Buda, R.\* , **Vukušić, K.\***, and Tolić, I.M. (2017). Dissection and characterization of microtubule bundles in the mitotic spindle using femtosecond laser ablation. *Methods Cell Biol* 139, 81-101.
4. **Vukušić, K.\***, Buda, R.\* , Bosilj, A.\* , Milas, A., Pavin, N., and Tolić, I.M. (2017). Microtubule Sliding within the Bridging Fiber Pushes Kinetochore Fibers Apart to Segregate Chromosomes. *Dev Cell* 43, 11-23 e16.
5. **Vukušić, K.\***, Buda, R.\* , and Tolić, I.M. (2019). Force-generating mechanisms of anaphase in human cells. *J Cell Sci* 132.
6. **Vukušić, K.\***, Buda, R.\* , Ponjavić, I.\* , Risteski, P., and Tolić, I.M. (2019). Chromosome segregation is driven by joint microtubule sliding action of kinesins KIF4A and EG5. bioRxiv 863381; doi: <https://doi.org/10.1101/863381> (preprint).
7. Ponjavić, I., **Vukušić, K.**, and Tolić, I.M. (2020). Expansion microscopy of the mitotic spindle. *Methods Cell Biol* 161 (in press).

\*These authors contributed equally to the work.